STUDIES ON THE ENVIRONMENTAL STRESS CORROSION CRACKING OF MODEL EPOXY-GLASS COMPOSITES.

by

JOHN WILLIAM ROCK. M.Sc.

A thesis in part fulfillment for the degree of Doctor of Philosophy of the University of Surrey. April, 1983.

SYNOPSIS

The stress corrosion cracking of model epoxy-glass $0^{o}/90^{o}/0^{o}$ crossply and 0^{o} unidirectional composites in aqueous sulphuric acid has been studied. Specimens, in the form of coupons cut from laminates were tested under conditions of uniaxial tension at constant load, whilst partially immersed in an acidic environment. Two different modes of failure, which resulted in fracture were observed. In the "so-called" Mode I failure, fracture occurred within that part of the composite immersed in the acid, whereas in Mode II, it occurred in the unimmersed part. Both failure modes were observed for crossply and unidirectional composites. In unstressed $0^{o}/90^{o}/0^{o}$ specimens a third failure mode (Mode III) was observed, in which the damage took the form of transverse and longitudinal cracking of the unimmersed part.

The failure mode depended upon the magnitude of the initial applied strain, the nature of the environment, and the type of environment cell. At initial applied strains of greater than about 0.15% only Mode I failure was observed. The similarity between the times-to-failure of laminates with those recorded for single E-glass fibres showed that the resin was not providing significant protection from the acidic environment. To account for this result it is postulated that the acid rapidly permeates these composites through environmental microcracks, which form parallel to the axis of the glass reinforcement.in the 0^{o} plies. The formation of these microcracks is due to a reduction in the resin/glass interfacial strength in the presence of acids. Confirmation of this phenomenon was obtained from experiments on the transverse cracking behaviour of crossply laminates, immersed in aqueous acid and tensile tested at constant strain rate.

At initial applied strains of less than about 0.15% and depending upon the experimental conditions, failure was by either Mode I or II. Mode II, which occurs in shorter times than Mode I was observed in acids (e.g. sulphuric acid) giving rise to relatively insoluble glass degradation products, providing evaporation of moisture from the unimmersed part of the specimen was possible. The Mode II failure mechanism has been identified with the transport of the aqueous acid along the glass resin interface from the immersed to the unimmersed part of the composite. Here precipitation of the less soluble glass degradation products causes a localised stress sufficient to initiate and propagate a stress corrosion crack. At these strains both Mode I and II failures occur at times significantly greater than those observed for glass fibres.

Mode III failure is similarly attributed to the precipitation of glass degradation products within the composite.

Microscopical examination of the stress corrosion fracture surfaces did not reveal any morphological differences between Mode I and II failure, apart from the appearance of more crystalline products in the Mode II fractures.

Although glass fibre fracture is the ultimate failure mechanism in these composites, stress corrosion of the fibre matrix interface was found to be a necessary precursor.

ACKNOWLEDGEMENTS

I am forever indebted to my supervisor Dr. F.R. Jones for his help, advice and invaluable discussion given throughout this work.

Also I gratefully acknowledge:

Professor J.E. Bailey for illuminating discussions and suggestions.

Dr. T.J. Sweeting for mathematical help and advice.

Mr. M.G. Bader for general discussion and encouragement.

Colleagues and staff for their valuable discussions.

The staff of the Micro-Structural Studies Unit for help with all things microscopical.

The staff of the Workshop in building apparatus.

My wife Denise for typing this thesis.

To my wife Denise
and my Parents.
Thank You.

CONTENTS

CHAPTER 1 INTRODUCTION AND LITERATURE REVIEW

1.1. INTRODUCTION

The phenomenon exhibited by many materials, whereby accelerated failure occurs because of a synergistic effect between a stress and a chemical environment, is often referred to as "Stress Corrosion","Stress Corrosion Cracking" or "Environmental Stress Corrosion". Since this type of failure can occur at low stresses, some materials cannot be used in certain environmental conditions. The stress may either be externally applied, or arise internally as for example, the thermal stresses in laminates produced on cooling from an elevated curing temperature, or the stresses generated by the cold working of a metal.

The stress corrosion cracking of metals and in particular, alloys which are especially prone to this phenomenon, has been studied for many years. However the complex nature of the process has made it difficult to elucidate the physical and chemical mechanisms involved. Possible mechanisms include hydrogen embrittlement and intergranular cracking (1).

The term "Static Fatigue" has been used to describe the time dependent failure of inorganic glasses. Once it was recognised that it was a stress assisted chemical process, and that water was one of the most active environments, "Static Fatigue" was retermed "Stress Corrosion". As with metals the mechanism has not yet been positively identified.

Of the polymeric materials, polyethylene is rather prone to stress corrosion cracking in a number of environments, of which the detergents

are the most active (2,3). However its resistance has been found to be dependent upon the degree of crystallinity, and morphology of the crystallites in the polymer. Failure is believed to be initiated in the inter-spherulitic regions. Thus totally resistant grades can be obtained by increasing the degree of polymerisation and narrowing the molecular weight distribution. Both result in a greater number of inter-spherulitic polymer chains.

Considering the diversity of materials in which stress corrosion is found, it is perhaps indicative of the complex mechanisms occurring, that no single theory can explain this phenomenon. Its existence in GRP is easily understandable in terms of the limited stress corrosion resistance of the glass reinforcement, together with the permeability of the matrix resins.

1.2. THE STRESS CORROSION CRACKING OF GRP

The simplest method of evaluating the chemical resistance of a material is to immerse it in potentially aggressive media, and monitor changes in its physical and mechanical properties. This type of test is known as an immersion test and has been extensively used in evaluating the chemical resistance of glass reinforced plastics (for example, see references 4,5,6). For economic and practical reasons it is necessary to use accelerated testing at elevated temperatures. The results of these tests are usually expressed as a percentage retention of the original properties. Table 1.1 shows the results of such a test on laminates fabricated using a general purpose (orthophthalic), an isophthalic and a bisphenol "A" polyester for the matrix resin. The better chemical resistance of the bisphenol "A" polyester resin is reflected in the good acid and alkali resistance of the laminates. The volume fraction of resin and the effectiveness of the barrier resins as gel coats have also been studied, and the following general conclusions on the resistance of GRP to aqueous environments have been reached.

1. The chemical resistance of a laminate decreases as the volume fraction of glass increases.
2. A resin rich outer layer, which is normally referred to as a gel coat, significantly improves the chemical resistance of the laminate.
3. The large reduction in the mechanical properties, which is observed in aqueous mineral acids, is primarily caused by chemical attack of the glass fibre reinforcement. Resin degradation is normally limited.

	HNO_3 5%	H_2SO_4 25%	HCl 15%	NaOH 5%	H_2O
Bisphenol-A Polyester					
Flexural Modulus[α]	71	72	59	55	71
Young's Modulus[α]	81	94	81	79	59
Isophthalic Polyester					
Flexural Modulus	52	44	49	Two[β]	65
Young's Modulus	67	70	65	Weeks	45
General Purpose Polyester					
Flexural Modulus	51	68	55	One	57
Young's Modulus	96	86	74	Week	59

α Shown as % retention

β Time to disintegration

TABLE 1.1 The deterioration of properties of 50/50 resin/glass "C" glass veil overlay laminates immersed for 1 month at 99°C. Data taken from reference 4.

4. The polyester resin is prone to blistering in alkaline environments which often results in complete disintegration of the laminate (see Table 1.1).

The general criticism of the immersion test is that it does not take into account the effect of externally applied stresses, and therefore does not realistically model the environmental conditions (7,8). The use of elevated temperatures to produce accelerated results has been criticised by Dewimille et al (9,10). They concluded, from a study of the damage produced in laminates immersed in water at various temperatures, that hot water did not simply accelerate lower temperature mechanisms. The use of strength retention data for predicting the long term behaviour of laminates has also been questioned by Aveston et al (11). They observed, as Metcalfe and Schmitz (12) had previously, that E-glass fibres immersed in water, retained most of their strength until final failure. Hence the extrapolation of short term test results will predict longer failure times than found in practice.

Rawe (13) also criticised the immersion test because of its failure to take into account the effect of externally applied stresses. Experiments where polyester or epoxy-glass laminates were exposed simultaneously to an applied stress and an aqueous environment,clearly demonstrated the existence of a synergistic effect. From the effect of various environments upon the creep rate of a glass reinforced anhydride cured-bisphenol "A" epoxy laminates, he classified the environments according to their possible corrosion mechanisms as follows.

1. "Non-aqueous liquids which do not chemically attack the laminate."
2. "Liquids which can be seen to attack the laminate chemically."
3. "Aqueous liquids that apparently do not chemically attack the laminate."

He gave no example of the first category. For category two he chose toluene as an example. Immersion testing for 1000 hours predicted a slight strength loss. However the simultaneous application of a load (1/3 ultimate fracture stress) produced total failure in 600 hours. Dilute aqueous acids and alkalies, which were included in category three were also responsible for failures which could not be predicted from immersion tests. Figure 1.1 shows the environmental creep of a laminate immersed in dilute acid. The initial creep rate was found to be independent of the applied load, but after an induction period, which was dependent upon the applied load, it increased rapidly, and failure of the specimen often followed. The results in Figure 1.1 are similar to those of Hogg, Hull and Spencer (14) for polyester laminates. Whereas these authors identified different stages in the process, Rawe was unable to discriminate between the different parts. He did however make preliminary attempts to fit power functions of time to the results for creep in air, water and dilute acid. Surprisingly he made no comment on the type of fractures observed. It is now recognized that stress corrosion fractures are distinctive in that they appear to be of a brittle nature, with very little fibre pull-out. This is in contrast to the tensile failure of a laminate which produces a brushlike fracture. Judd (6) observed that brittle tensile failures occurred in glass-epoxy laminates after immersion in boiling water for 72 hours. Bott and Barker (15) also commented on the brittle nature of fractures in filament wound glass polyester pipes, which

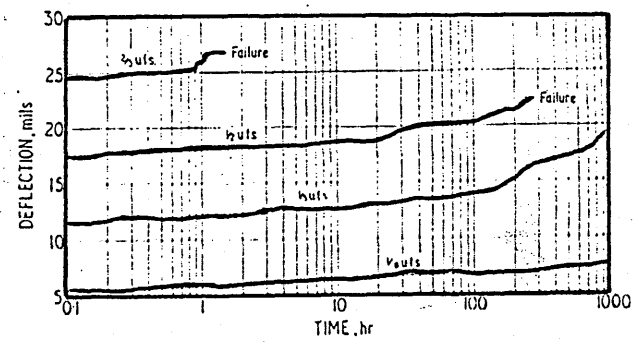

Figure 1.1 Environmental creep tests of an anhydride cured bisphenol-A epoxy laminates in acid (pH=5). Taken from reference 13.

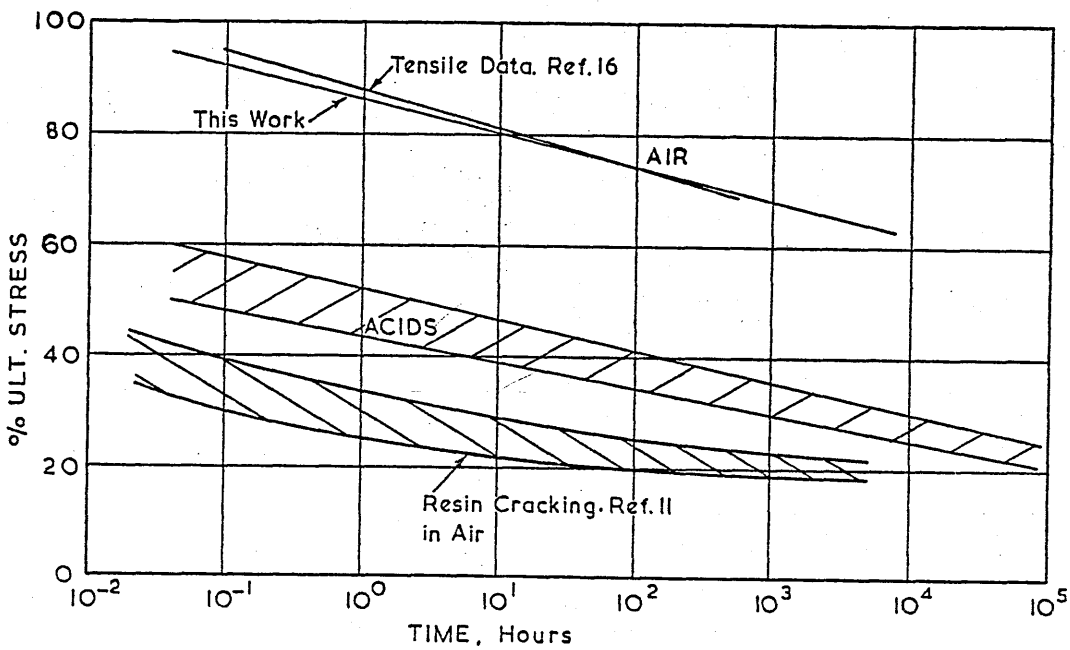

Figure 1.2 Comparison between environmental stress/rupture and damage in air. Taken from reference 7. Note references refer to original paper.

had been immersed in water at various temperatures.

Oswitch (16) applied the synergistic effect between the stress and the environment to obtain the effects of accelerated ageing, in a similar manner to the elevated temperature immersion test. However, he proposed to use the results to predict chemical rather than stress corrosion resistance. He fully appreciated that chemical attack could proceed more rapidly in stressed laminates, and commented that the laminates which survived this test would be expected to show good service life.

For a large number of metals and alloys, a stress corrosion limit below which fracture does not occur, has been identified. Similarly a limiting strain for GRP has been postulated. Collins (17) reported that strain corrosion failure of glass-polyester pipe did not occur at applied strains of less than 0.3%. But he also stated that "No systematic study of the effect of strain level on life-to-failure has been carried out." However other workers have carried out more systematic studies and found strong evidence for such a limit.

Aveston and Sillwood (18) measured the crack velocity as a function of its stress intensity for unidirectional polyester-glass laminates, in a direction normal to the reinforcement, whilst immersed in aqueous sulphuric acid. They attributed the deviation from linearity to be indicative of a stress corrosion limit. Jones et al (19) have also observed a stress corrosion limit, for polyester-glass coupons tested in 4-point bend and uniaxial tension. Roberts (7) postulated that the environment primarily

enters a laminate through cracks in the resin. If resin cracking is avoided then stress corrosion failure would require very long immersion times. His results are given in Figure 1.2, where the failure of chopped strand matt reinforced polyester laminates in times of up to 10^4 hours only occurs when the applied stress is sufficient to cause microcracking of the resin. Carswell and Roberts (20) and Barker, Baird-Smith and Jones (21) have suggested that environmental microcracks can form, in which case the results for resin cracking in Figure 1.2 would be at lower stresses. If resin cracking was primarily responsible for the stress corrosion failures, then more flexible matrix resins could be expected to enhance the stress corrosion resistance of the laminate. Hogg and Hull (22) have investigated the effect of resin flexibility using filament wound polyester pipe tested in diametrical compression. They found that the more flexible resins could be superior to the brittle chemically resistant resins. This they attributed to the mechanism of stress corrosion crack propagation. In the more brittle resins, the crack penetrates the resin between individual fibres and allowed the acid access to the glass fibres at the crack tip. However, with flexible resins, plastic flow at the crack tip prevents the exposure of the fibre with the result that the corrodent must diffuse through the resin to cause stress corrosion of the next fibre. With increasingly flexible resins of lower crosslink density, the diffusion of the corrodent becomes more rapid,with the result that there is an optimum resin flexibility for maximum stress corrosion resistance.

Wiederhorn and Bolz (23) found that whereas soda-lime glasses had a stress corrosion limit, E-glass and silica glass did not. Therefore, since

matrix resins do not provide an impermeable barrier to aqueous environments, it is difficult to conceive a stress corrosion limit in glass reinforced composites.

The effect of acid concentration has been reported by Collins (17) and Scrimshaw (24). Both found that the failure times of GRP were minimised when the hydrogen ion concentration was approximately 0.5-3.0 M. A similar concentration dependence was observed by Roberts (7), Scrimshaw (24) and Cockram (25), for the stress corrosion of E-glass strands. Collins (17) suggested that this was the result of the maximum hydrogen ion content of sulphuric acid, occurring within this range of concentration, whereas Roberts (7) interpreted it in terms of a reduction in the hydrogen ion activity, with increasing acid concentration. Both these explanations assume that the hydrogen ion alone is responsible for stress corrosion of E-glass. In section 1.3 other possible mechanisms for stress corrosion of glass will be examined.

Hull et al (14,22,26-28) have studied the failure of polyester-glass filament wound pipe, under diametrical compression, with the environment contained within the pipe according to ASTM 3681. Both constant load and constant displacement tests were carried out and changes in displacement or load (as appropriate) were monitored. These studies showed that the stress corrosion process, under constant load or strain, is fundamentally, the same. However the failure times are longer for the latter because of stress relaxation processes. They were able to identify five stages to the stress

corrosion process, which they described as follows:-

Stage I is the initial viscoelastic response of the material to the applied load and does not appear to be affected by the environment used.

Stage II shows an approximately linear relaxation of load which is associated with slow deformation and microfracture. During this stage stress corrosion cracks are nucleated and grow slowly. The number and distribution of cracks depends on the initial applied stress and the corrosive environment.

Stage III shows a sharp drop in load which is associated with the growth of large stress corrosion cracks and delaminations. The relaxation curves often show a series of steps indicating the discontinuous growth of the cracks.

Stage IV is a post stress corrosion failure region with a low relaxation rate.

Stage V is associated with the total collapse of the pipe in a constant load test.

Typical traces for experiments at constant load and constant displacement are shown in Figure 1.3 and the stages described above are indicated. Under constant load,final failure does not occur until the end of Stage V, although seepage of the acid out of the pipe could be detected during Stage III. Exactly when this occurs is uncertain so the end of Stage III is taken as failure. The nucleation of stress corrosion cracks in polyester-glass pipe has been shown by Barker et al (21) to occur by the fracture of individual glass fibres, normal to their axis. Hull et al showed that Stage II is caused by a similar nucleation process. During Stage III these individual stress corrosion cracks coalesce by shear

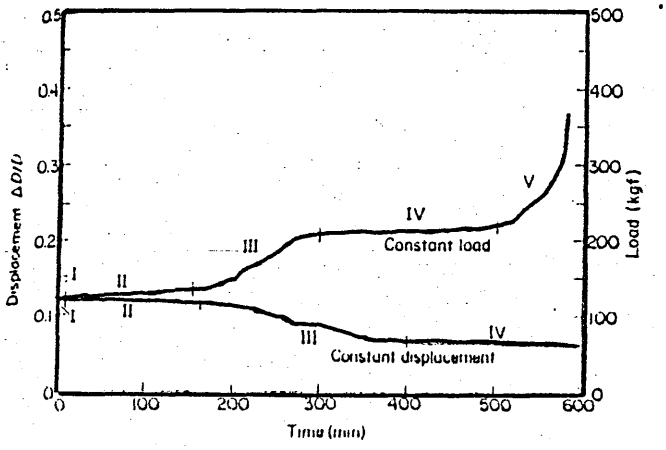

Figure 1.3 Comparison of constant load and constant displacement test showing the different stages of the fracture process. Taken from reference 14.

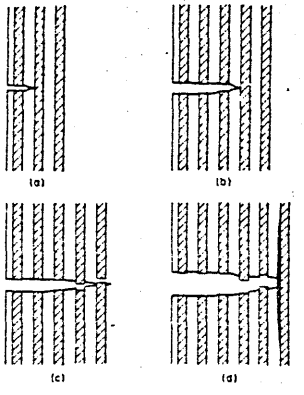

Figure 1.4 Model of the fracture process in unidirectional GRP structures tested in a corrosive environment,

(a) nucleation of first crack by acid attack on fibre
(b) growth of flat crack by fibre fracture at tip of resin crack
(c) development of small amount of pull-out due to out-of-plane fibre fracture
(d) delamination cracks at tip of flat crack

Taken from reference 27.

cracking parallel to the fibres to produce a fracture, with a stepped appearance, along the line of maximum tensile stress, at the bottom of the pipe.

The transverse failure strain of a unidirectional laminate is much less than the longitudinal. Thus when a $0^{o}/90^{o}/0^{o}$ crossply laminate is subjected to a stress, failure of the 90^{o} transverse ply occurs. The strain at which this happens is referred to as the transverse cracking strain. Generally this does not cause a total failure of the composite because the 0^{o} longitudinal plies can sustain the additional load placed upon them. With increasing applied stress further multiple transverse cracking occurs. The effect of these transverse cracks on the stress corrosion cracking of polyester-glass $0^{o}/90^{o}/0^{o}$ crossply laminates has been studied by Jones, Wheatley and Bailey (29). They observed, for coupons tested in 4-point bend, the transverse cracks penetrated the tensile 0^{o} longitudinal ply, where they nucleated stress corrosion cracks. A comparison of the results from 0^{o} unidirectional and $0^{o}/90^{o}/0^{o}$ coupons showed that the failure time of the 0^{o} longitudinal ply of a crossply coupon, had been significantly reduced by the presence of transverse cracks. However for similar coupons tested in uniaxial tension there were no significant differences between the failure times. They suggested (29) that under uniaxial tension, the transverse cracks had insufficient energy to penetrate the 0^{o} longitudinal plies. The greater energy of the transverse cracks generated in bend arises from the geometry of the test method. Under these conditions a symmetrical $0^{o}/90^{o}/0^{o}$ crossply laminate has a neutral axis at the centre of the transverse ply, between compressive and tensile zones. When the strain at the tensile $90^{o}/0^{o}$ interface

reaches the transverse cracking strain, failure of the 90^{o} ply will occur by a crack running towards the neutral axis. However in the 0^{o} ply there is a tensile strain gradient, with a maximum at the outer face of the ply, which aids the penetration of transverse cracks into the 0^{o} ply. Hull and Hogg (26) identified stress corrosion initiation regions in the ply adjacent to a transverse crack, which they interpreted as evidence for the transport of the aqueous environment into the laminate through the transverse cracks. A comparison of the stress corrosion results from 0^{o} and $\pm 55^{o}$ filament wound pipes, as a function of the strain in the glass fibres showed that transverse cracks significantly reduced the failure time. However it was not determined whether this could be accounted for by the enhanced stress placed on the adjacent plies, or by an initiation mechanism as described above. It is clear that transverse cracks reduce the durability of GRP and that laminates with a greater transverse cracking strain should have improved stress corrosion resistance. Jones et al (29) observed that, for polyester-glass crossply laminates postcured at different temperatures, those with the least thermal strain and hence highest transverse ply failure strain, showed the best stress corrosion resistance.

A preliminary study of the chemical aspects of acidic stress corrosion of polyester-glass laminates was carried out by Bailey, Fryer and Jones (30), who attempted to correlate laminate damage with the concentration of calcium, aluminium and sodium glass degradation products in the corrodent. They observed that the exposed glass at the cut edges of the transverse ply was attacked rapidly. The low calcium ion concentration in the corrodent led them to postulate that an insoluble calcium polyester soap could be formed

within the matrix resin. However whether this played any part in the stress corrosion process was not discussed.

From their studies of the fracture surfaces of stress corroded hoop and angle wound polyester-glass pipes, Hogg and Hull (27) identified three main morphological features.

1. Stress corrosion nucleation regions, where extremely planar fracture had occurred. Individual glass fibres had very smooth featureless fracture surfaces.
2. Stress corroded regions, where the fracture surface was less planar and the glass fibres had typical river line markings.
3. Small cliffs in the fracture surface. The number and height of these increased away from the crack nucleation regions.

Similar features have also been observed in the fracture surfaces of polyester-glass coupons tested in bend and tension (31), and appear to be common to all stress corroded GRP.

Kelly and McCartney (32,33) have used a bundle theory to predict the stress corrosion failure of non-impregnated E-glass strands. By assuming that the flaw distribution in the fibres could be described by a 2 parameter Weibull function, equation 1.1;

$$N = N_o \exp\{-(\sigma/\sigma_o)^m\} \qquad \ldots(1.1)$$

Where:-

N_o = Number of fibres in a large bundle.

N = Number of fibres surviving

σ = The stress in each fibre.

σ_o = The scale parameter, a constant for the material.

m = The shape parameter, a constant for the material.

and that their growth rate is dependent upon the stress intensity, as described by equation 1.2:

$$\frac{\delta a}{\delta t} = \alpha K_1^n \qquad \ldots(1.2)$$

Where:-

$\frac{\delta a}{\delta t}$ = Flaw growth rate.

a = Flaw length.

K_1 = Stress intensity.

α, n = Material constants.

they were able to calculate the failure times of unimpregnated bundles. Aveston, Kelly, McCartney and Sillwood (11) found good agreement between the predicted and experimental failure times, for stressed fibre bundles in water. However in order to predict the stress corrosion failure of laminates the theory requires considerable modification, because it makes no allowance for the properties of the matrix, and assumes that all the fibres in the bundle experience a similar environment. Thus at times to failure of less than

10^4 minutes they found that unimpregnated bundles failed first, whereas at times greater than 10^4 minutes failure occurred within similar times, from which they concluded that the water had completely penetrated the resin. The brushlike and planar fracture surfaces of unimpregnated and impregnated bundles respectively, were explained in terms of a short transfer length and the exponent n in equation 1.2. Thus for a hexagonal array of coupled fibres, the failure of a single fibre places an additional load of 1/6 onto its nearest neighbours. The value of n for E-glass in water is approximately 15, hence from equation 1.2 this will result in a 10 fold increase in the flaw growth rate. If the transfer length is short then this will be localised in the plane of the original fracture, and there will be a greater probability for a flaw in this region to propagate. An alternative mechanism for the planar fractures has been proposed by Hogg and Hull (25,26), in which the stress corrosion of the glass is limited to that exposed at the crack tip, as shown diagrammatically in Figure 1.4 for the growth of a stress corrosion crack in a brittle matrix resin. The main difference between the two theories is the localisation of the chemical attack upon the glass. In the former a general attack occurs on all the glass in the laminate, whereas in the latter it is limited to the vicinity of a crack.

Improved wet strength of glass reinforced composites is normally achieved by careful choice of an adhesion promotor, called a coupling agent. It is beyond the scope of this survey to review the adhesive mechanisms by which coupling agents are thought to work, and for further information the reviews of Plueddemann (34) and Ishida and Koenig (35) are recommended. The influence of coupling agents on the acidic stress corrosion properties of glass reinforced composites has not yet been studied.

1.3 THE STRESS CORROSION OF GLASS

The time dependent failure of glass has been studied since the end of the last century. The realization that the mechanism was a stress assisted chemical process, has resulted in it being termed stress corrosion. Many of the current ideas on the nature of this process originate from the work of Charles (36,37), who studied the corrosion and static fatigue of soda-lime glass, in water and steam. The activation energies for the stages involved, suggested that the diffusion of sodium ions within the glass, was rate determining, and that static fatigue was a stress assisted corrosion phenomenon. Previously Taylor (38) had also noted similarity between the activation energies of static fatigue and the diffusion of sodium ions in glass. Charles's theory may be divided into two parts. The first describes the chemical mechanism responsible for the corrosion. Thus hydrolysis of sodium silicate produces hydroxyl ions according to the reaction shown in Stage 1 below. These then react with the silica network as shown in Stage 2.

$$\text{-Si-O-Na} + H_2O \rightarrow \text{-SiOH} + Na^+ + OH^- \qquad \ldots(1)$$

$$\text{-Si-O-Si-} + OH^- \rightarrow \text{-SiOH} + \text{-SiO}^- \qquad \ldots(2)$$

$$\text{-SiO}^- + H_2O \rightarrow \text{-SiOH} + OH^- \qquad \ldots(3)$$

Reaction of the SiO^- group with water results in the regeneration of a hydroxyl ion (Stage 3) making the process autocatalytic. However the hydroxyl ion concentration does not increase indefinitely but stabilizes at a limiting pH, which is controlled by the acidity constant for silicic acid. He also observed that freshly drawn glass rods corroded faster than

those that had been annealed, and postulated that this was a result of a decrease in the Na^+ diffusion rate in the higher density glass. He suggested that a large triaxial stress would cause a rarefaction of the glass, with a subsequent increase in the rate of Na^+ diffusion. The most likely location for large triaxial stresses is at a crack tip where stress intensification occurs. Thus the glass will corrode fastest at this position. Uniform corrosion will blunt the crack tip and lower the stress intensity resulting in a decrease in the corrosion rate. The second part of Charles's theory deals with the preferential direction of flaw growth.

The stress concentration at the tip of an eliptical flaw orientated with its major axis normal to the applied stress is given by equation 1.3, and is proportional to the ratio of its major and minor axis.

$$\frac{\sigma_m}{\sigma_a} = \{1+(2x/y)\} \qquad \ldots(1.3)$$

Where:-

$\frac{\sigma_m}{\sigma_a}$ = Stress concentration.

x = Major axis.

y = Minor axis.

For failure at low applied stresses, the stress concentration at pre-existing flaws must be increased to a critical value.If the ratio of the flaw growth rates in the x and y directions is above a critical value, then the flaw is sharpened and unstable crack growth will occur. If it is below the

critical value the crack is blunted and an increase in the original strength is observed, as in the case of HF etching. This theory of flaw growth is applicable to any brittle solid and has been further developed by Hillig and Charles (39), and Weiderhorn, Fuller and Thomson (40) to predict the rate of growth of flaws from the activation and diffusion parameters for the chemical reactions, and geometry of the crack tip.

Mould and Southwick (41) investigated the effect of various mechanical surface treatments on the static fatigue of soda-lime glass in water. They found that their results could be represented by a Universal Fatigue Curve, providing the applied stress was normalized by dividing it by the instantaneous strength of the glass, which was obtained from the fracture strength at liquid nitrogen temperatures when static fatigue was believed to be absent. However, McKinnis (42) later reported that static fatigue was possible at liquid nitrogen temperatures. Nevertheless the Universal Fatigue Curve showed that a static fatigue limit existed. This has been confirmed by Weiderhorn et al (23) from crack velocity measurements. However a stress corrosion limit has not been observed for aluminosilicate (E-glass) or silica glass. Mould and Southwick (41) also compared their results with several theoretical models and concluded that Charles' theory gave the best fit to the experimental data, but it did not explain the whole curve. Subsequently Hillig and Charles (39) showed that their theory of stress corrosion could adequately explain the result of Mould and Southwick.

Metcalfe and Schmitz (12) do not agree that it is the growth of pre-existing flaws causes the failure of glass fibres. They claim that

the high strength of glass fibres indicates a flaw size of only a few atomic diameters, and that the Griffith type of flaw could not exist. Instead they believe that the flaws are generated by a tensile stress in the surface of the fibre, caused by an exchange of Na^+ for H^+ in the environment. Since the H^+ is smaller than the Na^+, a tensile stress is generated because the shrinkage of the fibre sheath is constrained by the unaffected core. This is in contrast to previous ion exchange theories where it has been assumed that the hydrogen ions in solution are always associated with water molecules, and water molecules thus brought into the surface of the glass will cause a swelling of the glass surface. Metcalfe et al (44) supported their mechanism with observations that unstressed fibres immersed in aqueous acids develop sheath core structures. The sheath may then spontaneously fracture by either multiple or spiral cracking. The development of a sheath core structure was also observed by Charles (36), for glass rods corroded in superheated steam, however the sheath occupied a greater volume than the original glass. Also Barker and Bott(45)have observed the formation of a surface layer in fibres immersed in aqueous acid and water. The ion exchange mechanism of Metcalfe et al cannot totally account for the observed strength retention in a HCl/NaCl solution, nor the strength recovery, which occurs on subsequently immersing the fibres in aqueous NaOH. The recovered strength was less than expected indicating that the mechanism was only partially reversible. The stress corrosion activation energy was similar to that obtained by Charles, which they interpreted as indicating that the rate controlling factor was the diffusion of the Na^+. E-glass is found to suffer a lower reduction of strength in alkali environments. This can be understood in terms of ion exchange, but

not in terms of Charles's mechanism.

Weyl (46) suggested that the interaction between the environment and the -Si-O- bonds under stress at the crack tip was responsible for subcritical crack growth. He postulated that a direct reaction between a molecule of the type ROH, where R is H, CH_3 etc, and the siloxanol groups in the silica network, according to the following equation, could occur.

$$-\overset{|}{\underset{|}{Si}}-O-\overset{|}{\underset{|}{Si}}- + ROH \rightarrow -\overset{|}{\underset{|}{Si}}-OR + -\overset{|}{\underset{|}{Si}}-OH$$

This type of reaction was rejected by Charles because of the lack of reactivity between silica and water. Hammond and Ravitz (47) measured the fracture strength of silica glass in various polar and non-polar liquids, and found limited correlation with the calculated lowering of the surface free energies. They used the value of surface free energy of quartz instead of that of silica glass, and this could account for some of the discrepancies. However ethanol, which is known to reduce the surface free energy of glasses did not cause premature failure. Therefore stress corrosion cannot be explained simply by changes in surface free energy.

Michalske and Freiman (48) have also discussed the stress corrosion in terms of reactions between the environment and the chemical bonds under stress at the crack tip. They believe that the size and the charge distribution of the attacking molecule are critical. That is, the molecule must be capable of forming a transition state with the -Si-O bonds, in which case the distance between the reacting centres must be close to that of the

-Si-O bond length of ≈ 1.63 Å. It must also possess a proton donating group at one end and an electron donor, such as lone pair electrons, at the other. They support their hypothesis with crack velocity measurements in various environments. They found that ammonia with its similar structure to water also had the same effect in increasing the crack velocity. Molecules of a different size or charge distribution were much less effective.

McKinnis (42) described stress corrosion as a consequence of a disperse phase in the glass, which he preliminary identified as crystobalite. Using a finite element analysis he calculated that a tensile stress existed across the interface with the dispersed phase. A reaction of the stressed bonds in the dispersed phase at the surface of the glass, with water was responsible for the formation of Griffith type flaws. He also postulated that water vapour could be more reactive than liquid water. This had also been noted by Charles, who explained it as a result of the greater concentration of alkaline corrosion products on the surface of the glass, producing an auto-catalytic effect on the rate of corrosion. This has also been observed by other workers (43,49).

It is expected that corrosion and stress corrosion of glass occurs simultaneously. Barker et al (21) observed that aqueous HCl and H_2SO_4 removed both calcium and aluminium ions from E-glass fibres. This may account for the irreversibility of the ion exchange mechanism proposed by Metcalfe et al (12). Furthermore El Shamy et al (50) have shown that the removal of calcium ions is dependent upon the composition of the glass and is not found for soda-lime glasses, and may explain the greater corrosion

resistance of this glass to acids. The solubility of silica decreases with increasing acid concentration, however Elmer and Nordberg (51) observed that for short time periods (less than 40 hours) the rate of dissolution of silica in nitric acid occurred fastest in acid of 0.8 M concentration. Their results show a similarity with those for the strength of E-glass strands and GRP, as a function of acid concentration (7,24,25). This suggests that a similar mechanism of dissolution of silica may be operating in both instances.

1.4 THE DIFFUSION OF AQUEOUS MEDIA INTO MATRIX RESINS AND GRP

One of the main functions of the matrix resin in a composite, is to provide chemical protection for the glass reinforcement. Unfortunately the diffusion coefficients for both liquids and gases in polymeric materials are large. Also there is a tendency for the permeating species, to interact with the polymer molecules for example, hydrogen bonding. Thus the absorption of water may cause any of the following (52).

1. An increase in the thermal expansion coefficient.
2. Lowering of the glass transition temperature.
3. Swelling of the resin.
4. A change in mechanical properties.

In most cases moisture absorption does not continue indefinitely, but reaches a limiting saturation or equilibrium value which is dependent upon the temperature and the relative humidity (53). Adamson (54) suggested that absorbed water could either occupy the free volume of the polymer, and be relatively free to move around, or be bound by hydrogen bonding, resulting in swelling of the polymer.

There is some evidence for the view that epoxy resins are not homogeneous single phase structures. Cuthrell (55) observed a two phase structure in several cured epoxy resin systems. For example the benzyldimethyamine cured bisphenol "A" system was reported to have a structure consisting of denser flocules of 20 - 90 μm diameter, in a matrix that "resembled the starting materials". The size of the flocules was found to be inversely proportional

to the curing temperature. Kenyon and Neilson (56) have also reported a two phase structure in several amine cured epoxy resin systems. However the size of the disperse phase were a magnitude smaller than those observed by Cuthrell. Adamson (54) has suggested that the slow filling of the disperse phase, which has a lower diffusion coefficient, is responsible for the slow approach to moisture equilibrium, shown by the resin .

The diffusion of water into epoxy resins is often described as Fickian, however interactions between the permeant and the polymer will result in non-Fickian behaviour. Fickian diffusion describes the concentration of the diffusant during absorption, by considering a non-stationary state of flow as described by equation 1.4 (57).

$$\frac{\delta C}{\delta t} = DS \frac{\delta^2 C}{\delta x^2} \qquad \ldots(1.4)$$

Where:-

$\frac{\delta C}{\delta t}$ = Change in concentration gradient with time.

$\frac{\delta^2 C}{\delta x^2}$ = Change in concentration gradient with distance x perpendicular to the cross section.

D = Diffusion coefficient.

S = Cross sectional area.

For a plane plate, immersed in a liquid, the quantity absorbed with time is given by equation 1.5 (58). Providing a steady surface equilibrium is immediately established.

$$\frac{M_t}{M_\infty} = \frac{4}{\pi^{\frac{1}{2}}} \left(\frac{Dt}{L^2} \right)^{\frac{1}{2}} \qquad \ldots(1.5)$$

Where:-

M_∞ = Wt absorbed at equilibrium.

M_t = Wt absorbed at time t.

L = Thickness of the plate.

D = Diffusion coefficient.

If the diffusion is Fickian then a plot of the weight of diffusant against the square root of time will be linear until approximately 60% of the equilibrium value has been absorbed, then it will curve over towards this value.

The effectiveness of gel coats as barriers to the diffusion of moisture has been questioned by Menges and Gitschner (53). They calculated (assuming Fickian diffusion) that a 3 mm thick gel coat would be penetrated within three months. Very little work has been carried out on the diffusion of solutes from aqueous solutions. However the work of Ashbee et al (59,60) on osmosis in polyester and epoxy resins suggests that diffusion rates are very much lower than that of water.

The sorption behaviour of composites is primarily dependent upon that of the matrix resin, although the glass resin interface may introduce complications. Dewimille et al (9,10) measured the diffusion of water into pultruded epoxy-glass rod. They found that up to 65^{o}C the diffusion was Fickian, and was approximately 3 times greater parallel to the fibres than

normal to them. Above 65°C the diffusion of water into both pure resin and its composite was non-Fickian, which suggested that the glass resin interface was not responsible for the change in behaviour. Regester (61) studied the effect of hydrostatic pressure on the permeation rate of water through a polyester-glass composite. From the lack of an effect he concluded that diffusion through the resin occurred, rather than transport along the glass matrix interface. In similar experiments using aqueous acids, only water was found to pass through the laminate. X-ray fluorescence spectrometry of laminates immersed in sulphuric and hydrochloric acids revealed that the chlorine ion penetrated considerably further than the sulphate ion. He postulated that a corrosion resistant layer might be formed in aqueous sulphuric acid. Collins (17) using an electron probe X-ray microanalysis, also observed that penetration of sulphuric acid into polyester-glass laminates was limited to the surface layer. Marshall et al (58,62), using a radio tracer technique employing tritium enriched water, determined the rates of diffusion of aqueous hydrochloric acid and water, into vinylester-glass fibre composites. They observed only small differences, and concluded that reaction of the aqueous acid with the glass, resulted in an immobilisation of the hydrogen ions which leads to a low diffusion coefficient being observed. In laminates, where the surface was damaged they found that diffusion could be up to 20 times greater in this region. This was attributed to an increased diffusion coefficient under the influence of a localised stress concentration.

The effect of a stress upon the diffusion rate has been reported by Hahn and Kim (63). They observed that the rates of absorption and desorption of water by an epoxy-graphite laminate were different. They attributed this

to the stress state at the outer surface. When water is absorbed, the resin swells and thus a compressive stress exists in the laminate surface, whereas upon desorption, resin shrinkage produces a tensile stress in the surface. Gillat and Broutman (64) observed that externally applied stresses increased the diffusion of water into an epoxy graphite crossply laminate, and that up to a critical combination of the external stress and the absorbed moisture, the diffusion could be described as Fickian. However above the critical limit, the rate of diffusion rapidly increased, which they attributed to microcracking of the transverse plies. Whitney and Browning (65) also observed an initial Fickian process,followed by non-Fickian uptake of water into both, an epoxy-graphite composite and the matrix resin. They attributed this to microcracking of the resin, rather than any fibre matrix debonding effect.

Theoretically it has been found difficult to predict the diffusion behaviour of laminates, and hence Fickian diffusion has usually been assumed. However as discussed above and in the next section, diffusion of moisture can generate internal stresses which may then modify the diffusion characteristics of the composite.

1.5 THE GENERATION OF INTERNAL STRESSES IN GRP LAMINATES

The mechanisms by which internal stresses in lamina and laminates are produced, is reviewed, because they are as equally effective as those externally applied in promoting stress corrosion failure.

In a lamina, internal stresses are the result of differences between the physical properties of the matrix and the glass reinforcement. For example, a difference in the thermal expansion coefficients, will result in an internal stress on cooling from an elevated curing temperature. Hull (66) calculated the strain parallel to the glass fibres, on cooling a unidirectional polyester from a cure temperature of 120^{o}C, is 1.5%. However the calculation of the stress is more difficult since it requires a knowledge of the viscoelastic response of the resin at elevated temperatures. The computation of the strain at 90^{o}C (normal) to the reinforcement is also difficult, because it is strongly dependent upon the volume fraction of glass fibre. At fibre volume fractions of less than 50%, the resin is the continuous phase, and because of its higher thermal expansion coefficient, will contract onto the glass fibres. Thus a compressive strain will exist in the resin. At volume fractions of glass greater than 50%, the resin may no longer be considered as the continuous phase, and isolated resin pockets will try to shrink away from the surrounding glass. Providing the resin-glass interface does not fail, the resin will be held in a state of tension (67). If the lamina does not possess a uniform distribution of glass fibres, both high and low volume fraction regions will exist, with the resin either in tension or compression.

In laminates, the thermal strains can also be generated by the mismatch in thermal expansion coefficients of the individual lamina. Schapery (68) derived the following equations to predict the expansion coefficients, for a unidirectional lamina, parallel α_ℓ and normal α_t to the direction of reinforcement.

$$\alpha_\ell = \frac{E_f \alpha_f V_f + E_m \alpha_m V_m}{E_f V_f + E_m V_m} \qquad \ldots(1.6)$$

$$\alpha_t = (1 + \nu_m)\alpha_m V_m + (1 + \nu_f)\alpha_f V_f - \alpha_\ell (\nu_f V_f + \nu_m V_m) \qquad \ldots(1.7)$$

Where:-

E_f = Modulus of the fibres.

E_m = Modulus of the matrix.

α_f = Expansion coefficient of the fibres.

α_m = Expansion coefficient of the matrix.

ν_f = Poisson ratio of the fibres.

ν_m = Poisson ratio of the matrix.

V_f = Volume fraction of fibres.

V_m = Volume fraction of matrix.

The computed expansion coefficients are shown as a function of volume fraction of glass in Figure 1.5. Thus at high volume fractions α_ℓ is dominated by that of the glass and at low volume fractions, α_t by that of the matrix, and the interaction of variously orientated lamina will lead to internal stresses. Parvizi (69) derived equations 4.1 and 4.2 (shown in Section 4.2) for $0^o/90^o/0^o$ crossply laminates.

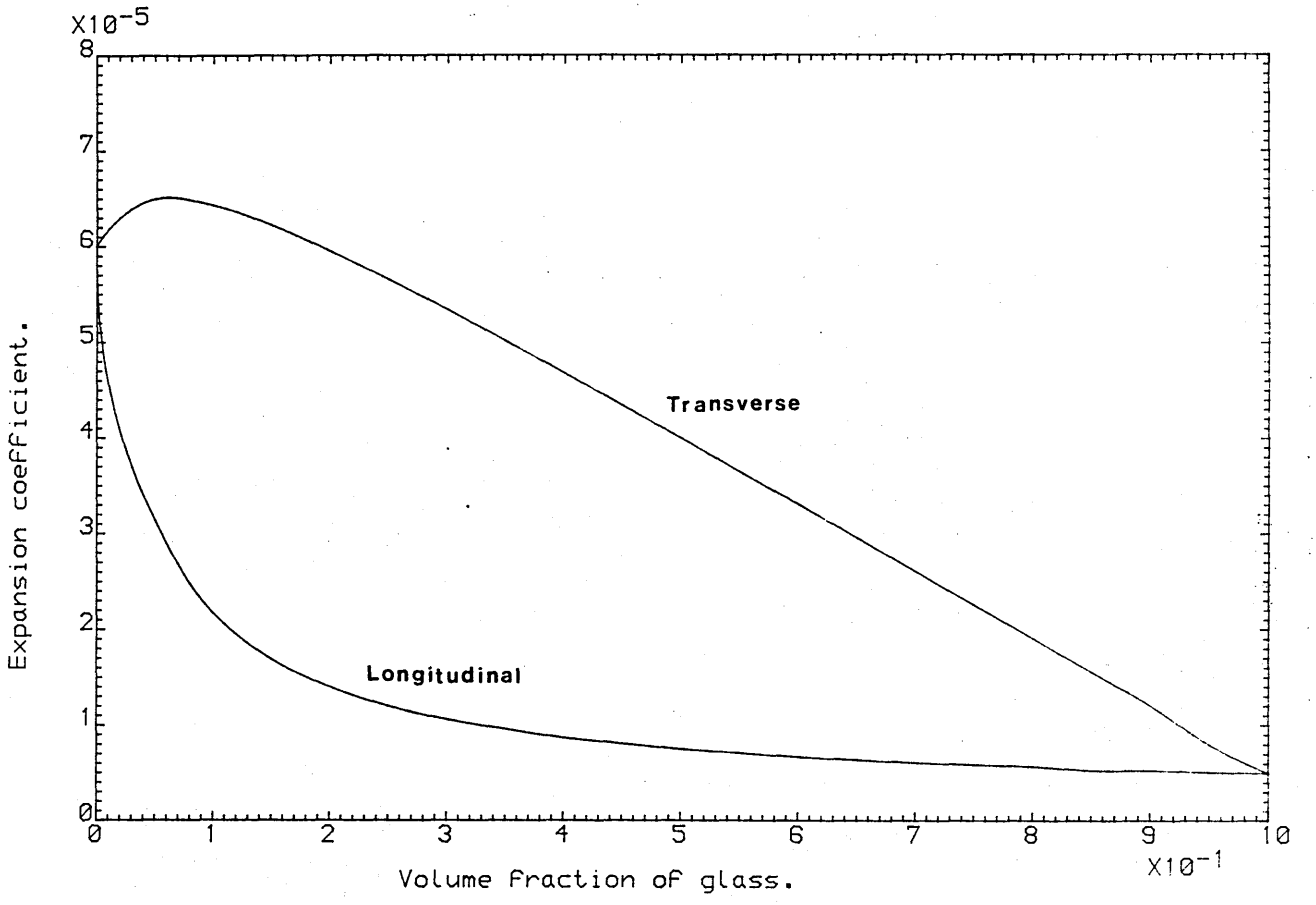

Figure 1.6 Variation in the transverse and longitudinal expansion coefficient of a unidirectional lamina with volume fraction of glass. Calculated using equations 1.2 and 1.3 and the data shown in Table 4.1.

The absorption of a liquid will also generate internal stresses, since swelling can be likened to the thermal expansion or contraction of the matrix. However the stresses may result from two different mechanisms. If diffusion has reached stationary conditions, they will be generated in an analogous manner to the thermal stresses. Menges and Gitschner (53) postulated that in a unidirectional lamina with a uniform glass distribution, swelling strains sufficient to cause microcracking can be formed. This is because the magnitude of the swelling coefficient in the transverse direction of a lamina, is also dependent upon the volume fraction of glass. They argue that as it is still possible to define resin and glass rich regions, then the interaction of the different swelling strains generated in these regions, will result in the production of internal stresses. In laminates, the interaction between variously orientated lamina will generate swelling stresses in a similar manner to the generation of thermal stresses. The longitudinal S_ℓ and transverse S_t swelling coefficients of a lamina may be calculated by replacing α_f and α_m with the appropriate swelling coefficients, in equations 1.6 and 1.7. These are then used to calculate the swelling strains, for example by equations 4.1 and 4.2. Since these strains are of opposite sign to thermal strains the latter will be relieved when moisture absorption takes place. If diffusion has not attained steady state conditions, then stresses will result due to the concentration profile of the diffusing species. These may be of sufficient magnitude to cause fracture in plastics, see for instance reference 70. On absorption the outer surface is placed in compression due to the swelling being constrained by the inner unswollen resin, which itself is placed under tension. Similarly upon desorption the outer surface is placed in tension whilst the inner portion is placed under compression. Menges and Gitschner (53) have

calculated that the tensile forces that arise in matrix resins during the desorption of water, are sufficient to cause microcracking.

Localised internal stresses may arise from osmotic pressure pockets. Ashbee et al (59,60) doped polyester and epoxy resin with potassium chloride, and found that penny shaped cavities with sufficient pressure to cause microcracking of the resin, resulted from the absorption of water. From studies on short fibre reinforced epoxy-glass composites, they observed that pressure pockets which formed at the fibre matrix interface, destroyed interfacial load transfer (71). In further studies (72) they observed the effects of freezing and boiling this phase separated water. Whereas freezing could induce microcracking of the resin, boiling did not. They explained this in terms of resin flow at the higher temperature, accomodating the internal stresses.

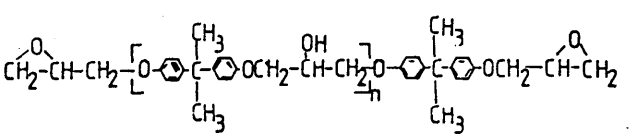

(a)

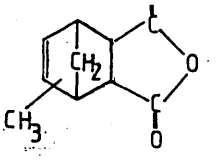

(b)

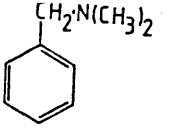

(c)

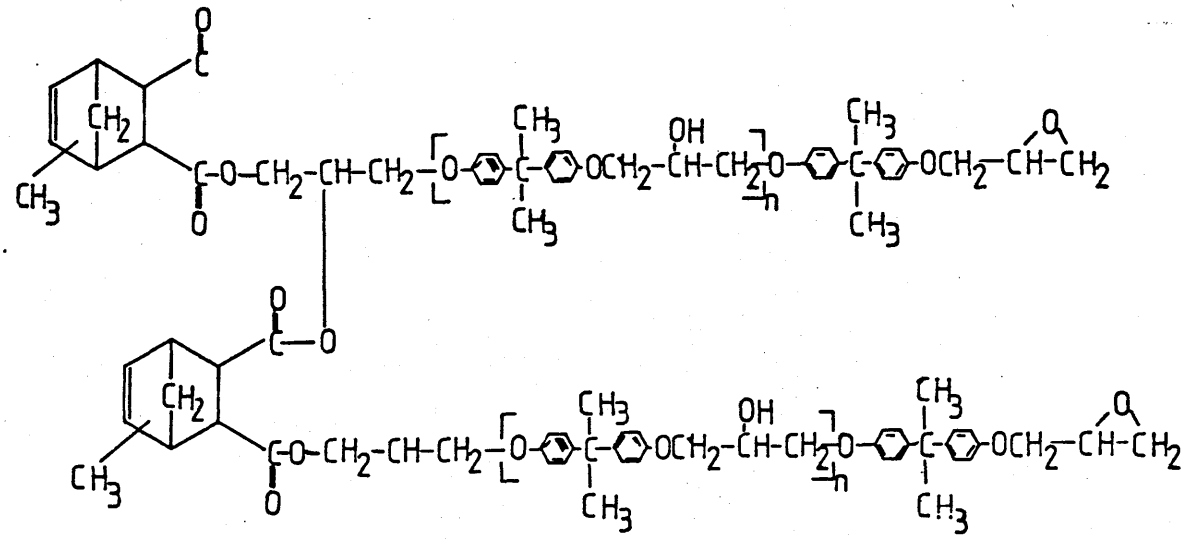

(d)

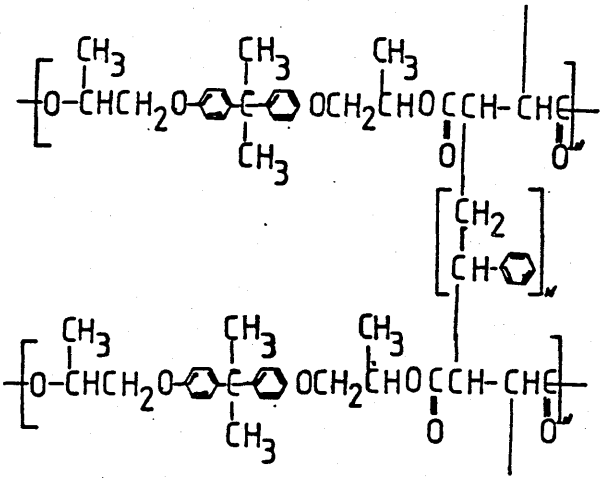

(e)

Figure 1.7 Molecular structures of (a) diglycidyl ether of diphenylolpropane, (b) nadic methyl anhydride (NMA), (c) benzyldimethylamine (BDMA), (d) anhydride cured bisphenol-A epoxy resin, (e) cured bisphenol-A polyester resin.

1.6. CHOICE OF THE COMPOSITE SYSTEM

As discussed in Section 1.2, much of the previous work on the stress corrosion cracking of GRP, has been carried out on glass polyester laminates, and in particular on filament wound pipes. Those studies in which pipe sections have not been used, have often involved composites containing glass fibres in the form of chopped strand matt. Whilst filament winding produces good test specimens, the non-linear strain fields associated with these structures, makes the comparison and interpretation of results rather difficult. The use of chopped strand matt as a reinforcement was considered undesirable since by the very nature of the material, uncontrollable orientation effects would be introduced. Therefore, it was decided to use 0^{o} unidirectional and $0^{o}/90^{o}/0^{o}$ crossply laminates. The former could be used to model a theoretical lamina, and the latter to assess the effects of thermal strains, and transverse cracking.

The matrix resin was chosen because:-

(a) The transverse cracking behaviour of epoxy-glass crossply laminates was well understood (69).

(b) Fibre matrix debonding of the 90^{o} ply had been observed at applied strains of less than that for transverse cracking. Thus the effect of debonding on the mechanism of stress corrosion could be studied.

(c) The anhydride cured bisphenol "A" epoxy resin has a crosslinked structure similar to chemical resistant bisphenol "A" polyester resins. A comparison of these molecular structures is shown in Figure 1.5, together with those of the epoxy system constituents.

CHAPTER 2 EXPERIMENTAL PROCEDURE

2.1 MATERIALS

The glass fibre used in this study, was Silenka 051P E-glass roving of 1200 tex. The roving is made up of four, one thousand filament strands, each filament being approximately 12 μm in diameter. It is finished with a polyester/epoxy compatible size.

The resin formulation was Epikote 828 (diglycidyl ether of diphenylol-propane, of epoxide equivalent 182 - 194) cured with either 80 phr or 90 phr Epikure NMA (Methylendomethylenetetrahydrophthalic anhydride) and catalysed with 1.5 phr BDMA (Benzyldimethylamine). All were obtained from Shell Chemicals Ltd. The chemical structures are shown in Figure 1.6.

2.2 LAMINATE FABRICATION

2.2.1 Frame Winding

The laminates were fabricated on 400 mm square steel frames, which were made from 25.4 x 5.5 mm strips of steel plate, spot welded together and smoothed with emery before use.

Initially the frames were hand wound, but difficulties in maintaining an even glass distribution, lead to the modification and use of a pre-existing winding machine. Using the improved resin impregnation technique described in section 2.2.2, it was no longer necessary to stack individual resin-impregnated, unidirectional laminae together, to fabricate a $0^{o}/90^{o}/0^{o}$ crossply laminate, as described in reference 69. They could be obtained in one stage by the technique illustrated in Figure 2.1. Thus consistent laminates with a uniform distribution of glass fibres could be fabricated.

The ply thicknesses of the $0^{o}/90^{o}/0^{o}$ crossply laminates could be varied by changing the number of layers of glass fibres. For laminates of approximately 2.2 mm thickness, eight layers of glass rovings were used.

2.2.2 Vacuum Impregnation

It was necessary to construct the vacuum chamber illustrated in Figure 2.2, to accomodate the size of the steel frames. For clarity, the impregnation technique has been itemised below, and shown diagrammatically in Figure 2.3.

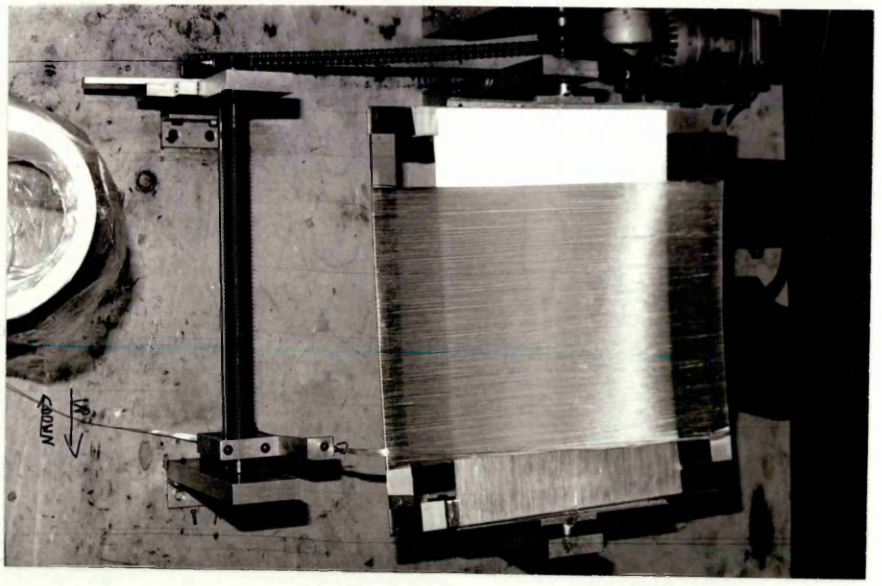

Figure 2.1 $0^{o}/90^{o}/0^{o}$ crossply laminate being wound on the frame winding machine.

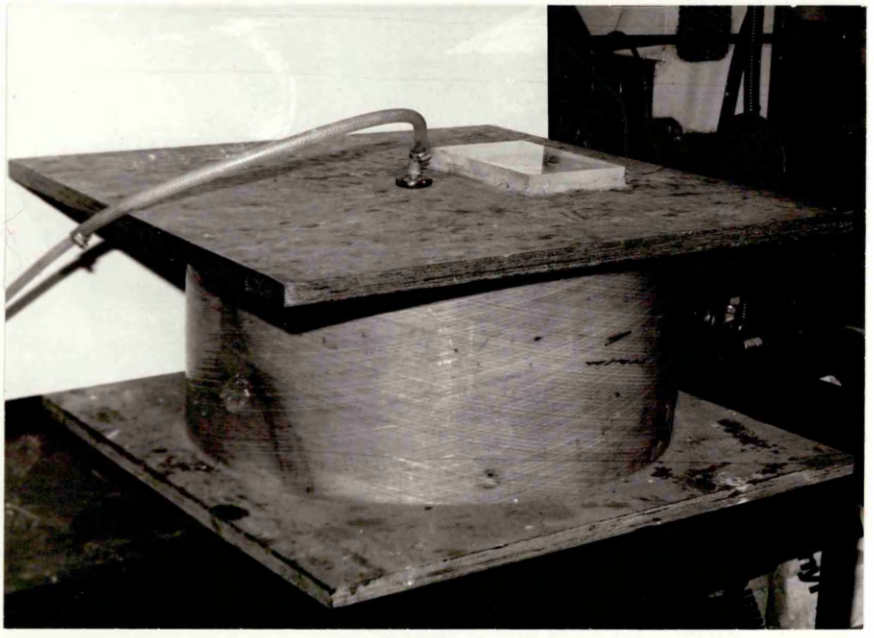

Figure 2.2 Vacuum impregnation chamber.

Stage 1 The resin was degassed under vacuum.

Stage 2 The resin was frozen by pouring it onto a "Melinex" covered precooled (-18°C) metal plate.

Stage 3 A preheated metal plate (+100°C) covered with "Melinex" was placed into the vacuum chamber.

Stage 4 When the resin is frozen, the following were stacked on top of the preheated plate, as shown in Figure 2.3.

(a) Wound frame.

(b) Inverted "Melinex" with the adhered frozen resin.

(c) Glass plate.

(d) 2.5 kg weight.

Stage 5 The chamber was closed and evacuated.

For good laminates it was essential that the resin remained frozen during evacuation, so that stages 4 and 5 were carried out as quickly as possible. The impregnation could be observed through the perspex window and was usually complete after about 30 minutes. It was found that cured resin adhered to the "Melinex", so that it was replaced with a silicone treated "Melinex" before curing the laminate.

2.2.3 Curing and coupon preparation

Initial curing of the laminates was for 3 hours at 100°C. This was carried out in an air circulating oven, with the laminate sandwiched between glass plates under a load of 300 kg/m^2. The loading weights were preheated because their large thermal inertia, compared to the laminate, could produce areas of delayed cure.

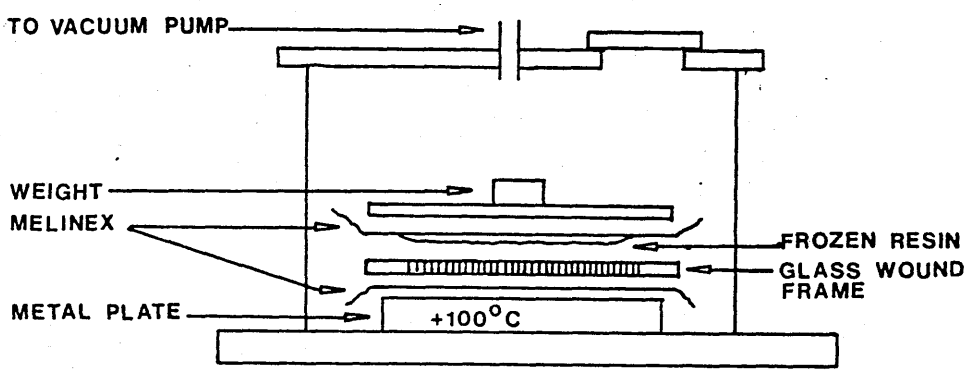

Figure 2.3 Schematic representation of the vacuum impregnation technique.

The laminate was allowed to cool outside of the oven, the release film removed, and the laminate cut from the frame and into coupons using a water cooled diamond wheel. The coupons were postcured for 3 hours at 150°C, except for coupons from laminates made with 90 phr NMA which were postcured for 24 hours at 200°C. All the coupons were removed from the oven whilst hot and allowed to cool.

Finally, the ends of the coupons were abraded and chromic acid-etched aluminium-end-tags were attached using "Araldite" cold setting adhesive. The coupons were then stored under conditions of constant temperature and humidity (20°C, 50% RH.).

2.3 LAMINATE CHARACTERIZATION

2.3.1 Tensile Measurements

Coupons that were intended for tensile characterization had a polyester film resistance strain gauge, PL 10, obtained from Tokyo Sokki Kenyuso Co. Ltd. bonded to them using "Araldite" cold setting adhesive. They were tested on an Instron Universal testing machine, Model 1195, at a constant displacement of 1 mm min^{-1}. Complete stress/strain curves were recorded for each laminate.

The transverse cracking behaviour of the crossply laminates was recorded photographically at 0.1% increments of strain.

2.3.2 Volume Fraction Measurements

Initially these were obtained using the "burn-off" method, but since the volume fraction of voids was found to be extremely low, the volume fraction of glass was deduced from the laminate thickness.

(a) Burn-Off Method

Preweighed laminate samples (±0.0001g) with accurately known dimensions (±0.01 mm) were placed in weighed crucibles with lids, and ignited in an electric muffle furnace at 600°C. From the weight of the remaining glass the

volume fraction was determined from the following equation

$$V_f = V_g / (V_r + V_g) \qquad \ldots(2.1)$$

Where:-

V_f = Glass fibre volume fraction

V_g = Volume of residual glass (W_g / ρ_g)

V_r = Volume of resin $(W_s - W_g)/\rho_m$

W_s and W_g are the sample and glass weights respectively.

ρ_m and ρ_g are the respective densities of the resin and glass and were taken to be 1.12 $g\ cm^{-3}$ and 2.55 $g\ cm^{-3}$ (66,69).

The volume fraction of voids was determined by comparing the measured volume of the sample with its theoretical volume, obtained from the values of V_g and W_s.

(b) Volume Fraction from the thickness of the laminate

An advantage of using a winding machine is that each lamina contains the same number of parallel rovings and therefore the same volume of glass. Providing the volume fraction of voids is small, the volume of resin and hence the volume fraction of glass in the laminate will be dependent upon its thickness and can be obtained from equation 2.2.

$$\frac{K_t\ N}{L_t} = V_f \qquad \ldots(2.2)$$

Where K_t is the theoretical thickness of a glass plate of equal area and volume as a single wound layer of glass (a constant for the winding machine used), L_t is the laminate thickness in millimetres, and N is the number of layers of glass in the laminate.

The value of K_t was determined by weighing a length of glass equivalent to that contained in a single layer of unit area. Figure 2.4 shows the relationship between V_f and laminate thickness for laminates containing eight layers of glass fibre.

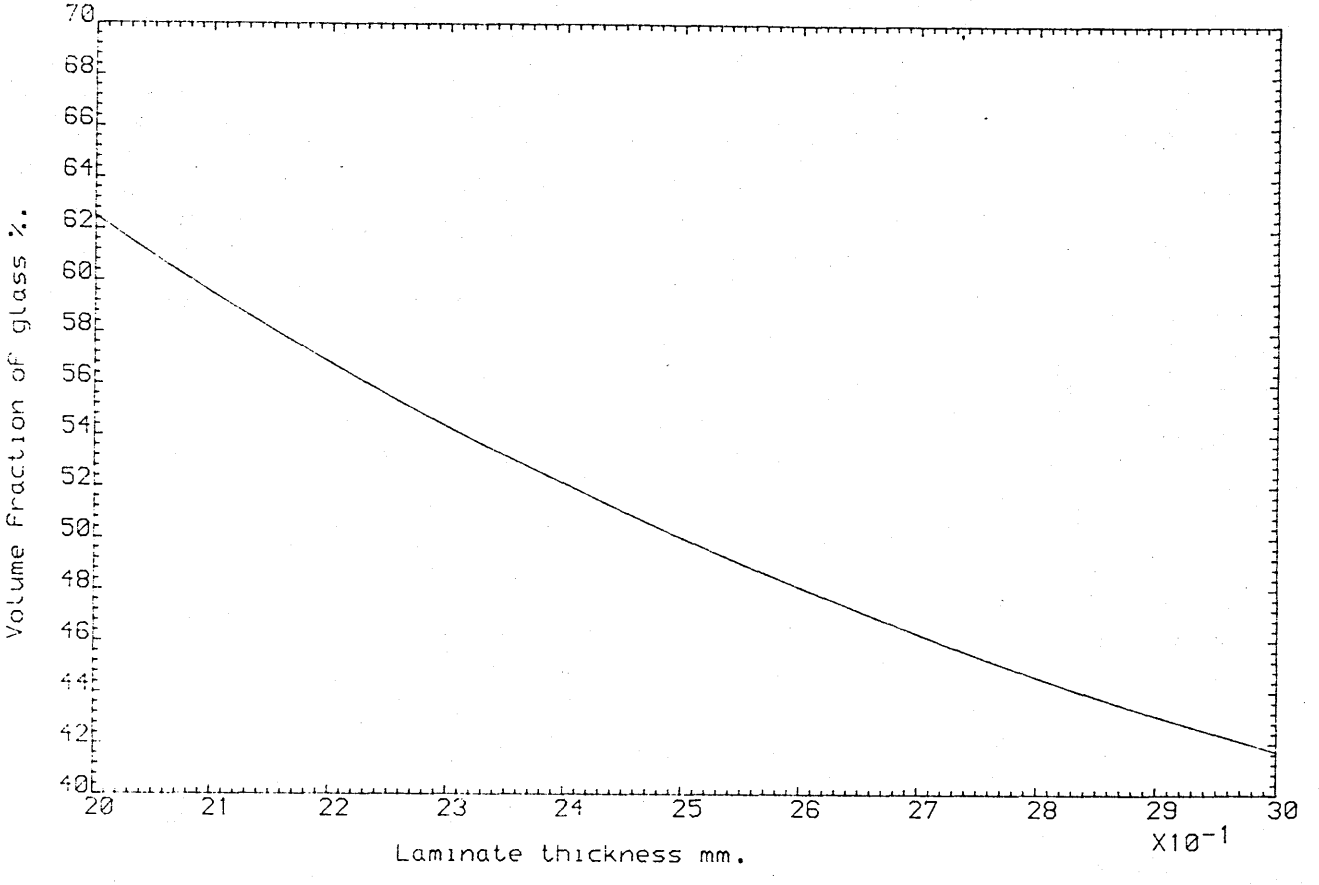

Figure 2.4 Variation in volume fraction of glass with the laminate thickness, for laminates containing eight layers of glass fibre.

2.4 STRESS CORROSION EXPERIMENTS ON LAMINATES

2.4.1 Introduction

The experiments were carried out under conditions of constant load on Emec Creep machines, Figure 2.5, using coupons of dimensions approximately 240 mm x 20 mm. The grips, Figure 2.6 were designed to minimize any misalignment, by allowing the head to freely pivot in 2 dimensions about the shaft. Three types of environmental cells were used to contain the aqueous environment (0.5 M sulphuric acid unless otherwise indicated). The load was applied to the coupons after the cells were filled with acid. The closed cell was filled by using a syringe to inject the acid into the side arm which housed the condenser. Physical changes and final failure were recorded by time lapse photography using Chinon CE4 single lens reflex cameras, fitted with power winders, electronic flash, and Pentax 50 mm macro lenses. The cameras were controlled using electronic timers that allowed a delay of between 10 seconds and 10 hours between photographs. The time of each exposure was confirmed by LCD (Liquid crystal display) digital watches attached to the grips and photographed with the coupon.

2.4.2 Open and closed environmental cells

Both types of cell were constructed from "pyrex" borosilicate glass. The open-cell, shown in Figure 2.7 consisted simply of a glass tube attached to the coupon by means of a split rubber bung, one half of which was rebated

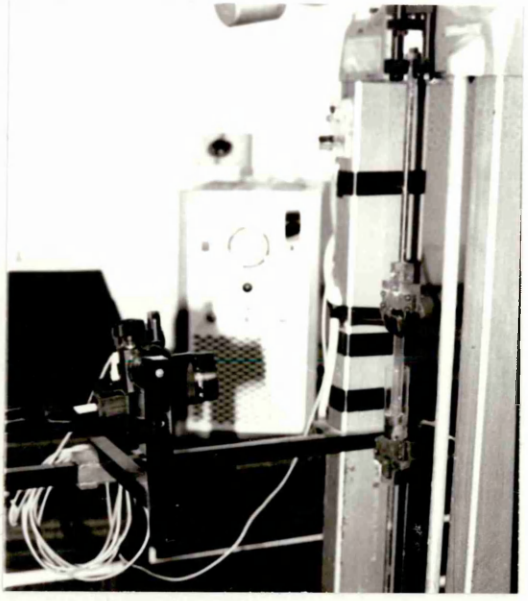

Figure 2.5 Emec Creep machine showing an open environmental cell, stress corrosion cracking experiment.

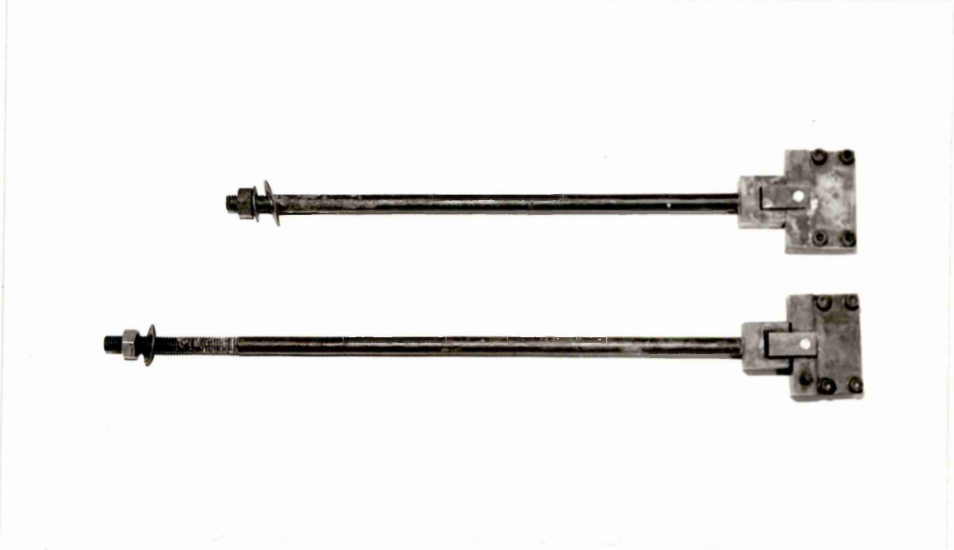

Figure 2.6 Specimen grips for use on the Emec Creep machine.

to accomodate the coupon. An acid tight seal was obtained by a smear of silicone grease, between the coupon and the rubber bung. Temperature control was not possible, but the room in which the experiments were carried out was fairly constant at 23 ± 3°C.

The closed-cell, illustrated in Figure 2.7(A) , allowed both the control of temperature, by means of circulating thermostated water from a Churchill Chiller-thermo circulator, and the atmosphere by purging with an appropriate gas. There was also a condenser to minimize loss by evaporation. The cell was affixed to the coupon in a similar manner as the open-cell, the glass cap was sealed using silicone putty.

2.4.3 Clamp-on environmental cell

To eliminate the effects of the unprotected cut-edges of the coupons, a clamp-on-cell, shown in Figure 2.8 was constructed. The cell was made from a polyethene vial cap, whose open face had been made flat using fine emery paper. The clamp was a normal laboratory rubber tube clamp. A leak proof seal between the face of the coupon was obtained with silicone grease. A 1 cm^3 syringe was used to fill the cell, when in place, through previously pierced holes, its capacity was 0.3 cm^3.

Larger glass cells were also used but necessitated the use of 40 mm wide coupons and the construction of special grips. They were affixed onto the face of the coupon using elastic bands. Problems of achieving a leak proof seal lead to the development of the polyethene clamp-on-cell.

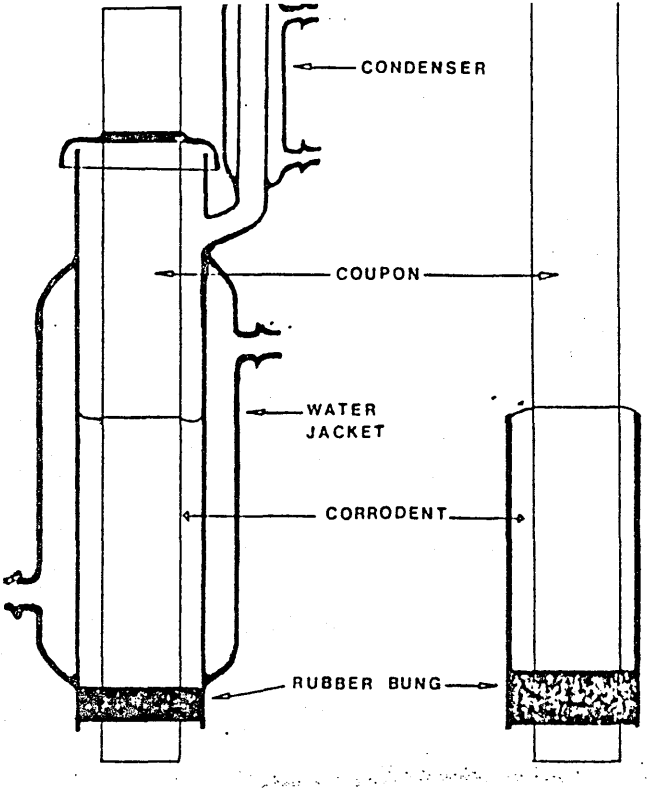

Figure 2.7 Types of environmental cell used for stress corrosion cracking experiments under constant tensile loads. (A) Closed, (B) open.

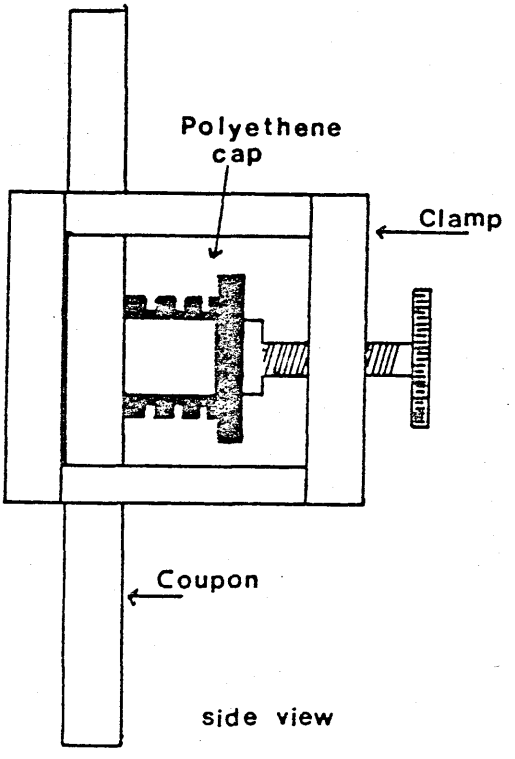

Figure 2.8 Diagrammatic representation of the clamp-on-cell in operation.

2.5 STRESS CORROSION EXPERIMENTS ON GLASS FIBRES

2.5.1 Mounting of single fibres

Individual glass fibres were separated from a Silenka 051P E-glass roving, and mounted on cardboard fibre testing windows using "Evostic" impact adhesive. Their diameters were then individually determined using forward light scattering, the technique is described in section 2.5.3. The fibre was removed from the frame and affixed to a glass rod and a cut rubber band in the manner shown in Figure 2.9. A 1 cm gauge length was chosen for testing. The rubber band formed a loop to support the glass loading weights, a small glass weight was attached to the rubber band to overcome its positive bouyancy.

2.5.2 Single fibre testing

Initially the fibres were tested individually in a small glass tank of 0.5 M aqueous acid. Their failure times were determined using a photoelectric sensor and chart recorder. As shown diagrammatically in Figure 2.9 the glass weight was positioned to stop the light beam from reaching the photoresistor, failure times could be measured to the nearest minute.

To allow eight fibres to be tested simultaneously the apparatus in Figure 2.10 was constructed. The Commodore PET Microcomputer, monitored the failure of individual fibres via eight magnetic reed switches and an input buffer; the arrangement of a single channel is shown diagrammatically

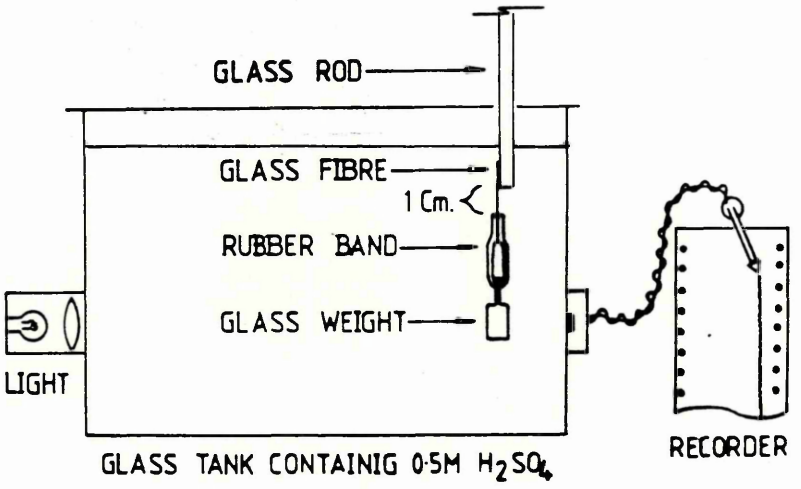

Figure 2.9 Initial experimental apparatus for the measurement of the stress corrosion of E-glass single fibres.

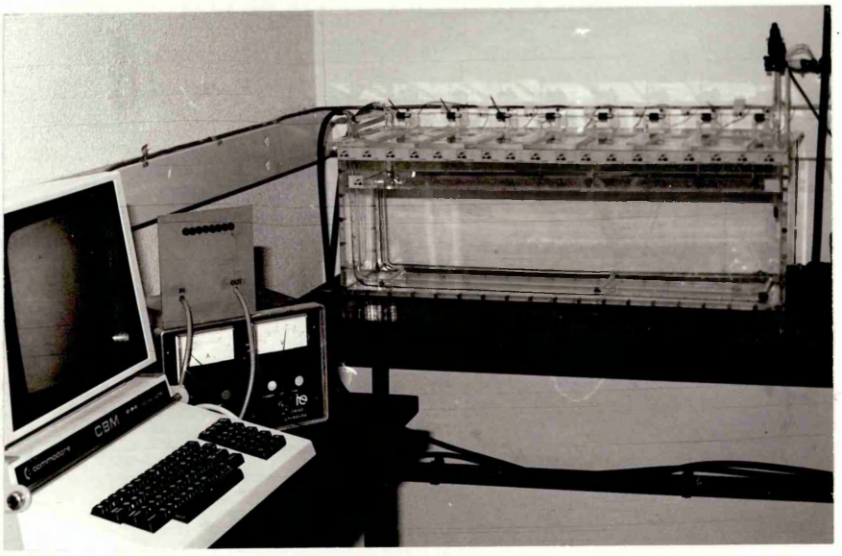

Figure 2.10 Experimental apparatus for the measurement of the stress corrosion of eight single E-glass fibres simultaneously.

in Figure 2.12. The computer programme shown as a flow diagram in Figure 2.11 was written in Basic, to give a continuous display of both the elapsed and failure times, to the nearest 0.1 min, for each of the eight channels. Temperature was controlled to $23^{o}C \pm 2^{o}$ by means of a contact thermometer and a Churchill Chiller-thermo circulator, which pumped thermostatted water through a glass spiral at the bottom of the tank.

2.5.3 Measurement of fibre diameter by forward light scattering

When a beam of coherent light is incident upon an opaque fibre, diffraction produces a pattern of alternate light and dark fringes in a plane normal to the axis of the fibre. If the fibre is transparent then interference between the reflected and refracted rays produces a similar pattern as diffraction. The fibre diameter is inversely proportional to the fringe period, and may be calculated using equation 2.3, (73).

$$N = \frac{2b}{\lambda}\left\{\left(\sin\frac{\theta_2}{2} + \left(\mu^2 + 1 - 2\mu\cos\frac{\theta_2}{2}\right)^{\frac{1}{2}}\right) - \left(\sin\frac{\theta_1}{2} + \left(\mu^2 + 1 - 2\mu\cos\frac{\theta_1}{2}\right)^{\frac{1}{2}}\right)\right\} \quad \ldots(2.3)$$

Where:-

N = Number of fringes within the included angle $\theta_2 - \theta_1$

μ = Refractive index of glass fibre

λ = Wavelength of laser radiation

b = FIBRE radius

The interference fringes were recorded on the apparatus shown in Figure 2.13. A 1 mW helium neon laser was used as the source of coherent light. The photo-transistor was attached to the X axis of a Bryant A3 chart

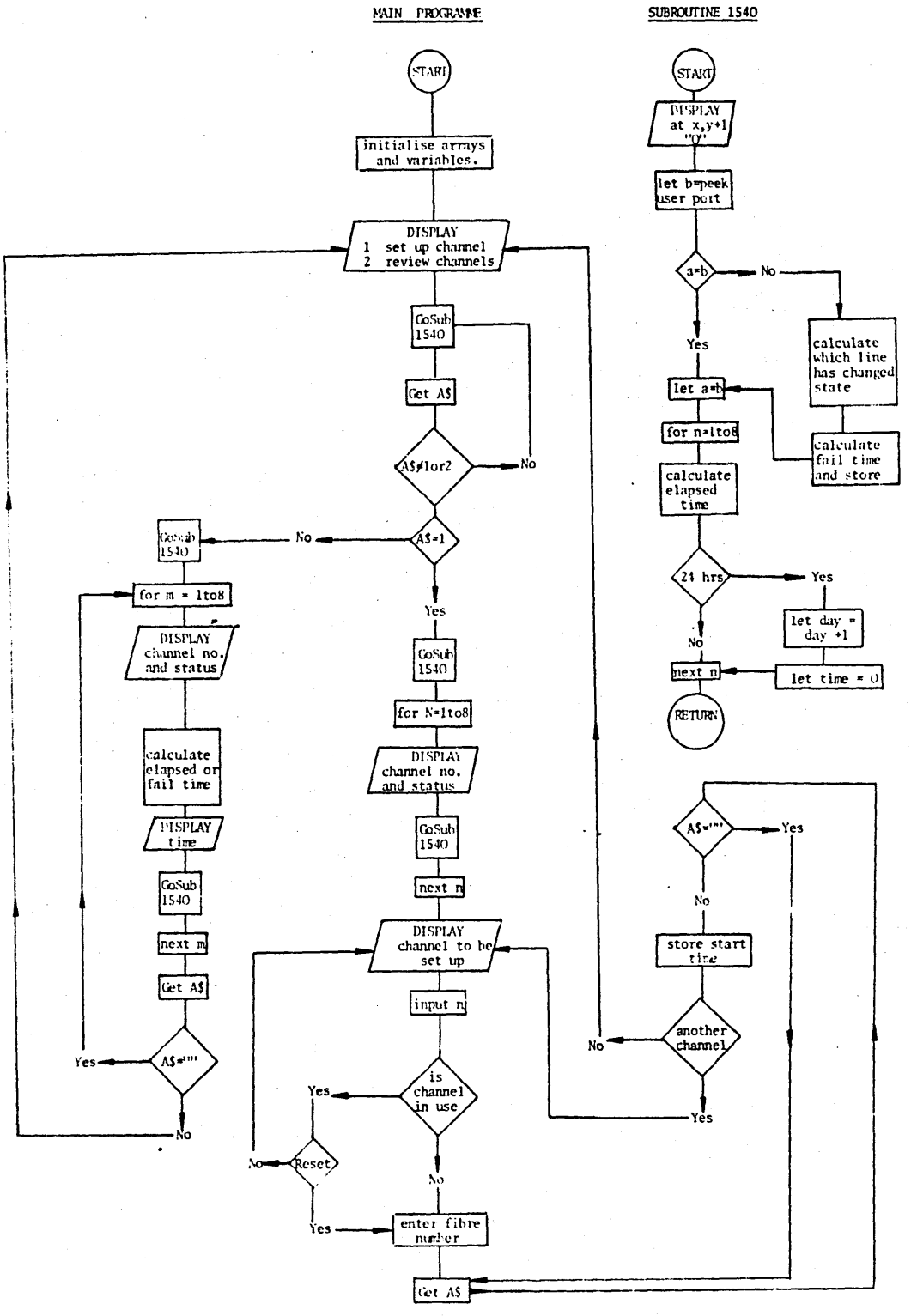

Figure 2.11 Flow chart of the PET Microcomputer programme, for monitoring and recording the stress corrosion failure of single E-glass fibres.

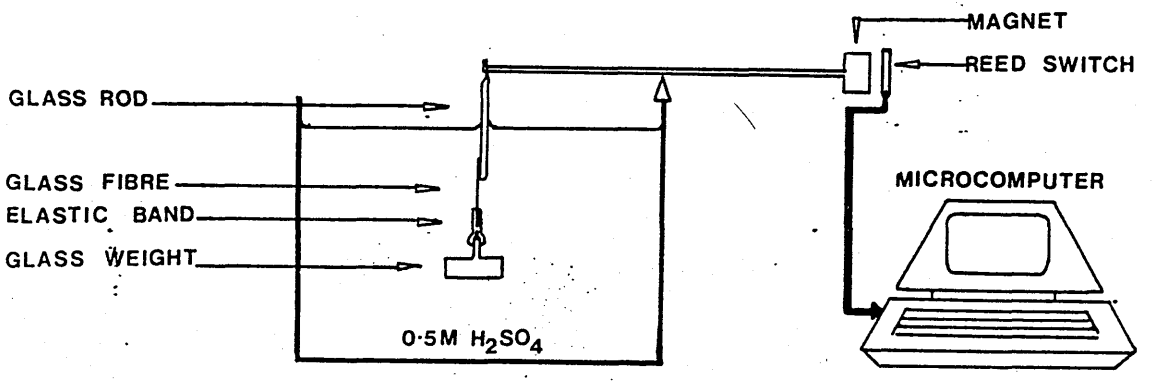

Figure 2.12 Diagrammatic representation of a single channel of the experimental apparatus shown in Figure 2.10.

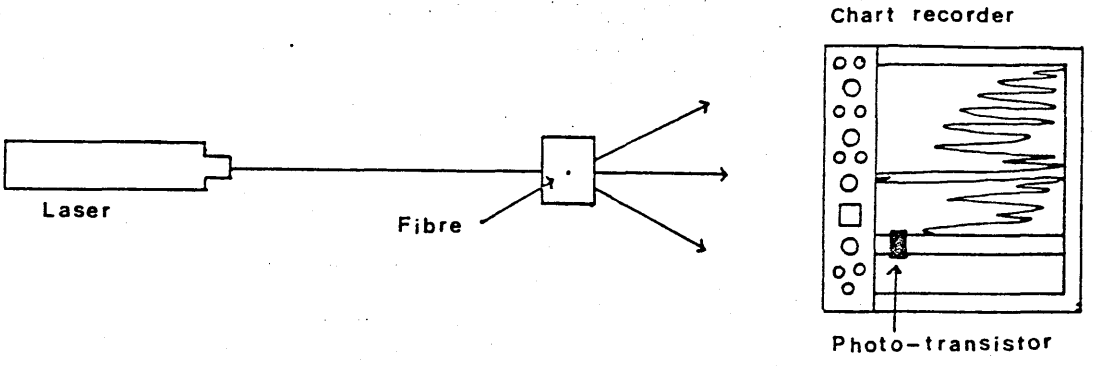

Figure 2.13 Experimental apparatus for the recording of interference fringes, to allow calculation of fibre diameter.

recorder. The time base was used to scan the interference pattern at 10 mm s^{-1} . The output of the phototransistor was amplified and used to control the Y axis, giving a trace of the intensity against the scattering angle. The diameters of the fibres were calculated using equation 2.3. Complications from diffraction at low angles were avoided by counting fringes from above a 6^{o} angle of scatter.

2.6 ENVIRONMENTAL TRANSVERSE CRACKING BEHAVIOUR OF CROSSPLY LAMINATES

Crossply coupons were tested on an Instron Universal testing machine model 1196 at a constant displacement rate of 0.5 mm min^{-1}. For those tested in 0.5 M aqueous sulphuric acid and deionized water, the environment was contained in an open-cell attached to the coupon as described in section 2.4.2. The transverse cracking was recorded photographically at approximately every 0.03% increment of strain. The exact stress at which each photograph was taken was recorded using the event marker attached to the Instron.

2.7 THE DETERMINATION OF RESIDUAL THERMAL STRAINS IN CROSSPLY LAMINATES

For the measurement of residual thermal strains, asymmetrical $0^o/90^o$ laminates were fabricated by stacking two unidirectional wound frames together before impregnation. Coupons of approximately 200 x 3-10 mm dimensions were cut from the laminates before postcuring.

Parvizi (69), using the Timoshenko bimetallic beam theory (74) derived equations 2.4 - 2.7, which relate the thermal strain in a $0^o/90^o/0^o$ coupon to the radius of curvature of an asymmetrical $0^o/90^o$ beam.

For d=b

$$\varepsilon_{t\ell}^{th} = \frac{E_\ell b}{E_\ell b + E_t d} \cdot \frac{P}{12\rho} \frac{E_\ell}{E_t} + 14 + \frac{E_t}{E\ell} \qquad \ldots (2.4)$$

$$\varepsilon_{\ell t}^{th} = \frac{E_\ell d}{E_\ell d + E_t b} \cdot \frac{P}{12\rho} \frac{E_\ell}{E_t} + 14 + \frac{E_t}{E_\ell} \qquad \ldots (2.5)$$

For $d \neq b$

$$\varepsilon_{t\ell}^{th} = \frac{E_\ell b}{E_\ell b + E_t d} \cdot \frac{P}{3\rho} \frac{(3\{1+m\}^2 + \{1+mn\}\{m^2 + 1/(mn)\})}{\{1+m^2\}} \quad \ldots(2.6)$$

$$\varepsilon_{\ell t}^{th} = \frac{E_\ell d}{E_\ell d + E_t b} \cdot \frac{P}{3\rho} \frac{(3\{1+m\}^2 + \{1+mn\}\{m^2 + 1/(mn)\})}{\{1+m^2\}} \quad \ldots(2.7)$$

Where:-

$\varepsilon_{t\ell}^{th}$ = Thermal strain in the transverse ply, longitudinal direction.

$\varepsilon_{\ell t}^{th}$ = Thermal strain in the longitudinal ply, transverse direction.

P = Semi-thickness of coupon.

ρ = Radius of curvature.

E_ℓ, E_t = Longitudinal and transverse moduli of a unidirectional laminate.

d = Inner ply semi-thickness.

b = Outer ply thickness.

$m = \frac{b}{d}$

$n = \frac{E_\ell}{E_t}$

The radius of curvature of a curved $0^o/90^o$ coupon was calculated from

measurements of the coupon length L (± 0.5 mm) and the displacement δ (± 0.01 mm) in Figure 2.14 using equation 2.8. Timoshenko (74) derived equation 2.9, which relates this curvature to the expansion coefficient,

$$\frac{1}{\rho} = \frac{2}{L} \cos^{-1} (1 - \delta/\rho) \qquad \ldots(2.8)$$

Young's modulus and thickness of the individual plies. The theory assumes there is elastic bonding between the plies, and the Young's modulus is temperature insensitive. Also no allowance is made for differences in the Poisson ratio of the plies, or any shear interactions that may arise.

$$\frac{1}{\rho} = \frac{6(\alpha_2 - \alpha_1)(T - T_0)(1 + m)^2}{h\{3(1 + m)^2 + (1 + mn)(m^2 + 1/mn)\}} \qquad \ldots(2.9)$$

Where:-

$m = \frac{a_1}{a_2}$ $\quad a_1, a_2$ Thicknesses of the individual plies.

$n = \frac{E_1}{E_2}$ $\quad E_1, E_2$ Young's moduli of the individual plies.

T_0 = Temperature at which bimetallic beam is flat.

T = Calculation temperature.

α_1, α_2 = Expansion coefficients of the individual plies.

h = The thickness of the beam.

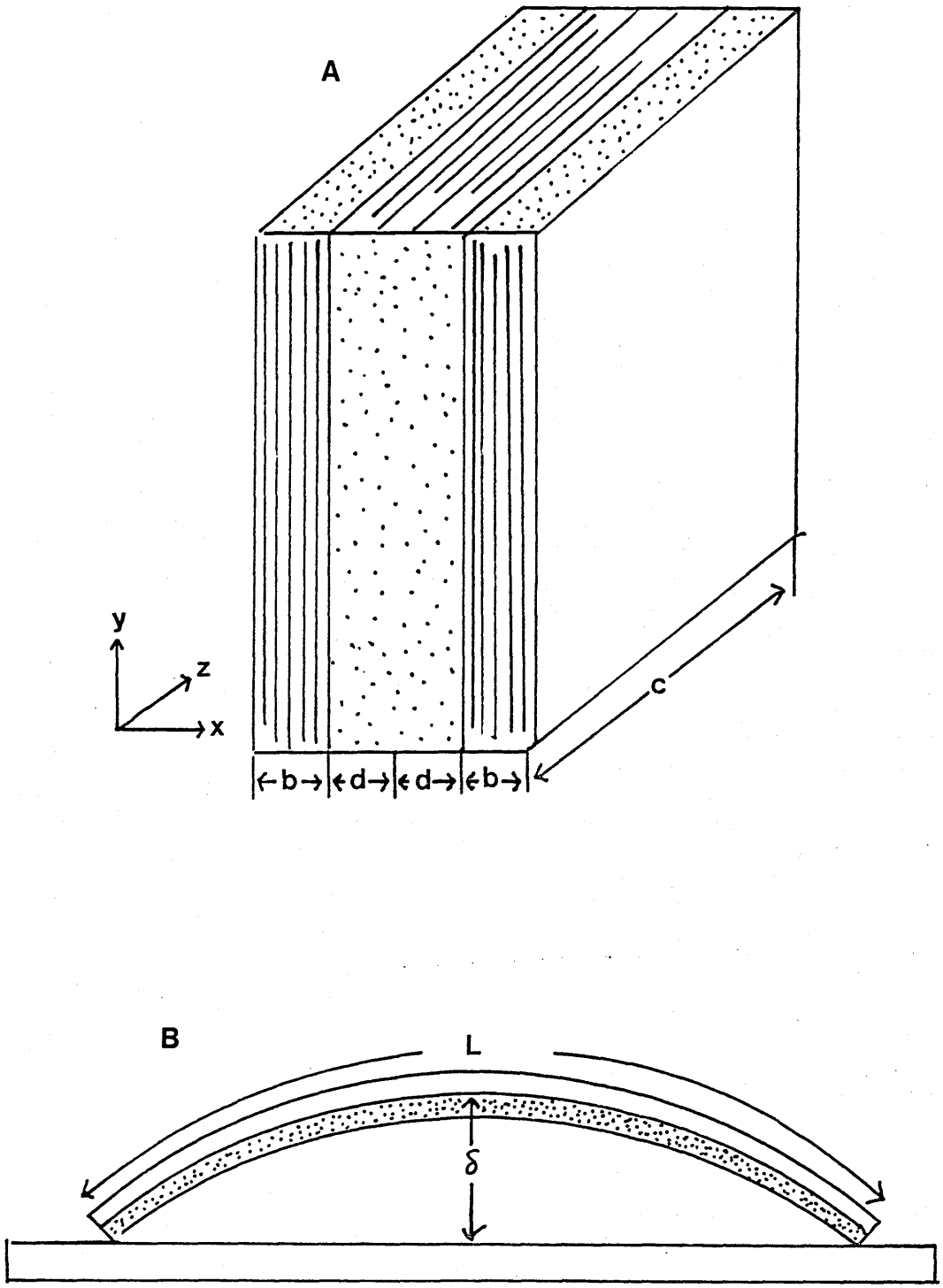

Figure 2.14 Illustration of the laminate models, (a) $0^{o}/90^{o}/0^{o}$ crossply (b) $0^{o}/90^{o}$ asymmetrical.

2.8 MICROSTRUCTURAL EXAMINATIONS

The microscopical examination of fracture surfaces were performed on both optical and electron (SEM) microscopes.

The use of optical microscopy was severely handicapped by its limited depth of field and its use was mainly confined to the examination of the edges or faces of coupons.

Specimens to be examined by SEM were affixed to aluminium stubs and coated with gold to provide a conducting surface.

The analytical examination of stress corroded fracture surfaces and single glass fibres were performed on carbon coated specimens using a JEOL JXA 50A microprobe.

The X-ray analysis of crystalline deposites found on the surfaces of coupons was performed using a JEOL 200X STEM.

CHAPTER 3 RESULTS

3.1 LAMINATE CHARACTERIZATION

The $0^{o}/90^{o}/0^{o}$ crossply and 0^{o} unidirectional laminates were characterized,as described previously. The transverse cracking behaviour of a $0^{o}/90^{o}/0^{o}$ crossply coupon is shown in Figure 3.1. Before the appearance of the first transverse crack, the coupon becomes increasingly opaque, this is termed stress whitening and has been shown to be associated with the debonding of the glass fibres (69). Initially, the transverse cracks appear randomly along the length of the coupon, but as their number increases, the crack spacing is seen to become more regular. The dark bands either side of a transverse crack are due to the partial rebonding of the glass fibres with the matrix, and the consequential increase in transparency of the coupon with the disappearance of the stress whitening. These bands are approximately 1-2 mm wide and show how rapidly the stress is built up again in the transverse ply.

At strains of approximately 0.7%, stress whitening of the longitudinal plies is observed, which is followed by longitudinal splitting. This is attributed to a transverse strain caused by a difference in the poissons ratios for the longitudinal and transverse plies (75).

The multiple cracking of the transverse ply in a crossply laminate results in a non-linear stress/strain curve, as shown in Figure 3.2. The first change in slope is associated with the stress whitening phenomenon, and the second with the onset of transverse cracking. In comparison, the 0^{o} unidirectional coupons have linear stress/strain curves.

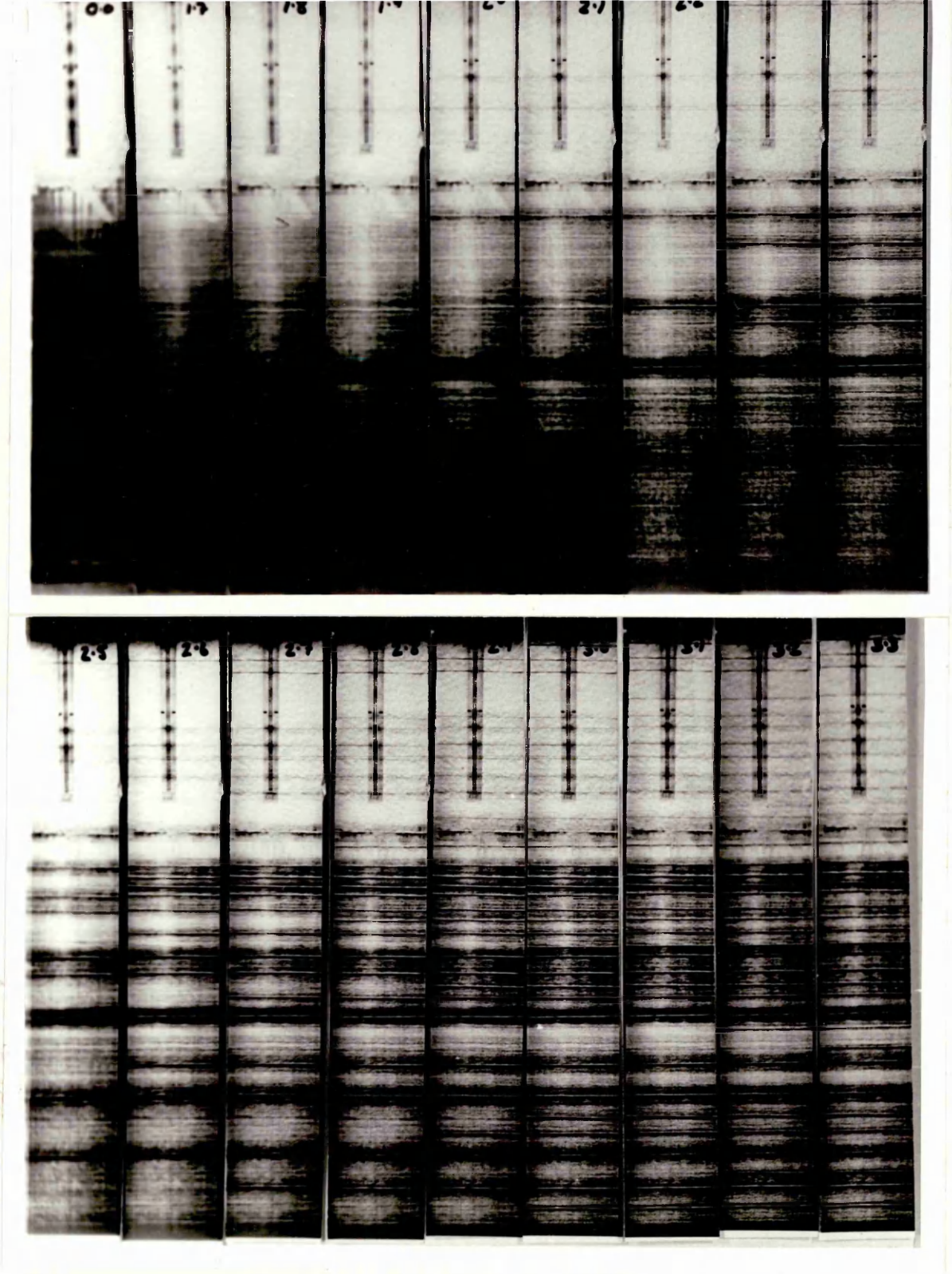

Figure 3.1 The transverse cracking behaviour of a $0^{o}/90^{o}/0^{o}$ crossply coupon over the strain range 0 - 0.66%. The strain in the coupon in each photograph is obtained by doubling the value marked on the coupon and dividing by ten.

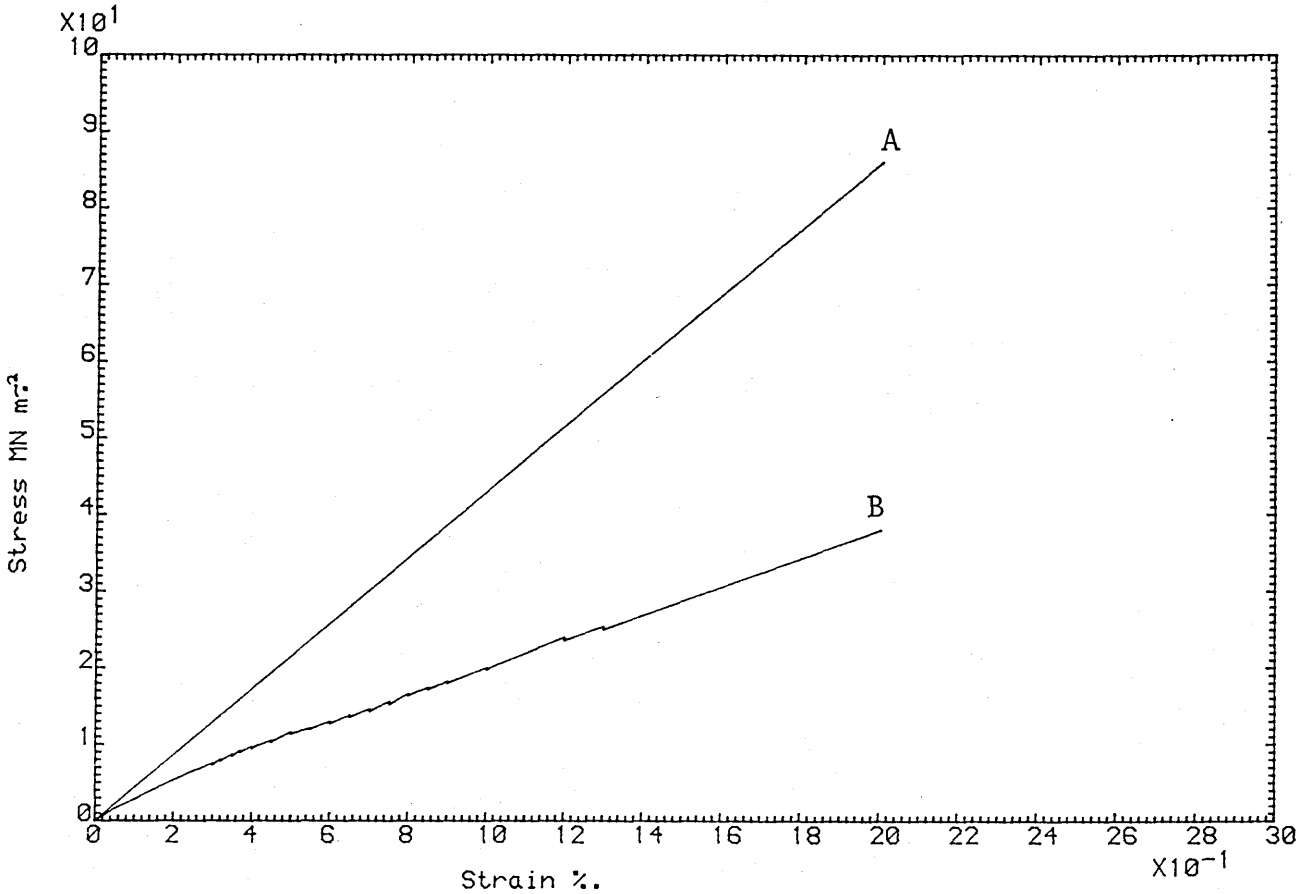

Figure 3.2. Typical stress-strain curves of (A) unidirectional and (B) $0^{o}/90^{o}/0^{o}$ crossply laminates.

The results of the laminate characterization are shown in Table 3.1. Whilst the moduli of the laminates are similar to those previously reported, the values of the first cracking strain $\varepsilon_{t\ell u}$ are considerably lower (69). This was found to be due to the greater thermal strain $\varepsilon_{t\ell}^{th}$ in these laminates, and is discussed in section 4.2.

Laminate			Cure		Volume Fraction*	Young's Modulus	1st transverse cracking strain
	Type	Geometry	Time Hrs	Temp °C	±2%	GN m^{-2}	±0.03%
A	d=b	$0^o/90^o/0^o$	3	150	57	26.2	0.34
B	d=b	$0^o/90^o/0^o$	3	150	56	26.8	0.33
M	d=b	$0^o/90^o/0^o$	3	150	57	26.3	0.32
N	d=b	$0^o/90^o/0^o$	3	150	56	25.9	0.32
P	d=b	$0^o/90^o/0^o$	3	150	58	26.4	0.28
R	d=b	$0^o/90^o/0^o$	3	150	56	27.1	0.28
Y	d=b	$0^o/90^o/0^o$	3	150	56	26.3	0.26
X	d=b	$0^o/90^o/0^o$	3	150	55	26.9	0.28
AZ	d=b	$0^o/90^o/0^o$	3	150	53	26.7	0.28
AC	d=b	$0^o/90^o/0^o$	24	200	55	26.6	0.10
U	d=2b	$0^o/90^o/0^o$	3	150	58	21.0	0.26
F	-	0^o	3	150	59	39.7	-
T	-	0^o	3	150	60	43.9	-
S	d=b	$0^o/90^o$	3	150	57	-	-

Table 3.1 Results of laminate characterization.

* Volume fraction of glass.

3.2 STRESS CORROSION EXPERIMENTS

3.2.1 $0^{o}/90^{o}/0^{o}$ Crossply laminates in Closed-Cells

The failure of a crossply coupon in a closed-cell is illustrated in Figure 3.3. The fracture of the coupon has occurred within the aqueous acid and this type of failure has been termed a Mode I failure. Initial loading of the coupon produced several transverse cracks because the applied strain of 0.49% was greater than the failure strain of the transverse ply, with time the number of cracks within the acid increased whereas out of the acid the number remained constant. After a specific period, dependent upon the temperature and the initial applied strain the longitudinal plies failed by a planar fracture adjacent to one of the initial transverse cracks, produced on loading. This has been arrowed in Figure 3.3. The failure times are shown in Table 3.2.

When the initial applied strain is less than the transverse ply failure strain,tensile transverse cracks do not form upon loading, but after an induction period, dependent upon how close the applied strain is to the transverse ply failure strain, cracks grow in the transverse ply from the cut-edges of the coupon towards the centre. This is illustrated in Figure 3.5 for a Mode II failure in an open-cell (See section 3.2.2), but the behaviour is identical for closed-cells. These cracks penetrate the thickness of the transverse ply and would span the entire width of the coupon were it not for the mutual interference of cracks growing from both edges.

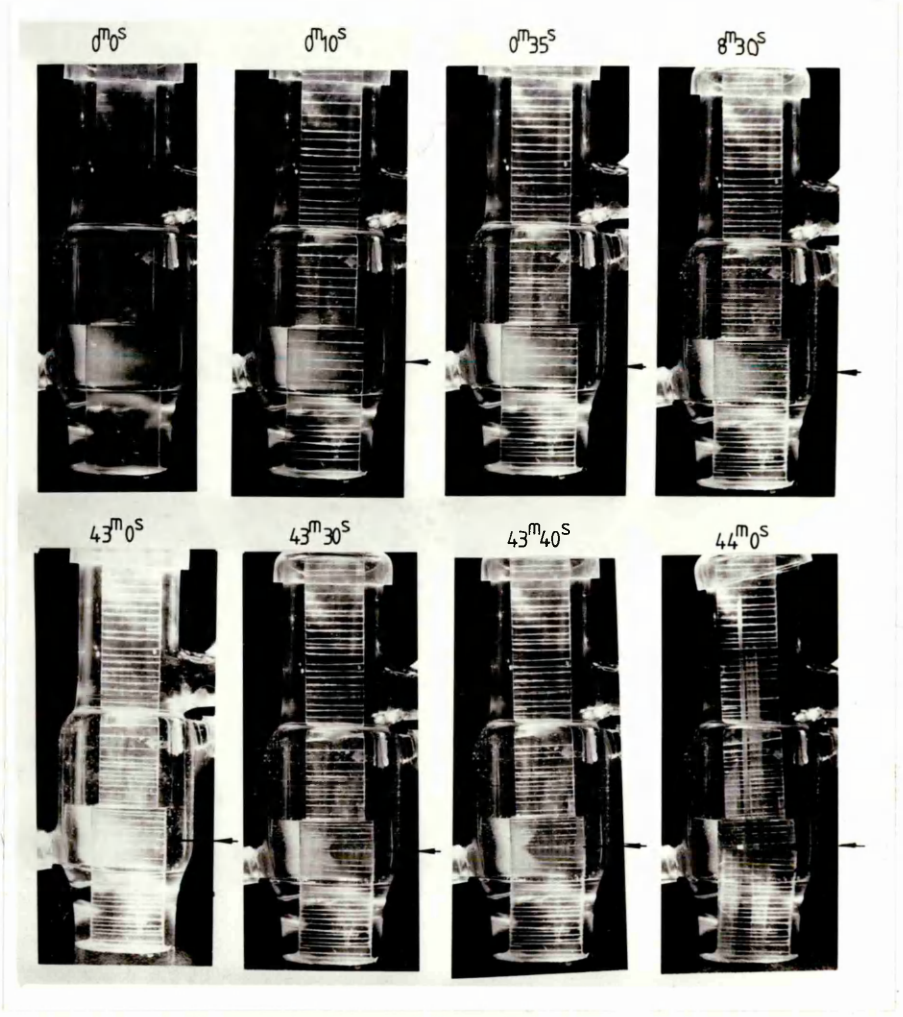

Figure 3.3 Mode I failure of a $0^{o}/90^{o}/0^{o}$ crossply coupon in 0.5 M H_2SO_4 at $23^{o}C$ and at an initial applied strain of 0.49%. The transverse crack adjacent to which failure occurred has been arrowed.

Coupon	Temp °C	Applied Stress MN m^{-2}	Initial Strain %	0° Ply Strain %	Fail Time min	Failure Mode
M 2	40	115	0.51	0.55	13	I
M 3	40	92	0.38	0.44	38	I
M 7	40	70	0.26	0.33	44	I
M 5	40	46	0.16	0.22	780	I
M 10	40	23	0.09	0.11	42,000	I
N 8	23	112	0.49	0.53	44	I
N 4	23	90	0.36	0.43	107	I
N 2	23	67	0.25	0.32	318	I
N 7	23	45	0.15	0.21	1,940	I
M 11	23	46	0.16	0.22	2,080	I
M 6	23	23	0.09	0.11	33,825	I
P 1	5	110	0.48	0.52	307	I
P 4	5	89	0.36	0.42	600	I
P 2	5	66	0.26	0.31	1,698	I
P 3	5	44	0.15	0.21	4,900	I
P 8	5	23	0.08	0.11	69,000	I

Table 3.2 Stress corrosion failure times of $0^{\circ}/90^{\circ}/0^{\circ}$ crossply coupons in closed cells.

Note. The 0° ply strain was calculated from equation 4.17.

The effect of temperature over the range 5^{o}-40^{o}C upon the failure time was investigated and the results are given in Table 3.2 and in Figure 3.4. As would be expected the higher the temperature the shorter the failure time at similar strains. However, below 0.2% strain the effect of temperature becomes less discernible, so that at 0.1% strain the failure times are similar. This suggests that at low applied strains the rate determining step is different. It will be shown in chapter 4 that the resin is only protective at these strains and therefore the temperature dependence of diffusion is different from that of stress corrosion of the glass fibres. Furthermore since the diffusion is possibly strain dependent, the reduction in the thermal strain at higher temperatures may reduce the rate of diffusion in opposition to the increase in the rate of stress corrosion of the glass.

Mode I failure only was observed at all initial applied strains in the closed-cells.

3.2.2 $0^{o}/90^{o}/0^{o}$ crossply coupons in open-cells

Unlike the closed-cell experiments described above two different types of failure were observed in the open-cells. At initial strains greater than 0.15%, failure occurred by the Mode I mechanism, whereas at lower strains, failure occurs in the unimmersed part of the laminate, as illustrated in Figure 3.5. This has been called Mode II failure. Unlike the Mode I failure, fracture of the coupon does not occur adjacent to an initial transverse ply crack, but by the growth of a crack propagating through both

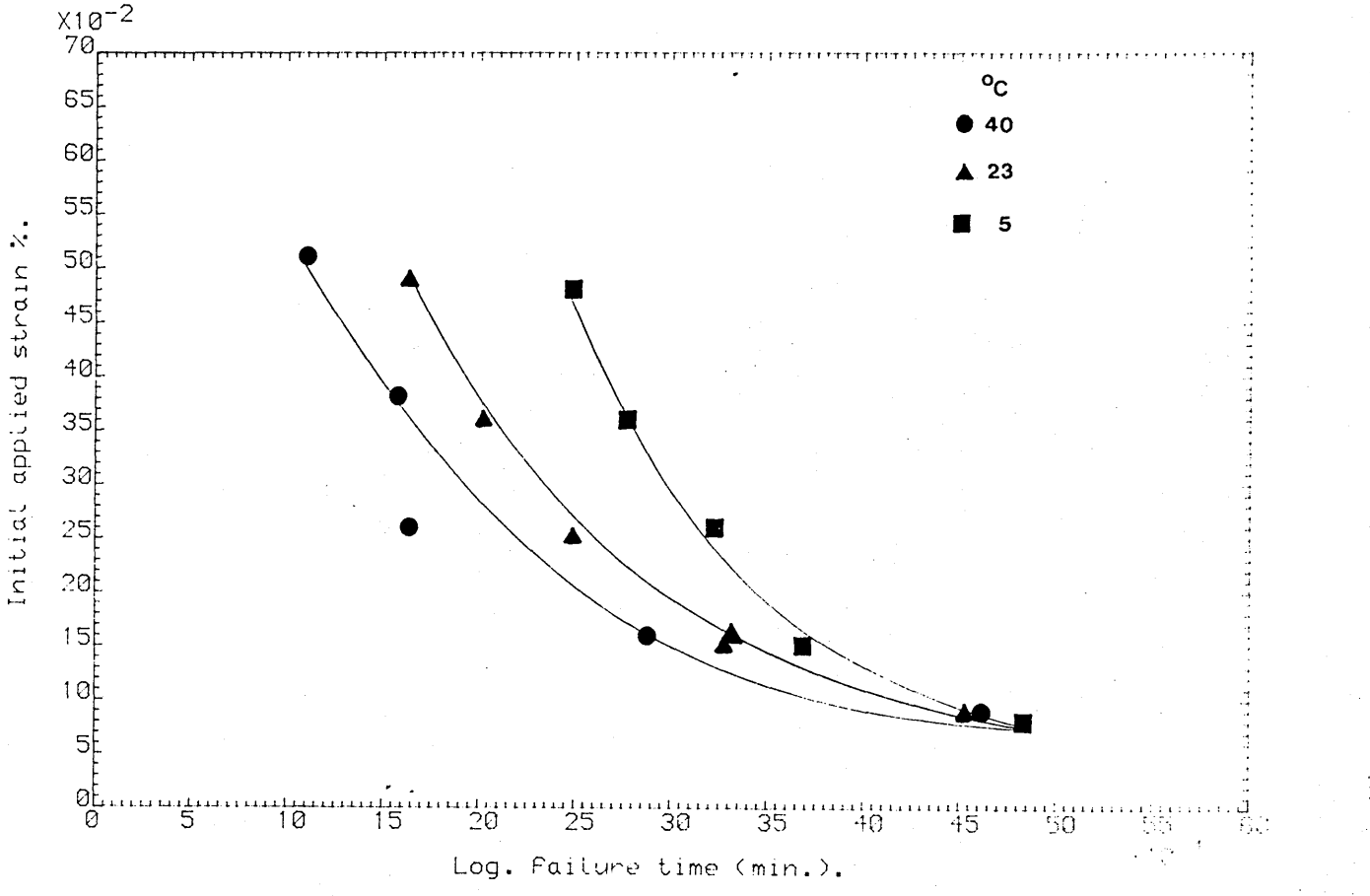

Figure 3.4 The effect of temperature upon Mode I stress corrosion failure times.

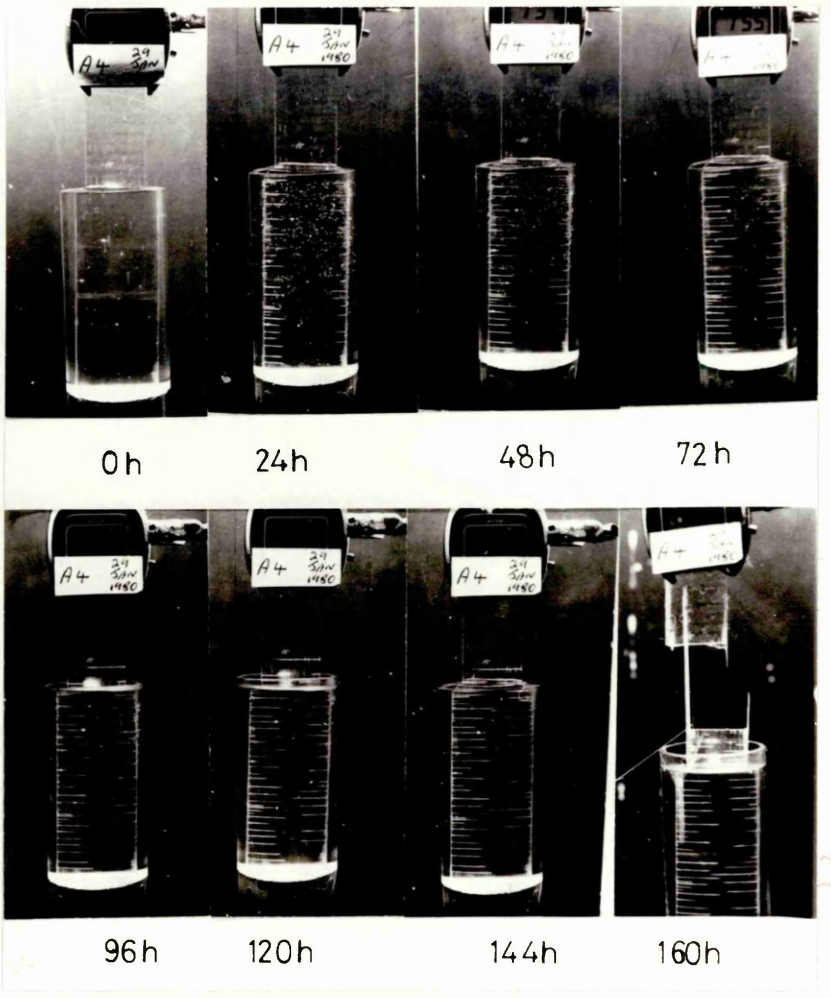

Figure 3.5 Mode II failure of a $0^{o}/90^{o}/0^{o}$ crossply coupon in 0.5 M H_2SO_4 at $23^{o}C$ and at an initial applied strain of 0.1%.

transverse and longitudinal plies concurrently. The initiation of this crack occurs well after the nucleation and growth of the edge-cracks within the acid (See Figure 3.5). The amount of damage within the unimmersed portion of the laminate varies from a single crack as shown in Figure 3.5 to considerable transverse cracking and longitudinal splitting, and is related to the applied strain on the coupon. The lower the strain, the more damage which appears before final failure. This damage is similar to that which occurs in crossply coupons under zero applied strain. Table 3.3 shows the times-to-failure of crossply coupons in the open-cells.

Figure 3.6 shows a comparison of the failure times of the coupons in the open and closed-cells. Mode II failure occurs in a shorter time than the Mode I fracture at similar strains. Mode I failures occur in both cells in similar times.

The effect of the sulphuric acid concentration on the failure time was investigated over the range 0.05 - 4.0 M at initial applied strains of $\simeq$ 0.1%. The results are shown in Table 3.4 and reveal that the failure time decreases with increasing acid concentration. However this effect appears to be minimal over the concentration range 0.50 - 2.00 M. Furthermore a change in the mode of failure occurs so that at concentrations greater than 2.0 M Mode II failures were not observed.

Coupon	Applied Stress $MN\ m^{-2}$	Initial Strain %	0^{o} Ply Strain %	Fail Time min	Failure Mode
R 10	119	0.50	0.57	49	I
Y 2	120	0.50	0.57	83	I
Y 3	97	0.40	0.46	94	I
X 5	119	0.50	0.56	50	I
R 11	94	0.38	0.44	139	I
R 1	72	0.27	0.34	288	I
P 7	46	0.16	0.22	790	I
N 3	45	0.16	0.21	2,000	I
R 7	24	0.10	0.12	3,420	II
Y 5	24	0.10	0.12	3,600	II
A 6	22	0.09	0.11	9,600	II
A 4	22	0.09	0.11	9,360	II
Y 8	24	0.09	0.11	4,300	II
M 9	23	0.09	0.11	7,920	II
B 11	11	0.05	0.06	21,600	II

Table 3.3 Stress corrosion failure times of $0^{o}/90^{o}/0^{o}$ crossply coupons in open-cells, at $23^{o}C$.

Note. The 0^{o} ply strain was calculated from equation 4.17.

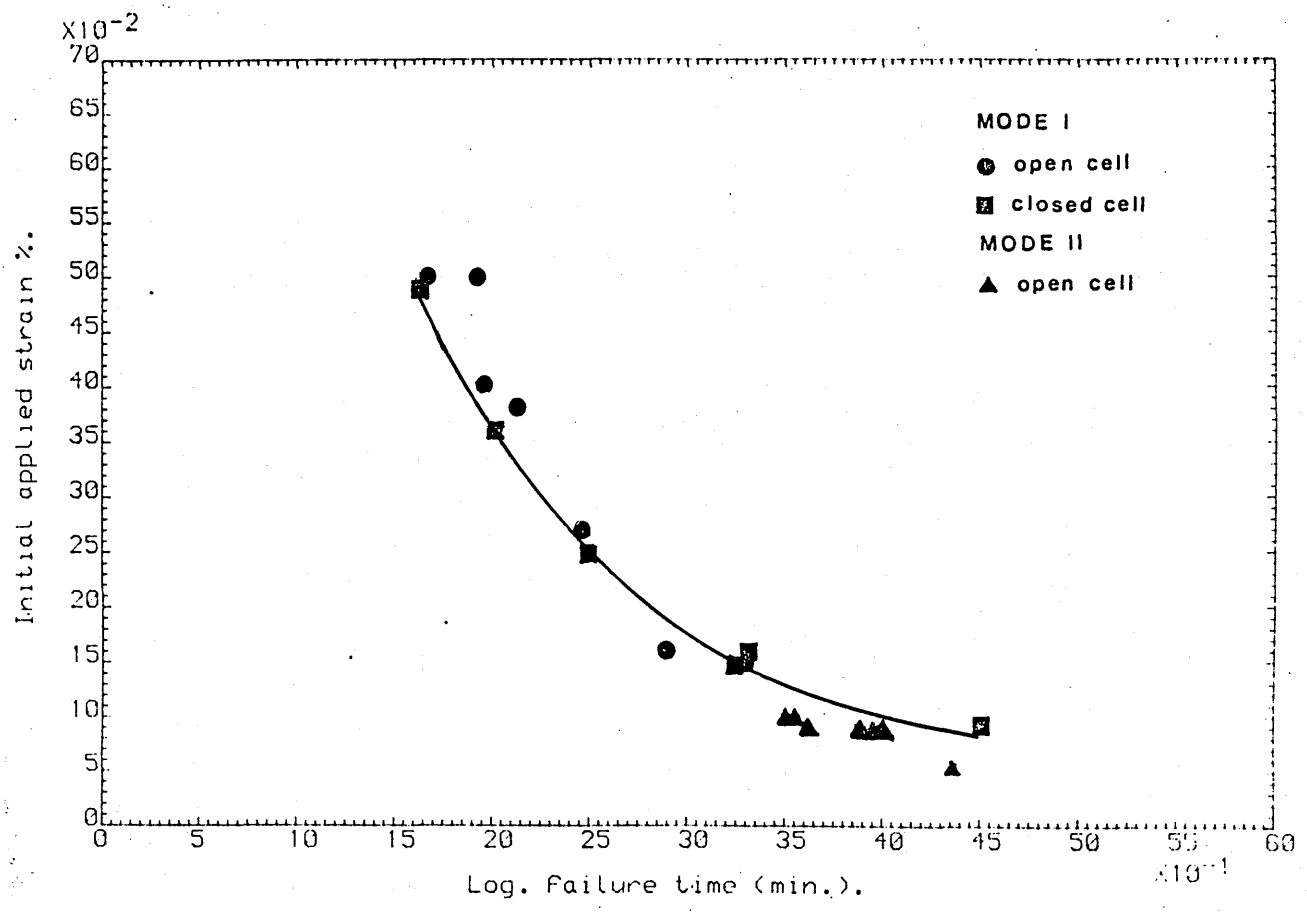

Figure 3.6 Comparison of the stress corrosion failure times of $0^{o}/90^{o}/0^{o}$ crossply coupons from open and closed cells.

Coupon	Applied Stress $MN\ m^{-2}$	Initial Strain %	0^o Ply Strain %	Fail Time min	Acid Molarity	Failure Mode
Y 10	24	0.09	0.11	No Fail	0	–
Y 9	23	0.09	0.11	13,440	0.05	II
R 9	25	0.10	0.12	7,200	0.25	II
R 2	25	0.10	0.12	5,340	1.00	II
R 4	24	0.09	0.11	6,600	2.00	I
A 25	24	0.09	0.11	1,380	4.00	I

Table 3.4 The effect of sulphuric acid concentration on the stress corrosion failure time of $0^o/90^o/0^o$ crossply coupons at 23^oC in the open-cell.

Note. The 0^o ply strain was calculated from equation 4.17.

3.2.3 Non-externally stressed $0^{o}/90^{o}/0^{o}$ crossply coupons

It had been observed that failed stress corroded coupons continued to develop damage even when they were removed from the environment, and had no external applied stress. In addition, this damage was more intense within the half of the coupon that had not been immersed in the acid. The nature of this damage was longitudinal splitting of the 0^{o} plies together with transverse cracking of the 90^{o} ply.

Experiments, where coupons were totally immersed or partially immersed in 0.5 M aqueous sulphuric acid, produced completely different results. Totally immersed coupons developed no longitudinal or transverse cracks, but showed a general acid attack of the exposed surface glass, giving a whitish appearance to the surface of the coupon. A slow attack at the edge of the 90^{o} ply similar to the type of edge cracking reported for polyester laminates also occurred (30). Figure 3.7, shows a coupon that has been totally immersed in acid for 20 months. However coupons that were only partially immersed, developed damage in the unimmersed half within three days, as shown in Figure 3.8 with no visible damage in the immersed half. The damage consists of longitudinal and transverse cracks and is similar in appearance to that found in the unimmersed half of coupons tested at initial applied strains of less than 0.1% in the open-cell, or that which develops in the unimmersed half of a previously stress corroded coupon. This type of damage has been termed Mode III failure. Coupons left exposed to acid vapour alone did not develop visible damage.

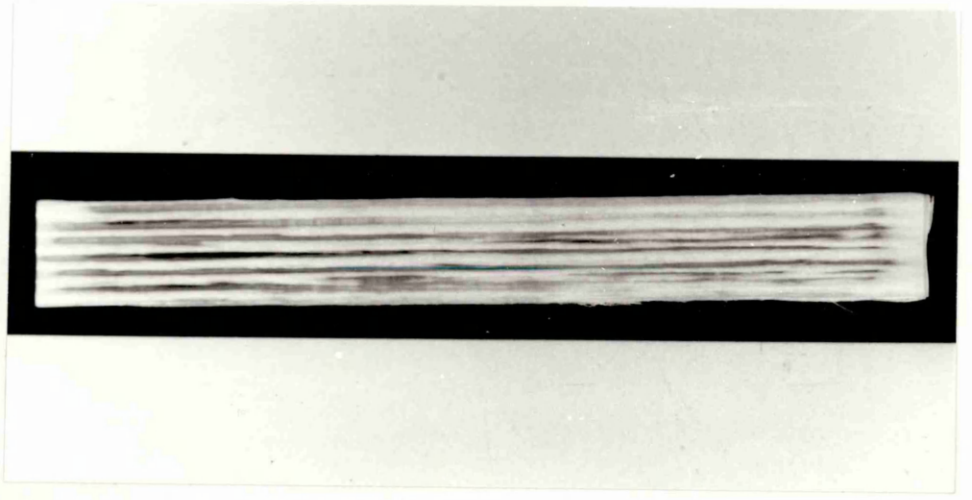

Figure 3.7 $0^{o}/90^{o}/0^{o}$ crossply coupon that has been immersed in 0.5 M H_2SO_4 at $23^{o}C$ for 20 months.

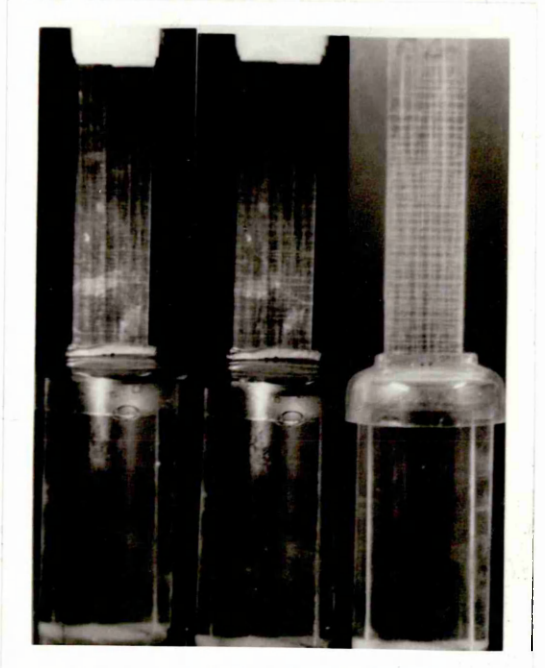

Figure 3.8 The development of Mode III damage in the unimmersed half of a non-externally stressed $0^{o}/90^{o}/0^{o}$ crossply coupon.

Since insoluble glass degradation products were thought to be responsible for the formation of Mode III damage (section 4.5) the effect of different acids whose corrosion products are of differing solubility, were studied.

No damage was observed with 0.5 M nitric acid and only one split in the longitudinal ply with 0.5 M hydrochloric acid, whereas Mode III damage was produced in both the immersed and unimmersed halves of the coupon,with 0.5 M phosphoric acid.

These results show a connection between the appearance of Mode III damage and the solubility of the major glass corrosion products which will be discussed fully in section 4.5.

3.2.4 $0^{o}/90^{o}/0^{o}$ crossply coupons with attached clamp-on-cells

The effect of the unprotected cut-edges of the coupons on the stress corrosion behaviour was determined by attaching a clamp-on-cell (see section 2.4.3), to one face of the coupon. Both the Mode I and Mode II type failures found in open-cell experiments, were observed. The times-to-failure are given in Table 3.5 and in Figure 3.9 and are compared with the results from crossply coupons in open-cells. The greater scatter in these results is considered to be due to the small area of contact with the environment, so that localized laminate irregularities will greatly influence the failure time. In the open-cell experiments the larger area of contact minimises the

Coupon	Applied Stress $MN\ m^{-2}$	Initial Strain %	0^o Ply Strain %	Fail Time min
AZ 3	110	0.47	0.53	392
AZ 4	100	0.41	0.48	210
AZ 8	93	0.38	0.44	240
AZ 12	77	0.30	0.37	2,200
AZ 14	67	0.26	0.32	431
AZ 22	54	0.19	0.26	27,360
AZ 18	46	0.16	0.22	2,200
AZ 13	22	0.09	0.11	4,320

Table 3.5 Stress corrosion failure times of $0^o/90^o/0^o$ crossply coupons using the clamp-on-cell, at 23^oC.

Note. The 0^o ply strain was calculated from equation 4.17.

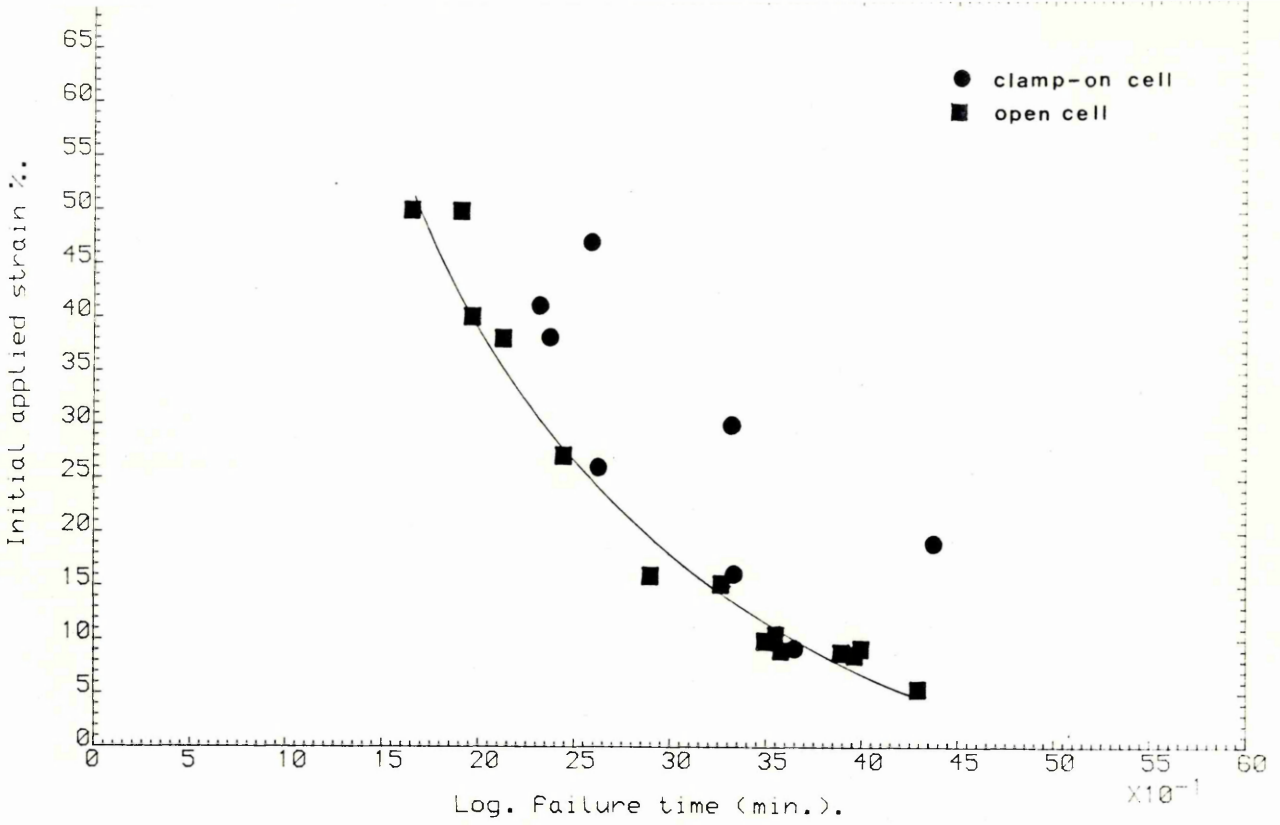

Figure 3.9 A comparison of the failure times of $0^{o}/90^{o}/0^{o}$ crossply coupons in open cells and the clamp-on-cell.

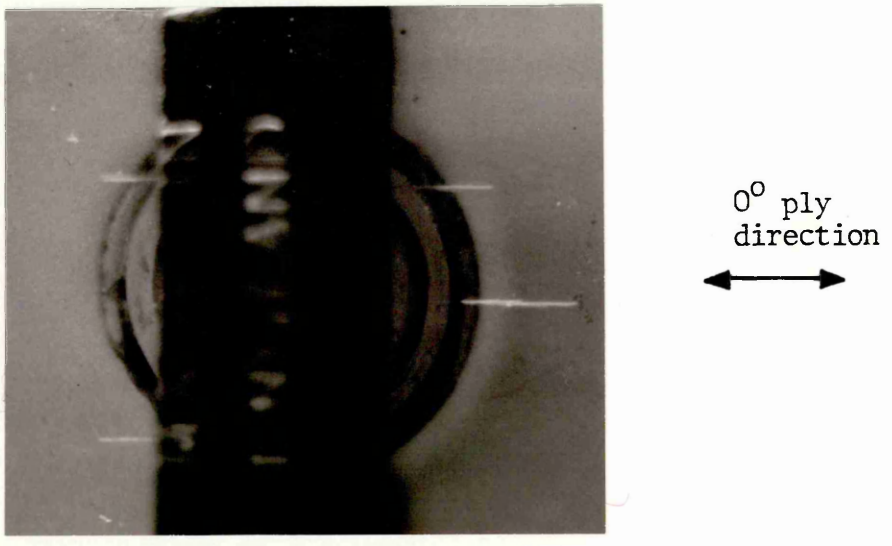

Figure 3.10 Initiation of Mode III damage in a non-externally stressed $0^{o}/90^{o}/0^{o}$ crossply coupon with an attached clamp-on-cell.

effect of such differences.

Mode III damage was also observed in experiments with the clamp-on-cell. Figure 3.10 shows the initiation of this damage by cracking of the longitudinal ply parallel to the glass reinforcement.

3.2.5 $0^{o}/90^{o}/0^{o}$ crossply coupons: NMA 90phr-200^{o}C postcure

The chemical resistance of the matrix resin was improved by using a near stoichiometric quantity of NMA (90phr) and postcuring for 24 hours at 200^{o}C (76,77). The lower concentration of NMA (80phr) together with the 3 hour postcure at 150^{o}C was used so that the laminates fabricated were similar to those previously studied (69). The failure times for the 200^{o}C postcured $0^{o}/90^{o}/0^{o}$ crossply coupons which have been tested in open cells are given in Table 3.6. Both Mode I and II failures were observed. In Figure 3.11 the results for the 150^{o}C and 200^{o}C postcured laminates are compared. The similar failure times indicate that the mechanism of stress corrosion is independent of the chemical resistance of this resin. Also shown in Figure 3.11 are stress corrosion failure times for polyester-glass laminates. The comparatively rapid failure of these epoxy glass laminates compared to the polyester-glass laminates is further evidence that the mechanism of stress corrosion does not involve the chemical attack of the resin. The chemical resistance of the epoxy resin is expected to be as good, if not better than the polyester resin (78).

Coupon	Applied Stress $MN\ m^{-2}$	Initial Strain %	0^{o} Ply Strain %	Fail Time min	Failure Mode
AC 9	128	0.53	0.61	40	I
AC 8	102	0.42	0.48	58	I
AC 3	79	0.29	0.38	133	I
AC 2	50	0.18	0.24	415	I
AC 10	25	0.10	0.12	11,000	II

Table 3.6 Stress corrosion failure times of $0^{o}/90^{o}/0^{o}$ $200^{o}C$ postcured crossply coupons in the open-cell at $23^{o}C$.

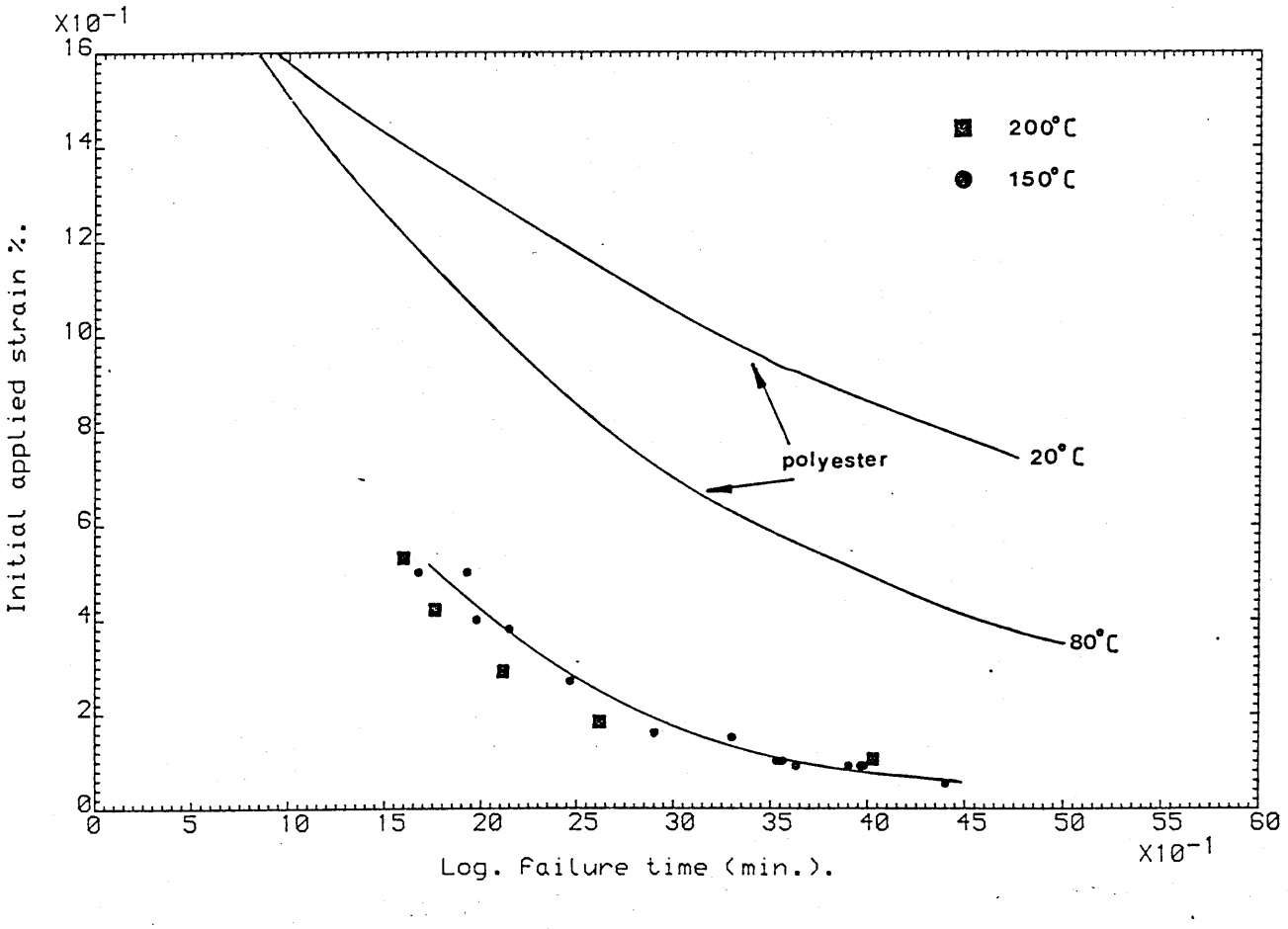

Figure 3.11 Comparison of the stress corrosion failure times of the 200°C postcured 0°/90°/0° crossply coupons with those given previously in Table 3.3. Also included are failure times of polyester glass crossply coupons postcured at 20°C and 80°C, taken from reference 90.

3.2.6 0^{o} unidirectional laminates in open-cells

The failure of the 0^{o} unidirectional coupons occurred in a similar manner to that of the $0^{o}/90^{o}/0^{o}$ crossply laminates, with the mode of failure dependent upon the initial applied strain.

The Mode I failure of a coupon at an initial applied strain of 0.35% is shown in Figure 3.12. Numerous individual stress corrosion cracks, which are easily visible in the photograph taken after 2.5 hours, have grown in the immersed half of the coupon. Failure results by the coalescence of a number of these cracks. The stepped topography of the fracture surface is in marked contrast to the planar crossply failures.

At applied strains of less than approximately 0.15%, failure occurs by the Mode II mechanism as shown in Figure 3.13. Before the initiation and growth of the failure crack, crystalline material was observed at the edge of the coupon and is arrowed in Figure 3.13. Its identification is separately reported in section 4.5. Once the failure crack had been initiated it proceeded to rapidly traverse the coupon, and gave a very planar fracture surface similar to those from the crossply coupons.

The initiation of stress corrosion cracks, above the aqueous acid, has also been observed at strains greater than 0.15%, giving rise to fracture by both Mode I and Mode II mechanisms, as illustrated in Figure 3.14. Since the failure results predominantly from the fracture within the aqueous acid these have been considered as Mode I failures.

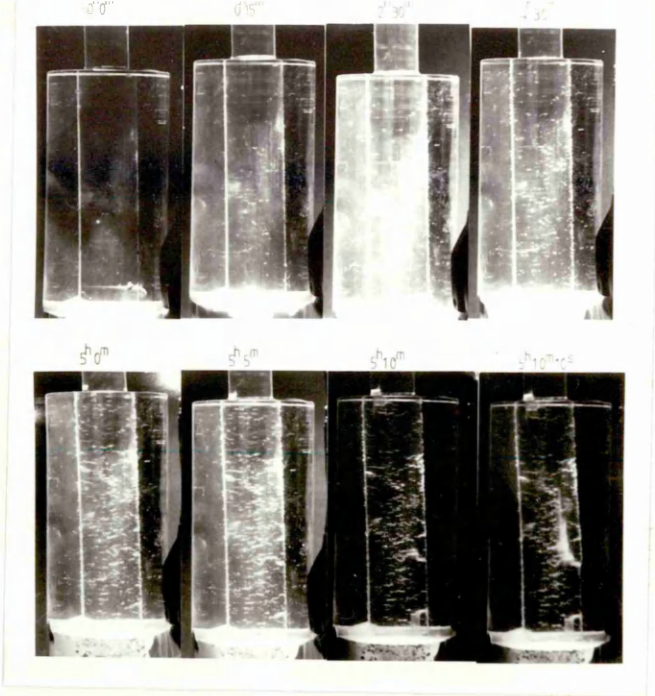

Figure 3.12 Mode I failure of a 0^{o} unidirectional coupon in 0.5 M H_2SO_4 at $23^{o}C$ and at an initial applied strain of 0.35%.

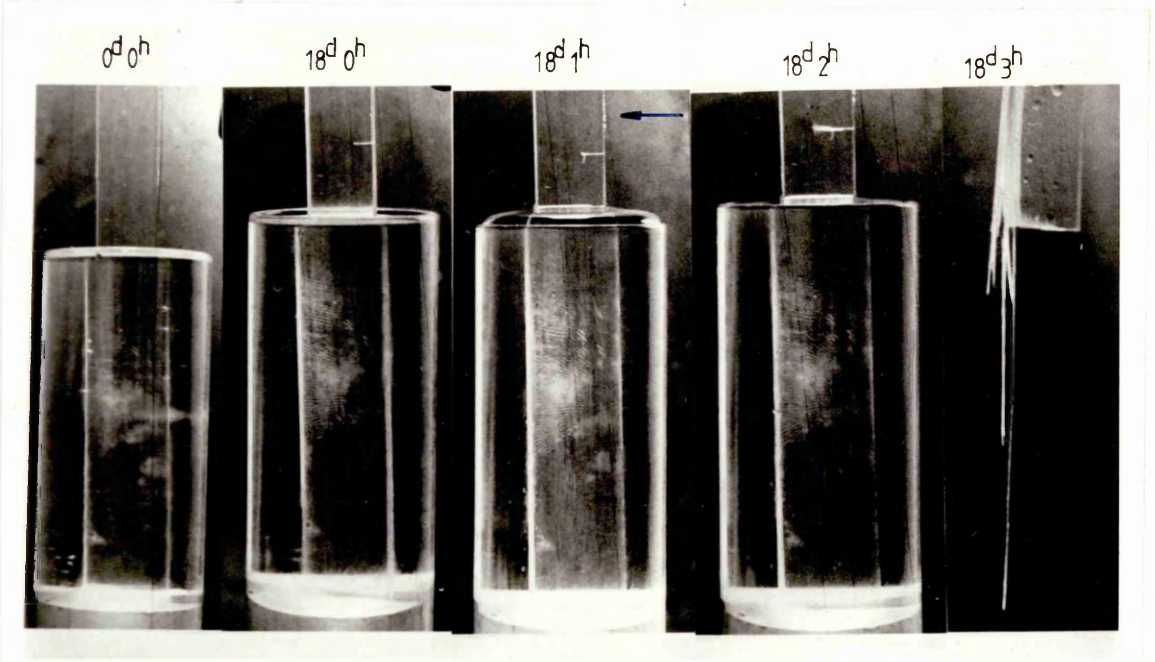

Figure 3.13 Mode II failure of a 0^{o} unidirectional coupon in 0.5 M H_2SO_4 at $23^{o}C$ and at an initial applied strain of 0.09%.

The failure times of the coupons are given in Table 3.7. In Figure 3.15 they are compared with the results from experiments with crossply coupons in open cells. At equivalent initial applied strains, the 0^{o} coupons take longer to fail.

Mode III damage has not been observed in partially immersed coupons, although deposition of crystalline material at the coupon edge occurs.

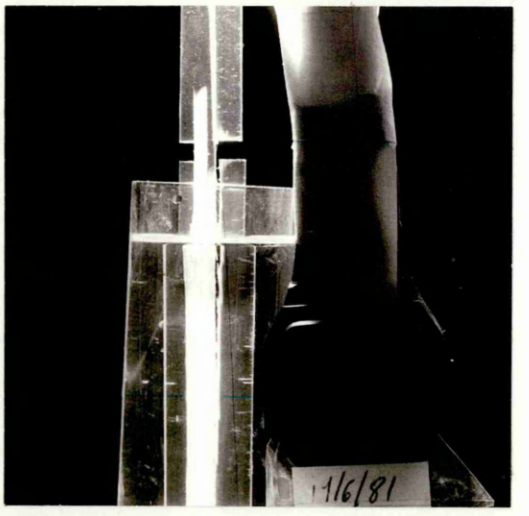

Figure 3.14 Mode I / Mode II failure of a 0^{o} unidirectional coupon at an applied strain of 0.27%.

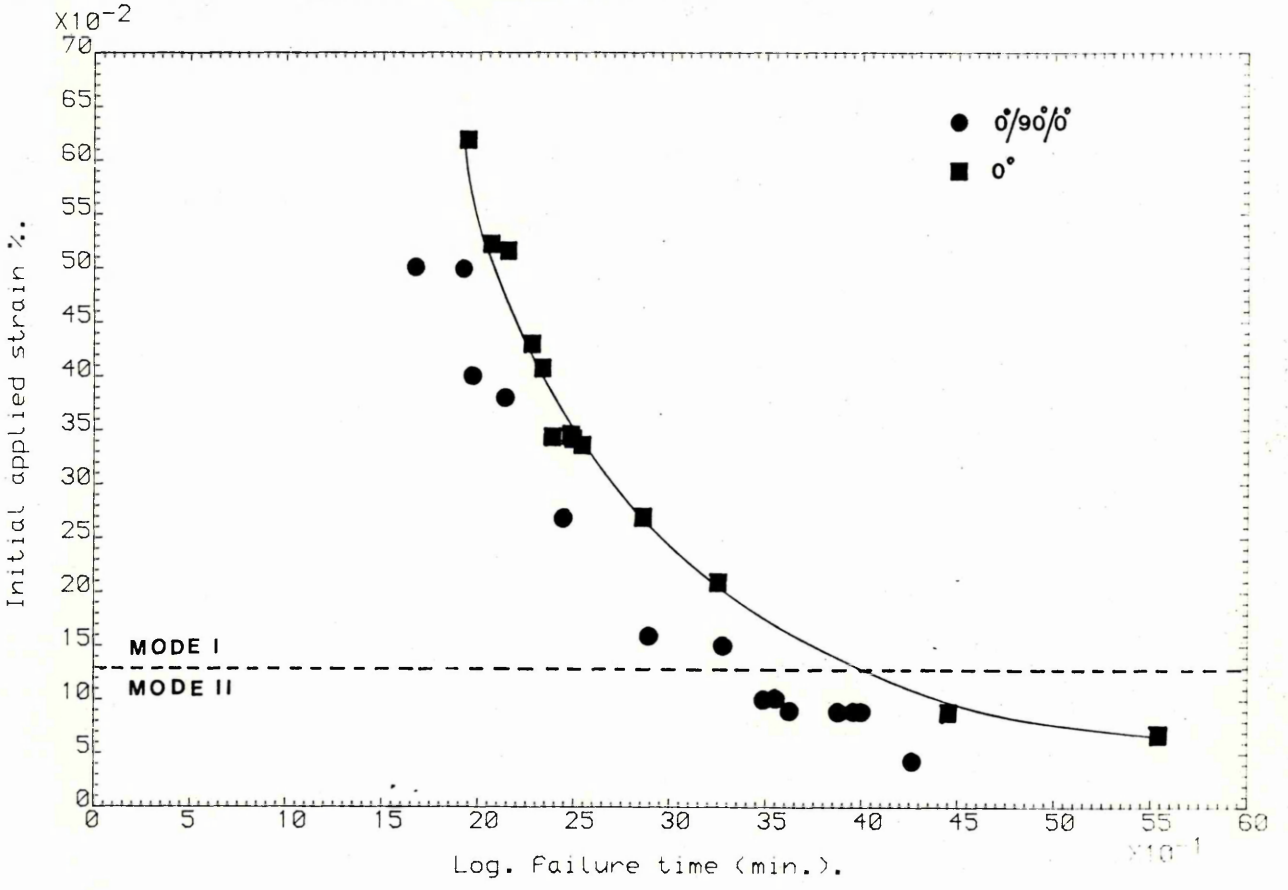

Figure 3.15 Comparison of the stress corrosion failure times of 0^{o} unidirectional and $0^{o}/90^{o}/0^{o}$ crossply coupons in open cells.

Coupon	Applied Stress $MN\ m^{-2}$	0^o Ply Strain %	Fail Time min	Failure Mode
F 2	262	0.62	90	I
T 7	220	0.52	120	I
T 12	220	0.52	145	I
T 8	184	0.43	195	I
F 3	174	0.41	213	I
T 9	148	0.35	325	I
T 10	147	0.35	309	I
F 1	145	0.34	257	I
T 11	113	0.27	746	I
F 4	87	0.21	1800	I
T 6	36	0.09	26,100	II
F 5	29	0.07	349,920	II

Table 3.7 Stress corrosion failure times of 0^o unidirectional coupons at 23^oC in the open-cell.

3.2.7 E-glass single fibres in 0.5 M sulphuric acid

An investigation of the stress corrosion of E-glass fibres was undertaken to determine the effectiveness of the matrix resin in providing chemical protection. One of the major difficulties, in such a study, is the determination of the fibre diameter, for calculating the strain from the applied load. Measurements from the forward light scattering method were compared to those determined by SEM. The former were found to give results which were approximately 0.5 μm larger, giving an error of approximately 5% in the value of the applied strain. Figure 3.16 shows a comparison of the times-to-failure for single glass fibres with those of the 0^{o} unidirectional coupons. The scatter in the data apparently falls into two classes: premature failure points which are almost certainly caused by specimen damage during handling; scatter within the main stream of the data expected from the known high coefficient of variation in the strength of commercial E-glass (79). There is good agreement between the failure times of single fibres and 0^{o} unidirectional coupons, above 0.2% initial applied strain. At lower strains the matrix resin is shown to provide some protection to the glass.

3.2.8 E-glass tows in 0.5 M sulphuric acid

To verify that Mode II failure was a laminate property and not that of the glass. Tows of E-glass were tested at nominal applied strains of 0.1%, in a similar manner to the experiments in open cells. Failure occurred within the acid by what would be considered to be a Mode I mechanism. It is noted that crystalline material is deposited in the unimmersed part of the tow. Crystalline deposits were also observed in unloaded tows of E-glass partially immersed in the acid.

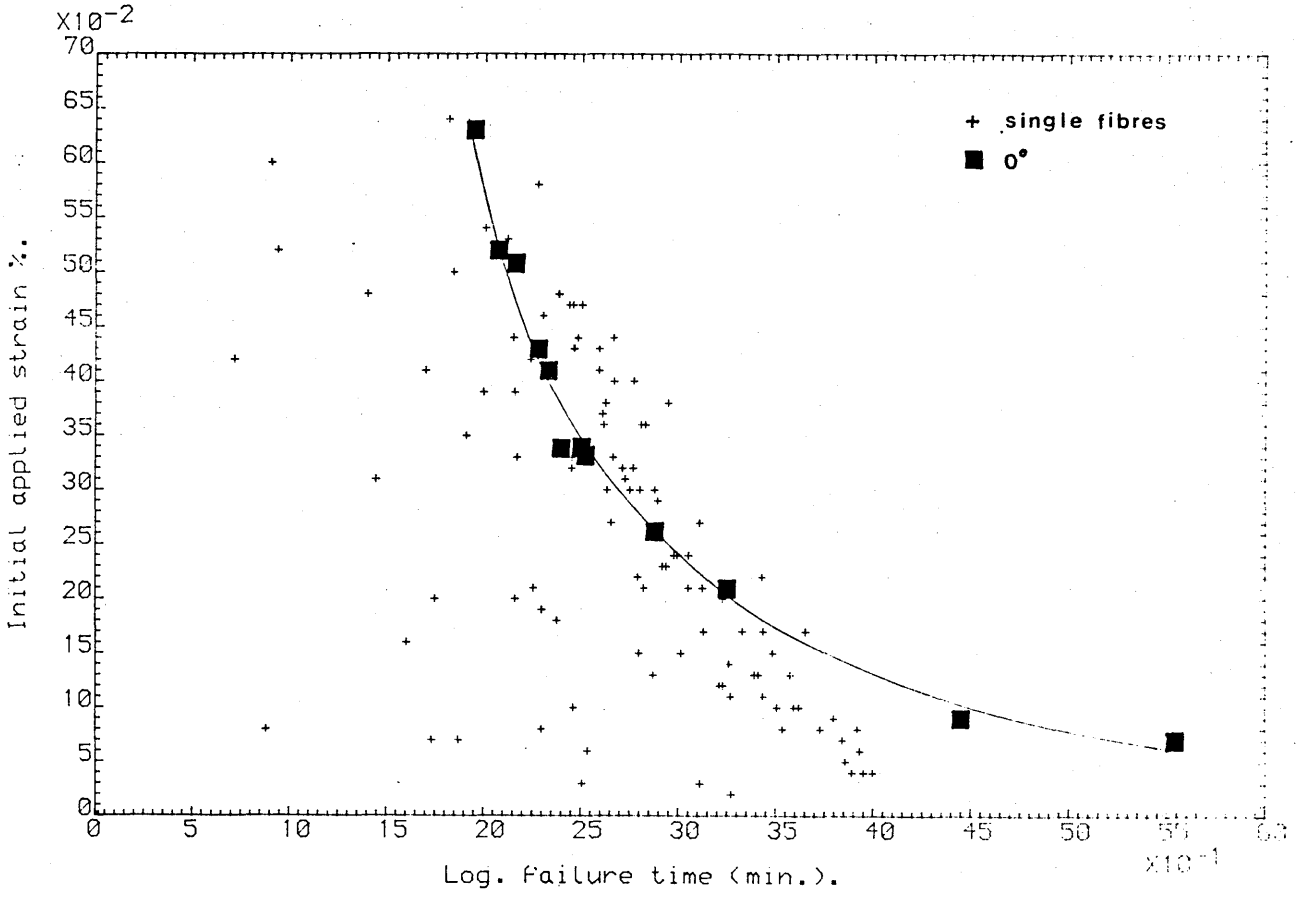

Figure 3.16 A comparison of the stress corrosion failure times for single E-glass fibres with those for 0^{o} unidirectional coupons in open-cells, at $23^{o}C$.

3.3 THERMAL STRAIN MEASUREMENTS

$0^o/90^o$ asymmetrical coupons were used to determine the thermal strain $\varepsilon_{t\ell}^{th}$ within the $0^o/90^o/0^o$ crossply laminates as described in section 2.7. It was found that the radius of curvature of a $0^o/90^o$ beam depended upon whether the beam was constrained i.e. kept flat, or allowed to bend during cooling. Keeping the coupon flat during cooling was expected to model the behaviour of a balanced crossply laminate more closely. The thermal strains calculated from the radii of curvature of both constrained and unconstrained $0^o/90^o$ coupons after cooling, are given in Table 3.8. The value of 0.22% for a crossply laminate with d = b is over twice the 0.094% reported previously (69). The larger thermal strain in these laminates accounts for the lower values of $\varepsilon_{t\ell u}$ reported in section 3.1. One effect which could be responsible for the larger values of $\varepsilon_{t\ell}^{th}$ was the rate at which the laminates were cooled. All the laminates used in this study were removed from the hot oven (+ 150^oC) and allowed to cool in air. Any increase in thermal strain on fast cooling was evaluated by placing them directly into a freezer at - 18^oC after postcuring at 150^oC. More slowly cooled laminates were left in the oven overnight. The resulting difference of 0.02% was well within experimental error and demonstrated that the higher values of $\varepsilon_{t\ell}^{th}$ could not be attributed to the rate of cooling.

In a further attempt to find the explanation for the larger thermal strain, the true softening point of the matrix,which is defined as the temperature at which the thermal strains are first built into the laminate, was determined. Thus the change in curvature as a function of temperature

was recorded in a glass fronted oven. The softening temperature was obtained by extrapolating the plot of $\Delta T(\alpha_\ell - \alpha_t)$ against T, $\Delta T(\alpha_\ell - \alpha_t)$ is directly related to the radius of curvature by equation 2.9, and the intercept on the T-axis gives the temperature at which the beam becomes flat. Figure 3.17 shows such a plot for a 150°C postcured $0^o/90^o$ unconstrained beam, and gives a softening temperature of 140°C. Therefore, the higher thermal strains in these laminates can be accounted for by a higher softening point and hence a larger cooling interval ΔT.

The relaxation of the thermal strains in crossply laminates immersed in aqueous environments, due to the swelling of the matrix resin was also investigated in a similar manner. Thus the change in curvature of an asymmetrical $0^o/90^o$ beam was monitored as a function of time. The results are shown in Figure 3.18 as a percentage retention of strain. The linearity of the plots against the square root of time implies Fickian diffusion. However a detailed investigation of the expected form of this graph was not carried out. On the other hand, the results do show that in the time periods of the stress corrosion experiments, reduction in the thermal strains present in crossply coupons is minimal.

Postcure Temperature °C	Postcure Time Hrs.	Thermal Strain $\varepsilon_{t\ell}^{th}$ Constrained Beam	Unconstrained Beam
150	3	0.22%	0.28%
200	24	0.37%	0.48%

Table 3.8 Thermal strains calculated from the radius of curvature of asymmetrical $0^{o}/90^{o}$ beams.

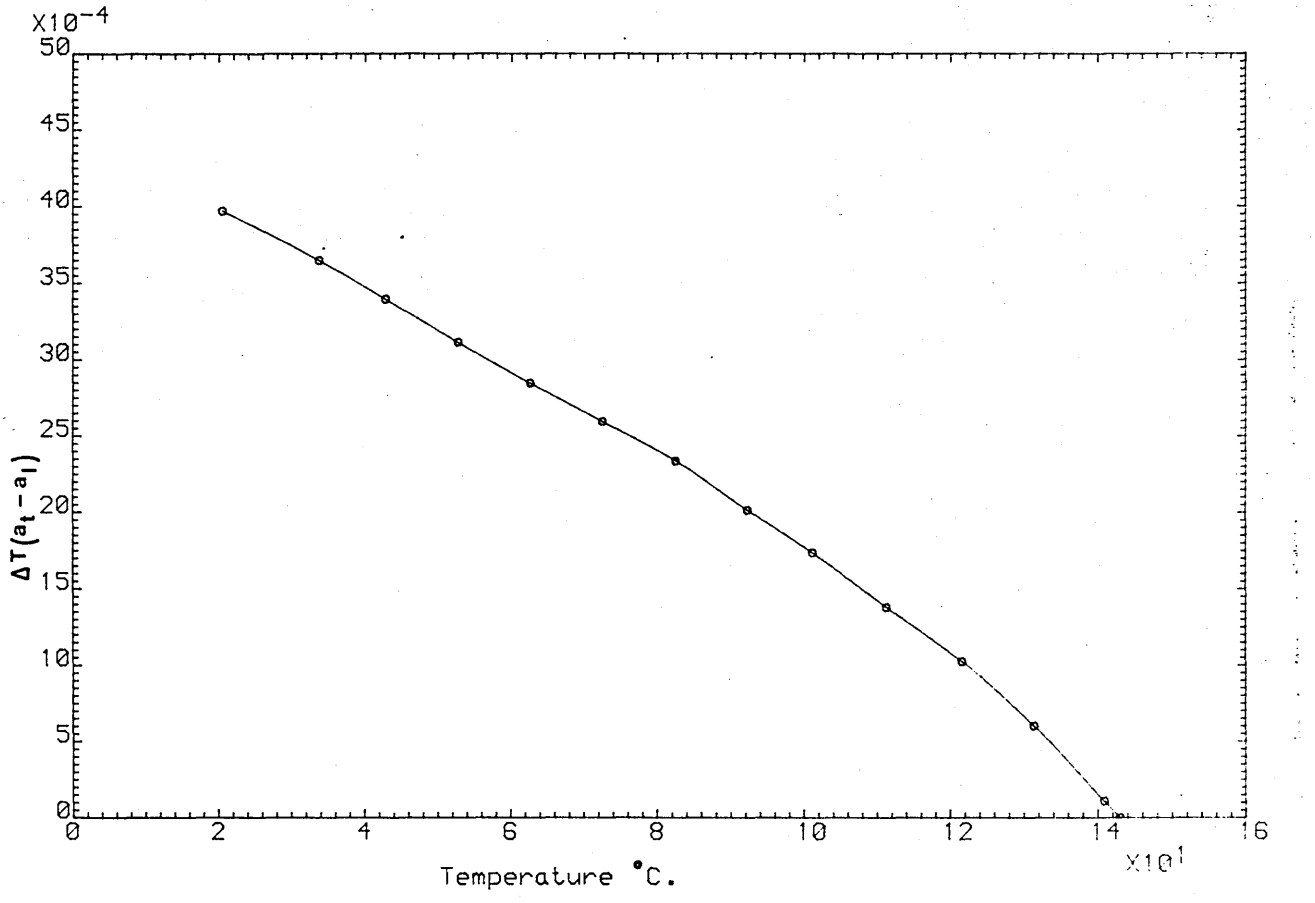

Figure 3.17 Graph of the function $\Delta T(\alpha_{\ell} - \alpha_{t})$ against T, for a $150^{o}C$ 3 hour postcured $0^{o}/90^{o}$ asymmetrical coupon, giving a predicted softening temperature of $\simeq 140^{o}C$.

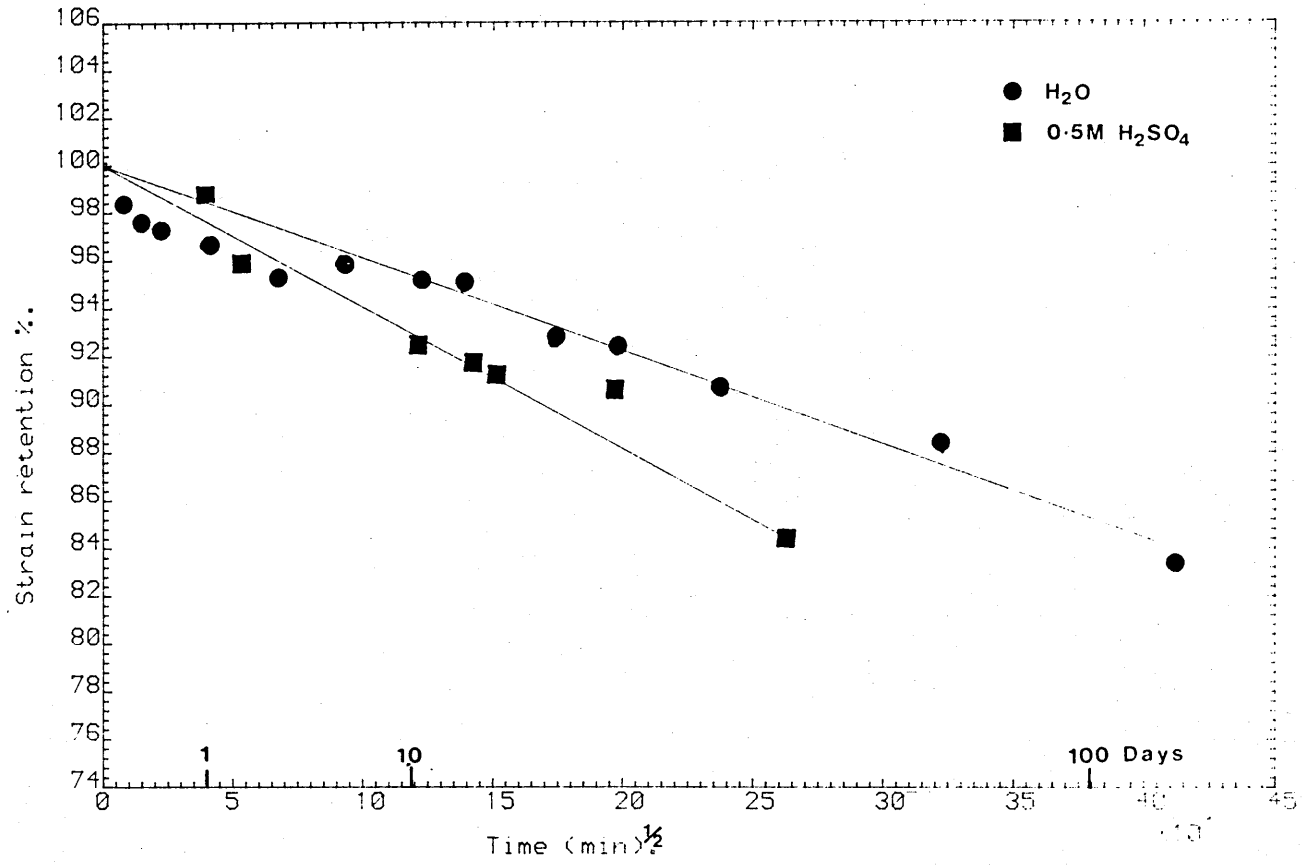

Figure 3.18 Percentage thermal strain retention as a function of time, as determined from the curvature of asymmetrical $0^{o}/90^{o}$ beams immersed in deionized water and 0.5 M aqueous sulphuric acid.

The average spacing was calculated from the photographs of the transverse cracking behaviour of $0^{o}/90^{o}/0^{o}$ crossply coupons, in and out of the aqueous environments, as follows. The number of transverse cracks were counted along one edge of the coupon only, and the average crack spacing calculated using equation 3.1. It was necessary to only count the cracks at one edge, because of their lower rate of growth in acid allowed stress relief between adjacent cracks growing from the opposite edges, as shown by the static environmental edge cracks in Figure 3.5. The total number of cracks would give an incorrectly low average, according to equation 3.1. In the case of coupons tested in air, the nearly instantaneous growth meant that the number of cracks at one edge equalled the total number present.

$$t_m = \frac{S}{(n + 1)} \qquad \ldots(3.1)$$

Where:-

t_m = Average measured crack spacing.

S = Specimen length.

n = Number of cracks.

The effect of transverse ply thickness on the crack spacing is shown in Figure 3.19. The shape of the curves is similar to that previously reported (69,80).

Since environmental edge-cracks do not form in crossply coupons under constant load at initial applied strains of less than $\varepsilon_{t\ell u}$ in deionized water, the transverse cracking behaviour under increasing strain should also be unaffected. This is confirmed by the crack spacing data given in Figure 3.20.

However when the coupons are tested in aqueous sulphuric acid, the crack spacing in both the immersed and unimmersed halves is reduced, in comparison with that in air, as shown in Figure 3.21. It is unlikely that the reduction in crack spacing for the unimmersed half is caused by the acidic vapour, because the unimmersed halves of coupons tested in both the closed and open-cells,under constant load at initial applied strains of less than $\varepsilon_{t\ell u}$, showed no inclination for edge-cracking. The few that were observed in the closed-cell can be explained by splashes of acid on filling. Thus this result indicates that the acid can be transported through the laminate during the experiment, before the coupon fails, as shown in Figure 3.23. Individual stress corrosion cracks, more typical of the 0^{o} unidirectional coupons under static load may be seen. However unlike the latter, they did not coalesce by longitudinal splitting of the 0^{o} plies. This is because of the localized additional stress placed on these plies adjacent to a transverse crack which acts to constrain individual stress corrosion cracks to growth in one plane only.

The coupons immersed in the aqueous acid without an externally applied strain, which were subsequently washed and dried (on a paper towel) prior to testing, had an intermediate reduction of the crack spacing, as shown in Figure 3.22. The significance of this result is discussed later in section 4.4.5.

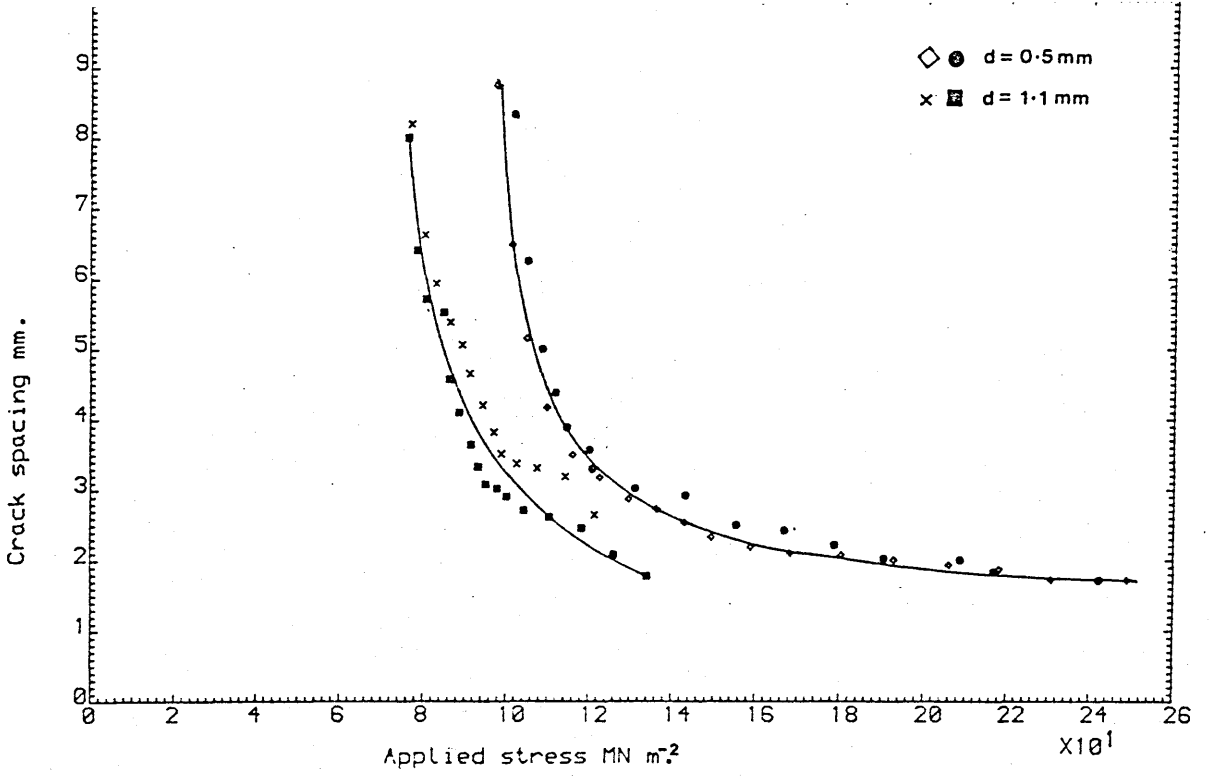

Figure 3.19 The effect of the transverse ply semi-thickness (d) on the measured average crack spacing (t_m).

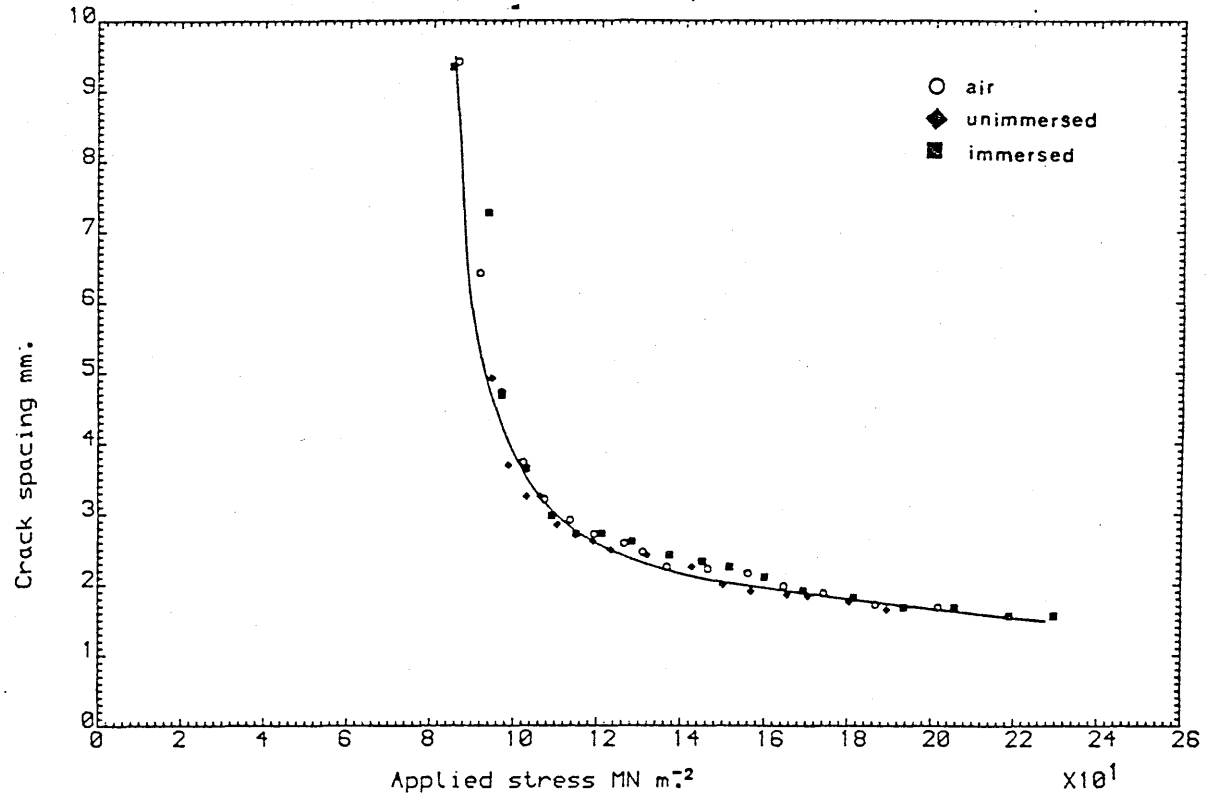

Figure 3.20 The effect of deionized water on the measured average crack spacing (t_m).

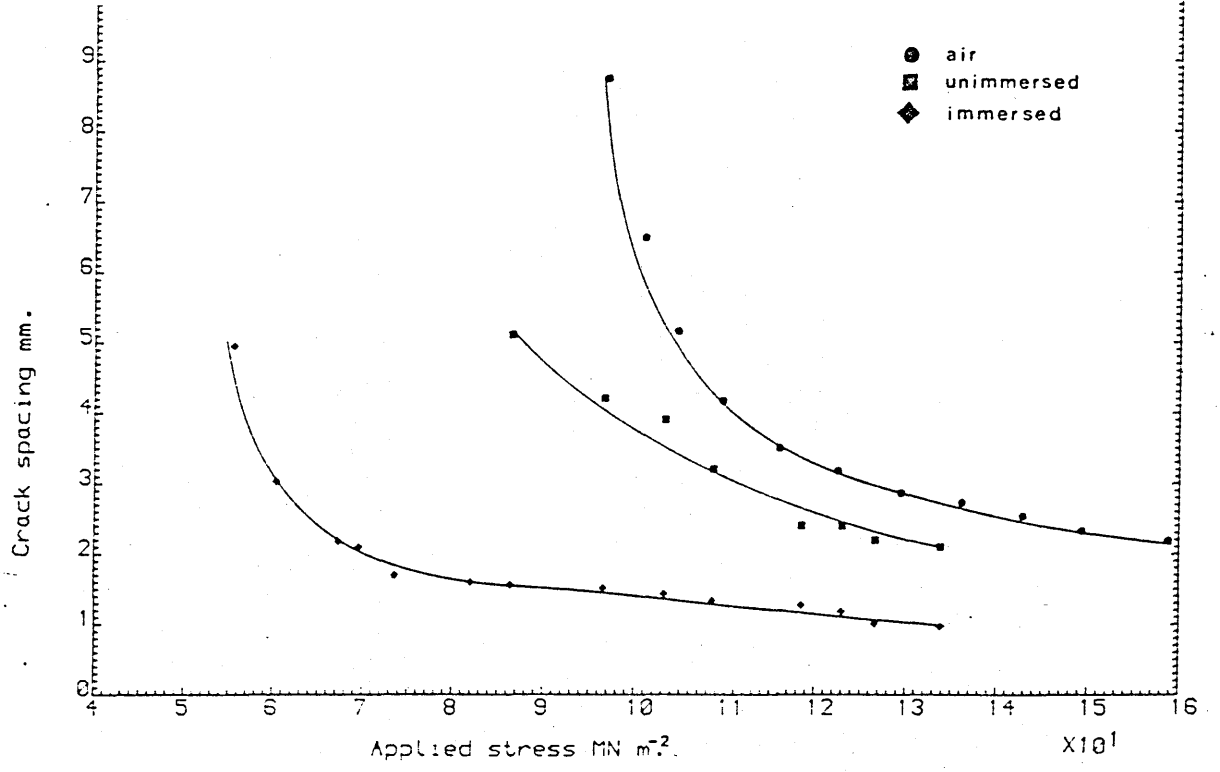

Figure 3.21 The effect of 0.5 M aqueous sulphuric acid on the measured average crack spacing (t_m).

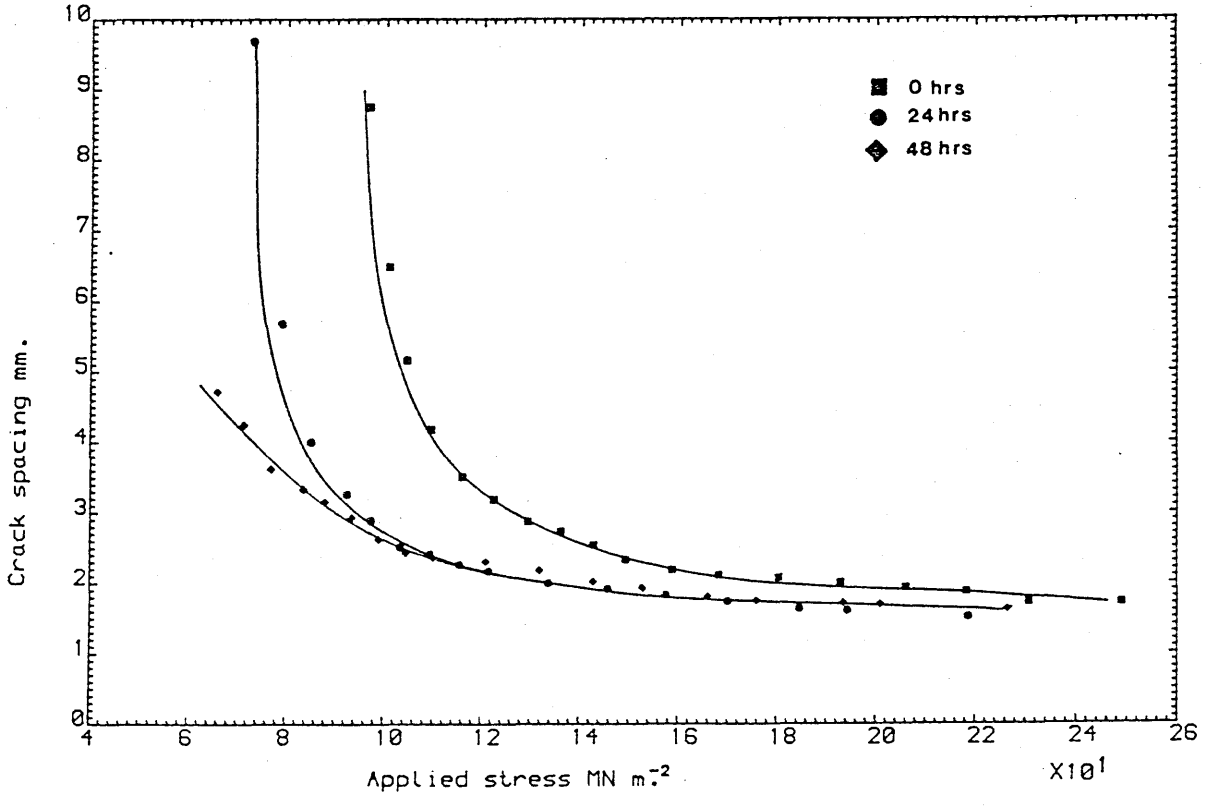

Figure 3.22 The effect of pre-immersing in 0.5 M aqueous sulphuric acid on the measured average crack spacing (t_m).

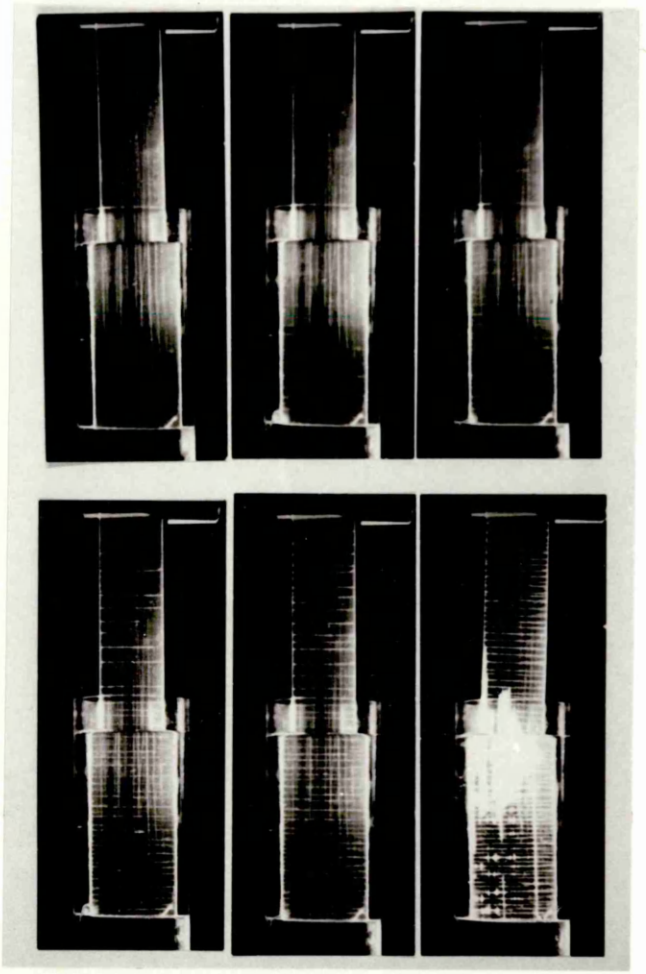

Figure 3.23 The environmental transverse cracking of a $0^{o}/90^{o}/0^{o}$ crossply coupon in 0.5 M aqueous sulphuric acid under dynamic* loading.

* CONSTANT DISPLACEMENT RATE OF 0·5 MM MIN^{-1}.

3.5 MICROSTRUCTURAL EXAMINATION OF THE STRESS CORROSION FRACTURE SURFACES

In this section examples of the microstructural morphological details of the fracture surfaces are given. The analysis of the crystalline material found in the fracture surfaces and at the edge of coupons, which failed by either a Mode II or Mode III mechanism, will be discussed separately in section 4.5.

The optical micrographs of transverse cracks and environmental edge-cracks are shown in Figure 3.24. They are clearly similar, and probably arise from the same mechanism. This is discussed further in section 4.4 where it is shown that these environmental edge-cracks are the direct result of the reduction in the transverse cracking strain by the stress corrosion of the fibre/matrix interface.

Figure 3.25 shows the stress corrosion nucleation region in a Mode II fracture surface. A similar area from a Mode I failure is shown in Figure 3.26. The size of these initiation regions varies considerably, but they are generally smaller, with larger initial applied strains. Both Figures 3.25 and 3.26 show that the fractured glass fibres are devoid of the usual river line markings, (see for example Figure 3.27). As shown in the higher magnification micrograph in Figure 3.26, the fractured fibres were found to be partially debonded. The importance of fibre debonding to the stress corrosion failure of these laminates is discussed in sections 4.4.5 and 4.5. However, very little fibre pull out was observed in these regions.

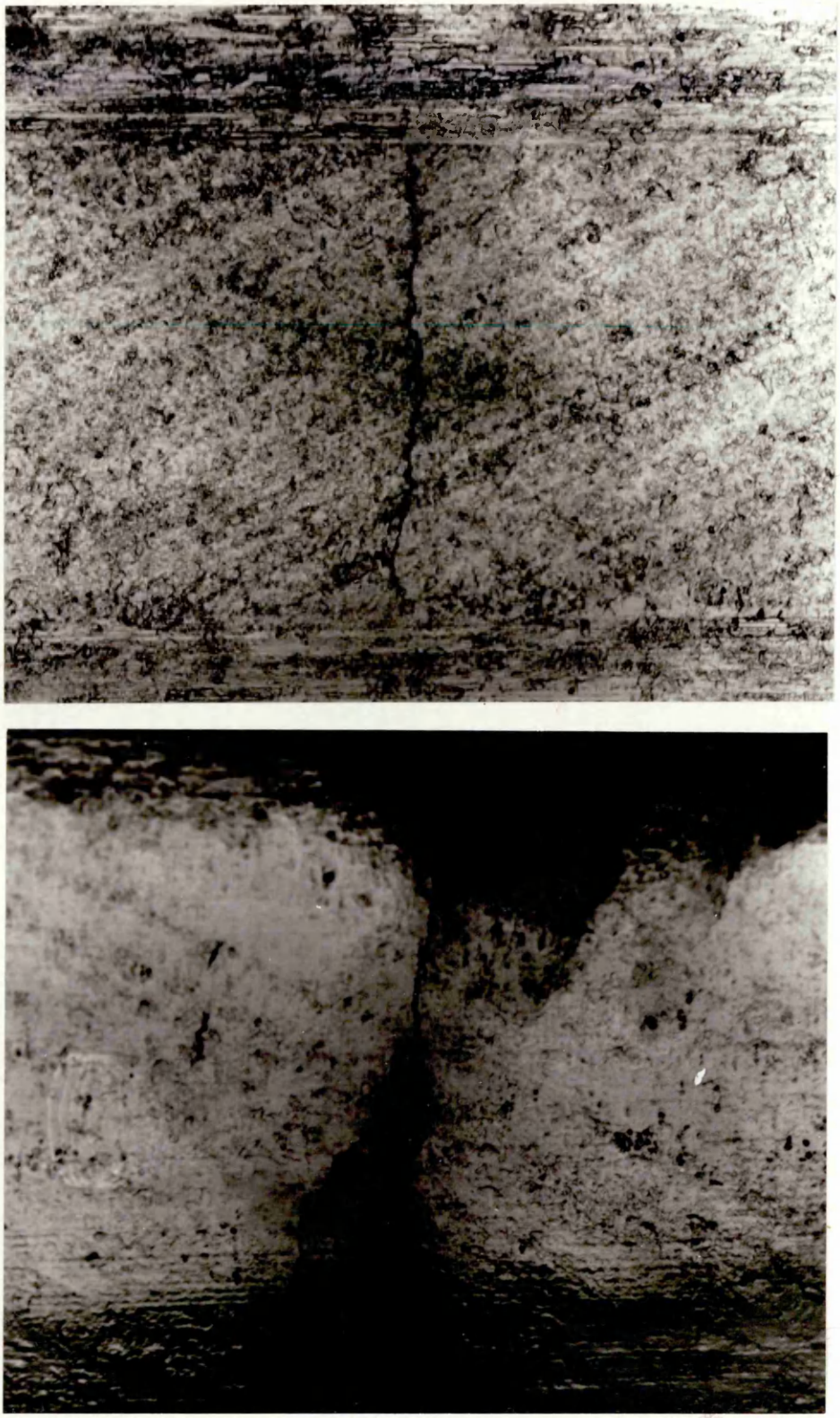

Figure 3.24 Optical micrographs of (a) transverse cracks, and (b) environmental edge cracks.

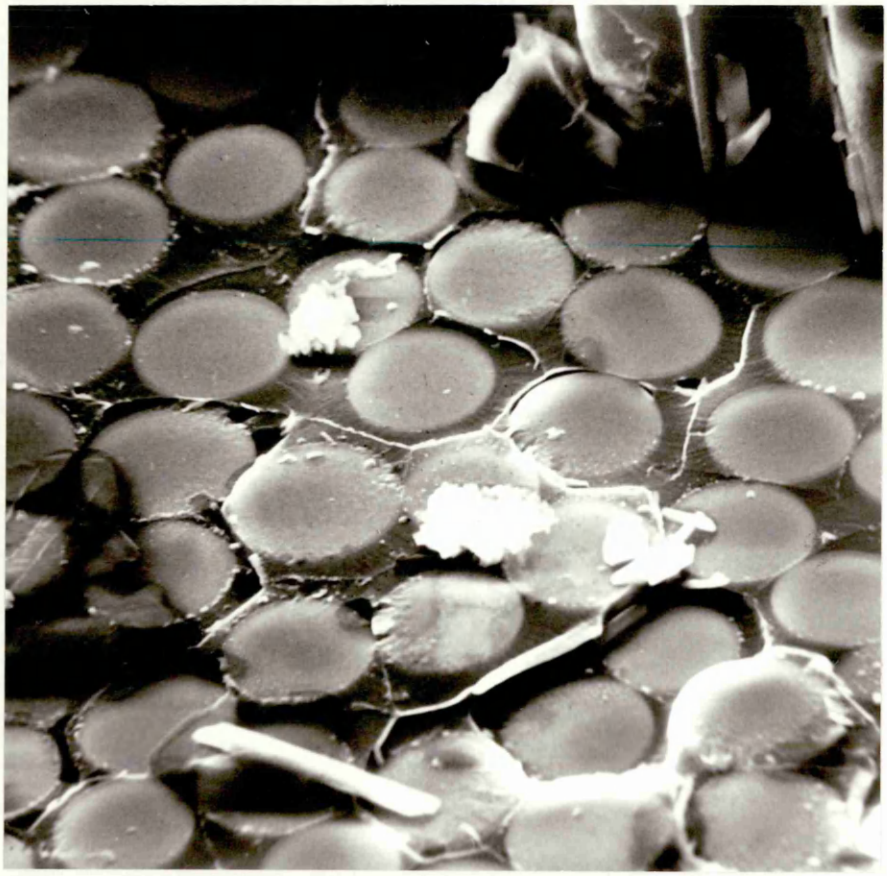

Figure 3.25 Stress corrosion nucleation region from a Mode II failure.

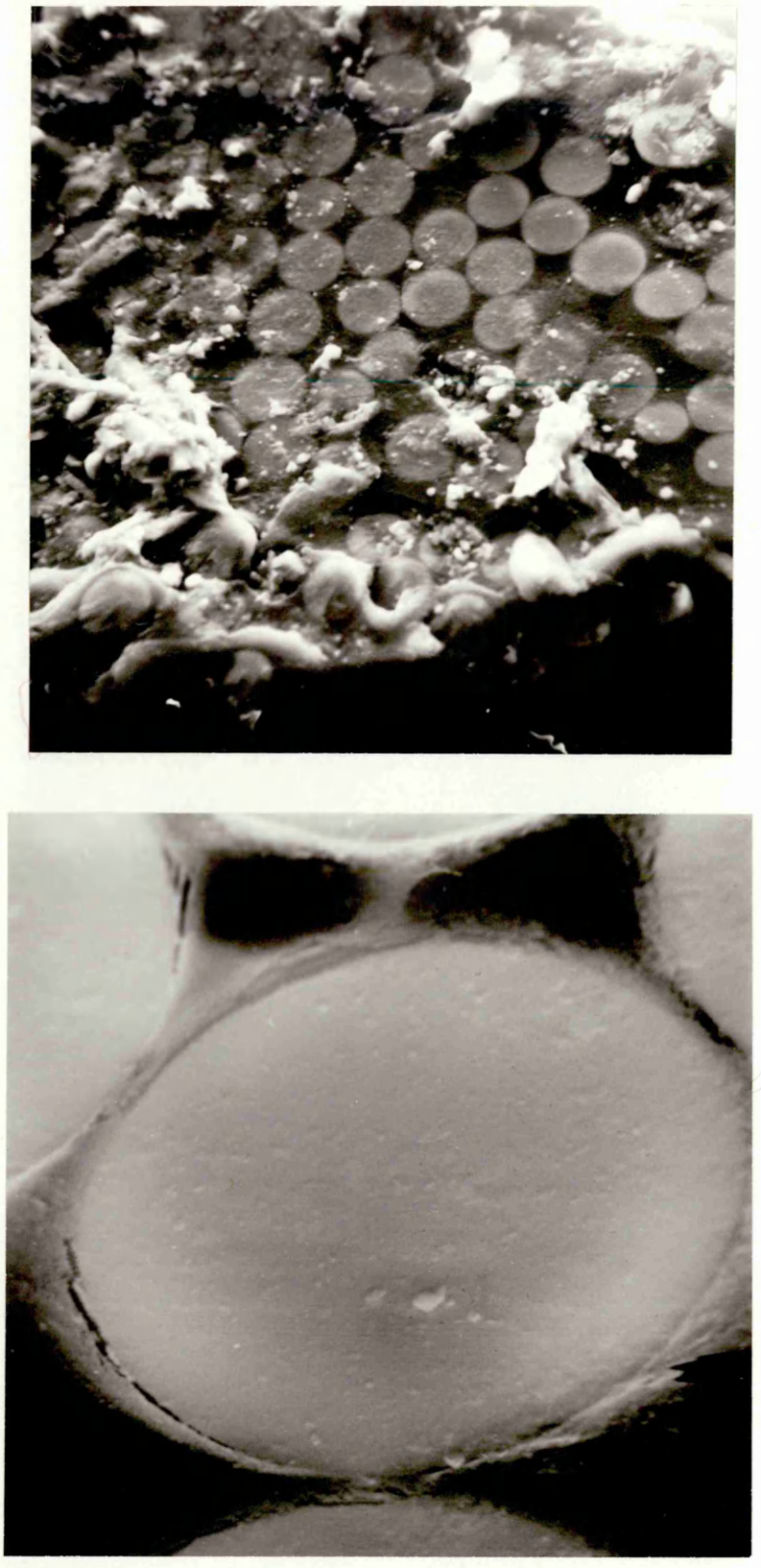

Figure 3.26 Stress corroded nucleation region from a Mode I failure, the lower micrograph shows partial debonding of the fibres.

Moving away from the stress corrosion nucleation regions, the fractured glass fibres have typical fracture markings, as shown in Figures 3.27 and 3.28. Where fracture began there is a smooth mirrored region, followed by a band of mist and then radial coarse hackle. These different regions are the result of the velocity of the crack, it is slowest in the mirrored region, and fastest in the area of coarse hackle. The appearance of these fracture markings indicates that the rate of crack growth in these fibres, is greater than that in the stress nucleation areas, where fracture of the fibres leaves them with a mirrored appearance. When fracture occurs very rapidly, forking or bifurcation of the fracture crack occurs as illustrated in Figure 3.27, giving rise to the glass segments shown in the micrograph. This only occurs when the velocity of the fracture crack approaches half the (transverse) speed of sound in the glass, and the angle of bifurcation is related to the ratio of the principal stresses (σ_y / σ_x). For low angles of bifurcation this ratio is -1, indicating that there is a considerable compressive component present. This value was obtained from a thin walled glass tube tested in torsion and not from glass fibres (81). In both Figure 3.27 and 3.28 the glass fibres are completely debonded, and there is more fibre pull-out evident than in the stress corrosion nucleation regions.

Figure 3.29 shows a low power SEM micrograph of a Mode I stress corrosion fracture of a crossply coupon. Of particular interest is the orientation of the "steps" (which appear as fine white lines in Figure 3.29) in the longitudinal ply, and which are orientated predominantly normal to the transverse ply. Figure 3.30 further illustrates these "steps" in a Mode II stress corrosion fracture. In section 4.7.1 a mechanism for the formation

Figure 3.27 Micrograph showing fracture markings on the stress corroded glass fibres.

Figure 3.28 Micrograph showing glass segments produced when bifurcation of the fracture crack occurs in the glass fibre.

of these "steps" is proposed, and in section 4.5 an explanation for the orientation of these "steps" normal to the transverse ply is given.

There was no basic morphological difference between the fracture surfaces found in Mode I and II failures. However there appeared to be more crystalline material in the Mode II fracture surfaces. Since very few spirally cracked glass fibres were seen in the fracture surfaces of all the coupons, it would appear that this phenomenon is irrelevant to the stress corrosion cracking of these laminates. Some core sheath structures, as illustrated in Figure 3.30, have been observed but these are quite rare and are believed to develop after stress corrosion failure has occurred.

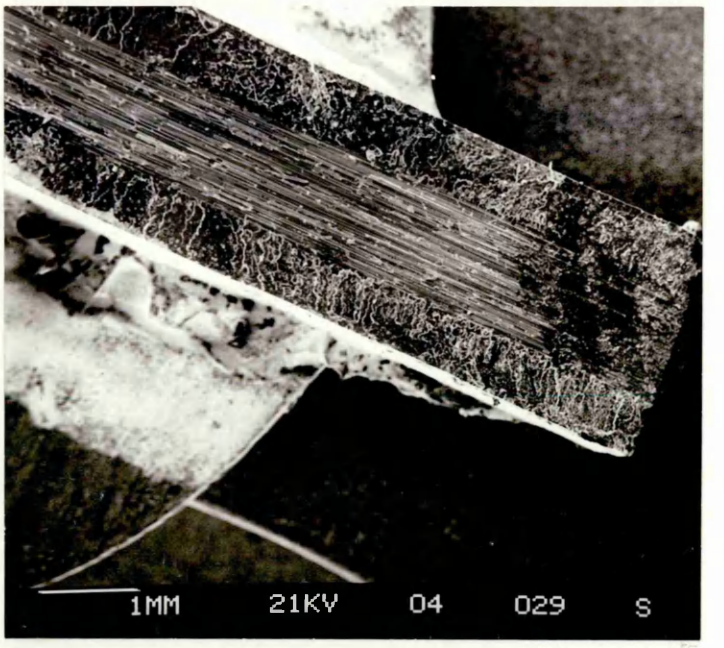

Figure 3.29 Low magnification SEM micrograph of a Mode I crossply stress corrosion failure. The fine white lines in the longitudinal ply are steps in the fracture surface, and are orientated normal to the transverse ply.

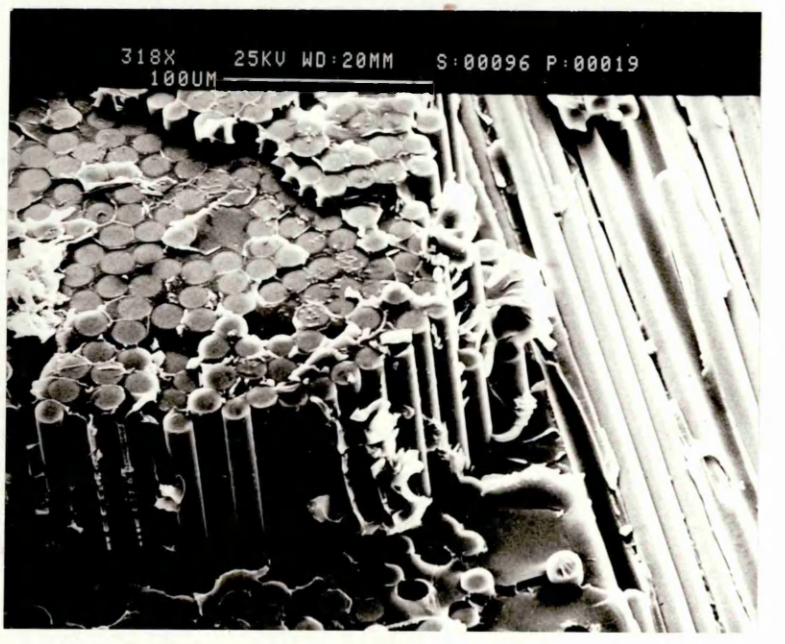

Figure 3.30 Mode II fracture surface showing steps.

CHAPTER 4 DISCUSSION

4.1 INTRODUCTION

The discussion has been divided into six sections and a brief outline of the contents of each is presented below.

The thermal strains in the longitudinal direction of the 90^{o} ply, $\varepsilon_{t\ell}^{th}$, of the crossply laminates used in this study were found to be larger than those previously reported. In section 4.2 it is shown that the laminates were fundamentally similar, but a greater degree of cure gave rise to a higher matrix softening temperature which resulted in an increased $\varepsilon_{t\ell}^{th}$. It is also shown that the thermal strains determined from the radius of curvature of unconstrained $0^{o}/90^{o}$ asymmetrical beams overestimate the magnitude of $\varepsilon_{t\ell}^{th}$ in $0^{o}/90^{o}/0^{o}$ crossply laminates, because stress relaxation has not been taken into account.

In section 4.3 the stress corrosion of E-glass fibres is considered. The previously reported core sheath structure was observed for unstressed glass fibres immersed in aqueous acid. Microprobe X-ray analysis confirmed the calcium and aluminium depletion of the sheath compared to the core of the fibre. The stress corrosion times-to-failure of single E-glass fibres are compared with those previously reported for E-glass strands.

In section 4.4 the transverse cracking behaviour of $0^{o}/90^{o}/0^{o}$ crossply laminates is considered. The Garrett and Bailey modified shear lag theory has been used to obtain the transverse ply failure strain from measurements

of the crack spacing as a function of the applied stress. In aqueous sulphuric acid the transverse ply failure strain has been shown to be reduced, suggesting that the environmental edge cracks are fundamentally the same as transverse cracks which form on loading, and that stress corrosion of the fibre matrix interface is occurring.

In the following sections the stress corrosion failures of this epoxy-glass composite system are discussed. In section 4.5, it is shown that Mode I failure is explainable in terms of the formation of environmental microcracks in the longitudinal ply, which form by the stress corrosion of the fibre matrix interface. In section 4.6, the mechanism of Mode II failure is discussed. It is concluded that at low initial applied strains, environmental debonding does not lead to microcracking. However, transport of the aqueous acid along the interfacial region to the unimmersed part of the laminate occurs, and the concentration of the glass degradation products, by the evaporation of moisture, leads to the nucleation of the failure crack.

In section 4.7, a mechanism for the formation of the "steps" observed in the stress corrosion fracture surfaces is proposed.

4.2 THE MEASURED AND PREDICTED THERMAL STRAINS

The thermal strain in a $0^o/90^o/0^o$ crossply laminate may be calculated as follows. The longitudinal and transverse linear expansion coefficients of a 0^o unidirectional lamina, α_ℓ and α_t respectively are calculated from equations 1.5 and 1.6. The theoretical thermal strain may then be calculated from these values by equations 4.1 and 4.2 (69).

$$\varepsilon_{t\ell}^{th} = \frac{E_\ell b}{E_\ell b + E_{td}} (\alpha_t - \alpha_\ell) \Delta T \qquad \ldots(4.1)$$

$$\varepsilon_{\ell t}^{th} = \frac{E_\ell d}{E_\ell b + E_{td}} (\alpha_t - \alpha_\ell) \Delta T \qquad \ldots(4.2)$$

Where:-

$\varepsilon_{t\ell}^{th}$ = Thermal strain in the 90^o ply, longitudinal direction.

$\varepsilon_{\ell t}^{th}$ = Thermal strain in the 0^o ply, transverse direction.

E_ℓ, E_t = Moduli of 0^o unidirectional laminate in the longitudinal and transverse directions respectively.

α_ℓ, α_t = Linear expansion coefficients of a 0^o unidirectional laminate in the longitudinal and transverse directions.

b = Outer ply thickness of $0^o/90^o/0^o$ crossply laminate.

d = Inner ply semi-thickness of $0^o/90^o/0^o$ crossply laminate.

ΔT = The difference between the matrix softening temperature and that at which the thermal strain is to be calculated.

The softening temperature of the laminate matrix was determined by the method described in section 3.2.4. It represents the true temperature at which thermal strains begin to develop, and was found to be 140°C, thus ΔT was known to be approximately 120°C. The modulus in the longitudinal direction, E_ℓ was calculated from the rule of mixtures, equation 4.3 The transverse modulus, E_t was taken as one third of the longitudinal modulus (69). The other values used in the calculation of the longitudinal and transverse expansion coefficients are shown in Table 4.1.

$$E_\ell = V_f E_f + (1-V_f) E_m \qquad \ldots(4.3)$$

The calculated value (for d=b, $V_f = 0.55$) of $\varepsilon_{t\ell}^{th}$ obtained was 0.28% and agrees with that determined from measurements of an unconstrained $0^o/90^o$ beam, as shown in section 3.3. Recently further research has shown that good agreement can be obtained over the whole of the cooling range for this composite system (82). Since such a good agreement between experiment and theory was achieved, an estimation of ΔT for Parvizi's laminates can be made. It is believed that Parvizi calculated the thermal strains from the curvature of a constrained beam. Thus 0.1% strain in a constrained beam would be equal to about 0.13% strain in an unconstrained beam. Using the values in Table 4.1, ΔT is estimated to be 90°C, thus the softening temperature was 100-110°C. The lower matrix softening temperature of her laminates is a result of a lower concentration of the curing catalyst BDMA (0.5phr). A softening temperature of 98°C is quoted in the literature for formulations with 90phr NMA and 1.0phr BDMA postcured at 150°C (81). This lower matrix softening temperature is further supported by her observation of the rebonding of the glass fibres in

previously stress whitened coupons after annealing at 100°C (69,83).

It is apparent that whilst a first approximation of the value $\varepsilon_{t\ell}^{th}$ may be obtained using equations 4.1 and 4.2, the effects of stress relaxation, as shown by the difference in the value of $\varepsilon_{t\ell}^{th}$ for a constrained and unconstrained beam in Table 3.8, need to be taken into consideration otherwise the thermal strain in the $0^{o}/90^{o}/0^{o}$ composite is over estimated.

Similar theoretical thermal strain calculations for a polyester-glass laminate were also found to give unsatisfactory predictions, although more accurate values of ΔT were known. Subsequently it has been shown that small quantities of water greatly enhanced the expansion coefficient of the polyester resin. Thus the use of the dry matrix expansion coefficient to predict the thermal strains present in normally "wet" laminates leads to a considerable under prediction of these strains (82). This enhancement of the expansion coefficient of the matrix is not observed for this epoxy resin system.

	Epoxy Resin (Matrix)	E-Glass (Fibre)
Young's Modulus GN m^{-2}	3.5	76.0
Poisson's Ratio	0.38	0.2
Expansion Coef. 10^{-6} K^{-1}	60.0	4.9

Table 4.1 Matrix and glass properties taken from reference 66.

4.3 STRESS CORROSION OF E-GLASS FIBRES

During the acidic corrosion of E-glass fibres previous workers have reported:

(1) The spiral or multiple cracking of an outer sheath (21,44).

(2) The leaching of metallic ions from the fibres by the aqueous acids. Microprobe examination has shown that both calcium and aluminium are preferentially leached out of the surface to form an outer sheath to the fibre leaving an unaffected central core (21).

Both these phenomena have been observed for unstressed E-glass fibres immersed in aqueous sulphuric acid, prior to using microprobe analysis for the examination of the stress corroded fracture surfaces. Figure 4.1 shows the spiral cracking phenomenon which is found in the majority of the fibres after a tow has been immersed in aqueous sulphuric acid. Figure 4.3 gives a comparison between the microprobe analyses of uncorroded and corroded fibres. The reduced height of both the aluminium and calcium peaks for the corroded fibre is evident. The sulphur peak found for the corroded fibre is a result of reaction with sulphuric acid and probably indicates the presence of calcium sulphate. Thus the reduction of the calcium and aluminium peaks in the X-ray spectra can be used to estimate the degree of acidic corrosion of the glass.

There is little published work on the stress corrosion of E-glass in 0.5 M sulphuric acid. Metcalfe et al (12,44) studied standard and modified

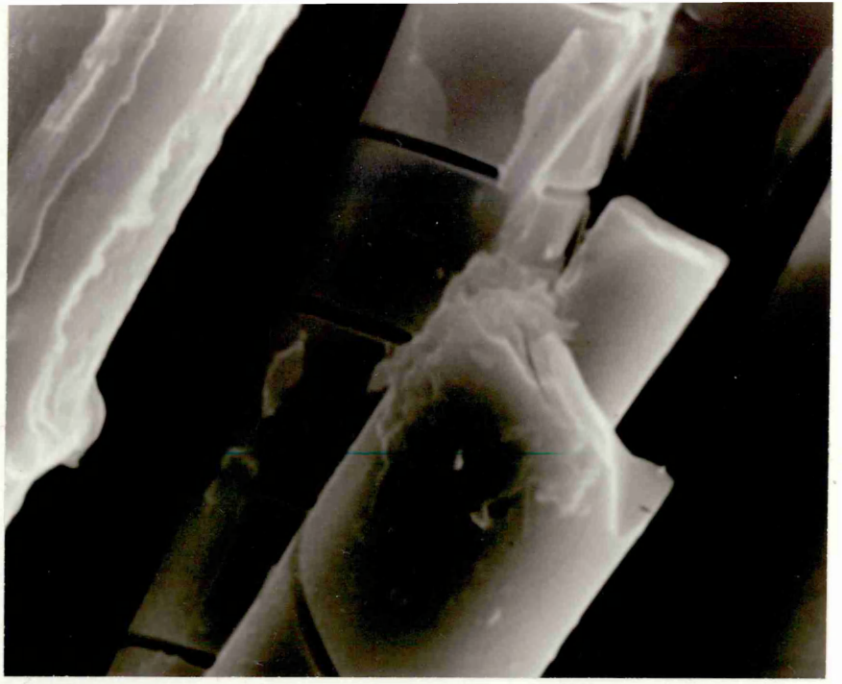

Figure 4.1 E-glass fibres showing "spiral cracking" after immersion in 0.5 M aqueous sulphuric acid

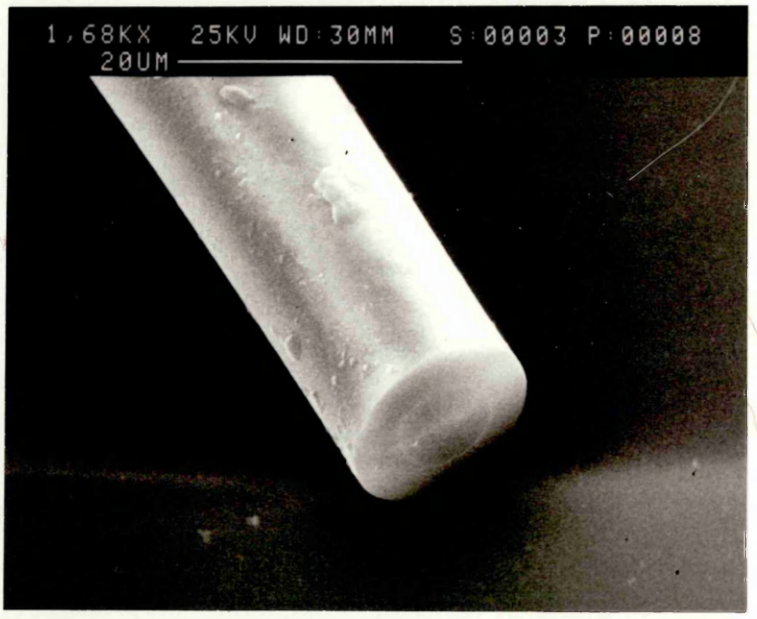

Figure 4.2 Stress corroded fracture surface of an E-glass fibre showing core sheath structure.

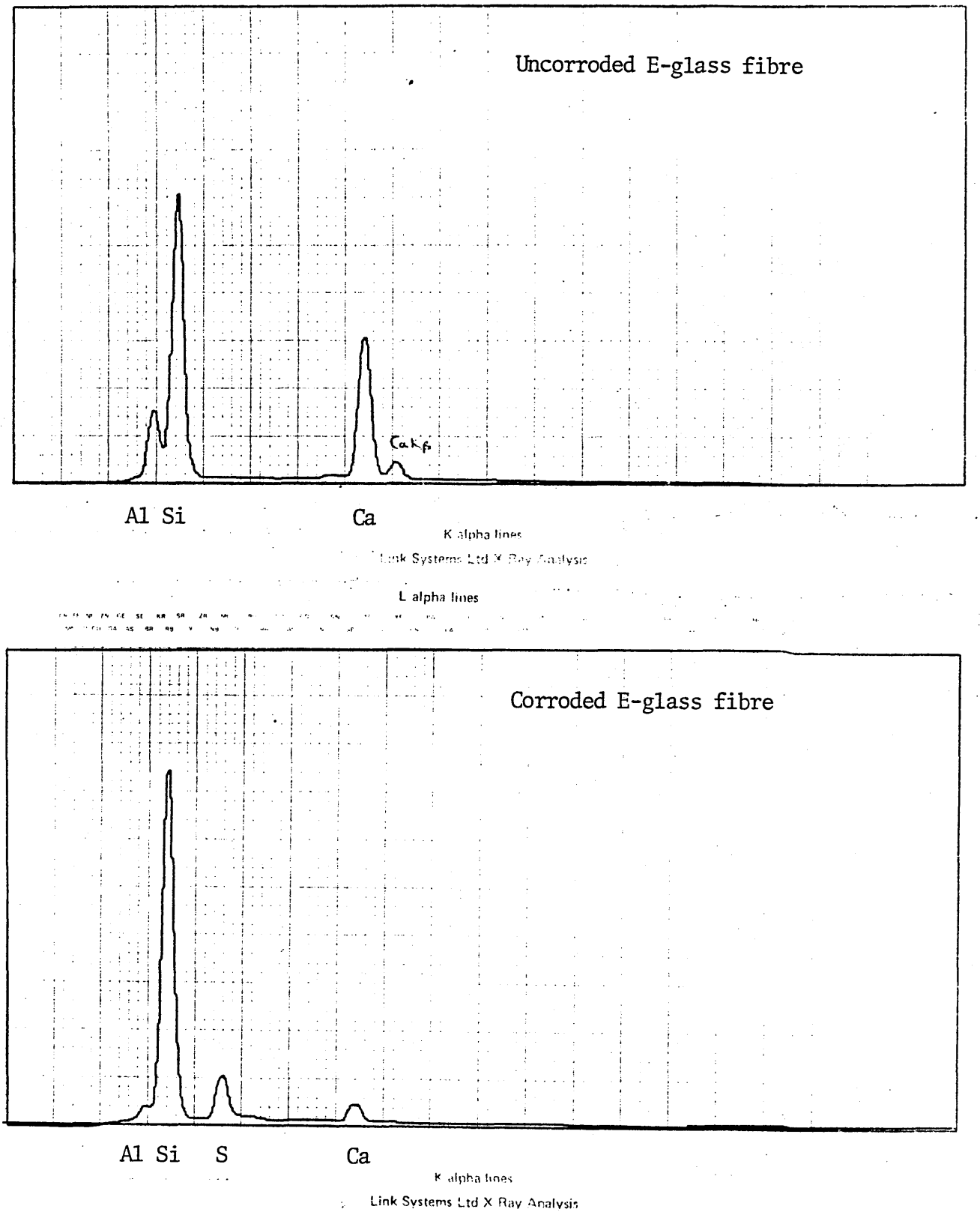

Figure 4.3 A comparison of the microprobe analysis of uncorroded and corroded E-glass fibres (0.5 M H_2SO_4).

E-glasses in solutions of various pH, but comparison of the results given in Figure 3.16 with their results is difficult because they used a simulated static fatigue technique, which represents high initial strains and gives failure times of 50 seconds in hydrochloric acid of pH=2. Roberts (7) presented the results for the stress corrosion of E-glass tows but he did not report the applied strain (or stress) at which the experiments were carried out. Scrimshaw (24) also presented stress corrosion data for E-glass strands, mostly in 2 M sulphuric acid, and a comparison between his data and the times-to-failure of the E-glass filaments is shown in Figure 4.4. It is noticeable that the slope of his data is less than that of the Silenka fibres, although at low applied strains the failure times are similar. His findings that the failure times in 2 M and 0.5 M sulphuric acid are similar excludes acid strength as the explanation. One possibility is a different glass composition, since he tested fibres manufactured by Pilkington Bros. More recent experiments however have demonstrated that both Silenka and Pilkington single glass fibres have statistically identical failure times (85). It seems more likely that there is either a bundle effect or a larger error in the applied strains reported by Scrimshaw.

Examination of the stress corroded fibre surfaces by SEM, showed a smooth featureless fracture, as shown in Figure 4.2, and similar to those found in GRP stress corrosion surfaces. Since GRP stress corroded fracture surfaces show very few and often no spiral cracks or core-sheath structures, in comparison with unstressed tows of E-glass, it is concluded that this phemomenon is not important in the stress corrosion failure of glass under external applied loads. The core-sheath structure shown in Figure 4.2 is

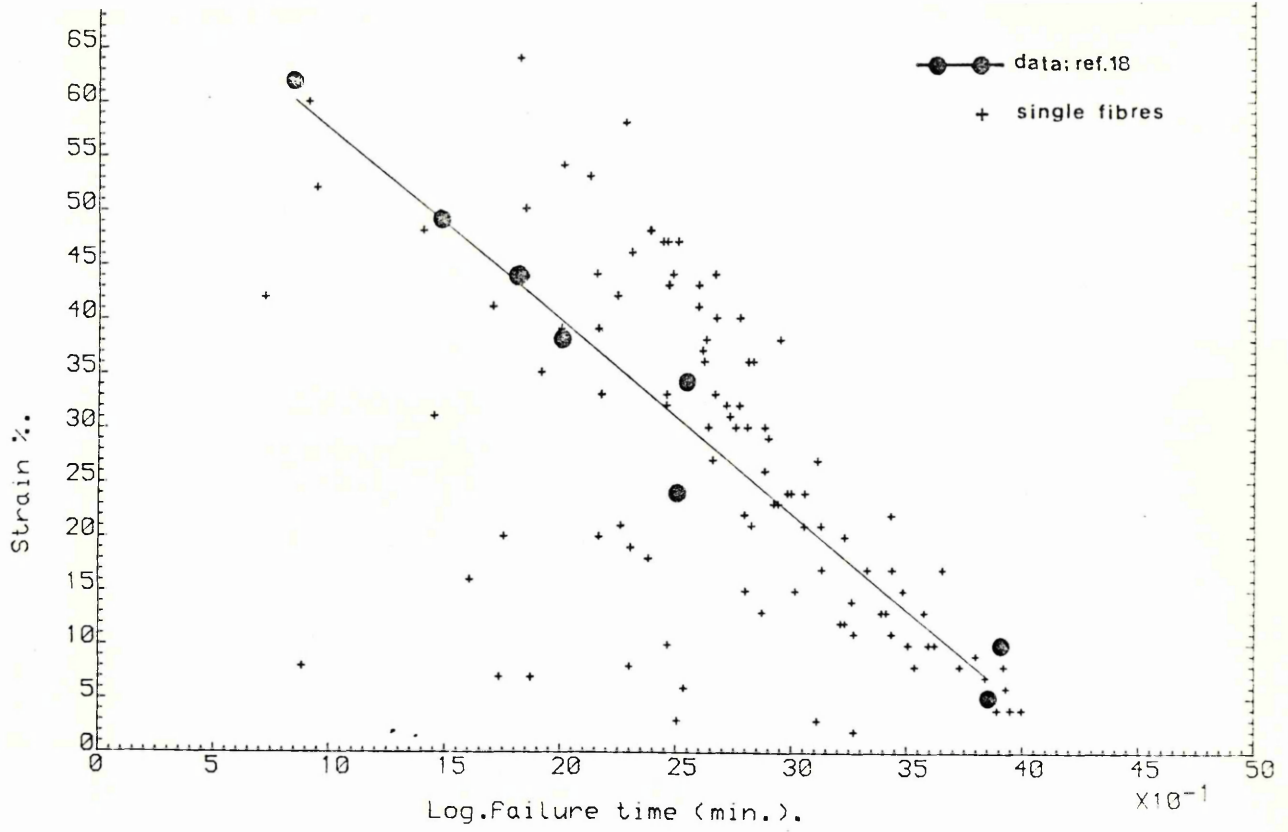

Figure 4.4 Comparison of the stress corrosion failure times of single E-glass fibres (this study) with E-glass strands, reference 24.

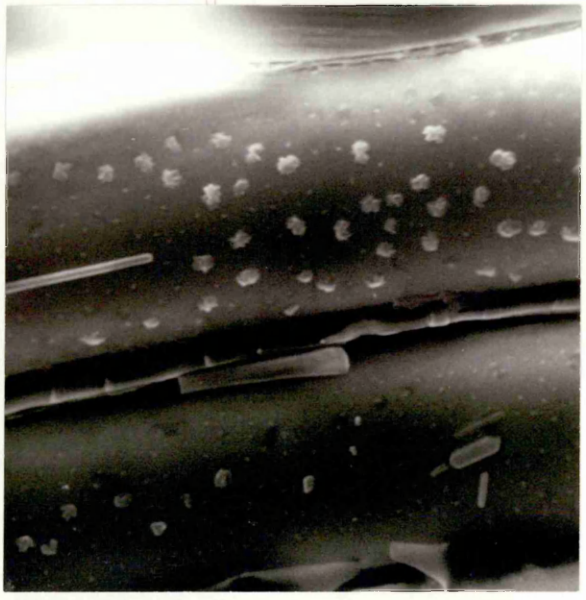

Figure 4.5 SEM micrograph of stress corroded glass in a Mode I fracture surface showing surface deposites.

believed to occur by corrosion of the glass after stress corrosion fracture. However the implication of spiral cracking is that the filaments have tensile stresses in the outer sheath, and compressive stresses in the core. These are neutralised under an applied load, and a stress corrosion crack can then run through the complete fibre.

SEM examination of GRP fracture surfaces has revealed glass covered in small particles, as shown in Figure 4.5. The exact nature of these has not yet been determined since they are too small for microprobe analysis, and practical difficulties have precluded their identification by scanning Auger spectroscopy. At present, it can only be speculated that these are some form of corrosion product, since they are not present on the virgin fibres. Similar surface marks for fibres immersed in both boiling water and alkali solutions have been reported by Barker and Bott (45). Thus the stress corrosion cracking of glass fibres appears to involve a stress enhanced chemical process which needs further study.

4.4 THE ENVIRONMENTAL TRANSVERSE CRACKING OF $0^{o}/90^{o}/0^{o}$ CROSSPLY LAMINATES

4.4.1 Introduction

It was shown in section 3.2 that $0^{o}/90^{o}/0^{o}$ crossply coupons were prone to environmental edge-cracking in the presence of an aqueous acid. Furthermore in section 4.5 it will be shown that these edge-cracks behave similarly to transverse cracks and transfer the load to the longitudinal plies, resulting in equivalent Mode I failure times of 0^{o} unidirectional and $0^{o}/90^{o}/0^{o}$ crossply coupons. In addition optical micrographs of transverse and environmental edge-cracks appear identical (section 3.5). Therefore it follows that the edge-cracks may result from a reduction in the transverse failure strain, ε_{tu} in the presence of the environment.

The conventional method of measuring the failure strain of the transverse ply ε_{tu}, is to add the first transverse cracking strain $\varepsilon_{t\ell u}$, to the value of the thermal strain $\varepsilon_{t\ell}^{th}$. However it was considered that the use of $\varepsilon_{t\ell u}$ as a measure of ε_{tu} would not be precise enough because the first transverse crack probably results from a gross edge or laminate defect, and will not be representative of the transverse ply as a whole. A similar view has been expressed by Garrett and Bailey (80), and Parvizi (69) who observed, that transverse cracks were always initiated in the cut edge of specimens polished on one edge only.

Furthermore a decrease in $\varepsilon_{t\ell u}$ may not be the result of an overall decrease in ε_{tu}, but the initiation of cracks along the edge of the coupon at positions dependent upon the ease of entry of the aqueous acid. Thus the cracking behaviour in the environment had to be shown to be fundamentally similar to that in air.

It was considered that a visual comparison of the graphs of crack spacing, t_m against applied stress σ_a, as shown in Figures 3.19-3.22, was insufficient proof that the cracking behaviour was similar (except for the case of deionized water where no effect was observed as shown in Figure 3.20). Therefore it was decided to estimate ε_{tu} from the crack spacing data using the modified shear lag theory of Garrett and Bailey (80). It is not proposed to describe the theory completely since a full description is given elsewhere (86). However a broad outline is presented to enable its use and limitations to be appreciated.

4.4.2 The Garrett and Bailey Modified Shear Lag Theory

Basically the theory states that an additional stress $\Delta\sigma_0$ is placed upon the adjacent longitudinal plies when a transverse crack forms. If the plies are assumed to be elastically bonded, then the magnitude of the stress transferred back into the transverse ply, $\Delta\sigma$ is a function of distance y from the crack and is given by equation 4.4.

$$\Delta\sigma = \Delta\sigma_0 \exp\ (-\phi^{\frac{1}{2}} y) \qquad \ldots(4.4)$$

Where:-

$$\phi = \frac{(E_c\ G_t)}{(E_\ell\ E_t)} \cdot \frac{(d + b)}{(d^2\ b)} \qquad \ldots(4.5)$$

E_c = Young's modulus of a $0^o/90^o/0^o$ crossply laminate.

E_ℓ = Young's modulus of unidirectional plies parallel to the fibres.

E_t = Young's modulus of unidirectional plies perpendicular to the fibres.

G_t = Transverse ply shear modulus.

b = Outer ply thickness, (see Figure 2.14).

d = Inner ply semi-thickness, (see Figure 2.14).

Garrett and Bailey derived equation 4.6 to predict $\Delta\sigma_0$ when moving from a crack spacing of 2t to t.

$$\Delta\sigma_0 = \sigma_{tu} \frac{d}{b} \{(1 + \exp\ (-\phi^{\frac{1}{2}}\ 2t) - 2 \exp\ (-\phi^{\frac{1}{2}}\ t)\}^{-1} \qquad \ldots(4.6)$$

Where:-

σ_{tu} = The transverse ply failure stress.

t = Crack spacing.

$\Delta\sigma_0$ is related to the applied stress σ_a according to equation 4.7.

$$\Delta\sigma_0 = \sigma_a\left(\frac{b + d}{d} - \frac{E_\ell}{E_c}\right) \qquad \ldots(4.7)$$

Equation 4.6 predicts discrete jumps in the crack spacings. If the first crack occurs midway in a specimen of length S, then the cracking sequence will be given by equation 4.8.

$$t = \frac{S}{2^r} \qquad \ldots(4.8)$$

Where:-

$r = 1,2,3....$

Figure 4.6 is taken from reference 80 and shows the predicted crack spacings obtained from equation 4.6. At any applied stress and from any initial position of the first crack, the crack spacing will lie between the bounds 2t and t. However, experimentally the average crack spacing, given by equation 3.1 does not follow the predicted stepped curve, but lies on a smoother curve, and it has been shown theoretically that providing the stress transfer length is small compared to the specimen length, then the average crack spacing is related to lower bound t in Figure 4.6 by equation 4.9 (87).

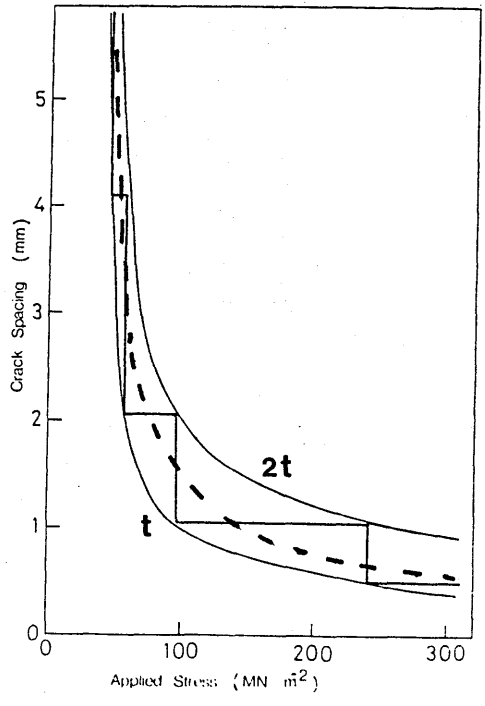

Figure 4.6 Theoretical crack spacing as a function of applied stress as predicted by equation 4.6. taken from reference 80.

$$t_a = 1.337\ t \qquad \ldots(4.9)$$

Where:-

t_a = Theoretical average crack spacing.

t = Crack spacing, lower bound in Figure 4.6.

4.4.3 The use of the Garrett and Bailey equation for predicting ε_{tu} from crack spacing data

Two separate methods have been used to estimate the transverse ply failure strain ε_{tu} from measurements of average crack spacing (t_m) at different applied stresses σ_a. Note these predicted values do not contain the thermal strain ($\varepsilon_{t\ell}^{th}$).

METHOD 1

ε_{tu} is obtained directly from equation 4.6 providing ϕ, t and $\Delta\sigma_0$ are known. ϕ can be calculated from equation 4.5 where the only unmeasured parameter, G_t was taken as 5 ± 0.5 GN m^{-2}. Garrett and Bailey, calculated this value for polyester glass laminates from the Tsai-Halpin equation (88). A value of 5.12 GN m^{-2} was computed from the same equation by Parvizi (69) for epoxy/glass laminates similar to those used here. Assuming that $t_m = t_a$ then t values can be computed from equation 4.9. For each cracking pattern the additional stress on the longitudinal ply $\Delta\sigma_0$ can be obtained from σ_a by equation 4.7.

The transverse failure strains predicted by this method will be referred to as $\varepsilon_{tu(1)}$.

Figure 4.7 shows a graph of $\varepsilon_{tu(1)}$ against t, for the data used previously in Figure 3.19 curve (a). A steady rise in $\varepsilon_{tu(1)}$ is predicted until the crack spacing has decreased to approximately 5 mm., this is then followed by a rapid fall of $\varepsilon_{tu(1)}$ with further decrease in the crack spacing. The implications of this behaviour will be discussed in section 4.4.4.

METHOD 2

Estimations of both ε_{tu} and ϕ may be obtained from equation 4.6, by rearranging it as follows:-

Let
$$X = \frac{b + d}{b} - \frac{E_\ell}{E_c} \qquad \ldots(4.10)$$

$$\psi = \frac{X}{\varepsilon_{tu} E_t \, d/b} \qquad \ldots(4.11)$$

Using equation 4.7 to replace σ_0, equation 4.6 may be rewritten;

$$\sigma_a \psi = (1 + e^{-\phi^{\frac{1}{2}} 2t} - 2e^{-\phi^{\frac{1}{2}} t})^{-1} \qquad \ldots(4.12)$$

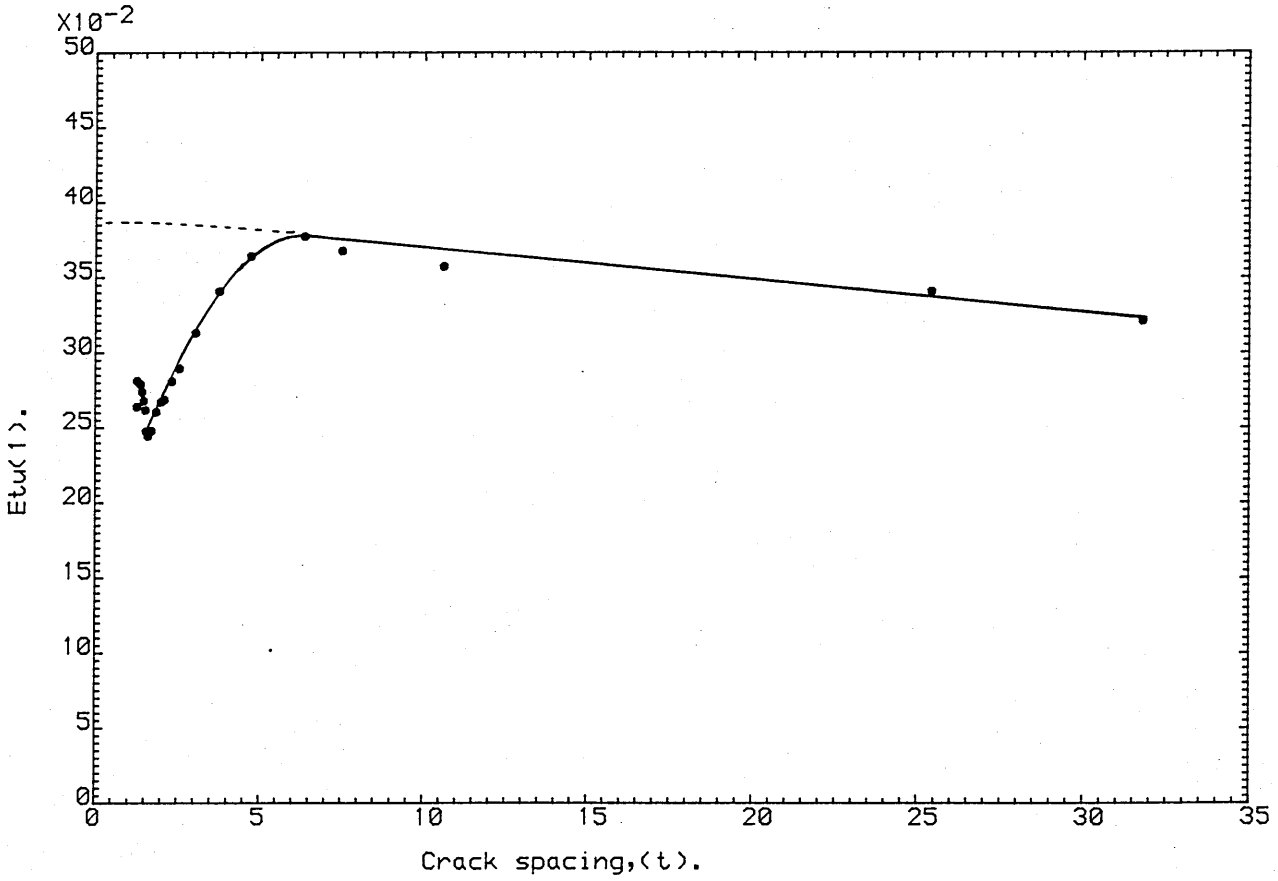

Figure 4.7 The transverse ply failure strain $\varepsilon_{tu(1)}$ as a function of crack spacing (t) for the data shown previously in Figure 3.19 curve ◆.

Let $Z = e^{-\phi^{\frac{1}{2}}t}$, equation 4.12 may then be rewritten,

$$\frac{1}{\sigma_a \psi} = 1 + Z^2 - 2Z = (1 - Z)^2 \qquad \ldots(4.13)$$

Equation 4.13 may be solved either quadatically or as given below.

$$\frac{1}{(\sigma_a \psi)^{\frac{1}{2}}} = (1 - Z) \qquad \ldots(4.14)$$

Resubstituting for Z, taking logs, and solving for t gives,

$$t = \frac{-1}{\phi^{\frac{1}{2}}} \ln (1 - 1/(\sigma_a \psi)^{\frac{1}{2}}) \qquad \ldots(4.15)$$

t is related to t_m as before, by equation 4.9, thus by plotting t against $\ln (1 - 1/(\sigma_a \psi)^{\frac{1}{2}})$, straight lines of slope $- 1/\phi^{\frac{1}{2}}$ should be obtained. A direct solution of equation 4.15 is not possible since ψ in equation 4.11 contains ε_{tu}. However, a solution was obtained by determining the correlation of t against $\ln (1 - 1/(\sigma_a \psi)^{\frac{1}{2}})$ for incremental steps in ε_{tu}. The value of ε_{tu} which produced the highest correlation was taken to be the failure strain of the transverse ply, and designated $\varepsilon_{tu(2)}$. The value of ϕ obtained from the slope will be distinguished thus $\phi_{(2)}$. The regression of t against $\ln (1 - 1/(\sigma_a \psi)^{\frac{1}{2}})$ was calculated by the method of least squares, using a stepwise incremental increase in the value of ε_{tu} of 0.0001. The procedure was carried out on the University Prime 750 computer. The results of this analysis, for the same data as in Figure 3.19 curve ◆ are shown in Table 4.2.

To eliminate the effect of the larger crack spacing, the results for each column were calculated as follows. The first column used all the crack spacing data, for the second column the largest crack spacing value was eliminated prior to calculation of the $\ln(1 - 1/(\sigma_a\psi)^{\frac{1}{2}})$ values, for the third column, the top two values were eliminated, and so on for each of the columns in Table 4.2.

4.4.4 Discussion of predicted values of ε_{tu}

Both methods predict an increase in the transverse failure strain ε_{tu} with decreasing crack spacing until $t \simeq 5$ mm, which can be explained in terms of random cracking at defects. The initial transverse cracks will remove the severest defects so that the average value of ε_{tu} rises. If this behaviour continued throughout the cracking process ε_{tu} would continue to rise, following the dashed curve shown in Figure 4.7 and become assymptotic at a value of ε_{tu}, which represented the failure stress of a defect free transverse ply.

Examination of equation 4.4 which is shown graphically in Figure 4.8, illustrates the rapid transference of the stress back into the transverse ply. For laminates where d = b, 95% of $\Delta\sigma_0$ has been transferred back within 2 mm, and for laminates where d = 2b a similar proportion is transferred back within 3.5 mm. If we consider the build up of the stress in the transverse ply between two cracks, then at spacings of greater than twice these values, a "plateau" will exist, as illustrated in Figure 4.9 where the variation in $\Delta\sigma_0$ will be extremely small. It is readily envisaged that the position of the next crack will depend primarily upon the location of any defects in

NO	STRESS	NO CRACK	CRACK SPACING	$\ln (1 - 1/(\sigma_a \psi)^{\frac{1}{2}})$													
	7.19	1	63.54	5.8179													
	7.86	5	25.42	3.0701	6.3534												
	8.34	7	21.19	2.6002	3.4772	3.4421											
	8.78	21	7.94	2.0252	2.8916	3.6336	5.5793										
	9.21	30	5.53	2.128	2.5536	3.0074	3.6005	5.4362									
	9.66	36	4.71	1.9673	2.3072	2.4335	2.991	3.5819	6.1661								
	10.08	49	3.43	1.8455	2.1329	2.3029	2.6559	3.0305	3.7875	5.6773							
	10.45	62	2.76	1.7545	2.0081	2.2294	2.4437	2.7289	3.205	3.8526	5.1514						
	10.95	77	2.23	1.6423	1.8692	2.0541	2.2262	2.4432	2.7691	3.1274	3.5489	4.3602					
	11.59	92	1.87	1.5385	1.7264	1.8778	2.0181	2.1852	2.4195	2.6505	2.9833	3.2084	3.8216				
	12.24	102	1.69	1.4446	1.6092	1.7405	1.8563	1.9926	2.1761	2.3474	2.5089	2.7144	3.032	3.8029			
	12.94	113	1.53	1.3594	1.5051	1.6193	1.7182	1.8324	1.982	2.1167	2.2391	2.3876	2.5994	3.0135	3.5942		
	13.61	120	1.44	1.2899	1.4214	1.5231	1.6102	1.7095	1.837	1.9495	2.0493	2.1673	2.329	2.6198	2.9619	3.8236	
	14.28	129	1.34	1.2292	1.3494	1.4414	1.5194	1.6074	1.719	1.8158	1.9004	1.9897	2.1301	2.3557	2.6005	3.0995	
	14.93	140	1.23	1.1773	1.2885	1.3728	1.4438	1.5232	1.623	1.7065	1.7825	1.8673	1.9789	2.165	2.358	2.7168	
	15.88	150	1.16	1.1113	1.2117	1.2871	1.35	1.4188	1.5065	1.5798	1.6425	1.7136	1.8055	1.9544	2.1028	2.3596	
	16.82	156	1.11	1.0652	1.147	1.2154	1.2721	1.3347	1.4116	1.4762	1.5309	1.5933	1.6709	1.7959	1.9174	2.1192	
	18.04	157	1.11	.9927	1.0757	1.157	1.1878	1.2427	1.3102	1.3663	1.4134	1.4659	1.5324	1.6365	1.7353	1.8945	
	19.29	162	1.07	.9333	1.014	1.0695	1.1151	1.1646	1.2248	1.2744	1.3159	1.3618	1.4185	1.5087	1.5922	1.7238	
	20.61	168	1.03	.8889	.9584	1.0091	1.0505	1.0953	1.1494	1.1939	1.2308	1.2715	1.3223	1.4002	1.4723	1.5841	
	21.93	175	.99	.8494	.9141	.9612	.9995	1.0409	1.0906	1.1312	1.1649	1.2018	1.2478	1.3177	1.382	1.4807	
	23.07	190	.91	.8133	.8739	.9178	.9534	.9918	1.0377	1.0751	1.106	1.1399	1.1818	1.2453	1.3032	1.3915	
	24.89	191	.91	.7676	.8232	.8693	.8957	.9305	.972	1.0057	1.0334	1.0636	1.101	1.1571	1.208	1.2848	
SLOPE				2.3916	1.8533	1.5727	1.296	1.1255	.9431	.8061	.7176	.6542	.598	.5317	.4813	.4114	
INT				-6.3885	-6.9855	-7.0451	-7.0403	-7.0577	-7.066	-7.0613	-7.0584	-7.0624	-7.0704	-7.0817	-7.0892	-7.0932	
CORR				.95837	.96175	.97996	.97927	.98044	.98984	.99373	.99509	.9946	.99212	.98932	.99001	.98752	
ETU				.292	.32	.34	.356	.373	.393	.402	.422	.436	.453	.478	.5	.532	

Table 4.2 Results of method 2 analysis of the data previously used in Figure 3.19. Note ETU = $\varepsilon_{tu(2)}$

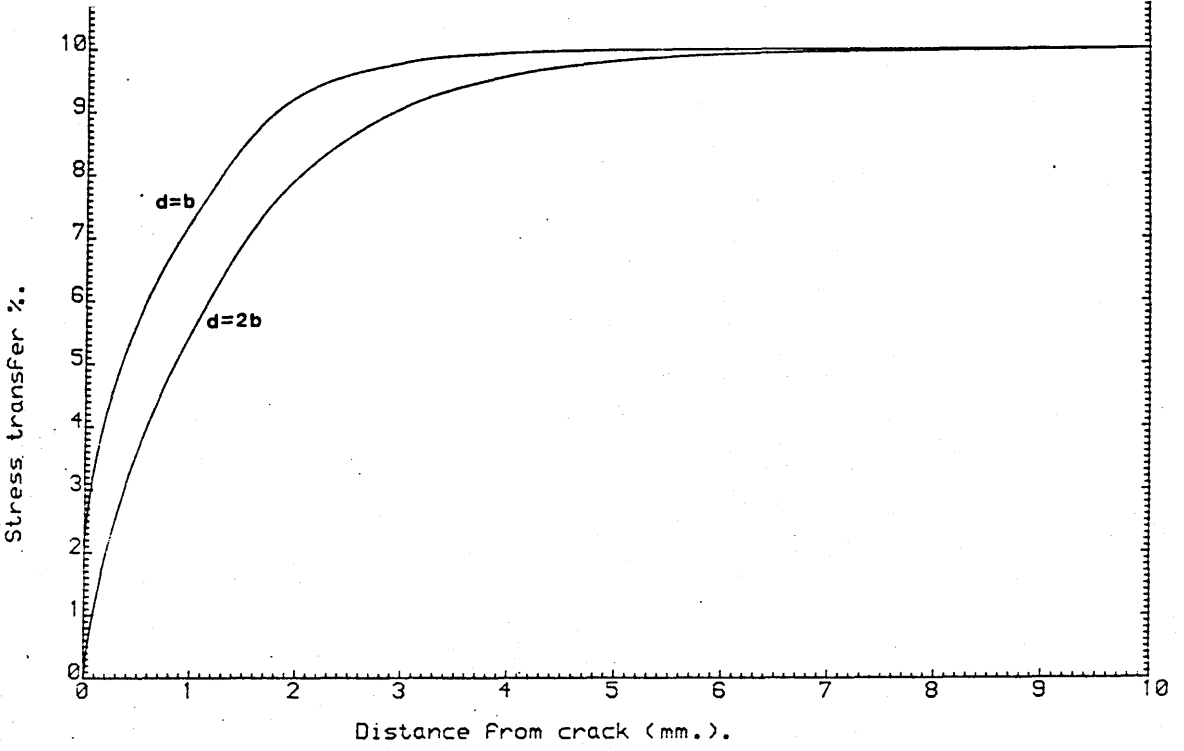

Figure 4.8 Stress transfer from the longitudinal ply to the transverse ply as a function of distance from a transverse crack, as predicted by equation 4.4.

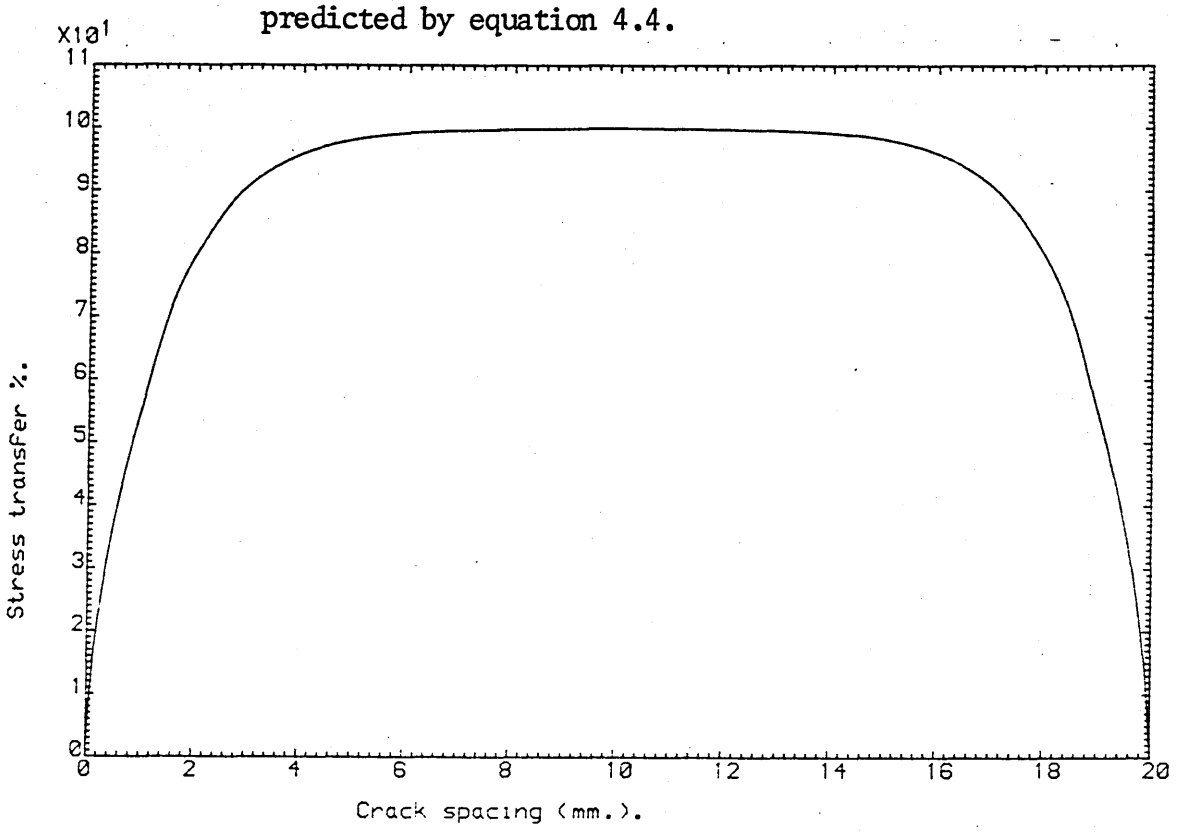

Figure 4.9 The build up of stress in the transverse ply between two transverse cracks.

this stress plateau and not that of the maximum stress, which according to equation 4.6 occurs equidistant between the two cracks. As the crack spacing is reduced, the length of this plateau is also reduced, and the new cracks will deviate proportionally less from the mid position. Finally when the crack spacing is such that the size of the plateau is small compared to the crack spacing i.e. the distance between cracks ≃ 5 mm, the modified shear lag theory would then be expected to operate.

The crack spacing at which the linear decline in $\varepsilon_{tu(1)}$, shown in Figure 4.7 begins, occurs at approximately twice the 95% $\Delta\sigma_0$ transfer length obtained from equation 4.4 for each of the coupons, and is shown in Figure 4.10 and tabulated in Table 4.3.

Comparison of the values of $\phi_{(2)}$ obtained by method 2 with those calculated from equation 4.5 are given also in Table 4.3. The similarity between the calculated and measured values occurs over only a relatively small range of crack spacings and indicates that the theory is applicable over only such a range.

The most puzzling phenomenon is the reduction of $\varepsilon_{tu(1)}$ values at small crack spacings. There are three possible explanations that could account for this:-

(1) Damage Zones

When the transverse ply fails, areas of damage could be formed either side of the crack. With decreasing crack spacing, an increasing number of

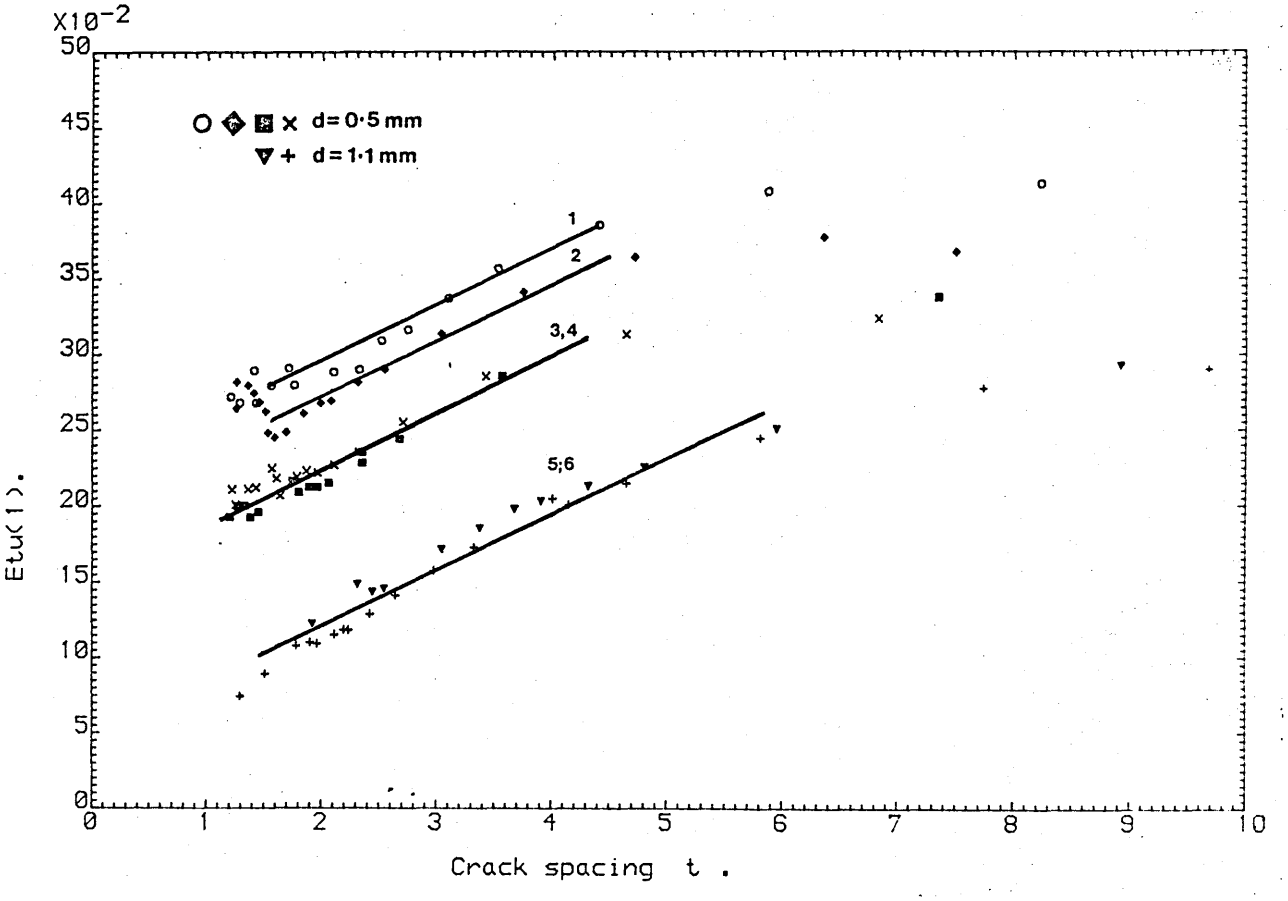

Figure 4.10 The effect of semi ply thickness (d) on the value of $\varepsilon_{tu(1)}$ as a function of crack spacing t, curves 1 - 4 are for coupons with a nominal inner ply semi-thickness of 0.5 mm., curves 5 and 6 for a thickness of 1.1 mm.

Coupon	Type	t at which linear decline in $\varepsilon_{tu(1)}$ begins	y at $\Delta\sigma/\Delta\sigma_0$ = 95%	$1/\phi^{\frac{1}{2}}$	
				measured	calculated
X (2)	d=b	4 mm	4.5 mm	0.0008	0.0008
Y (7)	d=b	4 mm	4.5 mm	0.0008	0.0008
R (3)	d=b	4 mm	4.5 mm	0.0006	0.0008
R (12)	d=b	4 mm	4.5 mm	0.0007	0.0008
U (10)	d=2b	6 mm	5.9 mm	0.0016	0.0015
U (11)	d=2d	6 mm	5.9 mm	0.0019	0.0015

Table 4.3 Comparison of the crack spacing t at which the linear decline in the value of $\varepsilon_{tu(1)}$ begins with the distance at which 95% of the stress $\Delta\sigma_0$ has been transferred back into the transverse ply, as predicted by equation 4.4. Also a comparison of the predicted values of $\phi_{(2)}$ obtained using method 2 with those calculated from equation 4.5 is given.

transverse cracks grow in these predamaged regions leading to a decrease in the average value of ε_{tu}. The exact nature of these zones is not known but they could be a product of the reversible whitening phenomenon which has been identified with the reversible debonding, observed for these laminates. Figure 3.1 shows dark areas either side of the transverse cracks, which had previously appeared white, where partial rebonding of the glass and resin had taken place due to the stress relief. Upon further debonding prior to transverse cracking, a cyclic process may lead to a reduction in the failure strain of these areas by a fatigue mechanism. Parvizi (69) observed that the coalescence of debonds into a microcrack often initiated the growth of microcracks in the surrounding area.

(2) Delamination

Parvizi (69) found that for laminates with an inner ply thickness of 4 mm, there was a sudden decrease in crack spacing above an applied stress of 130 MN m^{-2}, which could not be accounted for by the modified shear lag theory. She interpreted this in terms of delamination of the plys at these crack spacings. $\Delta\sigma_0$ is then transferred back by sliding friction over the delaminated region, and then elastically over the bonded region. The equation which Parvizi derived to confirm this mechanism (N.B. The equation in reference (69) is given incorrectly) is given below.

$$\Delta\sigma = \frac{\tau y'}{d} + \frac{b}{d}\left(\Delta\sigma_0 - \frac{\tau y'}{d}\right)\left(1 - \exp^{-\phi^{\frac{1}{2}} y - y'}\right) \qquad \ldots(4.16)$$

Where:-

τ = Limiting shear strength of the delaminated plies.

y' = Delaminated length.

Clearly whether stress transference occurs faster in the bonded or the delaminated case depends upon both the values of τ and y'. However Garrett and Bailey (80) found no evidence for delamination and considered that if it did occur then the stress transference at such areas would be less than in the elastically bonded case, predicting greater crack spacings than observed.

(3) Incorrect form of the stress transfer function

The rate of stress transfer may be lower than that given by the exponential function and therefore unable to predict the correct crack spacing (80). This is similar to (2) above except $\Delta\sigma_0$ would be transferred completely elastically.

The cause of the rise in $\varepsilon_{tu(1)}$ at small crack spacings, as shown by curve number 2 in Figure 4.10 is at present uncertain. It is apparent that further work on the cracking behaviour is needed, especially to discern the effects of the reversible debonding phenomena. However, for the purposes of this work, in which we are primarily concerned with identifying a reduction in ε_{tu} in the presence of an acidic environment, the theory can be used to estimate comparative values of ε_{tu} at crack spacings of 4-5 mm. for the d = b laminates and 6 mm. for the d = 2b laminates. In Table 4.4 the predicted values of $\varepsilon_{tu(1)}$ are compared with the experimental first transverse cracking strains. The similarity in the decline of $\varepsilon_{tu(1)}$ with decreasing crack spacing for each of the curves in Figure 4.10 shows that fundamentally the cracking behaviour was similar for each of the laminates. The different values of $\varepsilon_{tu(1)}$ for each of the laminates indicates that the transverse cracking strain for each was different. This is supported by the similarity

in the values of $\varepsilon_{tu(1)}$ for coupons taken from the same laminate,i.e. coupon 3 with 4, and 5 with 6 in Figure 4.10. A difference is to be expected for laminates with dissimilar transverse ply thicknesses, for example that found between laminates 1 - 4 with 5 and 6. However the differences between the transverse cracking strains of individual laminates of nominal transverse ply thickness 0.5 mm. were greater than expected. At first it was considered that these were due to the relaxation of thermal stresses during storage. However examination of the laminate preparation dates, showed that the one with the lowest $\varepsilon_{tu(1)}$ was made a considerable time after the others. A possible explanation is that each of the laminates possesses a differing level of thermal strain $\varepsilon_{t\ell}^{th}$. This could arise if the softening point of the resin varied, because this would lead to a variation in ΔT in equations 4.1 and 4.2. Loss of amine during the degassing of the resin, could cause differing states of cure. It has already been shown in section 4.2, that the increased amine concentration used in these laminates compared to those of Parvizi was responsible for a higher level of $\varepsilon_{t\ell}^{th}$. However, to explain this difference for laminates 1 and 4 solely in terms of a different matrix softening temperature, requires a change in this temperature of approximately $25^{o}C$. Since no detailed investigation into the variation of the matrix softening temperature between laminates was carried out, it is difficult to comment upon the validity of this value. But it is felt that this value is excessively high, and that differences in the transverse ply thickness of the laminates is partially responsible.

4.4.5 Experiments in aqueous environments

1. Deionized water

Since the growth of edge-cracks had not been observed in half immersed coupons at constant load in deionized water, its effect on the value of ε_{tu} was expected to be minimal. This was confirmed firstly, by a comparison of crack spacing data in Figure 3.20, where the close coincidence of the curves could only arise if the cracking behaviour was similar, and secondly, by analysing this data using method 1 described in section 4.4.3, to give the values of $\varepsilon_{tu(1)}$ shown in Figure 4.11.

2. Aqueous sulphuric acid

The transverse cracking patterns for the immersed halves of coupon in 0.5 M. acid have been analysed by the methods described in section 4.4.3. There is a similarity between the decline in $\varepsilon_{tu(1)}$ with decreasing crack spacing, for coupons tested in the aqueous acid and in air, as shown in Figure 4.12. There is also good agreement between the values of $\phi_{(2)}$ recorded in the different environments as shown in Table 4.5. Thus the cracking behaviour in the aqueous acid is fundamentally the same as in air, and the value of ε_{tu} in the presence of the environment can therefore be estimated by method 1. The transverse failure strain is therefore equated with the maximum value of $\varepsilon_{tu(1)}$ and is given for the immersed and unimmersed halves of the coupons in Table 4.5. The reduced value of $\varepsilon_{tu(1)}$ for the unimmersed part of the laminates implies that the transport of the environment to this part of the coupon occurs fairly rapidly.

Since the majority of stress corrosion experiments take longer than the

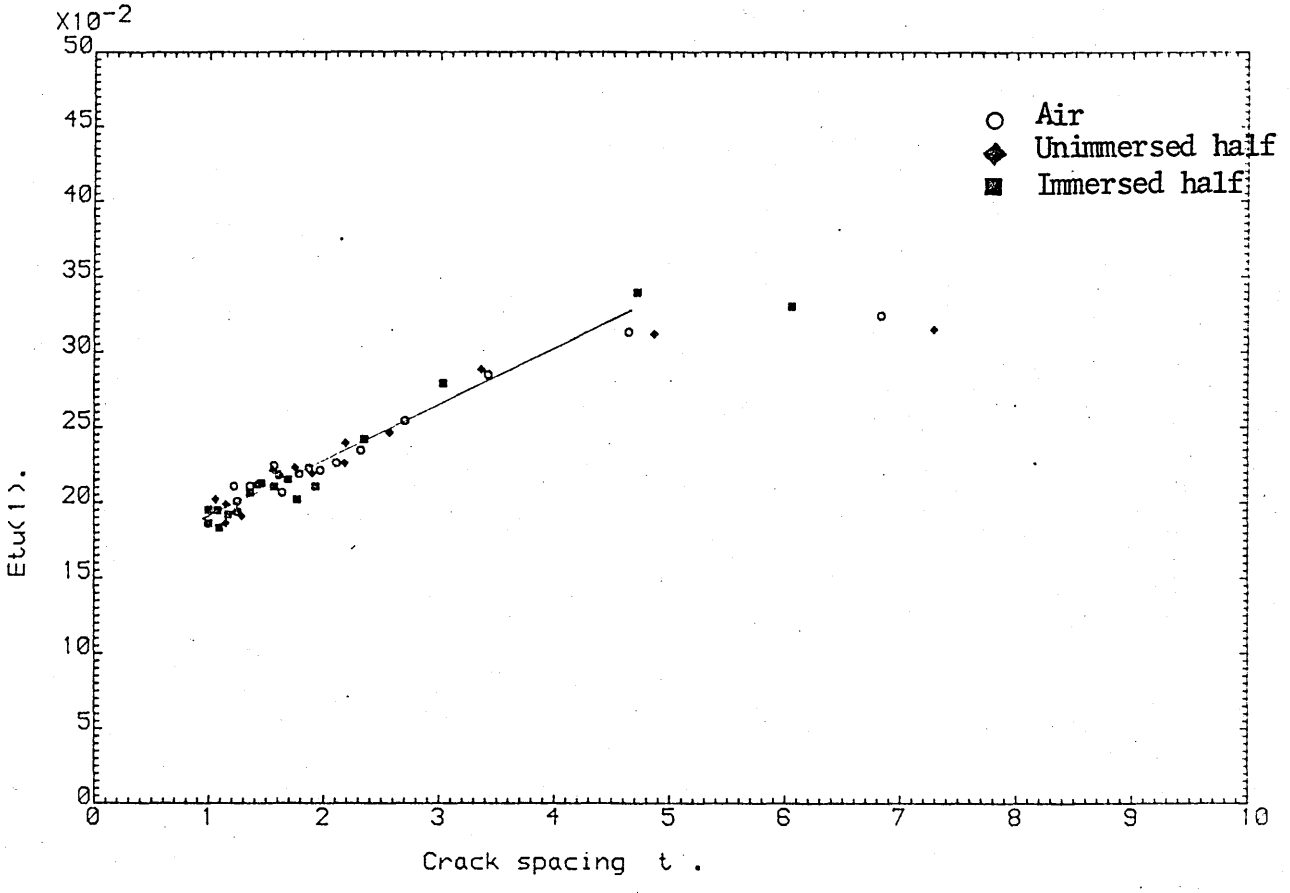

Figure 4.11 The effect of deionized water on the values of $\varepsilon_{tu(1)}$ as a function of crack spacing t.

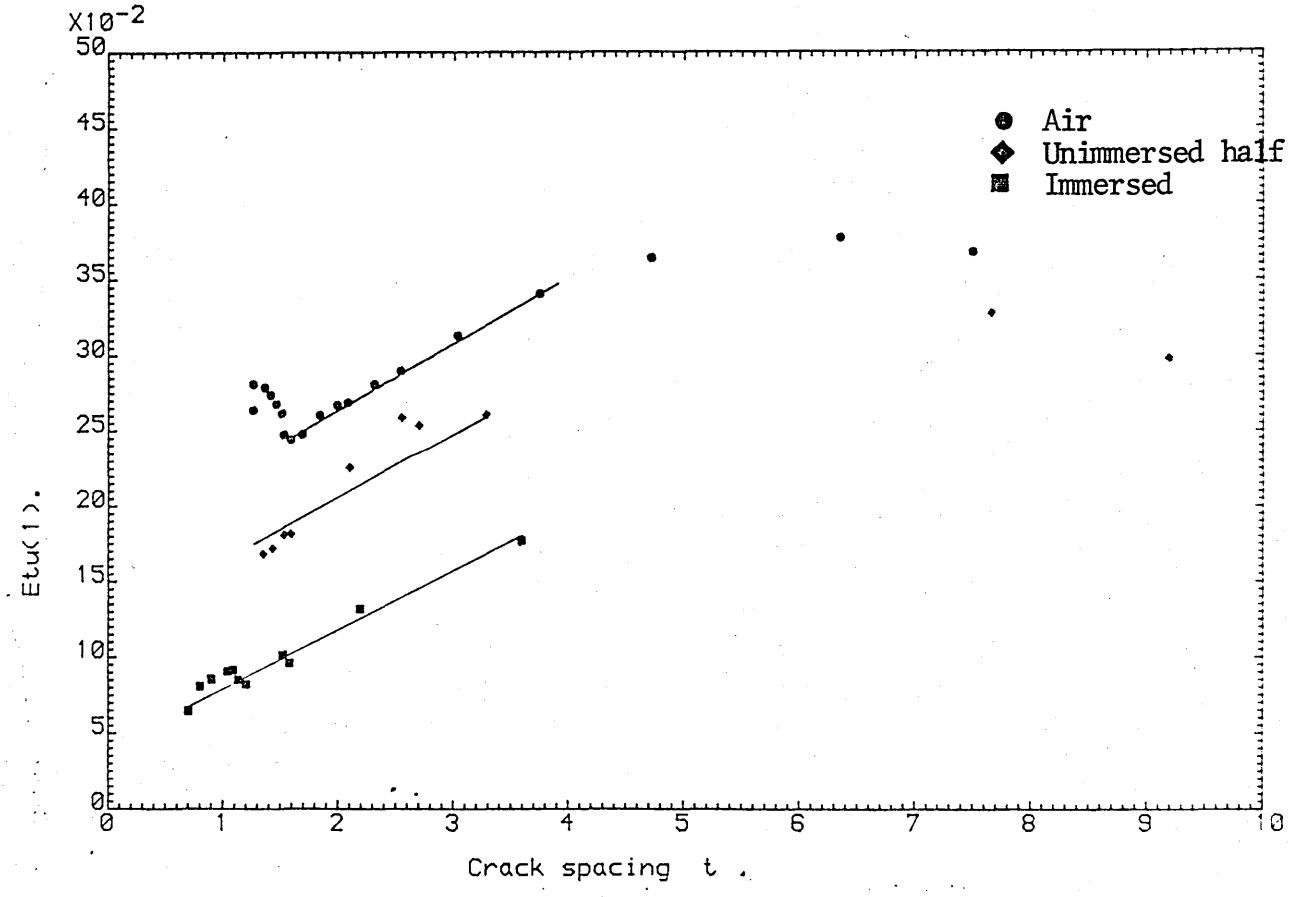

Figure 4.12 The effect of aqueous sulphuric acid 0.5 M on the transverse cracking strain $\varepsilon_{tu(1)}$ as a function of the crack spacing t. The laminate inner ply semi-thickness d = 0.5 mm.

Coupon	Type	$\varepsilon_{t\ell u}$	$\varepsilon_{tu(1)}$
X (2)	d=b	0.28	0.37
Y (7)	d=b	0.26	0.34
R (3)	d=b	0.28	0.29
R (12)	d=b	0.25	0.29
U (10)	d=2b	0.25	0.27
U (11)	d=2b	0.24	0.26

Table 4.4 Comparison of the measured first transverse cracking strain with $\varepsilon_{tu(1)}$ values predicted using method 1.

Laminate	Type	Environment	$\varepsilon_{t\ell u}$	$\varepsilon_{tu(1)}$	measured $1/\phi^{\frac{1}{2}}$
Y (7)	d=b	Air	0.26	0.34	0.0008
Y (11)	d=b	"Acid Vapour"	0.25	0.26	0.0012
Y (11)	d=b	Acid	0.20	0.23	0.0006
U (10)	d=2b	Air	0.25	0.27	0.0016
U (9)	d=2b	"Acid Vapour"	0.16	0.18	0.0014
U (9)	d=2b	Acid	0.14	0.12	0.0014

Table 4.5 Comparison of the predicted values of $\varepsilon_{tu(1)}$ with the measured values of $\varepsilon_{t\ell u}$ for coupons tested in air and aqueous acid. Note "acid vapour" refers to the unimmersed half of the coupon. $1/\phi^{\frac{1}{2}}_{(2)}$ values are also shown.

dynamic test, the reduction in $\varepsilon_{tu(1)}$ could be greater than indicated in Table 4.5. Environmental edge-cracks have been observed at applied strains of 0.05%, thus it is concluded that the transverse cracking strain can be reduced to a level approximating to that of the thermal strain i.e. $\varepsilon_{t\ell}^{th}$.

Bailey and Parvizi (83) investigated the transverse cracking mechanism of similar epoxy glass laminates, using a specimen configuration for constrained cracking. They found that debonding began at an applied strain of 0.1%, but it was not visible as stress whitening until 0.3%. The total strain in the transverse ply was then 0.38% ($\varepsilon_{t\ell}^{th}$ = 0.08%). Since the laminates used in this study possessed a $\varepsilon_{t\ell}^{th}$ = 0.22% (d=b) then visual stress whitening should be observable at around 0.15%. Figure 3.2 confirms that a change in slope does occur at approximately 0.15% strain and visually the crossply coupons are seen to whiten. Since they observed debonding when the total transverse ply strain was 0.18%, this would imply that some debonding occurs in the transverse ply of the laminates used in this study under the action of $\varepsilon_{t\ell}^{th}$ (0.22%) alone. Thus entry of acid into the laminate may occur through capillary action along debonded fibres in the transverse ply. They also observed that individually debonded fibres coalesced to produce microcracks, which grew into transverse cracks under the action of increasing applied strain (83). Therefore it appears that the effect of the acid in lowering the transverse ply failure strain is twofold. Firstly,it is responsible for debonding of the glass, and secondly, it promotes the formation of microcracks and transverse cracks. Both of these effects would allow the acid easy entry into the laminates and are further discussed in section 4.5.

It has been found that the transverse cracking behaviour of polyester glass coupons in the presence of aqueous acid is no different than in air so that $\varepsilon_{t\ell u}$ is not reduced in the short term (89). This explains the differences between the environmental edge-cracking observed for polyester and epoxy crossply coupons in acidic environments.

To further show the effect of acid on non-externally stressed coupons, the cracking behaviour, after 24 and 48 hours immersion,in aqueous acid of washed and dried coupons was examined. The crack spacing/applied stress curves are shown in Figure 3.22, and $\varepsilon_{tu(1)}$ against crack spacing is shown in Figure 4.13. What is not apparent from the crack spacing curves is that whilst the cracking behaviour after 24 hours is fundamentally similar to that in air, after 48 hours it is of the form expected if ε_{tu} possessed a single value. It is not proposed to draw too many conclusions from this experiment since on long immersion in acid it could be expected that values of moduli used in calculating these results are no longer valid. What the results do show however is that in the presence of aqueous sulphuric acid, and under no externally applied stress, a rapid fall in ε_{tu} is to be expected.

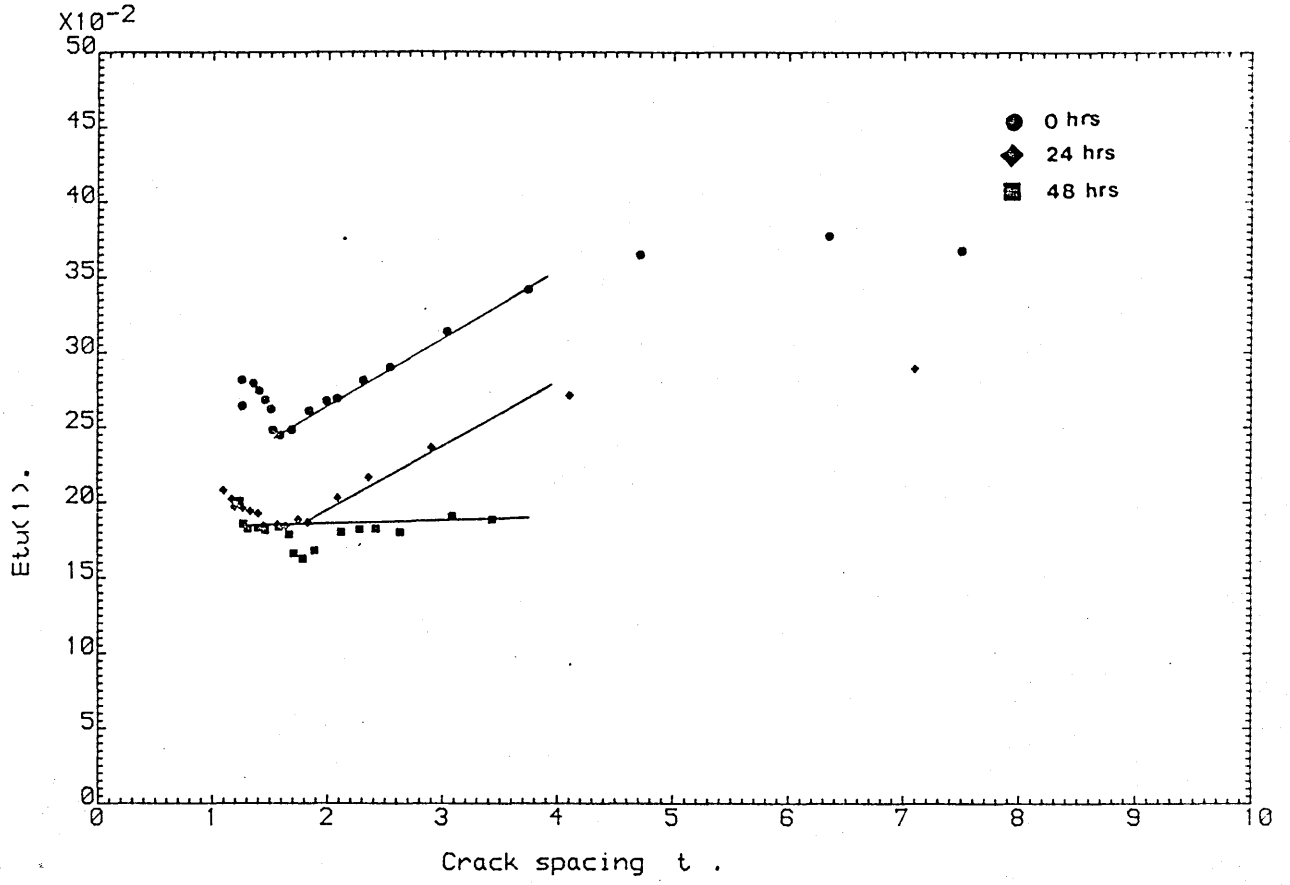

Figure 4.13 The effect of pre-immersion of a $0^{o}/90^{o}/0^{o}$ coupon in 0.5 M aqueous sulphuric acid on the transverse ply failure strain $\varepsilon_{tu(1)}$ as a function of the crack spacing t.

4.5 MODE I STRESS CORROSION FAILURE

Mode I failures of 0^{o} unidirectional coupons begin by the nucleation and growth of individual stress corrosion cracks in the surface of the immersed half of the coupon. Figure 4.14 shows the initiation and early stages of propagation, where fracture of individual, and small groups of fibres may be seen. Crack growth continues by the fracture of neighbouring fibres to produce a planar fracture surface, and in the time-lapse series of photographs shown in Figure 3.12, these stress corrosion cracks are clearly visible. Total failure results by the coalescence of the larger stress corrosion cracks. If these cracks are in different planes, as is often the case, then coalescence takes place by longitudinal splitting to produce the irregular fractures in the coupons shown in Figure 4.15. Similar stress corrosion crack initiation has been observed in polyester-glass composites (21).

The greater degree of irregularity to the fracture surfaces of these 0^{o} coupons in comparison to those from hoop wound pipes, tested in diametrical compression, can be explained in terms of a stress constraint effect. The growth of a stress corrosion crack occurs along the line of maximum stress (within the environment) at the bottom of the pipe (26). A similar constraining effect is found in $0^{o}/90^{o}/0^{o}$ crossply laminates. Figure 4.15 compares a 0^{o} unidirectional and a $0^{o}/90^{o}/0^{o}$ crossply coupon, which have failed at similar initial applied strains, the strain in the 90^{o} ply of the crossply coupon was recalculated to represent that in the longitudinal ply, adjacent to a transverse crack using equation 4.17. The planar fracture of the crossply coupon results from the additional stress, $\Delta\sigma_{0}$ placed upon the

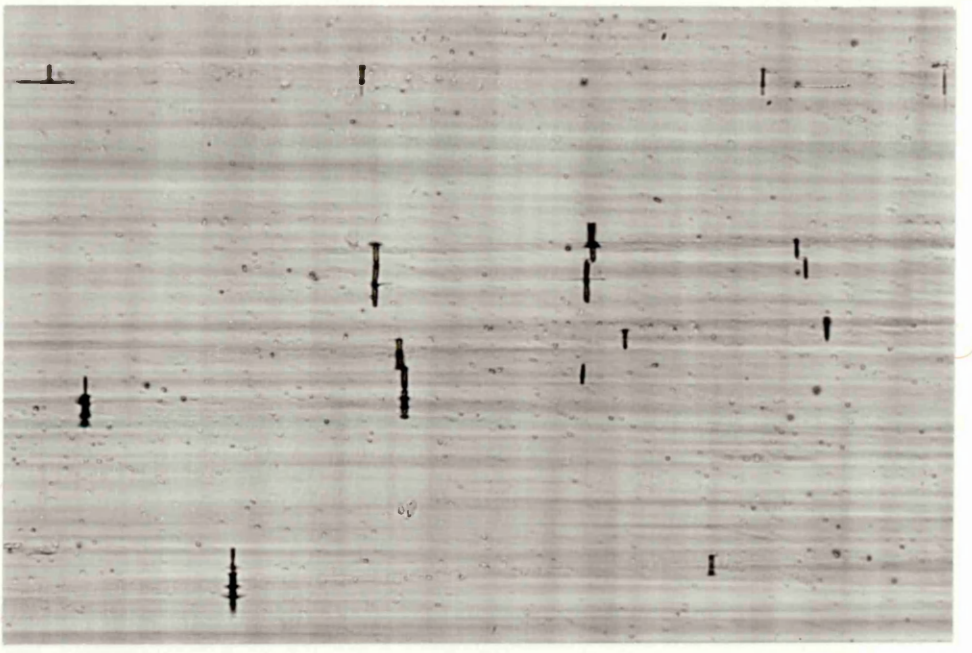

Figure 4.14 Initiation of stress corrosion cracks in the surface of the immersed half of a $0^{o}/90^{o}/0^{o}$ crossply coupon.

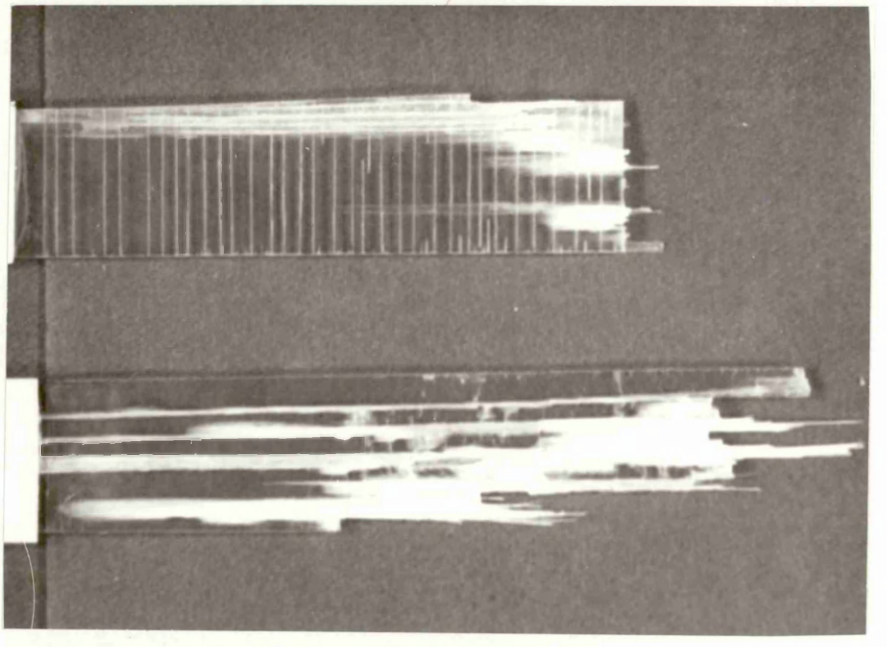

Figure 4.15 Comparison of the stress corrosion fracture of a 0^{o} unidirectional and a $0^{o}/90^{o}/0^{o}$ crossply coupon showing the constraining effect of the transverse crack. $\varepsilon_a \simeq 0.5\%$.

longitudinal plies adjacent to the transverse crack. Since $\Delta\sigma_0$ is transferred back into the transverse ply within a short distance of this crack, stress constraint will operate to restrain the stress corrosion crack to within a relatively narrow zone of increased stress adjacent to the transverse crack, in a similar manner to those restrained at the bottom of hoop wound pipes by the line of maximum stress. If the initial applied strain is insufficient to cause an immediate failure of the transverse ply, then as discussed in section 4.4, with time the transverse ply failure strain is reduced by stress corrosion in the aqueous acidic environment, and failure of the 90^{o} ply occurs. This results in a localized loading of the 0^{o} ply, similarly to that of a transverse crack.

Jones, Wheatley and Bailey (29) reported that polyester-glass $0^{o}/90^{o}/0^{o}$ crossply coupons tested in 4-point bend, showed reduced times-to-failure in comparison with those tested under uniaxial tension. They attributed this to the action of the transverse cracks, which notched the longitudinal plies, thereby providing initiation sites for stress corrosion cracks. Hull and Hogg (26) have also reported that transverse cracks formed on the loading of $\pm 55^{o}$ filament wound polyester pipe, reduced the stress corrosion times-to-failure by allowing the transport of the aqueous environment into the laminate, where stress corrosion cracks were initiated. To determine if either of these effects operated for these crossply laminates, it was necessary to recalculate the initial applied strains to allow for the localized increase in strain found in the longitudinal ply adjacent to a transverse crack. This was carried out using equation 4.17.

$$\varepsilon_{\ell}^{tc} = \frac{\varepsilon_c E_c}{E_{\ell}} \frac{(d+b)}{b} \qquad \ldots(4.17)$$

Where:-

ε_{ℓ}^{tc} = Strain in the longitudinal ply of a $0^o/90^o/0^o$ crossply laminate, adjacent to a transverse crack.

ε_c = Initial applied strain in $0^o/90^o/0^o$ composite.

E_c = Young's modulus of the composite in the 0^o direction.

E_{ℓ} = Young's modulus of a unidirectional laminate in the 0^o direction.

The similarity between the Mode I times-to-failure for 0^o unidirectional and $0^o/90^o/0^o$ crossply coupons after recalculation of the strain by equation 4.17, shown in Figure 4.16, illustrates that neither of the effects described above, have affected the times-to-failure of the crossply laminates. The absence of initiation of stress corrosion cracks, by the transverse cracks, is understandable in terms of the different strain fields in coupons tested in bend or in uniaxial tension. In the former, the transverse crack is being driven into the longitudinal ply by the increasing strain field, whereas in the latter no such driving force exists. Subsequently it has been found that stress corrosion cracks in polyester-glass coupons tested under uniaxial tension, were not initiated by transverse cracks (91). The similarity in Mode I times-to-failure also suggest that the failure of the 0^o plies of a $0^o/90^o/0^o$ crossply laminate is independent of the thermal strain. However, it will be shown below, that the rapid permeation of the aqueous acid into these composites can firstly, explain the lack of influence of thermal

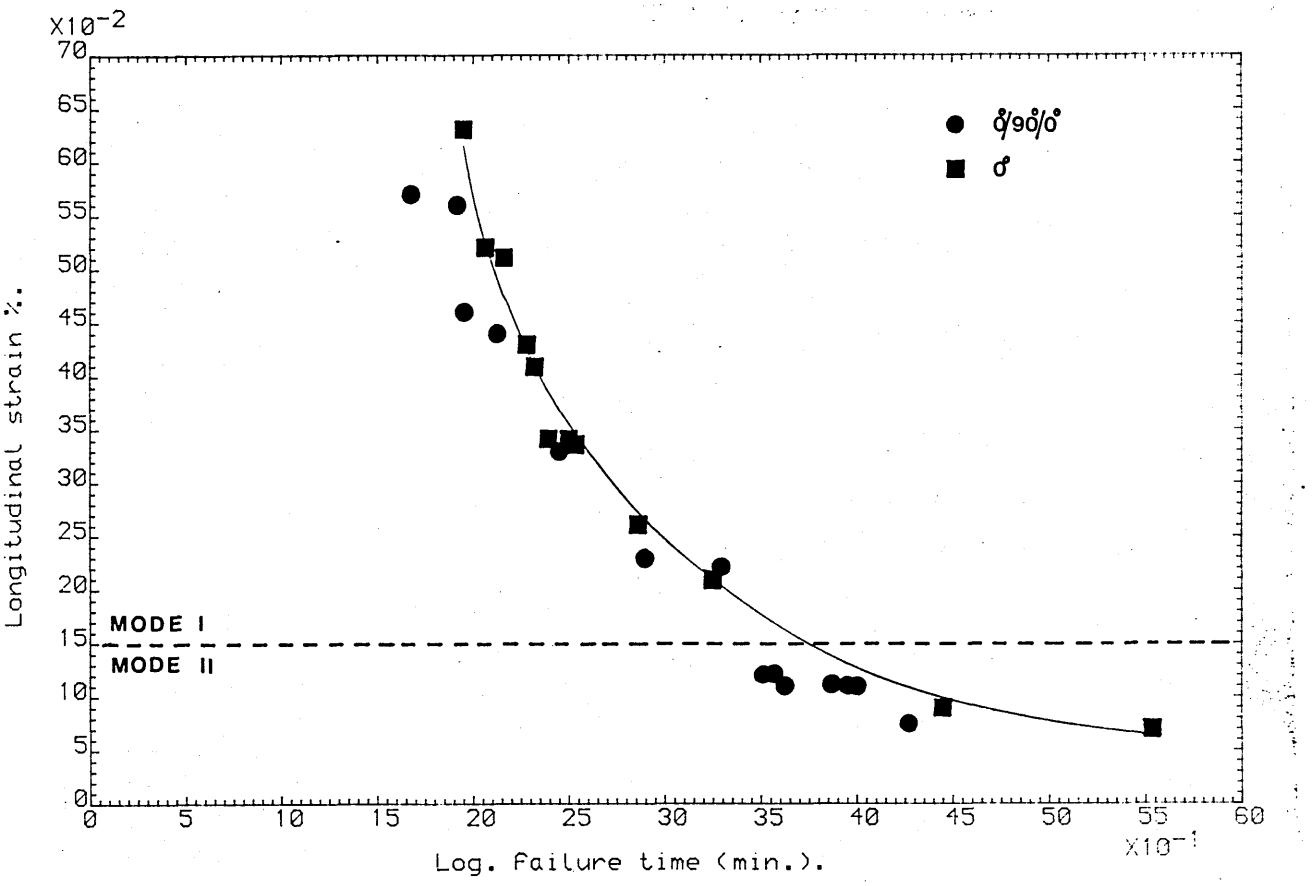

Figure 4.16 Comparison of the stress corrosion failure times between 0^{o} unidirectional and $0^{o}/90^{o}/0^{o}$ crossply coupons in open-cells. The initial applied strain in the crossply coupons has been recalculated to represent that in the longitudinal plies assuming the transverse ply is non-load bearing using equation 4.17.

strain on the Mode I times-to-failure of the $0^{o}/90^{o}/0^{o}$ crossply laminates, and secondly makes the transport of the aqueous acid into the laminate by transverse cracks unimportant.

It was not until the failure times of individual E-glass fibres had been measured, that the reason for the ineffectiveness of transverse cracks became apparent. Figure 3.16 shows a comparison of 0^{o} unidirectional coupons with times-to-failure of single fibres. The similarity between the times-to-failure at initial applied strains of > 0.15% suggests that the resin is not providing any chemical protection, and that the glass is failing in a similar manner as if it were an exposed single fibre. This indicates that the aqueous acid rapidly penetrates the longitudinal plies and stress corrodes the majority of the glass reinforcement. An alternative mechanism is that proposed by Hull and Hogg (26,27) whereby, attack of the glass is limited to that at the crack tip, the rest being protected by the resin. However the lack of influence of the transverse cracks on the stress corrosion is not consistent with this theory. The failure time of a 0^{o} unidirectional coupon will be dependent upon the number of stress corrosion cracks in any one plane normal to the reinforcement. The more cracks, the more rapidly the stress will be increased due to the reduction in the cross sectional area, and shorter the time-to-failure. Thus increasing the surface area of a 0^{o} unidirectional coupon should lead to a decrease in the failure time. A transverse crack may be thought of as doing this, since it allows access to the formerly protected inner surfaces, hence a reduction in failure time would be expected. Support for the transport of the aqueous acid through the 0^{o} plies is given in Figure 3.9, where the results from $0^{o}/90^{o}/0^{o}$ coupons with clamp-on-cells, are compared with those from the

experiments in the open cell. The similar failure times demonstrate that the acid is rapidly transported through the 0^{o} plies. Thus the ineffectiveness of the transverse cracks in reducing the Mode I failure times is due to the rapid transport of the acid, and at strains greater than 0.15%, a further decrease is not possible because failure is already occurring at similar times to unprotected single E-glass fibres. (At initial applied strains of below 0.15% Mode II failure was found in the clamp-on-cell, that is, the failure crack did not pass through the part of the laminate enclosed by the cell).

It has been shown in section 4.4 that the aqueous acid lowers the transverse ply failure strain by stress corrosion of the glass resin interface, the transport of acid within these laminates would be expected to occur by capillary action along the glass matrix interface. Entry of acid into the transverse ply is easily understandable since the cut edges will allow the acid direct access to the fibre interface. In the case of the longitudinal plies the acid firstly has to diffuse through the resin covering the surface glass, although direct interfacial attack of any exposed glass is another possibility.

The amount of work reported on the diffusion of aqueous acids within both composites and the matrix resins is severely limited, there has been more work carried out on the diffusion of water, although there is no general agreement as to the mechanisms involved. Menges and Gitschner (53) assumed Fickian diffusion, and calculated the times that water took to completely penetrate into various types of composite. For an epoxy-glass laminate similar to those used in this study, they estimated that complete penetration would be expected

in about 15 days. Similarly, rapid permeation into polyester-glass composites have been reported by Regester (61), and Marshall et al (58,62). However the rate of penetration by aqueous acid is reported to be slower, although Marshall et al consider that these lower diffusion coefficients are the result of reaction of the aqueous acid with the glass reinforcement. The effect of an applied tensile strain has been found to increase the diffusion coefficients of both water and aqueous acid.

The diffusion of aqueous acid parallel and normal to the direction of reinforcement may occur by three differing mechanisms.

(1) Diffusion through the matrix resin.

(2) Diffusion by capillary action along the fibre matrix interface.

(3) Diffusion through microcracks by a capillary mechanism.

Since, it has already been shown that the glass-matrix bond is susceptible to stress corrosion by aqueous acid, diffusion through the resin alone would only be expected to occur in the absence of, or at low applied tensile strains. Capillary diffusion is considered to occur approximately 500 times faster than diffusion through the matrix resin (35), therefore rapid movement of the acid will occur in the direction of the reinforcement. Diffusion normal to the reinforcement may occur by the aqueous acid crossing fibres at positions where they are in contact, i.e. high volume fraction areas. Furthermore since the transverse ply failure strain has been found to be reduced in the aqueous acidic environment, the applied strain needed to produce microcracks is also expected to be reduced. Since microcracking occurs normal to the direction of reinforcement, this would allow rapid diffusion of the

acid in this direction, followed by capillary action parallel to the fibre direction. Support for the formation of microcracks under the influence of the aqueous acidic environment has been found by employing microprobe X-ray analysis to examine the fibres near to what appear to have been microcracks in the fracture surfaces. Figures 4.17 and 4.18 show that fibres near to the microcracks have lost more aluminium and calcium than fibres in areas away from microcracks, thereby indicating that they have been in contact with the acid for a longer period.

At strains of below 0.15% failure occurs in longer times than unprotected E-glass fibres. It is not absolutely clear at present whether this is due to either, a lower rate of stress corrosion of the glass resin interface, or the cessation of microcrack growth. Since the Mode III behaviour of the crossply laminates indicates that diffusion of the aqueous acid occurs comparatively rapidly, parallel to the reinforcement in the longitudinal plies, it appears that the absence of environmental-microcracking reduces the diffusion rate.

Generally the chemical resistance of anhydride cured epoxy resins is thought to be superior to an isophthalic polyester (78). To further check that a chemical attack of the epoxy matrix was not primarily responsible for its poor stress corrosion properties, (See Figure 3.11 for a comparison with the polyester-glass coupons), the chemical resistance was improved by using a near stoichiometric proportion of NMA (90phr) and postcuring for 24 hours at 200^{o}C (76,77). No improvement in the stress corrosion resistance was found as shown in Figure 3.11 confirming that the mechanism was not dependent upon the chemical resistance of this resin.

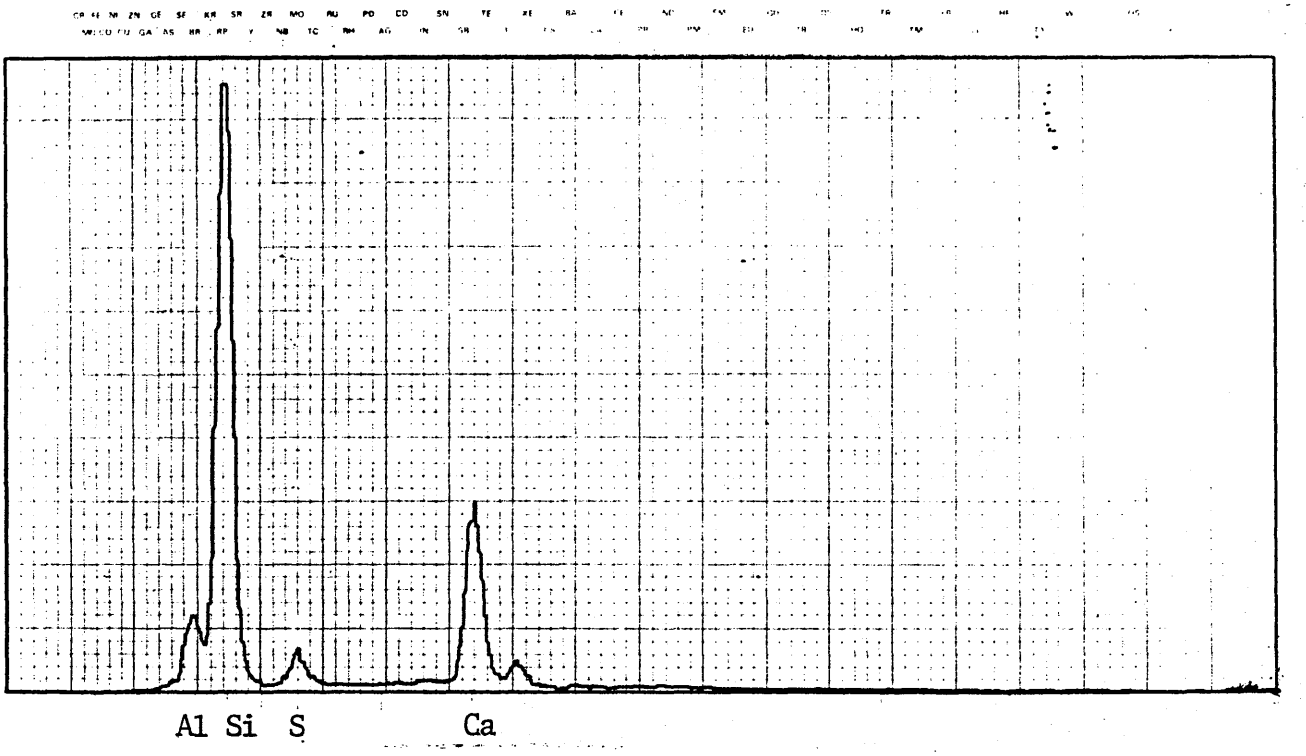

Figure 4.17 Microprobe analysis of glass fibres in stress corroded fracture surface away from microcracks. (Mode I failure)

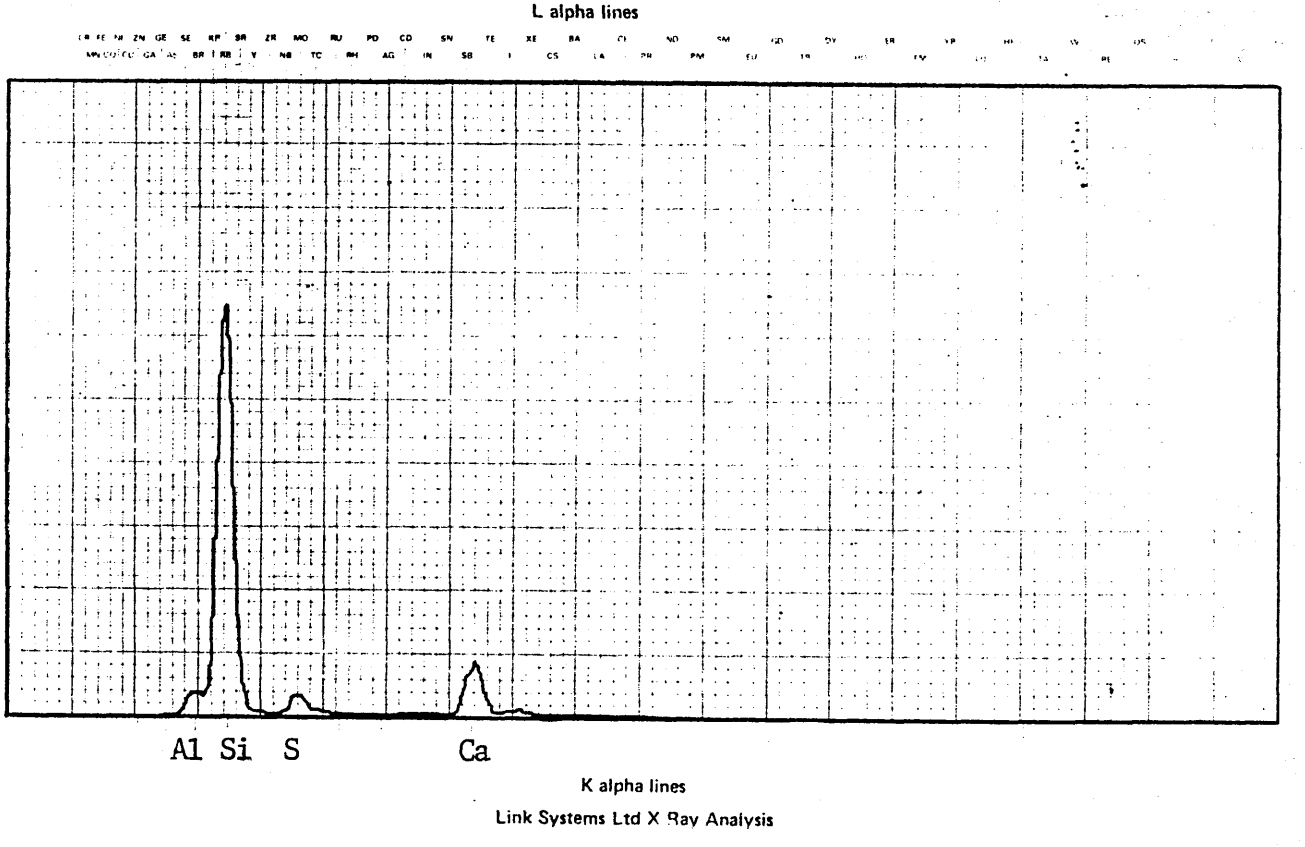

Figure 4.18 Microprobe analysis of glass fibres in stress corroded fracture surface near to microcracks. (Mode I failure).

It would be expected that the thermal strains present in the $0^{o}/90^{o}/0^{o}$ crossply laminates would influence the rate of stress corrosion, so that the 0^{o} unidirectional coupons would have longer failure times. The reasoning is that the generation of a thermal strain in the 90^{o} ply of a laminate will put the longitudinal ply into compression in the direction of the fibres. For laminates with d=b the compressive strain is one third of the thermal strain in the longitudinal direction of the transverse ply, i.e. approximately 0.07%. In an environment, resin swelling could lead to a reduction in the thermal strain, however in Figure 3.18 it is shown that within the times for failure by stress corrosion, relaxation is insignificant. Furthermore in section 4.2 it was shown that the glass fibres become debonded from the matrix under the action of an environment and an applied load. Therefore, since the decoupled fibres no longer have a compressive component the fibres in the 0^{o} longitudinal plies cannot be considered to be at a lower strain than the initial applied strain. Thus the stress corrosion times-to-failure as a function of the strain in the 0^{o} longitudinal plies are expected to be the same for 0^{o} and $0^{o}/90^{o}/0^{o}$ crossply laminates, as shown in Figure 4.16. In section 4.6 it is shown that the Mode II failure requires sufficient applied load to overcome the thermal compressive strains in the 0^{o} plies,otherwise the crack cannot propagate through the longitudinal glass fibres, and the coupon becomes damaged by the Mode III mechanism.

Thus Mode I failure at initial applied strains greater than 0.15% is due to the rapid diffusion of the acidic environment into the laminate resulting in stress corrosion of the glass fibres. The entry of the acid

seems to occur via environmental-microcracking and stress corrosion of the glass resin interface. At strains of below 0.15%. significantly longer times-to-failure than single glass fibres are found suggesting that environmental-microcracking does not take place.

4.6 MODE II AND MODE III STRESS CORROSION FAILURE

Mode II failures of both $0^{o}/90^{o}/0^{o}$ crossply and 0^{o} unidirectional coupons were observed in open-cells at applied strains of less than 0.15%. This failure mode was shown to be a property of the laminate and not of the glass, because E-glass tows in similar experiments, failed within the acid. Mode II is also characterised by failures in shorter times than Mode I, but micro-structural examination of the fracture surfaces showed no differences (Section 3.5), except that there appeared to be more crystalline material present in the Mode II fracture surface. Thus it appeared that the fracture of the longitudinal plies in a Mode II failure occurred in a similar manner to a Mode I failure, and that a mechanism operated which allowed the stress corrosion of the glass fibres to occur faster above the aqueous acid than in it. Since Mode II failure takes longer than the failure of single glass filaments at similar strains, the resin provides some chemical protection to the fibres. It was noted that the extent of the additional damage occurring in the unimmersed portion of a crossply laminate at strains below 0.15% seemed to be dependent upon the initial applied strain; the lower the strain, the more the damage. Thus the fracture process became more like the Mode III found in non-externally stressed crossply coupons.

Crystalline material was observed to form at the edge of 0^{o} unidirectional coupons tested in open-cells at initial strains of approximately 0.1%. Similarly, Mode III damaged crossply coupons had crystalline material present within the longitudinal splits and at their edges. Aluminium, sulphur and calcium were identified by X-ray spectrometry using a JEOL 200 CX STEM, as

the main elemental constituents of this crystalline material, see Figure 4.19. Furthermore, the needle shaped crystals separated from this material have been identified as aluminium sulphate (Figure 4.20).

The examination of the crystalline material found in the Mode II fracture surfaces using a JEOL JXA 50A microprobe showed it to be rich in calcium and sulphur as shown in Figure 4.21. There is some doubt as to when the material was formed, i.e. it may not have crystallized until after the fracture of the coupon. However since the corrosion of E-glass by aqueous acid occurs by leaching out the metallic elements, predominantly calcium, aluminium, potassium and sodium (50) and that calcium sulphate has only limited solubility in aqueous media it can be reasonably assumed that crystallization has occurred prior to fracture. On the other hand, aluminium sulphate is considerably more soluble, thus the crystalline deposits at the coupon edge can be explained by the transport of the soluble corrosion products from within the laminate to its edge, where evaporation of the water occurs. Therefore it was postulated that Mode II and III failures were caused by the precipitation of the less soluble glass degradation products within the laminate. The hypothesis is supported by Scrimshaw's observation of calcium sulphate in the ignited residue of stress corroded polyester-glass laminates (24). He also explained the weight gains found for polyester-glass laminates immersed in aqueous sulphuric acid as a result of the formation of in-situ calcium sulphate. Similar coupons tested in hydrochloric acid showed a loss in weight.

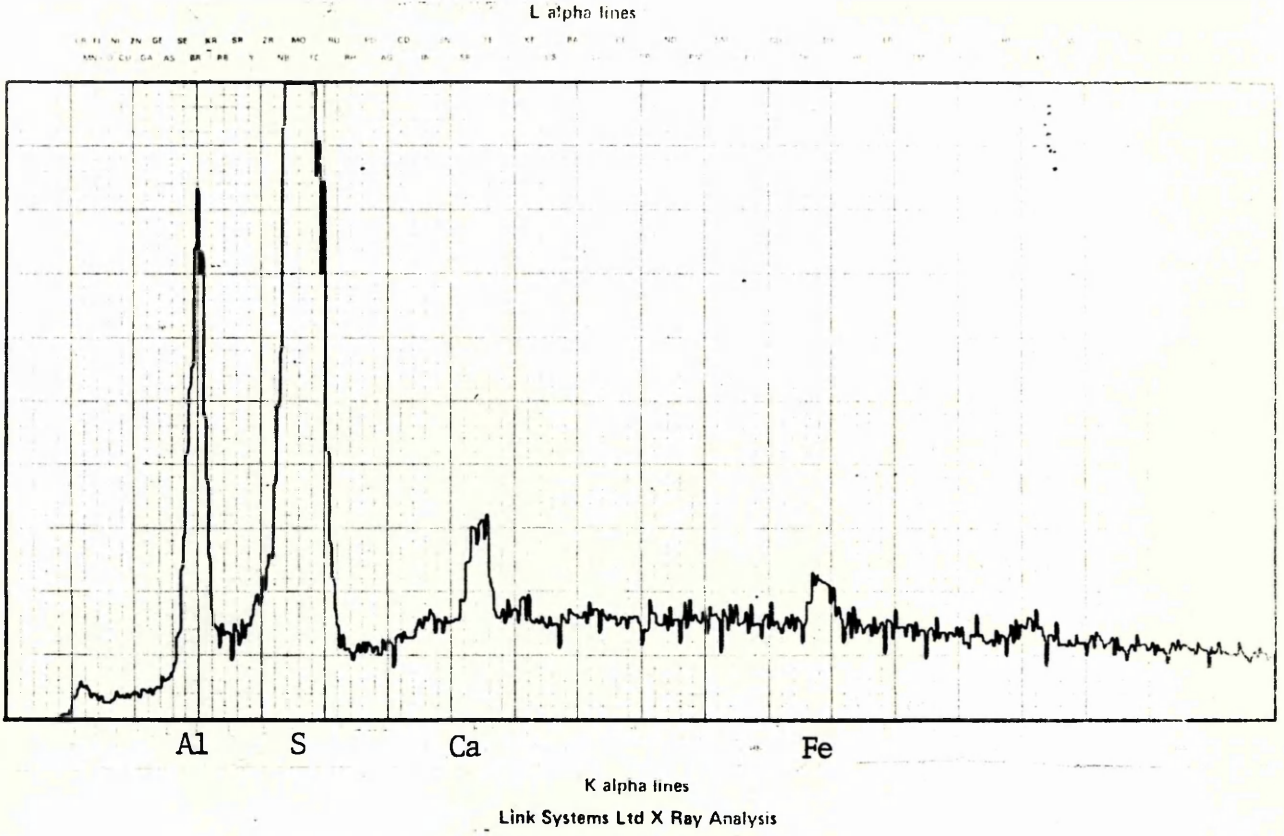

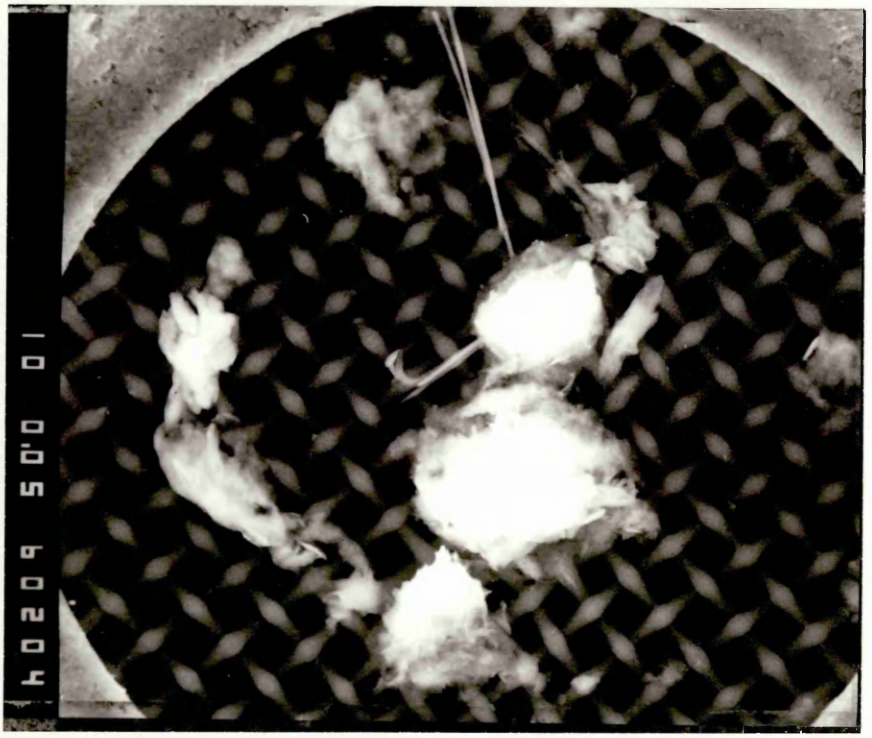

Figure 4.19 X-ray analysis of crystalline material found at the edge of a 0^{o} unidirectional coupon at an initial applied strain of 0.1%. The material analysed is shown in the micrograph.

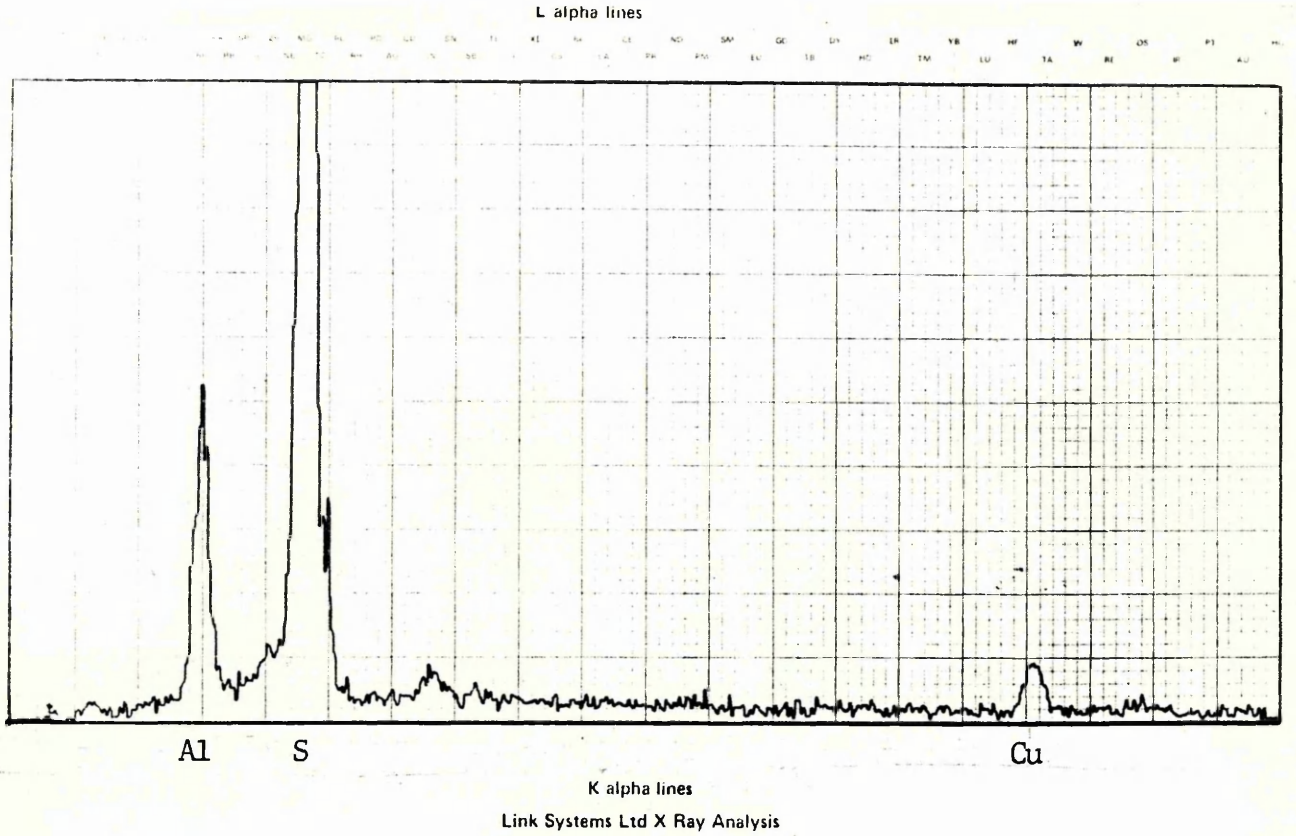

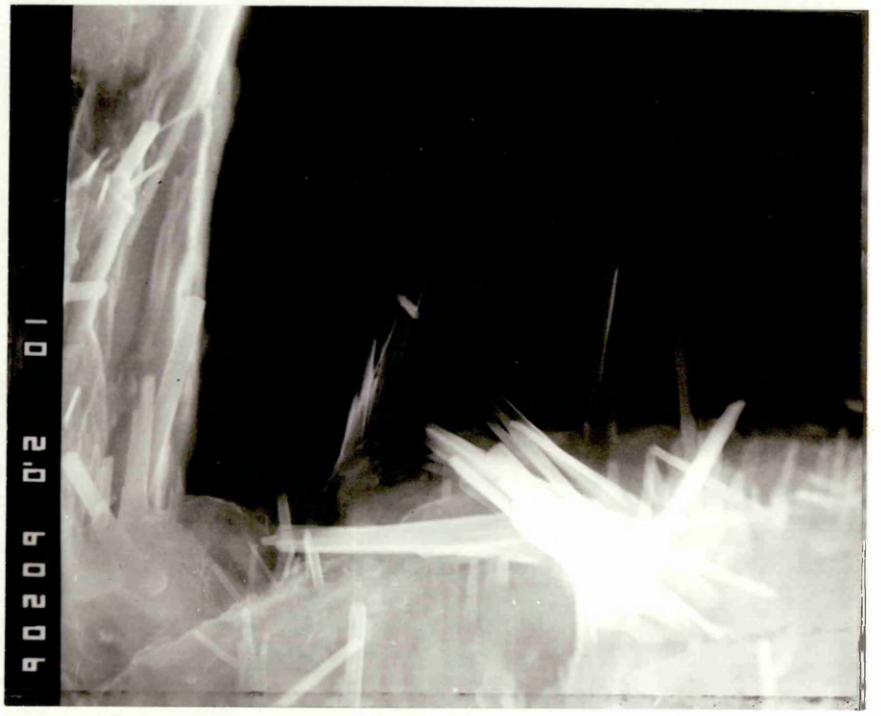

Figure 4.20 X-ray analysis of needle shaped crystals found in the crystalline material analysed in figure 4.19 and shown in the micrograph.

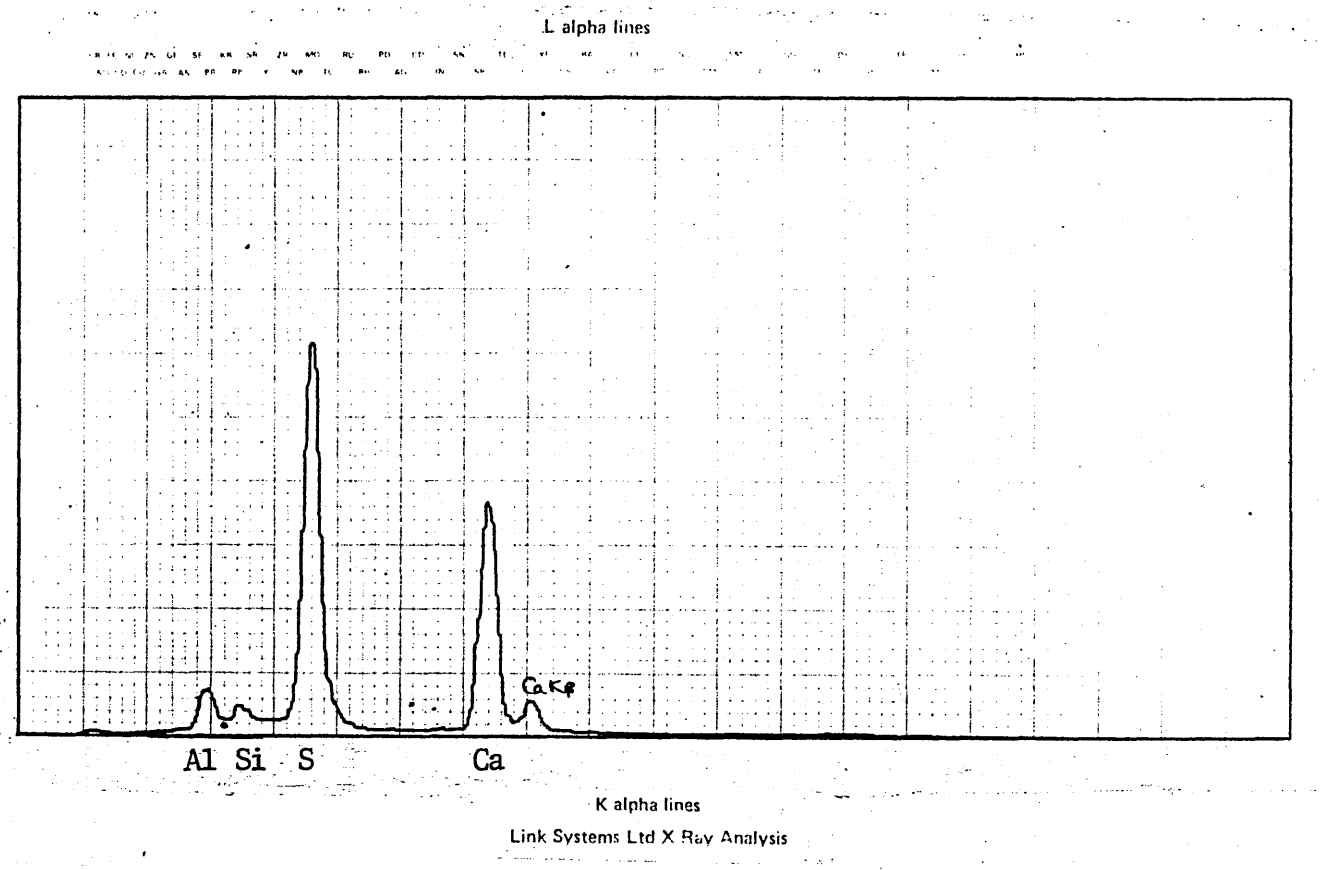

Figure 4.21 Microprobe analysis of crystalline material found in a Mode II fracture surface.

To confirm that Mode III damage resulted from insoluble glass degradation products, unloaded crossply coupons were immersed in nitric, hydrochloric and phosphoric acids of similar concentration. Damage did not develop in samples subjected to nitric acid, only one small transverse crack in the 0^{o} ply occurred in hydrochloric acid, whereas in phosphoric acid damage developed in both the immersed and unimmersed halves of the coupon. Comparison of the solubilities of the salts of calcium and aluminium formed in each of these acids, shown in Table 4.6, confirms that the formation of Mode III damage is directly related to the solubility of the glass corrosion products. Furthermore, since the calcium salts are the more insoluble, it appears that these are primarily responsible. The development of Mode III damage in phosphoric acid took considerably longer than in sulphuric acid, this is attributed to the lower acidity of the phosphoric acid, as shown by its greater pK_a value.

Further confirmation that Mode II failure was the result of insoluble glass degradation products was obtained by using hydrochloric acid of similar hydrogen ion concentration to the sulphuric acid. At initial applied strains of $\simeq$ 0.1% failure occurred within the environment by the Mode I mechanism, in a longer time than for Mode II failure in aqueous sulphuric acid, but in a shorter time than Mode I in the closed cells. The reduced time to Mode I failure shown by hydrochloric acid compared to sulphuric acid suggests that the hydrogen ion activity may be different. The interpretation of the differing effects of these acids needs further study.

Acid	H_2O	1M HCl	1M HNO_3	0.5M H_2SO_4	0.5M H_3PO_4
pK_a	-	-7	-1.4	-3	2.1
t_{III}	∞	∞	∞	3-7	>14
Salt	Solubility* /mol kg^{-1}				
$CaCl_2$	5.36	>5.36	-	-	-
$Ca(NO_3)_2$	6.2	-	>6.2	-	-
$Ca\ SO_4$	4.7×10^{-2}	-	-	4.4×10^{-2}	-
$Ca_3(PO_4)_2$	6.3×10^{-4}	-	-	-	3.5×10^{-5}
$Al_2(SO_4)_3$	0.91	-	-	-	-

* The solubilities in acidic environments are calculated from their solubilities in water and the appropriate solubility product (92,93)

Table 4.6 The time for onset of Mode III cracking (t_{III}/days) of $0^o/90^o/0^o$ epoxy-glass coupons half-immersed in aqueous acids, and its relationship with the acidity (pK_a) and solubility of the calcium and aluminium salts.

As discussed in section 4.5 it has already been shown that at low applied strains (< 0.15%), diffusion parallel to the glass reinforcement occurs much faster than at right angles to it. In crossply laminates the thermal strain $\varepsilon_{t\ell}^{th}$ has been shown to be sufficient for debonding to occur in the environment and allow the acid to penetrate the transverse ply. Thus the thermal strain $\varepsilon_{\ell t}^{th}$ in the longitudinal plies will also lead to debonding of the glass fibres in the presence of acidic environments with the subsequent rapid capillary diffusion in the direction of the reinforcement. The aqueous acid at the glass matrix interface will also leach the metallic ions from out of the glass fibre surface. Under capillary action the acid is transported to the unimmersed portion of the coupon, where concentration of the glass degradation products may result from the following processes.

(1) Absorption of water by the "dry" resin.
(2) Continued leaching of the metallic elements, without the opportunity to diffuse away into the bulk of the corrodent.
(3) Evaporation of moisture from the unimmersed portion of the coupon.

The effects of absorption of water by the resin, and/or loss by evaporation will be similar to a flame at the end of a wick, and thereby provide the driving force for more corrodent to be drawn into the immersed half of the laminate and be transported to the unimmersed part. That this is of major importance in concentrating the glass degradation products is shown by the suppression of Mode II failure in the closed-cells. The moisture saturated atmosphere surrounding the coupon stops the evaporation

of water and there is no driving force for the continual transport of the glass corrosion products to the unimmersed half of the coupon. Similarly in partially immersed non-externally stressed $0^{o}/90^{o}/0^{o}$ crossply coupons, Mode III damage begins near the top of the glass container where the onset of evaporation is most pronounced,as shown in Figure 4.22. This is confirmed when the cell is completely filled,because Mode III damage appears immediately above the surface of the environment as shown in Figure 3.8. This further indicates that a high relative humidity suppresses the damage by not allowing the concentration of the glass degradation products to occur.

The mechanism by which the environmental stress corrosion cracking is enhanced by the precipitation of degradation products in producing a Mode II failure is still not certain. There appears to be two possible mechanisms.

(1) Precipitation of the least soluble salt (calcium sulphate if sulphuric acid is the acidic environment) at the fibre matrix interface causing resin cracking, and allowing the acid access to previously protected fibres.

(2) Precipitation of the least soluble salt at the crack tip which then provides sufficient tensile force, due to crystallization pressure to open the crack.

That neither of these mechanisms is operative in the aqueous environment is due to the solubility of calcium sulphate, which is sufficiently large to remain soluble in the immersed laminate. However a more insoluble salt such as calcium phosphate will precipitate within the environment causing Mode III type damage.

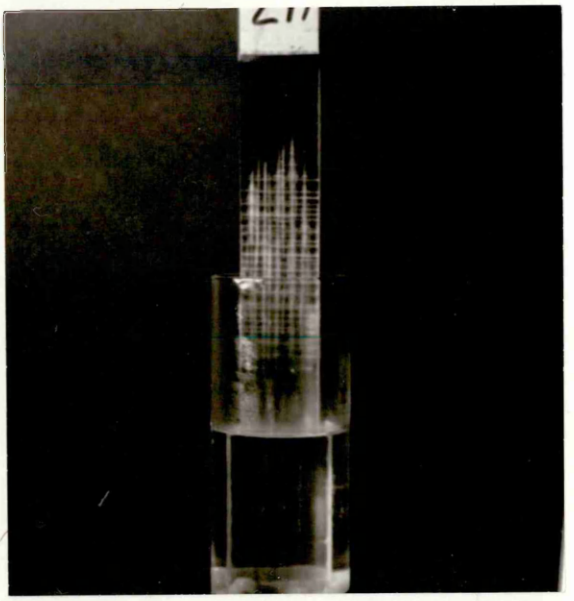

Figure 4.22 The development of Mode III damage near to the top of the glass container, as opposed to immediately above the environment.

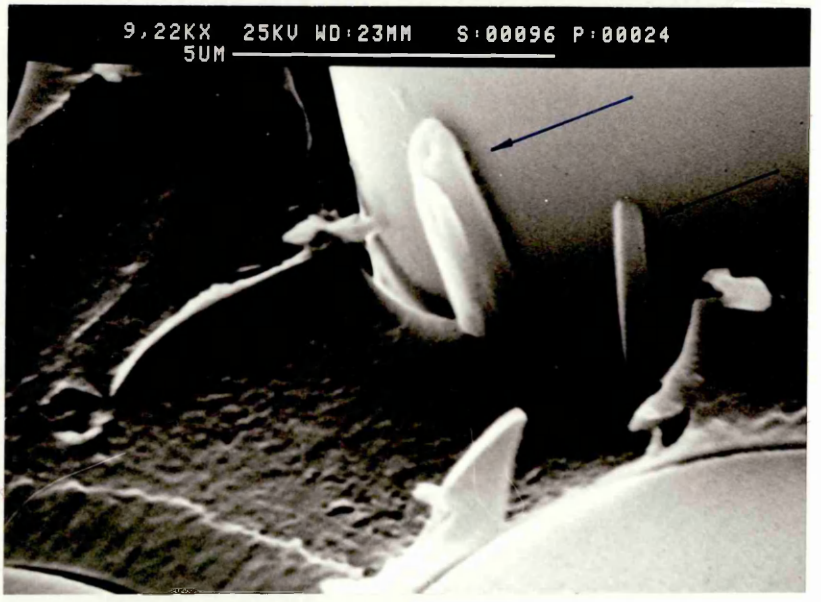

Figure 4.23 Material (crystalline) found at the fibre matrix interface in a Mode II failure fracture surface; shown arrowed in the micrograph.

The results of the low strain experiments carried out in aqueous sulphuric acid of increasing concentration are shown in Table 3.4. Above 1 M, Mode II failure was suppressed. There seems to be two possible explanations. Firstly, the observed Mode I failure is actually a Mode II failure which occurred within the aqueous acid because the common ion effect makes calcium sulphate less soluble in more concentrated sulphuric acid. Secondly, the increased acid concentration may lead to an increase in the rate of Mode I stress corrosion. The latter seems unlikely in view of the previous work (7,24,25) on the stress corrosion of E-glass bundles and laminates in acids of differing concentration where it was found that the most aggressive acid concentration is in the range of 0.5-2 M.

An example of the deposits found at the fibre matrix interface is shown in Figure 4.23. As yet no positive identification of this apparently crystalline material has been possible. Although it could be resin or glass splinters that have become lodged at the interface after fracture, the most likely explanation is that they are the crystals described here.

Thus Mode II failure results when the following four criteria are fulfilled.

(1) The resin provides sufficient chemical protection to produce longer times-to-failure than those for the unprotected single fibres.

(2) Moderately insoluble glass degradation products are formed.

(3) The corrodent can be transported to the unimmersed portion of a laminate.

(4) The glass corrosion products can precipitate on evaporation and/or dispersion of water.

Mode II failure has not been observed in polyester-glass coupons and this seems directly linked to the inability of the aqueous acid to attack the stressed fibre-matrix interface, as shown by the transverse ply failure strain remaining unaltered in the presence of acids, rapid transport of the environment to the unimmersed half of the coupon therefore cannot take place.

4.7 GENERAL MORPHOLOGICAL DETAILS

Hogg and Hull (26) identified three main structural features within stress corrosion fracture surfaces.

(1) Stress corrosion nucleation regions.
These were easily identified since the glass fibres were devoid of fracture patterns and the fracture plane ran through both the glass and the resin.

(2) Stress corroded regions.
The glass shows the usual fracture pattern, there is also fibre pull-out and debonding present.

(3) Steps.
Areas where the fracture shows a planar discontinuity.

The examination, by SEM, of both the 0^{o} unidirectional and $0^{o}/90^{o}/0^{o}$ crossply fracture surfaces of this study showed the presence of all three of these structures. Table 4.6 lists the Figure No. where examples of each structure may be found in this thesis.

Morphological Feature	Figure Number	Page Number
Stress Corrosion Nucleation Region	3.25	106
	3.26	107
	3.29	111
	3.30	111
Stress Corroded Region	3.27	109
	3.28	109
Steps	3.29	111
	3.30	111
	4.28	180
	4.29	180

Table 4.6 The location of SEM micrographs of morphological features within the thesis.

4.7.1 Step formation in the fracture surface

Hogg and Hull (27) observed that delamination occurred whenever the stress corrosion crack grew to a critical length, as illustrated in Figure 4.24. Furthermore, they found that increasing the initial applied strain, decreased the distance between delaminations. A similar mechanism has been observed in some of the 0^{o} unidirectional stress corrosion failures. Figure 4.25 shows one such coupon with two delamination cracks. Originally it was thought that a delamination process similar to that described by Hogg and Hull could explain the formation of the stepped fracture surfaces reported here, but operating on a reduced scale. However microscopical examination of the steps showed that they were not consistent with this theory, since if a step is formed by delamination, then there should be a crack at the base of the step. Figure 4.26 illustrates the formation of a step by delamination and the location of the crack at its base. In the majority of the fracture surfaces these base cracks were not observed showing that delamination was not responsible.

In section 4.5 evidence for the rapid entry of the environment through microcracks, formed by a stress corrosion mechanism was presented. It is therefore likely that the steps found in these fracture surfaces are the remnants of the microcracks. Stress corrosion within a microcrack will occur fastest at areas of greatest stress concentration, which will normally be where the crack is sharpest. This could produce two types of fracture depending whether stress corrosion cracks grow from different positions as illustrated in Figure 4.27. The stress corrosion cracks

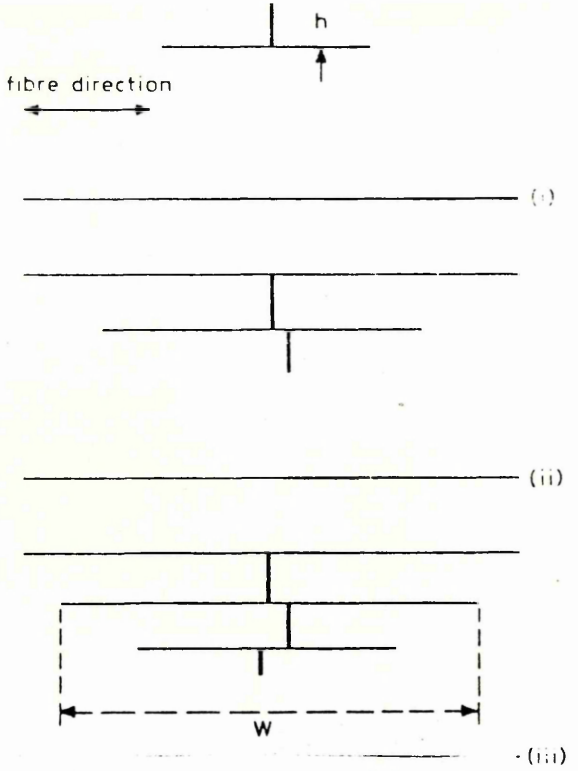

Figure 4.24 Schematic representation of formation of delamination crack at tip of strain corrosion cracks (1) nucleation of first delamination (2) further growth of strain corrosion crack (3) second delamination. Taken from reference 27.

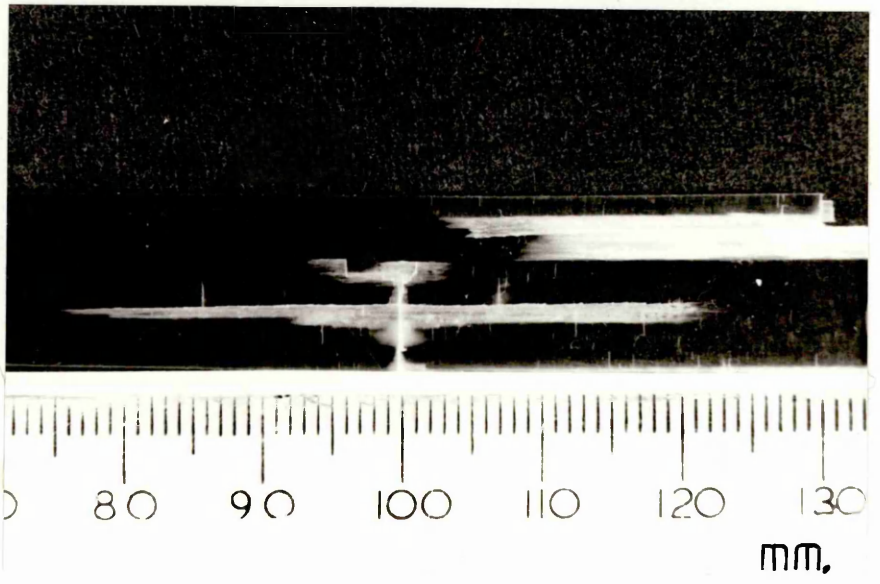

Figure 4.25 0^{o} unidirectional coupon showing two delamination cracks.

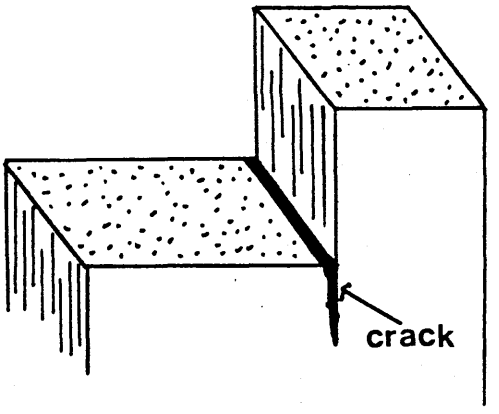

Figure 4.26 Diagramatic representation of the formation of a step by delamination, showing the position of the crack at the base of the step.

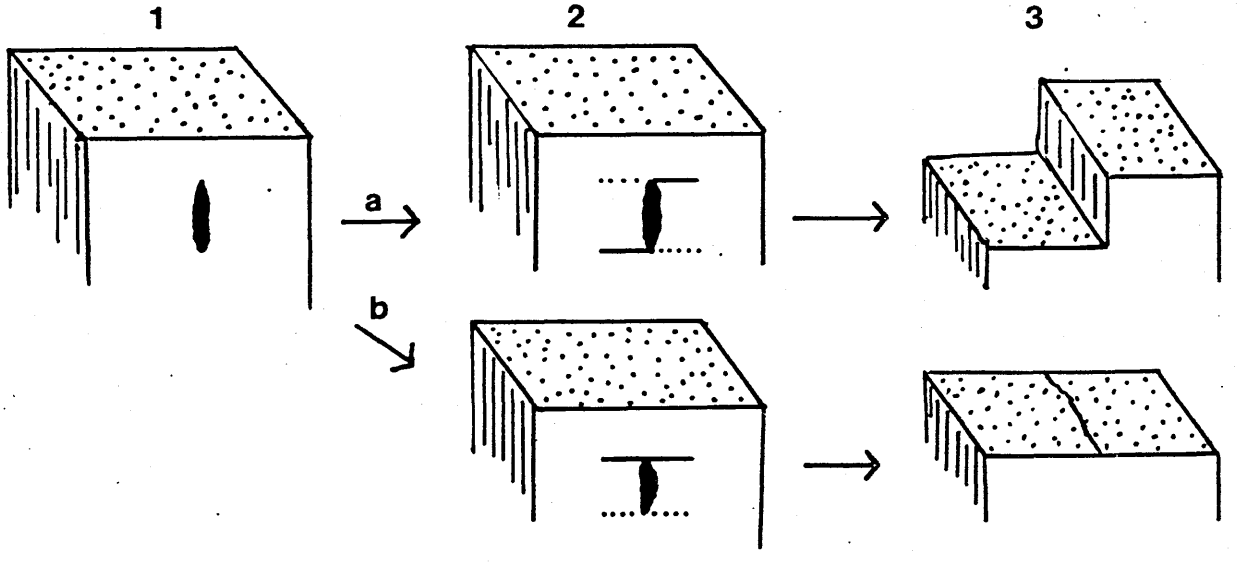

Figure 4.27 Formation of a step due to stress corrosion within a microcrack.

indicated by the dotted lines are not expected to grow so rapidly since they are in an area of reduced stress caused by stress relief from the mutual interference by the crack above or below it. Further evidence for this mechanism is given by the following observations.

(1) Microcracking in polyester (69) and epoxy laminates (94) generated under tensile loading occurs predominantly in fibre rich regions or at the borders between a resin rich-fibre rich regions. Further examination of these steps showed them to occur mainly at the interface between these resin rich-fibre rich areas as shown in Figure 4.28 Steps are not usually found in resin rich areas.

(2) In $0^{o}/90^{o}/0^{o}$ crossply coupons the steps are orientated predominantly normal to the transverse ply, as shown in Figure 4.29. This is similar to the expected orientation of the environmental microcracks which are allowing ingress of acid as described in section 4.5 and arises because of the thermal strain $\varepsilon_{\ell t}^{th}$ present within the 0^{o} plies.

The mechanism of step formation given above is consistent with and presents confirmatory evidence for the major feature of the stress corrosion of this epoxy-glass fibre laminate system. That is, the longitudinal ply is subject to stress corrosion, probably via the interface, as shown by the ease of debonding; with subsequent rapid transport of the environment by capillary action along the interface at low strains, and by environmental-microcracking at higher strains. Consequently at high strains the laminate failure times are the same as those for single glass filaments and Mode I fracture within

the environment occurs. At low strains Mode II and III mechanisms operate outside the environment. In conclusion, the interfacial properties of this laminate system control the long term lifetime of the material, in corrosive conditions.

Figure 4.28 Micrograph showing a step at the border between a resin-rich fibre-rich area.

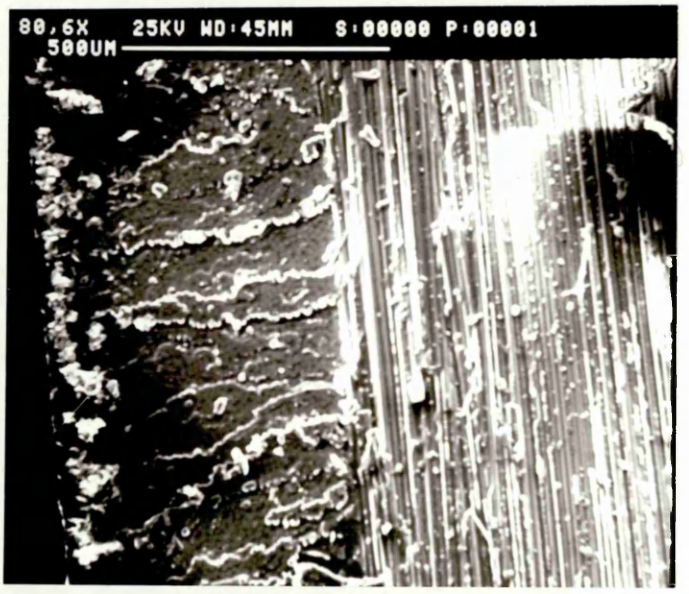

Figure 4.29 Micrograph showing the predominantly normal orientation of steps in the longitudinal plies to the transverse ply.

CHAPTER 5 CONCLUSIONS AND SUGGESTIONS FOR FURTHER WORK

5.1 CONCLUSIONS

The following conclusions about the mechanism of stress corrosion cracking of model glass fibre reinforced epoxy laminates, have been reached.

(1) The failure mode is dependent upon the magnitude of the initial applied strain, the nature of the aqueous environment and the type of environmental cell which controls the humidity of the atmosphere surrounding the immersed half. Three failure modes were identified.

Mode I: This occurs within the aqueous environment and was observed for both 0^{o} unidirectional and $0^{o}/90^{o}/0^{o}$ crossply coupons. At initial applied strains of greater than 0.15% it occurred in all the environmental cells, in similar failure times to those for unprotected E-glass fibres, and is associated with the rapid diffusion of the environment into the laminate. At strains of below 0.15%, Mode I is only observed if the more rapid Mode II failure is either suppressed, by removing the opportunity for concentrating the glass degradation products by the evaporation of water, as is the case in the closed cells, or in acidic environments such as hydrochloric acid, whose calcium salts are more soluble. At these low strains,Mode I failure occurs in longer times than that of the unprotected E-glass fibres.

Mode II: This occurs in the non-immersed half of the coupon and was found for both 0^{o} unidirectional and $0^{o}/90^{o}/0^{o}$ crossply laminates. At initial applied strains of less than 0.15% it occurs more rapidly than Mode I failure and is associated with the concentration and precipitation

of insoluble glass degradation products in the unimmersed half of the laminate, primarily by the evaporation of water.

Mode III: This has only been found in non-externally stressed $0^{o}/90^{o}/0^{o}$ crossply coupons and is related to Mode II failure, being similarly associated with the precipitation of insoluble glass degradation products.

(2) The results of the dynamic environmental transverse cracking experiments showed that the fibre matrix interface was susceptible to stress corrosion, leading to a partial debonding, and at applied strains greater than 0.15%, the formation of environmental-microcracks. It is the stress corrosion of the fibre matrix interface, that is responsible for the rapid stress corrosion cracking observed for these epoxy-glass laminates.

5.2 SUGGESTIONS FOR FURTHER WORK

The results in this thesis have identified two main areas for further study.

(1) Stress corrosion of the fibre-matrix interface.

The fibre-matrix interface in these laminates has been shown to be susceptible to stress corrosion, whereas the interface in polyester-glass composites appears to be resistant. Furthermore environmental microcracking can occur which leads to rapid permeation of these laminates by the aqueous acid. Further investigation of these phenomena are required to determine the effects of stress and aqueous acid on the glass-matrix interfacial chemistry, to better determine the matrix requirements necessary for environmental stress corrosion cracking resistance.

(2) Glass degradation products.

It has been shown that glass fibre degradation products may cause an accelerated failure where fracture occurs in that part of the composite not directly in contact with the environment. The mechanism of stress corrosion cracking of GRP by the crystallization of the glass degradation products is an area where further study is needed. Possibly, a microscopical study of model laminates, could determine how the glass degradation products affect the stress corrosion cracking resistance. The nature of these chemical degradation processes also tends to question the presently accepted mechanism of stress corrosion of glass fibres, and further study may lead to chemical ways of stabilizing the glass.

CHAPTER 6 REFERENCES

REFERENCES

1. Scully, J.C., in "The Fundamentals of Corrosion" (Pergamon Press, London, 1975) p. 179 - 208.

2. Vincent, P.I., in "Encyclopedia of Polymer Science and Technology" (Interscience Publishers, New York, 1967) Vol.7, p. 261 - 361.

3. Brydson, J.A., in "Plastic Materials" (Newnes Butterworths, London 1975) p. 202.

4. Feur, S.S. and Torres, A.F., Proceedings of the 15th S.P.I. Conference, Chicago, 1961. Section 5B p. 1 - 10.

5. Torres, A.F. and Feur, S.S., Proceedings of the 16th S.P.I. Conference, Chicago, 1962. Section 5D p. 1 - 13.

6. Judd, N.C.W., Lloyd, T., McMullen, P and Russell, E.W., Proceedings of the 15th S.P.I. Conference, Chicago, 1961. Section 5C p. 1 - 18.

7. Roberts, R.C., Reinf. Plast. Congress (BPF), Brighton, 1978, paper 19.

8. Sillwood, J.M., N.P.L. Report DMA (B) 1982.

9. Dewimille, B., Thoris, J., Mailfert, R and Bunsell, A.R., in "Adv in Composite Materials" Ed. Bunsell, A.R. et al. (Pergamon Press, Paris, 1980) Vol. 1, p. 597 - 612.

10. Dewimille, B and Bunsell, A.R., Composites, 14 (1983)35.

11. Aveston, J., Kelly, A., McCartney, L.N. and Sillwood, J.M., in "Progress in Science and Engineering of Composites" Ed. Hayashi et al.(Japan Soc. of Composites, Tokyo, 1982) Vol.2, p. 947.

12. Metcalfe, A.G. and Schmitz, G.K., Glass Technology, 13 (1972)5.

13. Rawe, A.W., Trans. J. Plast. Inst. 27 (1962)27.

14. Hogg, P.J., Hull, D. and Spencer, B., Composites, 12 (1981)166.

15. Bott, T.R. and Barker, A.J., Conf. Research Projects in Reinforced Plastics (The Plastics Institute) London, 1968, paper 10.

16. Oswitch, S., Reinforced Plastics, 8 (1964)174.

17. Collins, H.H., Plastics and Rubber: Materials and Applications, 3 (1978)6.

18. Aveston, J. and Sillwood, J.M., J. Mater. Sci. 17 (1982)3491.

19. Jones, F.R. and Wheatley, A.W., Personal Communication 1982.

20. Carswell, W.S. and Roberts, R.C., Composites, 11 (1980)95.

21. Barker, H.A., Baird-Smith, I.G. and Jones, F.R., Symp. Reinf. Plast. in Anticorrosion Appl. (N.E.L.) Glasgow, 1979, paper 12.

22. Hull, D and Hogg, P.J., Proceedings 13th Reinf. Plast. Congress (BPF) Brighton, 1982, paper 29, p. 115 - 120.

23. Wiederhorn, S.M. and Bolz, L.H., J. Amer. Ceram. Soc. 53 (1970)543.

24. Scrimshaw, G., Pipecon, London, 1980, paper 5, p. 1 - 17.

25. Cockram, D.R., Glass Technology 22 (1981)211.

26. Hull, D and Hogg, P.J., in "Adv. in Composite Materials" Ed. Bunsell, A.R. et al. (Pergamon Press, Paris, 1980) Vol. 1, p. 543-555

27. Hogg, P.J. and Hull, D, Metal Science, 14 (1980)441.

28. Hogg, P.J., Hull, D. and Legg, M.J., in "Composite Structures" Ed. Marshall, I.H., (App. Sci. London, 1981) Chapter 8, p. 106 - 122.

29. Jones, F.R., Wheatley, A.R. and Bailey, J.E., in "Composite Structures" Ed. Marshall, I.H., (App. Sci. London, 1981) Chapter 27, p. 415-429

30. Bailey, J.E., Freyer, T.M.W. and Jones, F.R., in "Adv. in Composite Materials" Ed. Bunsell, A.R.et al. (Pergamon Press, Paris, 1980) Vol.1, p. 514 - 528.

31. Jones, F.R. and Wheatley, A.W., Personal Communication 1982.

32. Kelly, A. and McCartney, L.N., Proc. Roy. Soc. Lond. A. 374 (1981)475.

33. McCartney, L.N., Fibre Science and Technology, 16 (1982)95.

34. Plueddemann, E.P., in "Composite Materials" Ed. Broutman, J.L. and Krock, R.H. (Academic Press, New York, 1974) Vol. 6, Ed. Plueddemann, E.P., p. 174 - 216.

35. Ishida, H. and Koenig, J.L., Polymer Eng and Sci. 18 (1978)128.

36. Charles, R.J., J. Appl. Phys. 29 (1958)1549.

37. Charles, R.J., ibid. 29 (1958)1554.

38. Taylor, N.W., ibid. 18 (1947)943.

39. Hillig, W.B. and Charles, R.J., in "High Strength Materials" Ed. Zackay, F., (John Wiley and Sons, New York, 1964) Chapter 17, p. 682 - 706.

40. Wiederhorn, S.M., Fuller, E.R. and Thomson, R., Metal Science, 14 (1980)450.

41. Mould, R.E. and Southwick, R.D., J. Amer. Ceram. Soc. 42 (1959)582.

42. McKinnis, C.L., in "Fracture Mechanics of Ceramics" Ed. Bradt, R.C. et al. (Plenum Press, New York, 1978) Vol. 4, p. 581 - 595.

43. Wang, F.F. and Tooley, F.V., J. Amer. Ceram. Soc. 41 (1958)521.

44. Metcalfe, A.G., Gulden, M.E. and Schmitz, G.K., Glass Technology 12 (1971)15.

45. Barker, A.J. and Bott, T.R., Trans. Inst. Chem. Engrs. 47 (1969)212.

46. Weyl, W.A., J. Amer. Ceram. Soc. 32 (1949)367.

47. Hammond, M.L. and Ravitz, S.F., ibid. 46 (1963)329.

48. Michalske, T.A. and Freiman, S.W., Nature, 295 (1982)511.

49. El-Shamy, T.M. and Douglas, R.W., Glass Technology, 13 (1972)77.

50. El-Shamy, T.M., Lewins, J. and Douglas, R.W., ibid. 13 (1972)81.

51. Elmer, T.H. and Nordberg, M.E., J. Amer. Ceram. Soc. 41 (1958)517.

52. Moy, P and Karasz, F.E., in "Water in Polymers" Ed. Rowland, S.P., (Amer. Chem. Soc. Washington, D.C. U.S.A. 1979) p. 505 - 514.

53. Menges, G. and Gitschner, H.W., in "Adv. in Composite Materials" Ed. Bunsell, A.R. et al. (Pergamon Press, Paris, 1980) Vol.1, p. 25 - 48.

54. Adamson, M.J., J. Mater. Sci. 15 (1980) 1736.

55. Cuthrell, R.E., J. Appl. Pol. Sci. 11 (1967)949.

56. Kenyon, A.S. and Nielson, L.E., J. Macromol. Sci. - Chem. A.3 (1969)275.

57. Hix, C.F. and Alley, R.P., in "Physical Laws and Effects" (John Wiley and Sons, New York, 1958) p. 75 - 77.

58. Marshall, J.M. Marshall, G.P. and Pinzelli, R.F., Proceedings of the 37th S.P.I. Conference, Washington, 1982 Section 9C p. 1 - 9.

59. Ashbee, K.H.G., Frank, F.C. and Wyatt, R.C., Proc. Roy. Soc. Lond. A. 300 (1967)553.

60. Farrar, N.R. and Ashbee, K.H.G., J. Phys. D. Appl. Phys. 11 (1978)1009.

61. Regester, R.F., Corrosion-Nace, 25 (1969)157.

62. Marshall, J., SAMPE Quarterly, 13 (1982)23.

63. Hahn, H.T. and Kim, R.Y., in "Advanced Composite Materials - Environmental effects" Ed. Vinson, J.R., (ASTM STP 658, 1977) p. 99 - 120.

64. Gillat, O. and Broutman, J.L., in "Advanced Composite Materials - Environmental effects" Ed. Vinson, J.R., (ASTM STP 658, 1977) p. 61 - 83.

65. Whitney, J.M. and Browning, C.E., in "Advanced Composite Materials - Environmental effects" Ed. Vinson, J.R., (ASTM STP 658, 1977) p. 43 - 60.

66. Hull, D., in "An Introduction to Composite Materials" (Cambridge University Press, Cambridge, 1981) p. 99.

67. Bott, T.R. and Barker, A.J., Trans. J. Plast. Inst. 33 (1965)153.

68. Schapery, R.A., J. Comp. Mat. 2 (1968)380.

69. Parvizi, A., Ph.D. Thesis, University of Surrey 1978.

70. Alfrey, T., Burnee, E.F. and Lloyd, W.G., J. Pol. Sci. Part C 12 (1966)249.

71. Wyatt, R.C. and Ashbee, K.H.G., Fibre Science and Technology, 2 (1970)29.

72. Nicholas, J. and Ashbee, K.H.G., J. Phys. D. Appl. Phys. 11 (1978)1015.

73. Smithgall, D.H., Watkins, L.S. and Frazee, R.E., Applied Optics. 16 (1977)2395.

74. Timoshenko, S., J. Optical Soc. Amer. 11 (1925)233.

75. Bailey, J.E., Curtis, P.T. and Parvizi, A., Proc. Roy. Soc. Lond. A. 366 (1979)599.

76. Wilson, G., Personal Communication 1982.

77. Lee, H. and Neville, K., in "Handbook of Epoxy Resins" (McGraw-Hill, New York, 1967) p.

78. Rosato, D.V. and Grove, C.S., in "Filament Winding" (Interscience Publishers, New York, 1964) Chapter 4, p. 88 - 95.

79. McCrum, N.G., in "A Review of the Science of Fibre Reinforced Plastics" (HMSO, 1971).

80. Garrett, K.W. and Bailey, J.E., J. Mater. Sci. 12 (1977)157.

81. Pye, L.D., Stevens, H.J. and LaCourse, W.C., in "Introduction to Glass Science" (Plenum Press, 1972).

82. Jones, F.R., Mulheron, M. and Bailey, J.E., in "Progress in Science and Engineering of Composites" Ed. Hayashi et al. (Japan Soc. of Composites, Tokyo, 1982) Vol.2, p. 1045 - 1052.

83. Bailey, J.E. and Parvizi, A., J. Mater. Sci. 16 (1981)649.

84. Epikote Technical Manuel E.P. 1.1.12. (Shell Co. Ltd.).

85. Lee, K.P., B.Sc. Project, University of Surrey 1982.

86. Parvizi, A and Bailey, J.E., J. Mater. Sci. 13 (1978)2131.

87. Kimber, A.C. and Keer, J.G., J. Mater. Sci. Letters, 1 (1982)353.

88. Ashton, J.E., Halpin, J.C. and Petit. P.H., in "Primer on Composite Materials" (Technomatic, Stamford, U.S.A., 1969) p.77 - 83.

89. Wheatley, A.R. and Jones, F.R., Personal Communication 1982.

90. Jones, F.R., Rock, J.W., Wheatley, A.R. and Bailey, J.E., in "Progress in Science and Engineering of Composites" Ed. Hayashi et al. (Japan Soc. of Composites, Tokyo, 1982) Vol. 2, p. 929.

91. Jones, F.R., Rock, J.W., Wheatley, A.R. and Bailey, J.E., Reinf. Plast. Congress (BPF) Brighton 1982. paper 32. p. 127.

92. Vogel, A.I., in "Textbook of Qualitative Inorganic Analysis" (Longmans, London, 1954).

93. Handbook of Chemistry and Physics, (CRC, Ohio, 1972).

94. Bailey, J.E. Jones, F.R. and Wheatley, A.R., in "Final Report and Progress report for S.E.R.C. and S.E.R.C./P.E.D. Funded research programmes. University of Surrey Dec. 1982.

CHAPTER 7 APPENDIX:- PUBLICATIONS

Environmental Stress Corrosion Cracking of GRP

F. R. Jones, J. W. Rock, A. R. Wheatley and J. E. Bailey
Department of Metallurgy and Materials Technology, University of Surrey, Guildford, Surrey, UK.

Abstract

The ESCC of epoxy and polyester glass fibre 0° and 0°/90°/0° composites has been studied. We have shown that the polyester resin protects the fibres in that the composites fail after a longer time than single filaments. The Mode I fracture of 0° coupons is nucleated at ESCC cracks in individual fibres. The transverse cracked 0°/90°/0° coupons are a special case where an enhanced stress in 0° ply adjacent to a transverse crack localises the failure. Post-curing of the 0° polyester coupons reduces the ESCC resistance.

Although the epoxy resin appears to be resistant to aqueous acid the transverse failure strain of 0°/90°/0° coupons is reduced by the combined influence of stress and the environment, with the effect that at strains >0.1% failure times of the coupons are found to be similar to those for single filaments. In addition, at strains <0.1% in which only half the coupon is immersed in the environment, Mode II failure of the 'dry' half occurs in a shorter time. The latter is related to the Mode III damage which occurs also in the unstressed half of unstressed coupons and appears to be caused by the growth of crystalline glass corrosion products.

Under bending moments, the transverse cracks in 0°/90°/0° polyester coupons have been shown to initiate a rapid stress corrosion fracture of the 0° plies.

1. Introduction

Glass fibre reinforced unsaturated polyester resins are becoming increasingly used in applications in which the material is in contact with acidic environments, such as process plant equipment, storage vessels and sewage pipes. The long term effect of aqueous acids on the carefully selected matrix resins and unstressed laminates has been shown to be minimal. However, GRP structures in service and during the laying of a buried pipe may also be subjected to stresses in addition to the corrodent. Typical tensile strains encountered in a GRP pipe may be of the order of 0.25% (1) well below the short term failure strain and would not be considered to lead to failure under normal conditions. However, a synergism between the stress and the environment has recently been shown to lead to unexpectedly rapid failures in a few hours at similar strains (1-3). The terms 'Environmental Strain Corrosion Cracking' and 'Environmental Stress Corrosion Cracking' have been used to describe failures of the GRP under constant strain or constant load respectively. In both cases the major characteristic of these failures is the smooth fracture surfaces. Hull and co-workers (5-7) have identified the initiation of the strain corrosion crack from the area of an SEM micrograph where the fractured glass fibres are devoid of flow lines typical of more rapid fractures.

Previous reports (1, 3, 5-7) have been concerned with tests on filament wound pipes subjected to a constant deflection or constant load in which the stress state is uncertain because there is a progressive change from a tensile to a compressive strain in a bent beam. Furthermore, because of their weak transverse properties useful composite materials have fibres at angles to one another. In the extreme case when the fibres are at right angles, an increased strain in the ply 90° to the applied stress leads to multiple transverse cracking at strains lower than the failure strain of either component. In addition, the transverse cracking strain can be reduced by thermal strains generated through the differential contraction of the individual plies, on cooling from the post curing temperature, which is dominated by the matrix in the 90° ply but is constrained by the higher modulus fibres in the 0° direction (7). It has also been observed that fibre matrix debonding can occur prior to transverse cracking at lower strains (9). Furthermore, higher thermal strains develop in polyester GRP than in the equivalent epoxy material (10, 11) where debonding was observed. It has been suggested (9), therefore, that the fibres in polyester laminates may be already debonded. We have, certainly, demonstrated the formation of microcracks in transverse plies of polyester GRP on cooling from the post-cure temperature. Cold cured laminates which have not experienced an elevated post-cure temperature nor an adventitious exotherm are free of microcracks (11).

We report here an extension of this study to the environmental stress corrosion cracking (ESCC) of carefully made, well characterised 0°/90°/0° crossply and 0° unidirectional coupons. The glass fibres chosen for the study were Silenka 051P 1200 tex with a polyester/epoxy compatible finish. The resin systems were an isophthalic unsaturated polyester filament winding resin (Crystic 272 — Scott-Bader Co. Ltd.) and a bisphenol 'A' epoxy resin (Epikote 828 — Shell Chemicals Ltd.) with NMA hardener and BDMA curing catalyst. The epoxy resin was chosen for its resistance to cracking and had previously been well characterised and could be considered to be a model for chemical resistant polyesters which are also based on bisphenol 'A' intermediates. We have identified different modes of failure and have investigated the importance of transverse cracks on the ESCC fracture of the load bearing plies.

2. Experimental

2.1 Laminate Preparation

The laminates were prepared by winding Silenka E glass 051P (1200 Tex) roving onto steel frames using a winding machine which ensured a uniform distribution of glass fibres and consistent volume fractions for the laminates. The Epoxy resin was Epikote 828 hardened with 80 phr NMA catalysed with 1.5 phr BDMA. Laminates free of entrapped air were prepared by a one stage vacuum-assisted resin impregnation technique. Full details will be given elsewhere (12). The laminates were cured between silicone treated 'Melinex' sheets and glass plates at 100°C for 3 hours, cut into coupons 25 cm x 2 cm and post-cured at 150°C for 3 hours and cooled out of the oven. The softening point of the laminate was found to be 140°C from the onset of curvature of a 0°/90° coupon on cooling (10). We have also examined coupons prepared with a stoichiometric quantity (90 phr) of NMA and post-cured at 200°C for 24 hours. Although the rate of decrease of the transverse cracking strain under an applied stress in the presence of the environment is slightly smaller (see Fig. 11) the overall stress-corrosion phenomena reported in section 3 are the same (12). The volume fraction of glass fibres was found to be 55%.

The polyester resin (Crystic 272) was cured with 2% Catalyst M and 0.25% Accelerator E (Scott-Bader Co. Ltd.). The laminates were prepared by a two-stage technique (11) in which the 90° ply was gelled for 24 hours prior to laying-up the 0° plies. After a further 24 hours at room temperature (no measurable exotherm was observed) the coupons were cut out with a water-cooled diamond wheel and post-cured for a) 170h at 110°C, b) 15h at 50°C, and c) 3h at 80°C. The volume fractions of glass fibres were 35% for crossply and 45% for the unidirectional laminates.

Each laminate was characterised by testing coupons in tension (polyester and epoxy) and in 4-point bend (polyester only) in an Instron to determine the transverse cracking loads and initial modulus. The strains were obtained from resistance strain-gauges attached to the coupons with cold setting epoxy adhesive.

2.2 Environmental Testing

Two types of tensile environmental cell constructed from borosilicate glass are illustrated in Fig. 1. The 'open' cell was a tube supported on the coupon with a split rubber bung, sealed with silicone grease. The 'closed' cell was designed so that the temperature could be controlled by circulating thermostatted water through the jacket and the atmosphere, by purging with an appropriate gas or left closed so that the atmosphere was saturated, more typical of a pipe or container in use. The cell was attached in the same manner with silicone grease to prevent leaks. The glass/epoxy was sealed with silicone putty. In 4-point bend the whole coupon supported in a stainless steel jig was immersed in the environment. The load was transmitted through a magnifying arm. A detailed analysis will be presented elsewhere (13). However, for comparison with the other tests, the loads have been normalised to the load required for the first transverse crack, F_{tc}.

The stress corrosion of the glass fibres was carried out on single fibres, separated from the tow, glued onto cardboard frames and their diameter determined by laser refraction. They were removed from the frames and glued to a glass rod with 'Evostik' high impact adhesive. Glass weights were hung onto the fibres by means of an elastic band glued to the other end. A small compensating weight was glued to the rubber band to overcome its positive buoyancy. The failures were monitored by reed switches interfaced to a PET computer programmed to store the failure times.

3. Results

The 0°/90°/0° model composite has been described previously (8, 9). In these experiments the thickness of the outer 0° ply was equal to half that of the inner 90° ply and was approximately 1mm. The environmental stress corrosion cracking (ESCC) of these glass fibre laminates has been studied in tension and in 4-point bend under a constant load. At low strains in tension of approximately 0.2% the epoxy glass laminates fractured within 24 hours whereas the polyester/glass coupons were still intact after 3 months. The latter, however, developed a series of transverse edge-cracks (14) but these did not lead to fracture of the 0° load bearing plies. We have, therefore, studied the polyester laminates both in tension and 4-point bend.

3.1 Environmental Stress Corrosion Cracking of Epoxy/Glass Laminates in Tension

The experiments have been carried out on coupons with an environmental chamber attached to specimens, so that only half of the coupon was immersed in the environment. Two types of cells were used in which the unimmersed half was exposed to the atmosphere ('open' cell) or enclosed so that the atmosphere was saturated with the most environment ('closed' cell).

The stress corrosion of the load bearing plies may occur either within the aqueous 0.5 M sulphuric acid, termed Mode I or outside the liquid

Fig. 1. ESCC of epoxy-glass laminates in 0.5M H_2SO_4.

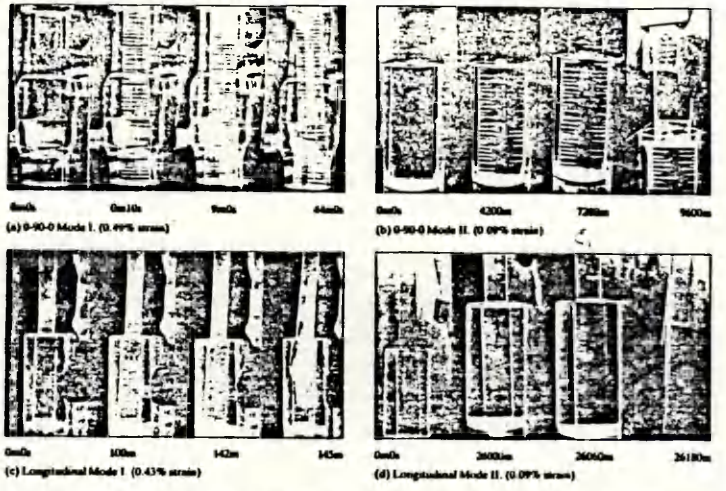

(a) 0-90-0 Mode I. (0.49% strain)
(b) 0-90-0 Mode II. (0.09% strain)
(c) Longitudinal Mode I (0.43% strain)
(d) Longitudinal Mode II. (0.09% strain)

The experiments have been carried out on coupons with an environmental chamber attached to specimens, so that only half of the coupon was immersed in the environment. Two types of cells were used in which the unimmersed half was exposed to the atmosphere ('open' cell) or enclosed so that the atmosphere was saturated with the most environment ('closed' cell).

The stress corrosion of the load bearing plies may occur either within the aqueous 0.5 M sulphuric acid, termed Mode I or outside the liquid in the unimmersed part of the specimen, termed Mode II. The mode of failure which occurs is dependent upon the type of environmental cell, the nature of the environment, and the initial applied strain. The difference between the two types of failure is illustrated in Fig. 1.

3.1.1 0°/90°/0° Crossply Laminates

At applied strains in the region of and greater than 0.15%, Mode I failures occur in both types of environmental cell. At lower strains Mode II fracture occurs in the 'open' cell and Mode I in the 'closed' cell.

Mode I failures occur by fracture of the longitudinal plies adjacent to one of the early microcracks in the transverse ply. As shown in Fig. 1a the initial applied strain was sufficient to induce transverse cracking and the transverse crack responsible for failure is indicated. However, at lower strains such that no transverse cracks would be produced in air, cracks are seen to form at the edge of the coupon, in contact with the aqueous acid, and propagate into the transverse ply. Examination of Fig. 1b demonstrates the growth of these edge-cracks during the test, in this case Mode II failure occurs but in the 'closed' cell and at higher strains in the 'open' cell they lead to a Mode I failure of the longitudinal plies adjacent to an early one. Since these edge-cracks lead to the same failure mode as 'true' transverse cracks, they can also be considered to have similar characteristics to the transverse cracks produced in dry specimens.

We have confirmed this effect in a dynamic tensile stress corrosion test in which the spacing of the transverse cracks in the coupon both in and out of the acid were compared. The number of cracks which formed in the environment was considerably larger and analysis (12) of the results indicated that the transverse cracking strain was greatly reduced (Fig. 11).

As shown in Fig. 1d, Mode II failure of the 0° plies occurs above the level of the aqueous acid. The crack grows simultaneously through both the width and thickness of the laminate before the edge-cracks have grown to sufficient length for a significant load to be transferred onto the 0° plies immersed in the environment, but the unfractured part of the laminate experiences an enhanced stress so that the 'edge-cracks' also grow at a faster rate.

In Fig. 2, the times-to-failure of crossply laminates at various applied stresses in the two environmental cells are compared. The dry transverse cracking strain is 0.3% and it is clear that at lower applied strains the failure times are consistent and independent of the environmental cell. However at applied strains lower than ≅ 0.1%, in the 'open' cell, the Mode II failure, which appears to be less sensitive to strain, occurs in apparently shorter times.

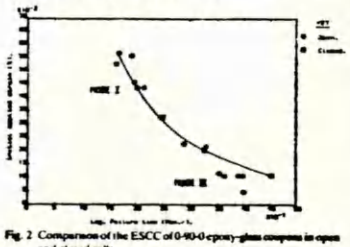

Fig. 2 Comparison of the ESCC of 0-90-0 epoxy-glass coupons in open and closed cells

3.1.2 0° Unidirectional Laminates

As shown in Figs. 1c and 1d, the 0° unidirectional laminates can also fail by either Mode I or Mode II depending upon the applied strain and the type of the environmental cell. The failure times are reported in Fig. 3a together with those for the crossply coupons in which the applied strain has been recalculated assuming that a microcracked transverse ply carries no load, so that the stress on the 0° plies is correspondingly larger. There is a close correlation between the failure times of both types of laminate.

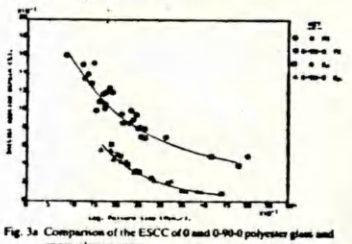

Fig. 3a Comparison of the ESCC of 0 and 0-90-0 polyester glass and epoxy-glass coupons

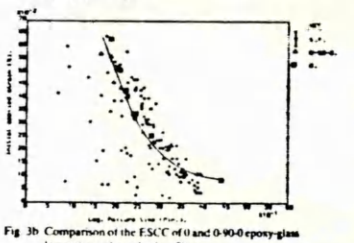

Fig. 3b Comparison of the ESCC of 0 and 0-90-0 epoxy-glass laminates with single glass fibres

Prior to failure by Mode I, coupons tested at applied strains ≥ 0.2%, a number of stress corrosion cracks are formed at random and grow until they coalesce by longitudinal splitting. This leads to a stepped fracture surface (Fig. 4b).

At lower strains, Mode II fracture occurs producing a smooth fracture surface typical of 0° plies in a stress corrosion cracked 0°/90°/0° laminates (Fig. 4a).

Fig. 4 Typical ESCC fracture surfaces

(a) Stress corrosion of the longitudinal ply of a 0-90-0 epoxy-glass laminate

(b) A strip formed by a longitudinal split in the 0 ply of a 0-90-0 epoxy-glass coupon

3.1.3 Stress Corrosion of Single Glass Fibres

In the absence of an applied stress, spiral cracks are formed in an outer sheath depleted of the metallic elements [1]. However, in the presence of an applied stress the fibres are embrittled and fail catastrophically after similar periods in the environment, as the 0° unidirectional epoxy laminates. These results are given in Fig. 3b.

3.1.4 Unstrained 0°/90°/0° Laminates

If coupons from crossply laminates are totally immersed in 0.5 M aqueous sulphuric acid there is no tendency for edge-cracks to form and acid attack is limited to the external faces of the laminate, where only the surface glass fibres show sign of damage. However, when the laminate is only half immersed in aqueous sulphuric acid in an 'open' cell, without an applied load, the unimmersed portion of the laminate shows both splitting of the 0° and transverse cracking of the 90° plies (termed Mode III damage) after approximately 72 hours. The

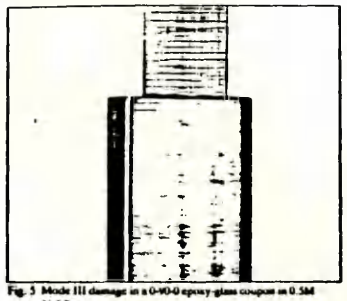

Fig. 5 Mode III damage in a 0-90-0 epoxy-glass coupon in 0.5M H_2SO_4

immersed half remains unaffected and quite transparent (Fig. 5). Furthermore, small crystals are seen to grow on the unimmersed edges of the coupon. With 1 M aqueous hydrochloric acid minor damage occurs and then only after three weeks.

3.2 Environmental Stress Corrosion Cracking of Polyester/Glass Laminates in Tension

3.2.1 0°/90°/0° Crossply and 0° Unidirectional Coupons Under a Constant Tensile Load

The most striking result of these experiments is the much longer failure times and higher strains involved for the Mode I fractures and the nature of the edge damage. These coupons showed a marked tendency to generate larger numbers of small edge-cracks at applied strains less than that for transverse cracking. The occasional crack appeared to run across the width of the specimen [14]. To date this type of damage has not caused catastrophic failure of cold cured coupons where the internal strain is minimised and strains approaching 0.6% can be applied prior to transverse cracking. Consequently catastrophic failure occurs at applied strains in excess of 0.6% and when the transverse ply is heavily cracked. The results are presented on Fig. 3a and the strain in the 0° plies is calculated assuming that the cracked transverse ply does not carry a load. The failure occurs adjacent to one of the transverse cracks and since the failure times are indistinguishable from those of the 0° unidirectional laminates we conclude, as shown earlier for epoxy/glass laminates, that the transverse crack acts only to throw the load onto the 0° plies without the enhanced effect which might be expected of a transverse crack acting as a notch.

The failure mechanism of the 0° laminate is similar to that of the epoxy/glass 0° coupons shown in Fig. 1d. Individual stress corrosion cracks in single fibres coalesce (Fig. 7) and eventually join together when the stress intensity at the crack tip is sufficient to induce longitudinal splitting. However, the failure times of both unidirectional and crossply coupons are much longer than both the epoxy laminates or the single glass filaments (Fig. 3) at similar strains demonstrating the effectiveness of the isophthalic polyester in protecting the glass fibres.

3.2.2 0°/90°/0° Crossply and 0° Unidirectional Laminates Under a Constant Four-point Bending Load

The experiments differ from those described in section 3.2.1 in that the whole coupon is immersed in the aqueous sulphuric acid. In 4-point bend the stress state is more complicated so that the tensile strain across the longitudinal ply has been determined by equating the strain at the 0°/90° interface with that required for transverse cracking in a tensile test. The tensile strain in the outer surface of 0° ply has been measured by a resistance strain gauge during the characterisation of the laminate in the bending jig. The results presented here have been normalised to the load required for the first transverse crack (F_{tc}). At lower loads transverse damage slowly accumulates at the cut edge, which is reduced by resin coating (Figs. 6a & 6b) but ESCC failure is apparently unaffected. Fracture occurs by the accumulation of individual ESCC cracks described in section 3.2.1 and 3.2.2 and shown in Fig. 7 where it is clear that nucleation occurs at random within the tensile face of the laminate. However, at loads above F_{tc} the

Fig. 6 ESCC of 0-90-0 polyester-glass laminates in four-point bending

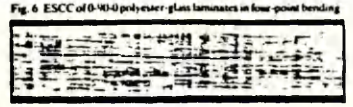

(a)

(b)

Appearance of (a) edge-coated and (b) non-edge-coated coupons after immersion for 100 days in 1M aqueous sulphuric acid when loaded below F_{tc}.

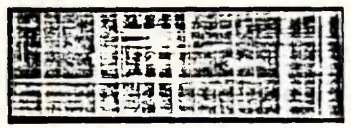

(c)

(d)

Appearance of (c) 0-90-0 coupon which has undergone mode Ib ESCC failure and (d) the failed 0 ply after sectioning from the original coupon. ESCC in the 0 ply (numbered 1-4) occurs adjacent to transverse cracks in the 90 ply which form on loading.

(e)

Transverse cracking in a 0-90-0 polyester glass laminate subjected to a four point bending load. These cracks form on loading, penetrate the 0 ply and act as initiation sites for subsequent mode Ib ESCC laminate failure.

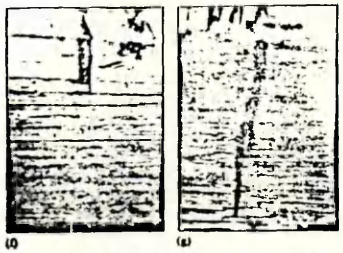

(f) (g)

Stages of propagation of mode Ib ESCC in crossply laminates. (f) & (g) show a 0 ply sectioned through a series of cracks as illustrated by the dashed line in (d). (f) shows the first stage of propagation from a pre-existing transverse crack tip. (g) shows the stage just prior to laminate failure.

transverse cracks have a profound effect on the failure times. Fig. 8 shows that in contrast to the tensile loaded coupons the stress corrosion failures can occur within a few hours. This is a result of the penetration of the transverse cracks into the load bearing 0° plies which then act as effective notches for ESCC. This is demonstrated in Fig. 6 by the growth of a transverse crack formed in the outer 90° ply into the more highly strained 0° ply. In both cases these are Mode I fractures but to differentiate between the two mechanisms we refer to the transverse crack dominated ones as Mode Ib and the cumulative failures as Mode Ia.

At loads in the region of F_{ss} the coupon may fail by either Mode Ia or Ib. This is illustrated in Fig. 7 where damage has accumulated in a transverse cracked specimen. This diffuse failure region is mainly

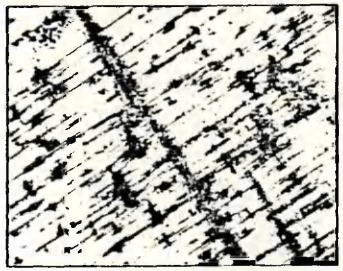

Fig. 7 Accumulation of mode I ESCC occurring in the 0 (tensile) ply of a 0-90-0 polyester-glass coupon loaded in four-point bend.

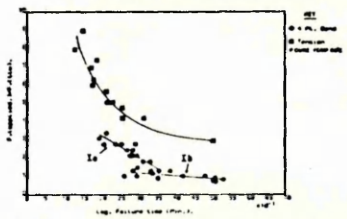

Fig. 8 Comparison of ESCC failure times of polyester glass 0-90-0 coupons in tension and in 4 point bend

confined to laminates post-cured at 80°C or above since the thermal strains which develop on cooling reduce the strain for transverse cracking and the applied load for Mode Ib failure so that the strain on the 0° fibres is proportionately lower.

In order to demonstrate the importance of 'sharp' notches on the stress corrosion behaviour in bending mode, 0° coupons were scratched with a scalpel blade prior to environmental testing. Whereas the un-notched specimens had not failed after 3 months at loads of up to 300 N, 150 N was sufficient to produce failure in approximately 20 hours (Fig. 9).

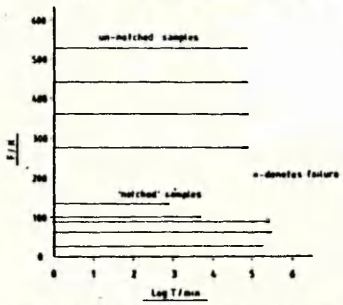

Fig. 9 ESCC behaviour of 0 unidirectional polyester-glass coupons in four point bending

3.2.3 0° Unidirectional Laminates Under Constant Tensile Strain — The Effect of Post-curing

In our study of the effect of transverse cracks on the ESCC in 4-point bend we examined coupons which had been transverse cracked in bend at an Instron test prior to loading to less than F_{ss} during the environmental test. The early results suggested that the post-cured laminates behaved differently. We have therefore carefully examined the Mode I failure of 0° coupons with and without post-curing at 50° and 80°C. The results are given in Fig. 10. It is clearly seen that the post-cured coupons are more susceptible to stress-corrosion cracking.

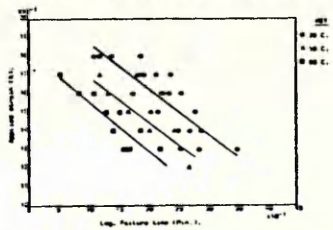

Fig. 10 The effect of postcure temperature on the ESCC of 0° polyester-glass coupons at constant strain

4. Discussion

4.1 Mode I Failure under Tensile Loads

4.1.1 Crossply Laminates

When the 90° ply of a crossply laminate fractures, the load that it supported is thrown onto the longitudinal plies, at a point adjacent to the transverse crack. Away from the transverse crack the stress is

transferred back into the 90° plies causing a further fracture of the transverse ply when an additional increment makes it greater than the transverse failure strain. Thus the shear lag model has been used successfully to predict the multiple cracking behaviour of these laminates (15). Transverse cracks can either act as notches, whose stress intensity is responsible for the stress corrosion crack, or amplify the load on the plies. Since the fracture of 0° unidirectional laminates from both resin systems occurs over the same period as equivalent crossply laminates (Fig. 6) we conclude that the effect of a transverse crack is simply to increase the load on the longitudinal plies by a calculable increment and not to reduce the failure times, which would be the consequence of a notch.

The failure times of the two composites are, however, significantly different and one of the reasons is the nature of the transverse cracking. In the polyester coupons, at strains below that for transverse cracking in air, failure occurs by the accumulation of small ESCC cracks at the tensile faces and although apparent transverse cracks form under the combined influence of the stress and the environment they are not effective in throwing the load on to the 0° plies, whereas in the epoxy composite 'true' transverse cracks are formed. We conclude, therefore that the transverse failure strain of these coupons is reduced under the combined influence of the stress and environment. This effect is confirmed in Fig. 11 where the transverse crack spacing from dynamic tensile tests on both 'dry' and 'wet' specimens is compared. The transverse cracking in air of this epoxy composite has been previously shown to be preceded by debonding at individual fibres (9). With a further increment of strain these debonds coalesce to form a transverse crack; it follows, therefore, that either stress corrosion of the resin or interface, or both, occurs, but the Mode III damage and the Mode II failures described in sections 3.1.3 and 3.1.4 and Figs. 1 and 5 strongly imply that stress corrosion of the interface occurs which allows the environment to reach the unimmersed half. Furthermore, the lack of protection of the glass fibres by the epoxy resin at applied strains greater than 0.1%, as shown by equivalent failure times of single fibres, can only be explained by the rapid transport of the environment within the coupon.

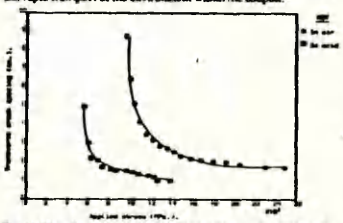

Fig. 11 The effect of the environment on the transverse crack spacing in 0-90-0 epoxy-glass coupons

4.1.2 0° Unidirectional Laminates

The stress corrosion failure of unidirectional laminates is strongly dependent on the resin. Although there is no evidence of chemical breakdown of the epoxy resin it does not appear to protect the glass fibres from stress corrosion whereas in the polyester composite the resin is shown to be quite effective.

In fact the random nucleation by ESCC of individual fibres appears to be faster in surfaces where the resin is thinnest.

It was anticipated that the thermal strains present in the matrix would put the fibres into slight compression thereby slightly improving the ESCC resistance. However, post-curing of the polyester coupons increases the probability of ESCC failure (Fig. 10). Since the strains involved should not be sufficient for resin cracking it follows, therefore, that either the matrix is subject to stress corrosion cracking or the rate of diffusion is enhanced by the thermal stresses in the resin. This effect is the subject of further study.

4.1.3 0°/90°/0° Laminates in Four-point Bend

The statistical probability of failure occuring in a 4-point bend test has been shown to be 1.27 greater than in a tensile test (16). However, Fig. 8 shows that Mode Ib ESCC failure is much more probable in 0°/90°/0° laminates because of the effectiveness of transverse cracks formed at the 0°/90° interface to propagate into the rising stress field, under the influence of the sulphuric acid.

4.2 Mode II Failures and Mode III Damage

Reproducible Mode II failures illustrated in Fig. 1 have so far been confined to the epoxy glass coupons and always occur at low applied strains in both 0° unidirectional and crossply laminates, as the unimmersed half of the coupon after apparently less time than an equivalent Mode I failure (Fig. 2). Various possible mechanisms such as attack by acid vapour and/or oxygen have been tested but it is always observed that crystalline deposits feature in the fracture surface and on the edge of the coupon. Whereas the former invariably are rich in calcium the latter are totally based on aluminium and traces of potassium. These results demonstrate the crystallisation of the less soluble calcium sulphate within the laminate and the more soluble aluminium sulphate and potassium aluminium sulphate on the exposed edges. Mode II fractures are also inhibited in the closed mill when the atmosphere is saturated with water vapour. Furthermore, in aqueous 1M HCl Mode I failure occurs at these low strains in the "open" cell. Both these experiments show that Mode II is inhibited when the calcium salts remain soluble as in the case of the more soluble calcium chloride. In addition, Mode III can occur in the whole specimen when half immersed in phosphoric acid whose calcium salt is much less soluble than calcium sulphate.

We postulate therefore that the stress state in the 0°/90°/0° coupons is sufficient for stress corrosion of the fibre-matrix interface allowing rapid transport of the environment into the laminates to corrode the glass fibres. The aluminium and calcium ions have been shown to be depleted from the outer sheath of the glass fibres (14). In sulphuric acid the lowly soluble calcium sulphate crystallises within the coupon outside the environment when the acid is concentrated by evaporation or diffusion of water away from the interface. In Mode III this crystallisation causes further stresses in the 'dry' half which allows the environment to rise further up the coupon causing progressive damage. Catastrophic failure does not occur because the 0° glass fibres are not stressed. However, when under a small tensile strain of e.g. 0.05% the first crack can propagate through the 0° plies to completely fracture the coupon.

5. Conclusions

The prime cause of ESCC fracture of GRP is the susceptibility of the glass fibres to stress corrosion cracking in acidic environments (17, 18). Therefore the prime function of the resin is to protect the glass fibres from the acid. In this study we have identified different ESCC mechanisms which can cause complete fracture of the GRP under the combined influence of aqueous sulphuric acid and an applied stress. The long term life of 0° unidirectional 0°/90°/0° crossply laminates under tensile loads is controlled by nucleation and propagation of individually stress corroded fractured fibres. In the transverse cracked crossply coupons the failure is localised by the enhanced strain in the 0° ply. The results from the study of the epoxy laminates demonstrate the most important requirement, which is that the glass fibre/matrix interface remains intact otherwise the environment can rapidly reach the fibres. Thus the interface should not be susceptible to stress-corrosion and the correct choice of glass finish and matrix is important. When the stress corrosion of the transverse ply occurs, caused by low thermal or applied stresses, the laminates can become debonded, resulting in unexpected catastrophic failures, outside the environment, in apparently unaffected composites.

Post-curing generates tensile thermal strains in both the matrix of unidirectional coupons and the transverse ply of crossply coupons. In the former the deleterious effect of post-curing on the ESCC resistance of the polyester coupons may be ascribed to the thermal strains becoming more significant at higher overall levels of strain. Under bending stresses, more typical of the stress state in pipes and containers, the thermal strains in crossply laminates can cause a large reduction in the stress which can be tolerated before rapid (Mode Ib) ESCC failure occurs. This is because ESCC cracks initiated at penetrating transverse cracks grow rapidly from the inside of the coupon and the transverse cracking load is controlled by the thermal strain in the coupon. We have previously reported thermal strains of 0.42%, after 80° cure, in Crystic 272 laminates which reduce the transverse cracking strain to 0.17% (11). The onset of rapid Mode Ib

failures in the polyester laminates is minimised by the level of thermal strain so that post curing is not necessarily beneficial to ESCC behaviour although the chemical resistance of the resin may be improved.

Thus GRP, for applications in which the combined effect of stress and aqueous acids is likely to be experienced, should be carefully manufactured under controlled temperatures to minimise the development of thermal strains. Where bending moments are encountered the laminate geometry should be designed to restrict the transverse plies from experiencing applied tensile stresses, otherwise penetrating transverse cracks may form which are effective notches in stress corrosion conditions. Furthermore, the ESCC resistance of each glass fibre composite should be tested since the fibre matrix interface may also be prone to failure.

6. Acknowledgements

We wish to thank the SERC for an equipment grant, a research studentship (J. W. R.), the Polymer Engineering Directorate for a research fellowship (A. R. W.), Scott-Bader & Co. Ltd. for the polyester resin and Silenka (UK) Ltd. for the glass fibres.

References

1. H. A. Barker, I. G. Baird-Smith and F. R. Jones, *Symp. Reinf. Plast. in Anticorrosion Appl.* paper 12, NEL, Glasgow, 1979.
2. R. C. Roberts, *Reinf. Plast. Congress (BPF)*, paper 19, Brighton, 1978.
3. H. H. Cobbs, *Plast. and Rubber: Mat. and Appl.* 1978, 3, 6.
4. S. Torp and R. Arnesen, *Proc. 34th Ann. Conf. SPI Reinf. Plast.*, paper 19-D, New Orleans, 1979.
5. D. Hull and P. J. Hogg in 'Adv. in Composite Materials', Ed. A. R. Bunsell et al, Pergamon, Paris, 1980, *Vol. 1*, 543.
6. P. J. Hogg and D. Hull, *Metal Science*, 1980, 441.
7. P. J. Hogg, D. Hull and M. J. Legg in 'Composite Structures', Ed. I. Marshall, App. Sci., London, 1981, 106.
8. J. E. Bailey, P. T. Curtis and A. Parvizi, *Proc. Roy. Soc., Lond., A*, 1979, *366*, 599.
9. J. E. Bailey and A. Parvizi, *J. Mat. Sci.*, 1981, *13*, 2131.
10. F. R. Jones and M. J. Mulheron, in preparation.
11. F. R. Jones, A. R. Wheatley and J. E. Bailey in 'Composite Structures', Ed. I. Marshall, App. Sci., London, *1981*, 415.
12. F. R. Jones and J. W. Rock, to be published.
13. F. R. Jones and A. R. Wheatley, to be published.
14. J. E. Bailey, T. M. W. Fryer and F. R. Jones in 'Adv. in Composite Materials', Ed. A. R. Bunsell et al, Pergamon, Paris, 1980, Vol. 1, 514.
15. A. Parvizi and J. E. Bailey, *J. Mat. Sci.*, 1978, *13*, 2131.
16. P. M. Braiden, 'An Introduction to Weibull Statistics', AERE Report R7165, Harwell, 1975.
17. A. G. Metcalfe, M. E. Gulden and G. K. Schmitz, *Glass Tech.*, 1971, *12*, 15.
18. A. G. Metcalfe and G. K. Schmitz, *Glass Tech.*, 1972, *13*, 5.

"Progress in Science and Engineering of Composites"
T. Hayashi, K. Kawata & S. Umekawa, Ed., ICCM-IV, Tokyo, 1982.

The Environmental Stress Corrosion Cracking of Glass Fibre Reinforced Polyester and Epoxy Composites

F. R. Jones, J. W. Rock, A. R. Wheatley, J. E. Bailey
Department of Metallurgy and Materials Technology, University of Surrey, Guildford, Surrey GU2 5XH, U.K.

ABSTRACT

The ESCC of epoxy and polyester glass fibre 0° and $0^\circ/90^\circ/0^\circ$ composites has been studied. The polyester resin protects the fibres in that the coupons have longer failure times than single filaments. Post-curing decreases the ESCC resistance of the composite. In contrast, the transverse cracking strain of the $0^\circ/90^\circ/0^\circ$ epoxy laminates is reduced, under the influence of the stress and the environment, with the result that at strains >0.15% the coupons had similar failure times to those for single fibres. At lower strains, fracture of the unimmersed half of the coupon occurs under the apparent influence of crystalline corrosion products.

INTRODUCTION

Glass fibre reinforced unsaturated polyester resins are becoming increasingly used in applications in which the material is in contact with acidic environments, such as process plant equipment, storage vessels and sewage pipes. GRP shows good chemical resistance to aqueous acids (1) but in the presence of a stress, rapid fracture can occur(2,3). The environmental stress corrosion cracking of these composite materials is to some measure determined by the susceptibility of E-glass fibre both to corrosion and stress corrosion (4,5). It has now been well established that stress corrosion fracture surfaces are essentially planar and normal to the applied stress with little evidence of fibre pullout (2,3,6-11). An explanation of the planar fracture surfaces, in terms of a short stress transfer length is given by Kelly et al from a comparison of the stress rupture of glass fibre strands and impregnated bundles (10,11). Hogg and Hull (6,7) have identified three stages in the stress corrosion cracking of pipes and demonstrated that stress and strain corrosion cracking are the same phenomenon.

We (12) have reported the nucleation of environmental stress corrosion cracking (ESCC) of polyester crossply coupons, in 4-point bend, at transverse cracks formed at $0^\circ/90^\circ$ interface. These propagate into the load bearing tensile 0° ply under the influence of the environment (13). Since the magnitude of the thermal strains determine the transverse cracking strain and have ESCC

resistance (12) we concluded that the transverse cracks were effective notches for the stress corrosion of the 0° ply. We have, therefore, extended our study to both $0^{\circ}/90^{\circ}/0^{\circ}$ and 0° coupons under a constant tensile load.

In addition, the more chemically resistant unsaturated polyester resins are based on Bisphenol 'A' intermediately so that an anhydride cured epoxy resin could be considered to be a model matrix resin. Furthermore $0^{\circ}/90^{\circ}/0^{\circ}$ composites from Epikote 828 cured with NMA and reinforced with Silenka 051P E-glass fibres have been shown to exhibit fibre-matrix debonding at lower strain than that for transverse cracking (14), enabling interfacial effects to be studied. In this paper therefore, we present a comparison of the ESCC of the glass fibre reinforced resins having ester links; one an unsaturated isophthalic and the other an anhydride cured epoxide with single glass fibres.

EXPERIMENTAL

The laminates were prepared from Silenka E-glass fibre 051P (1200 tex) by methods similar to those described elsewhere (12,18). Epikote 828 (Shell Ltd.) was cured with 80phr NMA and 1.5phr BDMA at $100^{\circ}C$ for 3h and at 150° for 3h. The softening point was $140^{\circ}C$ (16). Crystic 272 was cured with 2phr Catalyst M and 0.25% Accelerator E (Scott-Bader Ltd.) for 172h at room temperature or post-cured at $80^{\circ}C$ for 3h.

'Open' and 'closed' environmental tubes were attached to the 2 cm wide coupons so that only half was unimmersed. Either constant or dynamic tensile loads were applied. Single glass filaments, whose diameters were determined by laser refraction were fully immersed during stress corrosion (13,15). 0.5M and 1.0M aqueous H_2SO_4 were used.

RESULTS

The $0^{\circ}/90^{\circ}/0^{\circ}$ model composite has been described previously (14). In these experiments the thickness of the outer 0° ply was equal to half that of the inner 90° ply and was approximately 1 mm. The environmental stress corrosion cracking (ESCC) of these glass fibre laminates has been studied in tension under a constant load. At low strains of approximately 0.2% the epoxy glass laminates fractured with 24 hours whereas the polyester/glass coupons were still intact after 3 months. The latter however, developed a series of transverse edge-cracks but these did not lead to fracture of the 0° load bearing plies (17).

Environmental Stress Corrosion Cracking of Epoxy/Glass Laminates

The stress corrosion of the load bearing plies may occur either within the environment, termed Mode I, or in the unimmersed part of the specimen, termed Mode II. The mode of failure which occurs is dependent upon the type of environmentla cell, the nature of the environmental, and the initial applied strain. The difference between the two types of failures is illustrated in Fig. 1. Mode I failures of $0^{\circ}/90^{\circ}/0^{\circ}$ coupons occur by fracture of the longitudinal plies adjacent to one of the early microcracks in the transverse ply. In Fig. 1a the initial applied strain was sufficient to induce transverse cracking and the transverse crack responsible for failure is indicated. However, at lower strains such that no transverse cracks would be produced in air, cracks are seen to form at the edge of the coupon, in contact with the aqueous acid, and propagate into the transverse ply. These lead to Mode I fracture in the 'closed' cell but in the 'open' cell at strains >0.15% Mode II occurs at an earlier time, as shown in Fig. 2. Fig. 1c shows that Mode I failure of the 0° unidirectional occurs by random nucleation of ESCC cracks which coalesce and form a stepped fracture surface (13). The failure times in Fig. 3 correlate closely with those for the $0^{\circ}/90^{\circ}/0^{\circ}$ crossply coupons, when the applied strain is calculated assuming the cracked 90° ply carries no load. Fig. 4 demonstrates that the single glass filaments fail catastrophically within similar immersion times.

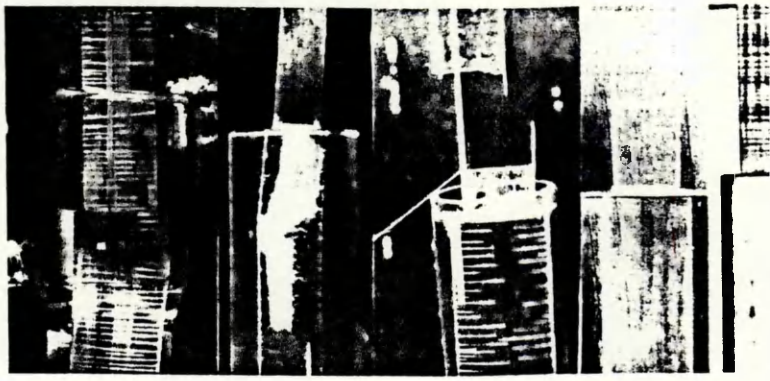

a b c d

MODE I MODE II

Fig.1. TYPES OF ENVIRONMENTAL STRESS CRACKING OF EPOXY G.R.P. a,c,e are $0^{\circ}/90^{\circ}/0^{\circ}$ and b, d are 0° coupons

If crossply coupons are totally immersed in 0.5M aqueous sulphuric there is no tendency for edge-cracks to form and acid attack is limite external faces of the laminate, where only the surface glass fibres sho of damage. However, when the laminate is only half immersed in aqueous acid in an 'open' cell, without an applied load, the unimmersed portion laminate shows both splitting of the 0o and transverse cracking of the (termed Mode III damage) after approximately 72 hours. The immersed hal unaffected and quite transparent (Fig. 1e). Furthermore, small crystals to grow on the unimmersed edges of the coupon. With 1M aqueous hydrochl only minor damage occurs after several weeks.

Environmental Stress Corrosion Cracking of Polyester/Glass Laminates

The most striking result of these experiments is the much longer times and higher strains involved for Mode I fractures (Fig.3), the abs Mode II and that nature of edge damage compared to the epoxy laminates. $0^{\circ}/90^{\circ}/0^{\circ}$ coupons showed a marked tendency to generate large numbers o edge-cracks at applied strains less than that for transverse cracking a the cold-cured samples, when the applied stress is maximised, did not fracture. Only heavily transverse cracked coupons with applied strains failed catastrophically. The close correlation between the failure time and $0^{\circ}/90^{\circ}/0^{\circ}$ coupons demonstrates that the failure mechanisms are simi those of the epoxy composites, in which the transverse cracks throw the on to the 0° plies. This result is in contrast to the ESCC under bendin where the transverse cracks nucleate a more rapid failure (13). Fig. 3 demonstrates that the post-cured coupons are less resistant.

DISCUSSION

Mode I Failures

When the 90° ply of a crossply laminate fractures, the load that orted is thrown onto the longitudinal plies, at a place adjacent to the erse crack. Away from the transverse crack the stress is transferred ba the 90° plies causing a further fracture of the transverse ply when an al increment makes it greater than the transverse failure strain. Thus lag model has been used successfully to predict the multiple cracking b

of these laminates (18), Transverse cracks amy also act as notches for the nucleation of stress corrosion cracks. Since the fracture of 0^o unidirectional laminates from both resin systems occurs within the same immersion time as equivalent crossply laminates (Fig. 3) we conclude that the effect of a transverse crack is simply to increase the load on the longitudinal plies by a calculable increment and not to reduce the failure times, which would be the consequence of a notch. This contrasts with the failure mechansim of the same polyester composite in 4-point bend where the transverse cracks have been shown to initiate stress corrosion cracks at $0^o/90^o$ interface (12,13).

However the failure times of the epoxy and polyester composites differ significantly. Most noticeable is the nature of the stress corrosion at applied strains less than that for transverse cracking in air. In the polyester coupons small ESCC cracks form in the tensile 0^o faces but within the timescale of these experiments (>100 days) no catastrophic fractures have been observed. In addition, edge-cracks grow in the transverse ply under the influence of the stress and the corrodent, which do not appear to lead-up the longitudinal ply, as shown by a lack of localised ESCC nuclei in the vicinity of them. Microscopy has demonstrated that these cracks do not span the thickness of the transverse ply (17). Some do however appear to run completely across the width. In contrast however, the ESCC fracture of the 0^o plies of the epoxy coupons at these low strains occurs adjacent to one of the early edge-cracks. These edge-cracks therefore, do load-up the 0^o plies and appear to behave like normal transverse cracks formed in air and the inference is that the transverse cracking strain is reduced, under the influence of the environment.

The Transverse Cracking Strain of the Epoxy Composites in the Environment

In order to determine the transverse failure strain under stress corrosion conditions, the following analysis was used. After Bailey and Parvisi (18) the additonal stress in the 0^o plies in the plane of the transverse crack, $\Delta\sigma_o$ is given by the modified shear-lag theory.

$$\Delta\sigma_o = \varepsilon_{t\ell u} E_t d[1 + \exp(-\phi^{\frac{1}{2}}t) - 2\exp(-\phi^{\frac{1}{2}}t/2)]/b \qquad ----(1)$$

where $\phi = E_c G_t (b+d)/E_\ell E_t bd^2$ and $\varepsilon_{t\ell u}$ is the transverse ply cracking strain, E_c E_ℓ and E_t are the Young's moduli of the composite and longitudinal and transverse plies respectively. G_t is the shear modulus of the transverse ply in the longitudinal direction, b and d are thicknesses of the longitudinal and semi-transverse plies. t is the transverse crack spacing.

$$\Delta\sigma_o = \chi\sigma_a \qquad ----(2)$$

where $\chi = (b+d)/b - (E_\ell/E_c)$ and σ_a = applied stress. Rearrangement of (1) and (2) and placing $\psi = \chi b/\varepsilon_{t\ell u} E_t d$ we get

$$1/\psi\sigma_a = [1 + \exp(-\phi^{\frac{1}{2}}t) - 2\exp(-\phi^{\frac{1}{2}}t/2)] \qquad ----(3)$$

Equation (3) is a quadratic expression in $\exp(-\phi^{\frac{1}{2}}t)$ whose solution is given by

$$-\phi^{\frac{1}{2}}t/2 = \ell n(1 \pm \sigma_a^{-\frac{1}{2}}\psi^{-\frac{1}{2}}) \qquad ----(4)$$

Equation (4) predicts a linear relationship betw-en the crack spacing, t and $\ell n\ (1/(1 \pm \sigma_a^{-\frac{1}{2}}\psi^{-\frac{1}{2}})$ with slope $2/\phi^{-\frac{1}{2}}$. Fig. 5 gives a plot of the experimental crack spacing for the epoxy/glass coupons compared to equation (4) with $\varepsilon_{t\ell u}$ for the best fit to the data. $\varepsilon_{t\ell u}$ is therefore determined from the cracking pattern of the coupon in the dynamic test, unpeturbed by the nucleation of transverse cracks at gross laminate defects. $\varepsilon^f_{t\ell u}$ was found to be 0.38%.

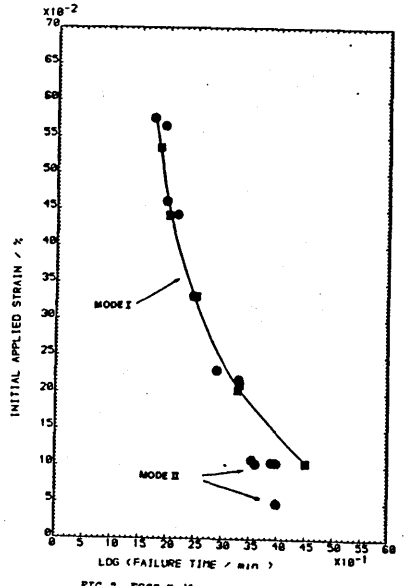

FIG.2. ESCC Failure Times of Epoxy $0^o/90^o/0^o$ Coupons in Open(●) and Closed(■) Cells. ε_a is that in the 0^o Plies.

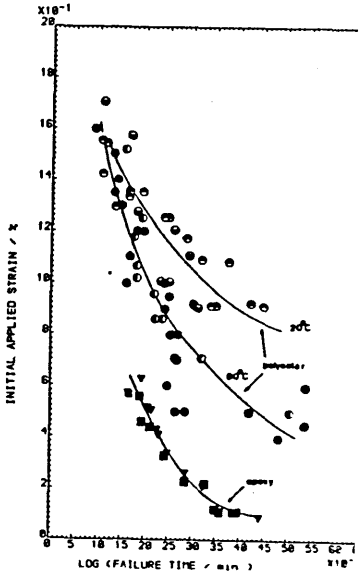

FIG.3. Comparison of the ESCC of Epoxy 0^o(▽), $0^o/90^o/0^o$(▲); Polyester 0^o(○,●), $0^o/90^o/0^o$(◐,◑). The Post-Cure Temperature is given.

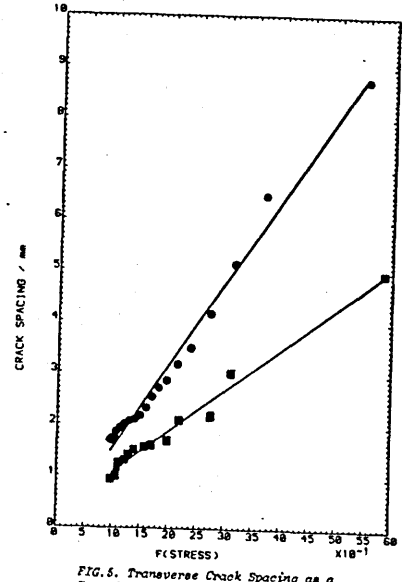

FIG.5. Transverse Crack Spacing as a Function of $\ell n\ (1/(1 \pm \sigma_a^{-\frac{1}{2}}\psi^{\frac{1}{2}}))$ According to Equation 4. In Air(●) $\varepsilon_{t\ell u}$ = 0.38%; H_2SO_4 aq.(■) $\varepsilon_{t\ell u}$ = 0.1%.

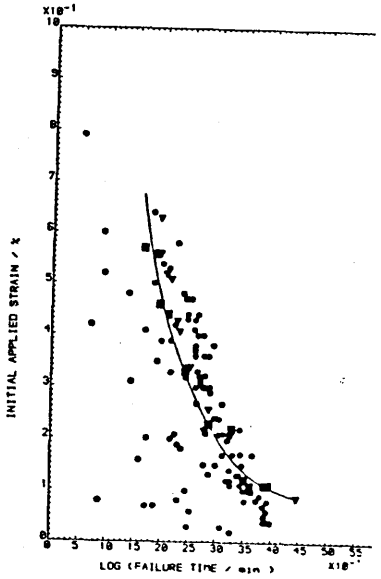

FIG.4. Comparison of Mode I Failure Times Epoxy $0^o/90^o/\overline{+}$(▲), 0^o(▽) with Single Glass Filaments (○).

Fig. 5 also includes the transverse crack spacing from a tensile test in which the coupon is half immersed in aqueous sulphuric acid. From the best fit to the data the transverse cracking strain in the environment $\varepsilon^{e}_{t\ell y}$ was found to be ≈ 0.1%. The dry half of the coupon had a crack spacing typical of the test in air. Similar experiments with the polyester composite showed no discernable reduction in the transverse cracking strain.

The transverse cracking in air of this epoxy composite has been previously shown to be preceded by debonds at individual fibres, which coalesce to form a transverse crack at a higher strain. It follows therefore, that either stress corrosion of the resin,or interface, or both, occurs. The Mode III damage and the Mode II failure described strongly imply that stress corrosion of the interface occurs. In order to estimate the debonding strain in the environment we make use of equation 5 (14).

$$\varepsilon^{b}_{tu} \; / \; \varepsilon^{nb}_{tu} \; = \; 1/(\; 1 - V_f \;) \qquad \text{----(5)}$$

where V_f = fibre volume fraction. Since V_f of the epoxy coupons was 55% this ratio should be ≈ 2. Debonding was shown to be responsible for the first 'knee' in the stress-strain curve at 0.25% and $\varepsilon_{t\ell u}$ = 0.55%. $\varepsilon^{th}_{t\ell}$ was also reported as 0.08% (14). Therefore

$$\varepsilon^{b}_{tu} \; / \; \varepsilon^{nb}_{tu} \; = \; (\; \varepsilon_{t\ell u} + \varepsilon^{th}_{t\ell} \;) / \; \varepsilon^{b}_{tu} - (\; \varepsilon_{db} + \varepsilon^{th}_{t\ell} \;) = 0.63/ \; 0.3 \approx 2 \qquad \text{----(6)}$$

where ε_{db}, ε^{b}_{tu} and ε^{nb}_{tu} are respectively the debonding strain, and failure strains of the bonded and non-bonded transverse ply.

The higher softening point of the coupons used in this study meant that $\varepsilon^{th}_{t\ell}$ = 0.22% and that $\varepsilon_{t\ell u}$ = 0.28%. Eqaution 6 predicts that ε_{db} = 0.03% which is very close to the observed whitening strain at 0.05%. Fig. 5 shows that $\varepsilon_{t\ell u}$ is reduced to at least 0.1% during a dynamic tensile test whereas $\varepsilon^{th}_{t\ell}$ is not reduced significantly over much longer periods in the environment, as demonstrated by relatively slow increase in the radius curvature of a $0^{o}/90^{o}$ beam (15). The debonding strain therefore will also be reduced and equation 6 predicts that the coupon will debond in the environment. Furthermore, for this laminate configuration $\varepsilon^{th}_{t\ell}$ is equivalent to the thermal strain in transverse direction of the longitudinal ply $\varepsilon^{th}_{\ell t}$. It follows therefore that under the influence of the environment and stress, the longitudinal plies will also become debonded and the equivalent stress corrosion failure times of the single glass fibres and the epoxy crossply laminates can be understood by the stress-corrosion of the interface leading to a rapid transport of H_2SO_4. The equivalent failure times for 0^{o} and $0^{o}/90^{o}/0^{o}$ coupons suggests that diffusion is probably more important than transport along a transverse crack to the interface. Menges and Gitschner (19) show that diffusion through the ≈ 5 μm layers of the resin between the fibres will have occurred during the time scale of these experiments.

Since the stressed 0^{o} epoxy coupons at strains >0.2% also have similar ESCC failure times as the single glass fibres, we conclude that debonding can also occur. The mechanism of these failures is still uncertain but the inmplication is that the stress state derived either from the longitudinal thermal, Poisson or swelling strains can cause debonding or resin cracking in the vicinity of the fibres. These failures are the subject of further investigation.

The polyester coupons are less susceptible to ESCC cracking than the equivalent epoxy composites. The result cannot be accounted for by a volume fraction effect since it has been possible to produce the composites with similar compositions. However, the difference in thermal strains which exist in post-cured coupons might be expected to improve the ESCC resistance by putting the fibres into compression. Furthermore, since the transverse ply interface does not appear to be sensitive to stress corrosion it seems likely that the diffusion of the acid through the resin, which is probably stress enhanced, is the most important factor.

Mode II Failure and Mode III Damage. Reproducible Mode II failures illustrated in Fig. 1 have so far been confined to the epoxy glass coupons and always occur at low applied strains in both 0^{o} unidirectional and crossply laminates, in the unimmersed half of the coupon after apparently less time than an equivalent Mode I failure (Fig. 2). Various possible mechanisms such as attack by acid vapour and/or oxygen have been tested but it is always observed that crystalline deposits feature in the fracture surface and on the edge of the coupon. Whereas the former invariably are rich in calcium the latter are totally based on aluminium and traces of potassium. These results demonstrate the crystallisation of the less soluble calcium sulphate within the laminate and the more soluble aluminium sulphate and the potassium and sodium aluminium sulphates on the exposed edges. Mode II fractures are also inhibited in the closed cell when the atmosphere is saturated with water vapour. Furthermore, in aqueous 1M HCl Mode I failure occurs at these low strains in the 'open' cell. These experiments show that Mode II is inhibited when the calcium salts remain soluble. In addition, the Mode III damage can occur in the whole specimen when half is immersed in phosphoric acid whose calcium salt is much less soluble than calcium sulphate. We suggest therefore that the H_2SO_4 is transported through the debonded immersed half of and epoxy $0^{o}/90^{o}/0^{o}$ coupon to the unimmersed half, where the interface is still intact. Wicking is no longer possible and the environment diffuses into or permeates through the 'dry' region. The change in concentration causes the lowly soluble glass corrosion products to precipitate. The more soluble ions can be transported to the edge of the coupon. Continuous crystallisation of calcium sulphate at the glass/resin interface produces an additional stress which causes the Mode II crack to run from the edge of the coupon. In the absence of a stress $\varepsilon^{th}_{\ell t}$ is sufficient to environmentally debond the 0^{o} fibres, which are in compression so that only progressive transverse and longitudinal cracking occurs. A strain of 0.05% is sufficient for Mode II. The Mode II failure of the 0^{o} epoxy coupons can be similarly explained.

CONCLUSIONS

The prime cause of ESCC fractures of GRP is the susceptibility of the glass fibres to stress corrosion cracking in acidic environments (4,5). Therefore the prime function of the resin is to protect the glass fibres. In this study we have identified different ESCC mechanisms which can cause complete fracture of the GRP under the combined influence of aqueous sulphuric acid and an applied stress. Two composite systems based on 'polyester' matrices, one a conventional unsaturated polyester and the other an anhydride cured epoxide and an epoxy/polyester compatible glass. Important differences in the rate of stress corrosion cracking ahve been identified. The failure mechanism of the epoxy laminate demonstrates that the interface can also be prone to stress corrosion cracking and that this is the major factor since the fibres become accessible. Low strain fractures can also occur when diffusion along the fibre interface dominates the corrosion progress.

ACKNOWLEDGEMENTS

We wish to thank the SERC for an equipment grant, a research studentship (J.W.R), the Polymer Engineering Directorate for a research fellowship (A.R.W), Scott-Bader and Co Ltd. for the polyester resin and Silenka (UK) Ltd. for the glass fibre.

REFERENCES

1. Norwood, L.S. and Farebrother, T., "The Importance of the Anti-corrosion Barrier Layer in GRP Process Plant Applications", Symp. Reinf. Plast. in Anti-corrosion Applications, National Engineering Laboratory, Glasgow 1979, paper 8.

2. Barker, H.A., Baird-Smith, I.G., and Jones, F.R. "Larger Diameter GRP pipes in Civil Engineering - The Influence of Corrosive Environments", Symp. Reinf. Plast. in Anti-corrosion Applications, N.E.L. Glasgow 1979, paper 12.

3. Roberts, R.C. "Design Strain and Failure Mechanisms of GRP in a Chemical Environment", Reinf. Plast. Congress (BPF), Brighton 1978, paper 19.

4. Metcalf, A.G. and Schmitz, G.K. " Mechanisms of Stress Corrosion in E-glass Filaments", Glass Tech. 13. 1972,p5-16.

5. Metcalf, A.G., Gulden, Mary E. and Schmitz, G.K. "Spontaneous Cracking of Glass Filaments", Glass Tech. 12, 1974,p15-23.

6. Hogg, P.J. and Hull, D., "Micromechanisms of Crack Growth in Composite Materials Under Corrosive Envionrments", Metals Science, 1980,p441-449.

7. Hull, D. and Hogg, P.J. "Nucleation and Propagation of Cracks during Strain Corrosion of GRP" in Advances in Composite Materials (Ed. Bunsell, A.R. et al), Pergamon, Vol.1, 1980, p543-555.

8. Hogg, P.J.,Hull, D. and Legg, M.J. "Failure of GRP in Corrosive Environments" in Composite Structures (Ed. Marshall, I.H.) App. Sci. 1980, p 106-122.

9. Collins, H.H. "Strain Corrosion Cracking of GRP Laminates", Plast. Rubb: Mat. and Appl., 1978,p6-10.

10. Aveston,J.,Kelly, A. and Sillwood, J.M. "Long Term Strength of Glass Reinforced Plastics in Wet Environments" in Advances in Composite Materials, Pergamon, Vol.1,p556-568.

11. Kelly, A. and McCartney, L.N. "Failure by Stress Corrosion of Bundles of Fibres", Proc. R. Soc. Lond. A 374, 1981, p475-489.

12. Jones, F.R., Wheatley, A.R. and Bailey, J.E. "The Effect of Thermal Strains on the Microcracking and Stress Corrosion Behaviour of GRP" in Composite Structures (Ed. Marshall, I.H.) App. Sci. 1980, p415-429.

13. Jones, F.R., Rock, J.W., Wheatley, A.R. and Bailey, J.E. "Environmental Stress Corrosion Cracking of GRP", Reinf. Plast. Congress (BPF),B righton, 1982.

14. Bailey, J.E. and Parvizi, A. "On Fibre Debonding Effects and the Mechanism of Transverse-Ply Failure Strain in Cross-ply Laminates of Glass Fibre Composites", J.Mat.Sci. 16, 1981,p649-659.

15. Jones, F.R. and Rock, J.W. in preparation.

16. Jones, F.R. and Mulheron, M.J. "Origins of Thermal Strains in Polyester Composites", ICCM 4, Japan, 1982.

17. Bailey, J.E., Fryer, T.M.W. and Jones, F.R. "Environmental Stress-Corrosion Edge-Cracking of Glass Reinforced Polyesters" in Advances in Composite Materials, Pergamon, Vol.1, p514-528.

18. Parvizi, A. and Bailey, J.E. "On Multiple Transverse Cracking in Glass Fibre Epoxy Cross-ply Laminates", J. Mat. Sci. 13, 1978, p2131-2136.

19. Menges, G. and Gitschner, H.W. " Sorption Behaviour of Glass Fibre Reinforced Composite" in Advances in Composite Materials,Pergamon, Vol.1, p25-48.

The Environmental Stress Corrosion Cracking of Glass Fibre Reinforced Laminates and Single E-glass Filaments

by

F.R. Jones, J.W. Rock and J.E. Bailey

Department of Metallurgy and Materials Technology

University of Surrey, Guildford, England

ABSTRACT

The environmental stress corrosion cracking of Epoxy/glass fibre crossply, unidirectional coupons and single E-glass filaments have been compared. At initial applied strains > 0.15% the resin does not protect the fibres as shown by their equivalent failure times. The failure occurs in the environment and planar fractures occur because of the localised stress in the load bearing plies adjacent to a transverse crack in the 90^{o} ply of the $0^{o}/90^{o}/0^{o}$ coupons. These transverse cracks result from stress corrosion of the glass/resin interface, which leads to a reduction of the transverse cracking strain.

At applied strains <0.15% fracture occurs within the unexposed half of the coupons and is thought to be caused by rapid transport of glass corrosion products where they crystallise within the coupon.

This phenomenon is also responsible for the progressive transverse cracking that occurs in both the 0^{o} and 90^{o} plies of the unimmersed half of the crossply coupon under zero load.

INTRODUCTION

With increasing use of GRP for the fabrication of structures such as chemical plant and pipelines, which are subjected to aggressive environments, the effects of chemical degradation and particularly that of stress corrosion has become increasingly important if efficient and economic designs are to be attained. Whereas the resins are normally resistant to acidic environments (1) glass fibre reinforced polyester pipes have been shown to be susceptible to cracking under the combined influence of a stress and the environment (2-7). It is now well established that environmental stress corrosion failures have essentially planar fracture surfaces which show little evidence of fibre pull-out and occur normal to the load-bearing reinforcement(5).

A comparison of the stress corrosion of unimpregnated and resin impregnated glass fibre bundles lead to an explanation of the planar fracture in terms of the stress transfer length between fibre and matrix and the increase in the rate of growth of flaws near to fractured fibres (8). Planar fractures have also been explained by localised acid attack on the fibres at the stress corrosion crack tip (6). Hogg and Hull have identified four distinct stages to stress corrosion and have also shown that stress and strain corrosion are esssentially the same phenomena (7).

Recently(9,10) however, the usual matrix resins have been shown to be only partial barriers to water and aqueous acids, so that the retained strength of GRP correlates closely to that of E-glass fibres (11). Therefore the susceptibility of E-glass to both chemical and stress corrosion (12-14) places the onus onto the matrix resin to provide for chemical durability of the laminates. However crossply laminates are susceptible to transverse cracking and Jones et al (15) showed that these can nucleate catastrophic failure of polyester coupons under 4-point bend. Furthermore, the magnitude of the tensile thermal strains in the 90^{o} ply can significantly reduce the threshold for transverse cracking (15). In addition, under tensile loading the polyester coupons were susceptible to edge-cracking at low strains but at higher strains the transverse cracks did not apparently promote a rapid stress corrosion fracture (16).

NMA cured Bisphenol 'A' epoxy resins and chemical resistant unsaturated polyesters have similar molecular structures so that a glass laminate from the former, whose failure has been extensively studied previously (17,18), could be considered to be a model system. There is also a lack of published information available on the stress corrosion cracking of epoxy GRP. In this paper therefore, we report a detailed study of the stress corrosion cracking phenomena of model epoxy resin glass fibre laminates.

EXPERIMENTAL METHODS

Laminate Preparation and Characterisation

The laminates were prepared by using a winding machine to wind Silenka 051P 1200 T E-glass roving onto preformed steel frames. This ensured a uniform distribution of glass and consistent volume fractions. The wound frames were impregnated with degassed resin of formulation: Epikote 828 cured with 80phr Epikure NMA (Methylendimethylenetetrahydrophthalicanhydride) and catalysed with 1.5 phr B.D.M.A (Benzyldimethylamine) (Shell Chemicals Ltd) using the following technique, shown schematically in Fig. 1. The resin was frozen by pouring it onto a precooled metal plate at $-18^{o}C$ covered in "Melinex" sheet. The release film with the adhered resin was inverted and placed with the glass fibres on top of a heated metal plate For good impregnation it was essential that the resin did not soften prior to evacuation.

After 30 minutes the resin impregnated frame was removed, inspected and the "Melinex" sheets replaced with a silicone treated "Melinex" to prevent the cured resin adhering to the untreated film. The laminate was cured for 3 hours at $100^{o}C$ under a load of 300 kg/m^{2} in a circulating air oven, removed from the frame and cut into coupons of dimensions 25 x 2 cm using a water cooled diamond wheel. These were postcured at $150^{o}C$ for 3 hours. For testing, etched aluminium end-tags were attached using "Araldite" cold setting epoxy adhesive. Additonally coupons for tensile testing had resistance strain gauges bonded to them.

Each laminate was characterised by tensile testing for the initial Youngs modulus. For the crossply laminates the multiple cracking behaviour was recorded photographi The softening point of the laminates was found to be $140^{o}C$ from the onset of curvat on cooling coupons cut from a $0^{o}/90^{o}$ unsymetrical laminate (19).

Stress Corrosion Experiments

The stress corrosion of coupons was carried out on creep machines at constant load. Physical changes and the mode of failure were recorded by time-lapse photography. Two different types of environmental cell were used, both constructed from Borosilicate glass and are illustrated in Fig. 2. The open cell was simply a tube supported on the coupon. The closed cell allowed control of both temperature, by the circulation of thermostatted water, and the atmosphere if desired by purging with an appropriate gas. Both types of cell were supported on the coupon by a split rubber bung with silicone grease to provide a leak-free seal.

The experiments on single glass fibres (Silenka 051P E-glass) were carried out in the apparatus shown diagramatically in Fig. 3. Eight fibres could be tested at any one time. The single fibres were separated from the roving and their diameters determined by forward light scattering (20). They were then glued to the glass rods and elastic bands with "Evostik" high impact adhesive. The fibres were loaded whilst immersed in the environment to prevent prestressing. All the failures were examined to ensure that they had occurred away from the adhesive.

RESULTS

Laminate Characterisation

The model $0^{\circ}/90^{\circ}/0^{\circ}$ coupons used for this study have been described previously and we have made use of the transverse cracking phenomenon for the control of the laminates (17,18).

Table 1 gives the properties of the laminates used in this study. The softening point of the resin was found to be $140^{\circ}C$.

0-90-0 Crossply laminates in 0.5M H_2SO_4

The stress corrosion of the load bearing plies may occur either within the aqueous acidic environment, and this we have termed a Mode I type of failure, or outside of the environment, termed a Mode II. The mode of failure is dependent upon the type of environmental cell, the nature of the environment and the initial applied strain. The two types of failure are illustrated in Figs.4 and 5.

Mode I failures occur at strains greater than ≈0.15% in both environmental cells, whereas at lower strains Mode II occurs only in the open-cells. Mode II failure ha not been observed in the closed-cells at any applied strain.

Above ≈0.15% strain the times to failure of the coupons in the open and closed cells are shown in Fig.6 to be identical whereas at strains less than 0.15% the Mode II failures occur earlier than the Mode I failures.

A comparison of the fracture surfaces using scanning electron microscopy (S.E.M.) from Mode I and Mode II failures revealed no significant differences, other than presence of more crystalline deposits in the latter.

0° Unidirectional laminates in 0.5M H_2SO_4

Failure of unidirectional coupons may also be either by Mode I or Mode II (Figs. and 8). In order to compare the results from 0° unidirectional and the $0^{\circ}/90^{\circ}/0^{\circ}$ crossply coupons, the maximum strain in the longitudinal plies of the crossply coupons has been calculated (ie. the stress in the longitudinal plies in the same plane as a transverse crack). The result of such a calculation is given in Fig. 9 Above ≈0.15% the Mode I failure times for both laminate configuraions are found t be identical. At lower strains, the Mode II failure times are also similar but fa on a line of different slope.

As shown in Fig. 10, the fracture surfaces of 0^{o} coupons subjected to initial applied strains greater than 0.15% (ie. Mode I)are considerably stepped in appearance in contrast to the planar fractures of the crossply coupons. At ≈ 0.1% strain and below they are as planar as the crossply failures. Examination of the fracture surfaces by SEM did not reveal any significant differences with those of the crossply coupons.

Crossply Coupons in various Acids under zero load

Crossply coupons partially immersed in 0.5M sulphuric acid quickly develop damage in the unimmersed half of the laminate, whilst the immersed part showed no sign of damage (Fig.11). This damage, termed Mode III consists of longitudinal splits and transverse cracks, and has not been observed in longitudinal coupons. If the acid is replaced by hydrochloric or nitric acid of similar concentration, then no damage occurs,(hydrochloric acid gave very slight damage after 2 weeks), whereas phosphoric acid produces damage in the immersed half also, but after a considerably longer time than sulphuric acid.

A crossply coupon totally immersed in 0.5M H_2SO_4 for 15 months has shown no tendency to longitudinal split or transverse crack, the attack is apparently limited to the exposed surfaces only.

Stress Corrosion of Single Glass Fibres and Tows

At strains of 0.15% amd above single glass fibres failed in similar times to those of both the unidirectional and crossply coupons. (Fig. 12). At lower strains the fibres failed more rapidly than laminates failing under Mode II conditions.

Glass fibres stored in 0.5M H_2SO_4 became embrittled, and spontaneous spiral cracking of the outer sheath occurred in the majority of fibres of the tow.

Tows of fibres always failed within the acid under applied strains of 0.1% in an open-cell experiment. Under these conditions the laminates would have failed by Mode II.

DISCUSSION

Glass Fibres

Fig. 12 shows that, above an applied strain of 0.15%, the times-to-failure of single glass fibres and laminates are similar, demonstrating that the acid rapid reaches the fibres in the laminates. Below 0.15% the laminates take longer than the glass fibres to fail.

Relatively few spiral-cracked fibres have been found in the laminate fracture surfaces compared with the number in unstressed tows. This suggests that spiral cracks are only formed when the fibres are not stressed and therefore their role in the stress corrosion of laminatesmay be unimportant. The fracture surfac of single fibres were shown to be smooth and similar to those reported by Charles (21)and to those found in stress corroded laminates (2-7). Some indication of a core-sheath structure has been observed, but it is believed to be caused by corrosion after stress corrosion fracture. Few core sheath structures have been observed in laminate fracture surfaces. Glass tows failed within the acid when te in open cells, so that the Mode II fracture can be considered to be a property of the laminates.

Mode I Type Failure

Mode I failure of crossply laminates occurs by fracture of the longitudinal plies adjacent to an initial transverse crack in the 90^{o} ply. This is shown in Fig.4 where the crack which lead to failure is arrowed. These failures can be explained as follows: When the transverse ply of a crossply coupon fractures, the load that it supported is redistributed onto the longitudinal plies. The modified shear lag theory of Garrett and Bailey (22) describes how this additional load on the longitudinal plies is transferred back into the transverse ply as a function of distance, and predicts a transfer length of less than 2 mm for 90% of this additional load.

Thus the longitudinal ply adjacent to a transverse crack experiences a greater stress than at a short distance away. Therefore, stress corrosion will be most rapid in this area, and failure will occur adjacent to the initial transverse crack. The effect of this localised highly stressed region is that crossply coupons that fail in this manner have planar fracture srufaces, whereas those from longitudinal coupons, which have no localised laminate stress concentrations, have a stepped topography (Fig. 10).

The failure of 0^{o} coupons at strains greater than 0.2% begins by the initiation and growth of individual stress corrosion cracks randomly over the immersed half of the coupon, as shown in Fig. 13. These cracks occur normal to the applied load and on the microscale are seen to cross individual fibres normal to their axes. With time, these cracks increase in size and coalesce by longitudinal splitting, and are easily visible over the whole of the immersed surface, in Fig. 7. When the crack reaches a critical size, failure of the coupon results.

At applied strains of less than that for transverse cracking of crossply laminates, instantaneous failure of the transverse ply does not occur on loadi but in the aqueous acidic environment there is a slow growth of "edge-cracks" the specimen which are clearly seen in Fig. 5. These"edge-cracks" do not span entire width of the coupon because of their mutual interference. However, we h shown by comparison of the transverse cracking of crossply coupons in air and in aqueous acids that they behave similarly to transverse cracks produced in a and may be considered to be identical (23,24). It appears therefore, that the transverse cracking strain of the crossply coupons is reduced under the combin influences of the stress and the acidic environment.

Experiments with polyester coupons, in bend, lead to the hypothesis that trans cracks would cause a more rapid failure, of the longitudinal plies of a $0^{o}/90$ laminate than those of a 0^{o} laminate, since not only would they allow the acid enter the laminate, but could also act as sharp notches where stress corrosion cracks would be initiated. Since the times-to-failure of unidirectional and crossply coupons above 0.15% are shown in Fig. 9 to be the same, it is conclu that neither factors significantly affect the fracture of the crossply coupon This result is in agreement with experiments with polyester laminates under tensile loads where the failure times were also unaffected by the presence of transverse cracks (24,25).

The transverse cracking of this laminate system in air was shown previously to be preceded by debonding at individual fibres, which coalesce to form a transverse crack at a higher strain (18). Since the transverse cracking strai ε_{tlu}, is reduced by stress corrosion, it follows that the debonding strain wil also be reduced. It can be shown that ε_{tlu} is reduced to 0.1% in short term environmental tests, and since for this laminate configuration where the inner play thickness is twice the outerply, the thermal strain in the longitudinal direction of the transverse ply is equivalent

to that in the transverse direction of the longitudinal ply and that these strains do not decay significantly in the environment over the timescale of the experiments, then it follows that the 0^o plies will also become debonded. Therefore, equivalent failure times of the single filaments and the $0^o/90^o/0^o$ coupons can be understood in terms of the stress corrosion of the interfaces leading to rapid transport of the aqueous acid. Since the stressed 0^o coupons, at applied strains > 0.2% also have similar failure times, it would appear that debonding of unidirectional coupons can also occur. Experiments with small cells clamped to the faces of these laminates gave similar results which demonstrate that diffusion through the surface resin to the interfacial region is important (26).

Mode II Type Failure

The Mode II failure of crossply coupons, unlike the Mode I failures, are not preceeded by transverse cracks, but rather the failure crack grows through both the transverse and longitudinal plies concurrently. At strains < 0.15% the Mode II type of failure occurs in shorter times than Mode I , but not so rapidly as single glass fibres. At higher strains when failure of single glass fibres occurs in similar time to that of laminates, Mode II has not been observed. Although stress corrosion cracks may nucleate just above the aqueous acid in 0^o coupons, these do not lead to final failure. Therefore, the mode II mechanism only operates when resin is protecting the glass fibres and is suppressed in "closed-cells" when the atmosphere surrounding the unexposed half is moist. Enrichment of the atmosphere with oxygen had no effect on the time or mode of failure which eliminated oxidation as the mechanism.

Observations that the dry half of fractured crossply coupons became increasingly damaged when removed from the environment, which could not be accounted for by differential shrinkage stresses on drying out, led to the discovery of cumulative damage in the unexposed halves of partially immersed unstressed coupons. We have termed this Mode III (Fig.11). There was however, a crystalline deposit always present on the unexposed edges and within the longitudinal splits.

X-ray analysis in the transmission electron microscope showed it to be rich in alumin and sulphur with traces of calcium and potassium. Furthermore, Mode III was supressed in hydrochloric and nitric acids but could form within the environment in the case of phosphoric acid (Table 2). It is well documented (12) that acids leach the metallic ions from glass and for E-glass these are Al^{3+}, Ca^{2+}, and Na^{+}, and the trend in Table 2 appears to be related to the solubility of these salts. The apparently lower rate observed in phosphoric acid can be ascribed to its reduced acidity, as shown by a more positive pK_a. In addition, as the initial applied strain in the laminate is decreased, additional Mode III damage, whose extent is increased, appears in the unexposed half of crossply coupons that fail by Mode II. It is therefore apparent that the mechanism responsible for stress corrosion Mode II failures is the same as that for Mode III damage within partially immersed coupons, under zero load.

The crystalline material found in Mode II fracture surfaces was found by microprobe analysis to be rich in calcium and sulphur with traces of aluminium, potassium and iron.

Fig. 8 shows that aluminium-rich crystals are also deposited at the edge of these low strain coupons. Therefore it is clear that, for aqueous H_2SO_4 the more insoluble calcium salts are precipitated within the laminate, whilst the more soluble aluminium salts are transported to the surface of the coupon, where precipitation occurs by evaporation of water. Acids, with soluble calcium and / or aluminium salts do not cause Mode III damage. Its absence in the immersed half of coupons in aqueous

sulphuric acid shows that the glass degradation products can remain in solution and not cause damage. This is in contrast to phosphoric acid, whose calcium salts are more insoluble. Further support for the mechanism is given by the fact that, in IM HCl, at 0.1% strain, a delayed Mode I fracture occurs (in the environment), and that the fracture surfaces are devoid of crystalline deposits.

Thus the Mode II fractures and Mode III damage are caused by additional local stresses from the crystallisation of the rather insoluble calcium salts. The glass corrosion products can clearly be transported to the unimmersed half by capillary action at the stress-corroded interfaces, since the thermal strains are sufficient to debond the fibres of a laminate whose transverse failure strain is reduced under the influence of the acid environment (23,24). The continued evaporation of moisture from the laminate surface, or diffusion from the interface into "dry" resin, effectively maintains a concentration gradient within the laminate which produces an additional driving force for acid transport. When distillation is not possible, as in the case of the closed-cells and fully immersed coupons, Mode II or Mode III behaviour is suppressed.

At applied strains of < 0.15% diffusion through the resin normal to the fibres is slower than along the stress-corroded fibre interfaces so that crystallisation and hence the Mode II crack is initiated at the edge of the coupon, just above the environment where the fibres are not debonded. Crossply coupons develop thermal strains in the matrix which put the fibres into compression so that coupons under zero load are subject to cracking rather than fibre fracture. The stress state, associated with the Mode III cracks, causes further debonding and acid transport and the unexposed half becomes progressively damaged with time.

The planar fracture surfaces in the stress corrosion of GRP have been explained by Hogg and Hull (6), as localised acid attack upon exposed fibres at the crack tip. However, at applied strains > 0.15% the equivalent failure times for crossply 0° unidirectional and single glass filaments favour the explanation of Aveston, Kelly and Sillwood (8) that the rate of growth of flaws in fibres adjacent to the fractured filament is increased tenfold. At lower strains the resin provides some protection to the glass fibres so that the former mechanism of localised corrosion at the crack tip formed under the stresses generated by the crystallisation proce could also operate. The true reason for the planar fractures, therefore is dependent on the detailed stress corrosion mechanism.

CONCLUSIONS

The prime cause of environmental stress corrosion of these epoxy glass fibre composites is the susceptibility of the glass fibres to stress corrosion. Therefo the main function of the resin is to protect the glass fibres from the environmen However, the glass/resin interface will stress corrode with the result that the a penetrates the laminate, so that at initial applied strains greater than 0.15% th Mode I failure times are the same as for single filaments. At lower strains the resin protects the glass fibres and the laminates are more resistant to stress corrosion, but a second mechanism termed Mode II is available which leads to a st corrosion fracture more rapidly than by Mode I failures at these strains. Mode I is associated with the crystallisation of calcium rich glass degradation products in the unexposed half of the coupons. In crossply coupons under zero load this results in Mode III cracking because the localised stresses are unable to overcom the compressive forces in the load bearing fibres with the result that the unimme half becomes progressively more damaged with time.

Thus the environmental stress corrosion resistance of GRP is not only controlled by the rate of diffusion of the acid through the resins to the glass fibres but by the degradation of the interface and the accumulation of crystallisable glass corrosion products in unexposed areas of the composite. Furthermore the change in mechanism at low strains shows that high strain control tests may not predict the long term-low strain life of a GRP structure.

ACKOWLEDGEMENTS

We thank the Science and Engineering Research Council for a research studentship (JWR), and an equipment grant, and Silenka (UK) for the glass fibres.

REFERENCES

1. L.S. Norwood and T. Farebrother, Symp. Reinforced Plastics in Anticorrosion Applications, National Engineering Laboratory, Glasgow 1979, paper 8.
2. H.A. Barker, I.G. Baird-Smith and F.R. Jones, Symp. Reinforced Plastics in Anticorrosion Applications, National Engineering Laboratory, Glasgow, 1979 paper 12.
3. R.C. Roberts, Reinforced Plastics Congress (BPF) Brighton 1978, paper 19.
4. H.H. Collins, Plast. Rubber. Mat. and Appl. 1978, 6.
5. P.J. Hogg, D. Hull and M.J. Legg in "Composite Structures" edited by I.H. Marshall (Appl. Science, 1980), p. 106.
6. P.J. Hogg and D. Hull, Metals Science, 1980, 441.
7. P.J. Hogg and D. Hull in "Advances in Composite Materials" Vol. 1, edited by A.R. Bunsell et al. (Pergamon, Paris 1980) p.543.
8. J. Aveston, A. Kelly and J.M. Sillwood in ref. 7. p.556.
9. R.F. Regester, Corrosion, 25 (1969) 157.
10. J.M. Marshall, G.P. Marshall and R.F. Pinzelli, S.P.I., Reinforced Plastics Conference,Washington, 1982.
11. G. Scrimshaw, Pipe Conf. London 1980 , paper 5.
12. R.W. Douglas and T.M.M. El-Shamy, J.A. Ceram Soc. 50 (1967) 1.
13. A.G. Metcalfe and G.K. Schmitz, Glass Tech 12 (1971)15.
14. A.G. Metcalfe and G.K. Schmitz, Glass Tech 13 (1972) 5.
15. F.R. Jones, A.R. Wheatley and and J.E. Bailey in ref. 5, Ch. 27, p. 415.
16. J.E. Bailey, T.M.W. Fryer and F.R. Jones in ref. 7. p.514
17. J.E. Bailey, P.T. Curtis and A. Parvizi, Proc. Roy. Soc. Lond. A 366 (1979) 599.
18. J.E. Bailey and A. Parvizi, J.Mater.Sci.16 (1981) 649.
19. F.R. Jones, M. Mulheron and J.E. Bailey, International Conference on Composite Materials IV, Tokyo, 1982.
20. D.H. Smithgall, L.S. Watkins and R.E. Frazer Jr.,Applied Optics, 16 (1977) 2395.
21. R.J. Charles. J. Appl. Phys. 29 (1958) 1549.
22. K.W Garrett and J.E. Bailey. J. Mater. Sci. 12 (1977) 57.
23. F.R. Jones and J.W. Rock, in preparation.
24. F.R. Jones, J.W. Rock, A.R. Wheatley and J.E. Bailey, International Conf. on Composite Materials IV, Tokyo 1982.
25. F.R. Jones, A.R. Wheatley and J.E. Bailey, Reinforced Plastics Congress, BPF, Brighton, 1982.

26. F.R. Jones and J.W. Rock, unpublished results.

27. A.I. Vogel "Textbook of Qualitative Inorganic Analysis" Longmans 1954.

28. Handbook of Chemistry and Physics" CRC, Ohio 1972.

FIGURE CAPTIONS

Fig. 1. Schematic Representation of the vacuum impregnation technique.

Fig. 2. Types of environmental cell used for ESCC studies under constant tensil loads. (a) Closed-(b) open-cells

Fig. 3. The experimental method for the study of the stress corrosion of singe glass filaments.

Fig. 4. Mode I failure of $0^\circ/90^\circ/0^\circ$ coupon in 0.5M H_2SO_4 at 23°C. ε_a = 0.49%. The transverse crack adjacent to the failure is arrowed.

Fig. 5. Mode II failure of a $0^\circ/90^\circ/0^\circ$ coupon in 0.5M H_2SO_4 at 23°C. ε_a = 0.1%.

Fig. 6. ESCC failure times of epoxy $0^\circ/90^\circ/0^\circ$ coupons in open (●) and closed-cells (■). The applied strain is that on the composite obtained from the stress-strain curve of the characterisation coupon for each laminat

Fig. 7. Mode I failure of a 0° unidirectional coupon in 0.5M H_2SO_4 in an open-cell with an initial applied strain ε_a of 0.34%.

Fig. 8. Mode II failure of a 0° unidirectional coupon in 0.5M H_2SO_4 in an open-cell at an applied strain ε_a of 0.09%. Note the crystalline deposit on the cut edge above the growing crack.

Fig. 9. A comparison of the Mode I and Mode II failure times of $0^\circ/90^\circ/0^\circ$ (●,○) and 0° (■,□) coupons in open-cells. The open points are Mode II failu The initial applied strain in the former has been calculated assuming t 90° is not load bearing.

Fig. 10. Stress Corrosion Fracture Surfaces: (A) $0^\circ/90^\circ/0^\circ$ with ε_a = 0.1% (B) The same $0^\circ/90^\circ/0^\circ$ fracture surface close to the final failure zone. (C) Single glass filament. (D) Comparison of 0° and $0^\circ/90^\circ/0^\circ$ failures at ε_a = 0.5%.

Fig. 11. Mode III damage in the unexposed half of a $0^\circ/90^\circ/0^\circ$ coupon without an external applied strain. The damage is initiated just above the 0.5M H_2SO_4 after about 3 days and progresses up the coupon.

Fig. 12. A comparison of failure times of 0° coupons in open-cells (■) with sin glass filaments (●). Mode II occurs at $\varepsilon_a < 0.1\%$. An error of ± 0.5 μm in the fibre diameter gives an error of ± 10% on applied strain for 10 single filaments.

Fig. 13. Micrograph of 0° coupon showing initiation and growth of individual st corrosion cracks.

Figures and Tables not included, they are all present in the thesis.